Configurational studies of asymmetric star polymers

Stuart William Reynolds

Configurational Studies of Asymmetric Star Polymers

by

Stuart William Reynolds
Graduate Society
University of Durham

A thesis submitted in partial fulfilment of the requirements for the degree of Doctor of Philosophy

Department of Chemistry
University of Durham

2001

Configurational Studies of Asymmetric Star Polymers

Stuart William Reynolds

Submitted for the degree of Doctor of Philosophy

2001

Abstract

A series of miktoarm star polybutadienes were investigated in the melt and dilute solution state by neutron and light scattering and viscometry techniques. The stars had 8-arms, with a single asymmetric arm of varying molecular weight. Living anionic polymerisation synthesised the arms to be coupled by chlorosilane core molecules, with the molecular weight of the hydrogenous arms being 3×10^4 g mol^{-1} and increasing for the deuterated arm from 3×10^4 g mol^{-1} to 3×10^5 g mol^{-1}. Global properties of $\bar{M}_W$, R_G, A_2, D_0 and $[\eta]$ were ascertained for these stars in the good solvent of cyclohexane, and over a temperature range in the θ-solvent of 1,4-dioxane. Branching ratios calculated from the cyclohexane data indicated that increasing the asymmetric arm length yielded values similar to a linear polymer of equivalent molecular weight, with a reduction of segment density near the star core. This was seen more clearly by calculating the size ratios of R_T/R_G, R_H/R_G and R_V/R_G from the equivalent sphere radii. Aggregation of the stars was found with the dioxane solutions, as the $\bar{M}_W$ of these stars increased with decreasing temperature to values higher than obtained in cyclohexane, where they remained constant and equal to the good solvent data for the linear polymers. Small-angle neutron scattering was used to determine the R_G and interaction parameters for the asymmetric arm in the melt and solution states. The increase of R_G in the order of unperturbed linear equivalent<melt<cyclohexane was due to the presence of the branch point and the excluded volume effect. Higher R_G values obtained in the θ-solvent suggested aggregation. An increase in temperature in the melt state was found to promote inter-star mixing of the asymmetric arms and this was greater for shorter arms. In cyclohexane, the intra-star interaction parameters were found to decrease with increasing asymmetric arm length, and lower values were found in 1,4-dioxane as the solvent became thermodynamically more favourable.

Memorandum

The research presented in this thesis has been carried out in the department of Chemistry, University of Durham, between April 1998 and March 2001. It is the original work of the author unless otherwise stated. None of this work has been submitted for any other degree.

Acknowledgements

I would like to acknowledge my supervisor, Professor Randal Richards, for his vigorous support and assistance during my studies. His advice in the sacrifice of lunches for the pursuit of science is well noted. I must also thank Dr. Lian Hutchings who guided me through the unforgiving world of anionic polymerisation. His technical skill and patience (with postgrads) was always an inspiration. I would also like to thank Mr Douglas Carswell for performing all the size exclusion chromatography experiments, and all the technical and support staff (I have retired two glass blowers) in the Department of Chemistry. Neutron scattering experiments were performed at the Institute Laue-Langevin, with the help of the instrument scientists of Drs Robert Cubbit and Isabelle Grillo. Financial support for this work was provided by the EPSRC and IRC.

My colleagues in the chemistry department, past and present have helped to provide a pleasant and stimulating working environment. I must especially acknowledge the following colleagues for their contribution to my reasearch (and sanity): Ian (the "Kid") Anderson, Andrew (Splitter) Brown, Andreas (Crawl Master) Kilbinger, Dave (Anglo-Saxon warrior) Parker, Edoardo (Steady-Eddy) de Luca, Wilfried (Mr President) Lovenich, Alison (Bungle/Mongrel) Stoddart, Simon (City Scum) Aldersley, Richard (Forme de Poire) Thompson, Aline (cheers for the leg room) Miller and Mark (@computer-surf.non-ac.uk) Wyatt.

I would to thank friends who have provided a distraction away from the desk and laboratory bench. These include members of the Durham Graduate Society (you know who you are), and the Loughborough (Phil, Steve, Gareth and James) and Birmingham (Gas, Bads, H) lads. I must especially thank Helen for being so supportive during my write-up period, being a constant reminder that there is more to life (3 requirements maintained) and for no longer preparing tuna pasta.

Finally, I must thank all the members of my family, especially Mum, Dad and Steven for their constant guidance and support during my studies.

To my Family

Table of Contents

Chapter 1

Introduction to Asymmetric Star-Branched Polymers

1.1 Star Polymers- The Simplest Branched Polymers

Random branching of polymers is a common occurrence.[1] Chain transfer reactions can cause short and long-chain branching during polymerisations, such as the high pressure polymerisation of ethylene. Branching can also be induced intentionally by the use of multifunctional monomers, for example divinylbenzene. Graft polymerisations can also induce long chain branches on to a polymer backbone, the branches often being chemically different from the backbone. Properties of branched polymers are quite different from those of linear polymers of the same molecular weight. The bulk viscosities as well as concentrated and dilute solution viscosities are lower for branched polymers than linear polymers of the same molecular weight. Melt processing behaviour can be manipulated by alterations in the average molecular weight, molecular weight distributions, and the frequency and length of long branches in the macromolecules. This leads to an obvious need to correlate and characterise the type and degree of branching in a polymer, with its effect on the physical properties in solution or in the melt.

Branching in a polymer cross-linked network can be totally random, where the frequency of branching and the length of segments in between the branch points and of branch can vary. A mixture of branched and linear material exists, and therefore the properties of the material will be an average of all the species present. The diversity of these species causes the

interpretation of the effect of branching to be difficult. Any calculations involving these structures will be complex and so theory needs to be tested by the simplest model possible. To consider the most simplest model of a branched polymer is to focus on a single branch point, and this can be modelled by a star polymer (Figure 1).[1-4] A star polymer is considered to be a single branch point structure, with a number of linear polymers chains radiating away from the common junction point. There are three variable to such a model: the number of star arms (*f*), the molecular weight of the arm and the polymer type. Regular star polymer models are produced when all the arms are of the same polymer type and molecular weight. Asymmetric star polymers have also been synthesised by varying the molecular weight of the arms and/or having arms of different chemical type. Stars that contain arms of differing chemical type are called miktoarm star polymers.

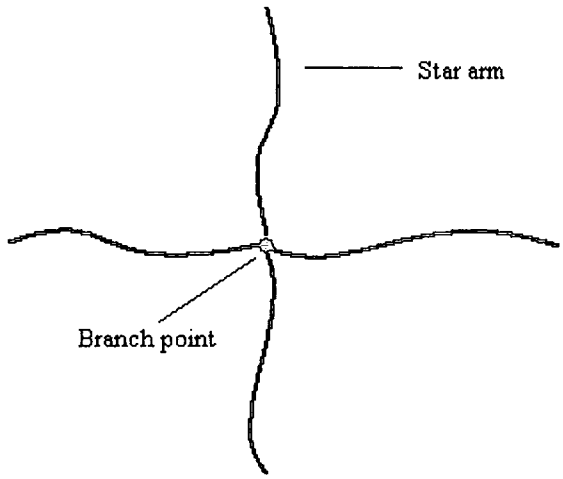

Figure 1: A star polymer with f arms.

To study branching in polymers, the characteristics of the model star polymers must be known precisely, so that reproducible results can be achieved. Characteristics such as the average number of arms attached to the core and the molecular weight of the arms must be ascertained, so that results of properties obtained can be interpreted properly. To produce precise model stars, special synthetic procedures such as anionic polymerisation techniques have been used to yield linear polymer chains with narrow molecular weight distributions. The star arms were coupled together with linking agents such as the chlorosilanes, the number of chlorosilyl groups determining the functionality of the resulting stars. The average molecular weights of the arms and of the whole stars can be found by utilising the

characterisation technique of size exclusion chromatography. Overall the use of anionic polymerisation and functional chlorosilanes can yield model compounds with a known number of arms and molecular weight.

Branched polymers have increased segment densities at the junction points when compared to linear polymers. High segment densities can be achieved at star cores by increasing the number of arms attached to the single branch point. Regular star polymers with high segment densities have been produced with over 200 arms.[1, 4] The effect of high segment density at the core has led to the concept that the arms are stretched in order to relieve the steric crowding at the core, and this has been modelled by Daoud and Cotton.[5] This model considered the star to be in a solution with the arms existing in different concentration scaling regions, where melt-like conditions prevailed at the inner core region. A different model by Grayce and Schweizer[6] considered the polymer arms to be pushed out due to differential excluded volume interaction between the core and corona regions of the star, but this could only be applied to concentrated solutions and the melt state. Increasing the length of the arms reduced the effect of core expansion had on the overall properties, and therefore a reduction in the relative increase of the arm dimensions. Star polymers with molecular weight asymmetry can be used to investigate the effect of core has on arm stretching, by varying the length of a single arm.

Model star polymers can be studied in the melt state, and also in concentrated and dilute solutions.[2] The usefulness of a dilute solutions is that the star polymers can be treated as isolated species, and be characterised on a individual basis. Changing the thermodynamic quality of the solvent, influences the interactions of the polymer arms with the solvent molecules, and subsequently affecting the dimensions of the star The thermodynamic quality of the solvent for the polymer can be quantified using the virial coefficients, where only the second virial coefficient needs to be considered in dilute solutions. Global dimensions of the star can be characterised by the radius of gyration, which is the average distance of the polymer segments to its centre of mass. Dynamic solution properties of the stars in solution, such as the translational diffusion coefficients and intrinsic viscosity have also been investigated. These global properties can be determined by dilute solution characterisation techniques such as static and dynamic light scattering and viscometry.

Global properties ascertained can be interpreted as an equivalent sphere that behaves in a similar manner to the polymers in solution. The hydrodynamic, viscometric and thermodynamic radii are the equivalent sphere radii for the translational diffusion coefficient, intrinsic viscosity and second virial coefficient respectively. Equivalent radii can be compared to the radius of gyration of the polymer by the calculation of size ratios and the values obtained will depend on the segment density near the core. Alternatively, the properties of these star-branched structures can be compared to linear polymers of the same molecular weight. This has been achieved by calculating branching ratios for the star polymers and comparing experimentally determined values to theory and simulation. Branching ratios g, h and g' have been devised for the radius of gyration, hydrodynamic radius and intrinsic viscosity respectively. The radius of gyration of a single arm can be obtained in the melt state and in solution as well, with interaction parameters between different regions within the star polymers and between different stars.[7] This has been achieved by labelling a specific arm within the star and using the technique of small angle neutron scattering (SANS).

The polymer physics used to characterise these star polymers is outlined in section 1.2. Chain models of linear polymers that define the conformational dimensions and a description of the ideal chain are discussed. A review of the behaviour of linear polymers in solution is presented and the effect of the thermodynamic quality of the solvent on the global properties of these polymers, such as the radius of gyration and second virial coefficients. The concept of the distribution of molecular weight of polymers is also described and the importance of molecular weight averages. Polymer behaviour in more concentrated solutions and the melt state is then outlined, with the concept of semi-dilute solutions. Dynamical properties of polymers in solution will also be reviewed, with a discussion of translational diffusion coefficients and intrinsic viscosity, and the effect of solvent on these properties. Section 1.3 reviews the work already published on the characterisation of star polymers in solution and in the melt state. Section 1.4 describes the motivation of this work and the investigation of molecular weight asymmetric star polymers in the solution and in the melt state.

Chapter 2 reviews the synthesis of regular and asymmetric star polymers. The polymerisation techniques and coupling centres that have been used to produce and link the star arms is discussed in section 2.2, with the advantages and disadvantages that were found. An outline for the choice of polymerisation and star synthesis procedures used for this project are presented at the end of this section. Section 2.3 of this chapter discusses the synthesis followed to obtain the model stars used for this study. A description of the technique of anionic polymerisation is provided with the choice of monomers that can be used, polymerisation initiator, solvent and other reaction conditions. The synthetic method of deuterium labelling and the production of the chlorosilane core molecules are also presented. The method of synthesising model star polymers with a labelled arm is described, with the average molecular weight results obtained for the arms and for the overall stars being listed. An in-depth description of experimental methods for the synthetic methods applied in this study are given in section 2.4.

Chapter 3 discusses the dilute solution characterisation of the model polymers synthesised. A description of the techniques of static and dynamic light scattering and viscometry is provided in section 3.2 and the global properties obtained from them. Section 3.3 reviews the experiments performed on these star polymers using these techniques. The results for the stars are given in section 3.4, with comparisons to the data in the literature. Two solvents with different thermodynamic quality that affects the global properties of the stars were used The polymers were characterised by calculating branching ratios, equivalent sphere radii, size ratios and other dilute solution properties as well. At the end of this chapter a summary of all the results and findings is presented.

Chapter 4 is devoted to the characterisation of the labelled star polymers in solution and in the melt state by SANS. An overview of the technique of SANS is provided in section 4.2 and the properties of star polymers that can be ascertained. The experimental section 4.3 then outlines the analysis of the model star polymers by this technique. Section 4.4 presents all the results obtained that includes the radius of gyration of the labelled arm and the interaction parameters in the solution and the melt state. The experimental data will be compared to previous work and a summary of results is provided. The final chapter summarises all the results and the general conclusions that can be drawn. A description of future work is also presented.

1.2 Properties of Linear Polymers in Solution and in the Melt

1.2.1 The Configurations of Polymer Chains

Linear homopolymers can be considered as consisting of many identical chemical residues (monomers) covalently bonded in a linear fashion, to form a long chain of repeating units. Each monomer along the chain has a certain degree of rotation about the axis of the preceding monomer unit.[8-10] This yields a chain with flexibility and a huge number of different polymer configurations, so that the polymer can be considered to be similar to a flexible string. The internal rotations of successive monomer units cannot take place independently because their constituent atoms or atomic groups interact with each other when they become close. These correlated internal rotations yield the chain with some resistance against bending or twisting and the chain cannot be considered to be perfectly flexible. A degree of flexibility still remains though, as these correlations between monomer units only persists over a few successive monomers, which is short in comparison to the entire length of the polymer chain.

To investigate the flexible nature of polymers over the entire chain length, hypothetical models of segments of equal length (b) connected at universal joints (N of them) have been devised. The simplest hypothetical chain is the freely-jointed model (random flight model), where the universal joints are placed on a 2-dimensional lattice and successive joints are allowed to take any position on the lattice, with free bond angle and segment rotation. Such a model linear polymer chain has a Gaussian probability distribution function of intramolecular distances and the mean square end-to-end distance is:

$$\left\langle R^2 \right\rangle_0 = Nb^2 \tag{1}$$

Equation 1 demonstrates that the size of a Gaussian chain scales with $N^{1/2}$. If the bond angle of the chain is fixed and the monomer units are allowed to take any angle of rotation, then this leads to the freely-rotating chain model. The constraint of the fixed bond angle can be overcome in this model by changing the length of the rigid rods in between the universal joints. The freely-jointed model is invalid in the respect that a pair of monomer units

separated by more than a chain segment can come close due to the deformation of the intervening chain. As the monomers cannot occupy the same volume, they tend to repel each other as one monomer excludes the other approaching monomer unit. These interactions are long-range and are modelled by placing beads at the universal joint positions, with intra-chain (inter-chain as well) interactions only acting between the beads. Each segment (or rod) between the beads is now treated as a phantom. The freely-jointed model no longer contains any information on primary chemical structure and local interactions and is therefore only useful in formulating large scale or global behaviour. A global property is determined by its entire length (or molecular weight) as well as it overall flexible nature and by long-range interactions of its monomers. The random flight model is not always convenient for the theoretical formulation of global properties due to the constraint of fixed segment length. A less constrained model is the spring-bead chain (Figure 2), where the chain segments in-between the beads are represented by a spring, whose end to end distance fluctuates with a Gaussian distribution function and is often referred to as the Gaussian spring. The spring is also considered as a phantom, with the interactions still being only between the beads.

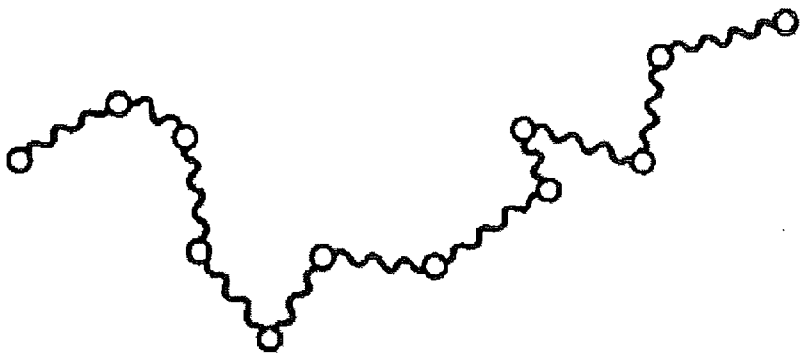

Figure 2: The spring-bead model for a polymer chain.

When moving along a random flight or a spring-bead chain a discontinuous change in direction is encountered at each bead. To remove this structural detail, the polymer chain is coarse-grained to smooth out the microscopic discreteness, so that the chain can now be represented as a continuous space-curve with a certain contour length (L), and this curve is called the continuous chain model. A continuous chain can be represented by a limiting process in which all the segments of a freely-rotating chain are shortened to zero and at the

same time the bond angle approaches 180°. This type of model is called a wormlike chain or Kratky-Porod chain and has the feature of no longer being a flexible chain, as a resistance to bending now exists. The wormlike model is useful in the formulation of global behaviour of stiff or semi-flexible polymers chains. A continuous chain can also be derived by making all the springs in the spring-bead chain vanishingly short, with its total contour length fixed. This is an example of the Edwards continuous chain and the segment length is now represented by the Kuhn segment length (b_K), which is a measurement of the stiffness of a polymer chain. The end to end distance of a Gaussian polymer calculated by this model is:

$$\left\langle R^2 \right\rangle_0 = Lb_K \tag{2}$$

The interactions between the beads of the hypothetical linear chain determine the global properties. If a dilute gas of chains is considered, the beads are not allowed to occupy the same volume and a repulsive force exists between them. The strength of this force depends on the separation between the beads, the chemistry of the bead, and the temperature and pressure of the gas. If a solvent is introduced, the polymer beads now interact with the solvent molecules and the resultant force that now results between the beads is no longer equal to the vacuum value. If the bead-solvent interactions are more favourable than bead-bead interactions, the solvent is said to be good and *vice-versa* for poor solvent conditions. An ideal thermodynamic state can be achieved where all interactions are the same and the solvent is described as a θ-solvent for the polymer.

The bead-solvent interactions has an effect of inducing some additional force (solvent mediated force) between a pair of beads and the thermodynamic behaviour of a polymer solution can be formulated by applying the well known Van-der-Waals theory of gases. In a good solvent the bead-solvent interactions tend to pull a pair of beads apart and the solvent mediated force is repulsive. In a poor solvent the solvent mediated force is attractive and pulls a pair of beads together. This prevention of chain from occupying the same space, and the intra-chain and inter-chain segment-segment interactions are described by the excluded volume of the polymer.

The polymer physics of such systems are not concerned with the individual polymer conformations, but those averaged over the ensemble of such conformations. The polymer conformation and hence global properties are significantly influenced by the potential energy stored in the polymer chain, that results from binary, ternary or higher bead interactions. The Hamiltonian of the chain is the total potential energy calculated from the elastic energy stored within the springs and the mean potential force from the cluster of beads. In dilute solutions, binary-interactions are only considered (the binary cluster approximation) and the mean potential force is related to the excluded volume strength, β (sometimes called the binary cluster integral). This leads to the conformation of a linear polymer in a solution being dependent on the effect the solvent has on the binary interactions of the chain. The total potential energy stored in an Edwards continuous chain is described by the Edwards Hamiltonian. It is specified by four parameters of L, b_k, β_c and λ, where β_c is the excluded volume strength for binary interactions for an Edwards continuous chain. The term λ is the cut off length that prevents self-interactions of the beads. The increase in chain dimensions as the beads start to repel each other can be described by the universal function F:

$$\left\langle R^2 \right\rangle = \left\langle R^2 \right\rangle_0 F\left(z, \frac{\lambda}{L}\right) \tag{3}$$

The universal function depends on the excluded volume variable z, defined for a continuous chain as:

$$z = \left(\frac{3}{2\pi}\right)^{3/2} \beta_c b_k^{-1/2} L^{1/2} \tag{4}$$

It can be seen in equation 4 that the excluded volume variable depends on the excluded volume strength, and the Kuhn segment and contour length of the polymer chain. Equation 3 shows that $\langle R^2 \rangle$ is governed by 3 combined parameters of Lb_k, z and λ/L. If $\lambda/L < 1$, then $\langle R^2 \rangle$ depends only on Lb_k and z, and dilute polymer solutions fitting to this expectation is called two-parameter theory. The use of the Edwards Hamiltonian and the condition $\lambda/L < 1$ is referred to as the two-parameter approximation.

The radius of gyration (R_G) is a more useful size dimension of macromolecules as it can be related to branched systems as well, and is obtained directly from scattering methods. It is the mean-square distance of the chain units from the centre of mass of a polymer configuration. The mean-square radius of gyration, $\langle R_G^2 \rangle$, is the size dimension averaged over all possible configurations, and for a bead-spring chain of $N + 1$ beads, $\langle R_G^2 \rangle$ is defined as:[8, 9]

$$\left\langle R_G^2 \right\rangle = \frac{1}{N+1} \sum_{j=0}^{N} \left\langle R_j^2 \right\rangle \tag{5}$$

$\langle R_j^2 \rangle$ is the mean-square distance between bead j and the centre of mass of the chain. The radius of gyration can be related to end to end distance by:

$$\frac{\left\langle R_G^2 \right\rangle_0}{\left\langle R^2 \right\rangle_0} = \frac{1}{6} \tag{6}$$

The subscript of 0 in equation 6 signifies unperturbed dimensions. The expansion of the radius of gyration in a thermodynamically more favourable solvent can be seen measured by radius expansion factor, α_S^2;

$$\alpha_S^2 = \frac{\left\langle R_G^2 \right\rangle}{\left\langle R_G^2 \right\rangle_0} \tag{7}$$

In the two parameter approximation, the expansion factor becomes a universal function of the excluded volume variable. In thermodynamically favourable (good) solvents, this factor approaches asymptotic regime as the chains exclude each other more strongly. When z reaches infinity, the chains no longer have a chance to form binary clusters and this extreme is called self-avoiding. The radius of gyration of a polymer chain increases with size and hence with molecular weight. This dependence of R_G on molecular weight has a scaling described by the Flory exponent of ν:

$$\left\langle R_G^2 \right\rangle^{1/2} \sim M^{\nu} \tag{8}$$

In a θ-solvent linear polymers have a Flory exponent of ½ and the chain has a Gaussian distribution of intramolecular distances. These polymer chains are termed ideal. Under good solvent conditions, the polymer dimensions are no longer Gaussian and have perturbed dimensions, with the value of the Flory exponent being 3/5. These polymer chains are described as non-ideal.

1.2.2 Polymer Chains in Solution

The formation of a polymer solution requires a negative Gibbs free-energy of the mixing (ΔG_M) of its components.[11, 12] This free-energy of mixing is described by Flory-Huggins theory, which postulates that the formation of a polymer solution is by the transfer of the polymer from a perfectly ordered state, to a state of disorder on a 3-dimensional lattice, with the inclusion of solvent molecules (Figure 3). This lattice contains a number of equal sized sites, with the polymer segments and solvent molecules occupying these sites. The connectivity of the polymer chains cause all the chain segments to occupy adjacent sites, with the solvent molecules filling the remaining surrounding sites. The combinatorial entropy of mixing (ΔS_M) of the polymer and the solvent on the lattice can be calculated by:

$$\Delta S_M = -k(N_1 \ln \phi_1 + N_2 \ln \phi_2) \tag{9}$$

N_1 and N_2 are the number of lattice sites occupied and ϕ_1 and ϕ_2 are their volume fractions of the solvent molecules and polymer segments respectively. The Boltzmann constant is k. During the mixing of the polymer and the solvent, an energy or heat change occurs. The enthalpy change of mixing (ΔH_M) of the two components is determined from the formation of new binary polymer-solvent contacts, and from the loss of polymer-polymer and solvent-solvent contacts:

$$\Delta H_M = kT\chi_1 N_1 \phi_2 \tag{10}$$

T is the absolute temperature and χ_1 is the interaction parameter. The interaction parameter is the energy difference between a solvent molecule being immersed in pure polymer, to when it is immersed in pure solvent. The free energy of mixing of the components can be calculated from the enthalpy and entropy of mixing using the Gibbs free energy equation at

a specific temperature ($\Delta G_M = \Delta H_M - T\Delta S_M$), with the assumption of incompressibility (no volume change):

$$\Delta G_M = kT\left(N_1 \ln \phi_1 + N_2 \ln \phi_2 + N_1 \phi_2 \chi_1\right) \tag{11}$$

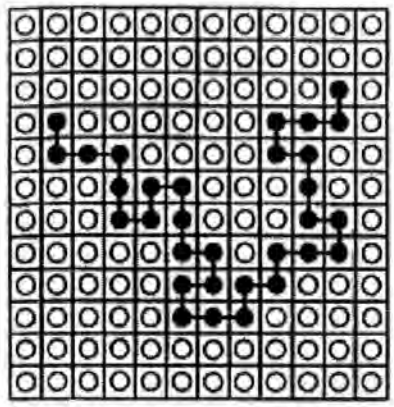

Figure 3: The Flory-Huggins lattice model of polymer solutions where filled and open circles represent polymer segments and solvent respectively.

A negative free energy of mixing leads to the formation of a polymer solution, where a positive free-energy of mixing leads to phase separation. The partial molar free energy of mixing ($\overline{\Delta G_1}$) can be determined, after multiplying by the Avogadro`s constant (N_A):

$$\overline{\Delta G_1} = RT\left[ln(1-\phi_2) + \left(1 - \frac{1}{x}\right)\phi_2 + \chi_1 \phi_2^2 \right] \tag{12}$$

R is the gas constant and x is the ratio of molar volumes of polymer to solvent. The partial free energy of mixing is related to the osmotic pressure by:

$$\left(\mu_1 - \mu_1^0\right) = -V_1 \pi = \overline{\Delta G_1} \tag{13}$$

V_1 is the molar volume of the solvent. The osmotic pressure is defined as the pressure that must be exerted on a solution to raise the chemical potential of a solution (μ_1), to that of pure solvent (μ_1^0). Insertion of equation 12 into equation 13 leads to:

$$\pi = -\frac{RT}{V_1}\left[\ln(1-\phi_2)+\left(1-\frac{1}{x}\right)\phi_2+\chi_1\phi_2^2\right] \tag{14}$$

If the logarithmic term in equation 14 is expanded in terms of a Taylor's series and with the low powers only being retained, then the following expression for the osmotic pressure can be formulated:

$$\pi = \frac{RT}{V_1}\left(\frac{\phi_2}{x}+\left(\frac{1}{2}-\chi_1\right)\phi_2^2+....\right) \tag{15}$$

Expansions of equation 15 leads to the virial coefficients, where the second virial coefficient is defined as:

$$A_2 = \frac{\bar{V}_2^2}{V_1}\left(\frac{1}{2}-\chi_1\right) \tag{16}$$

The partial specific volume of the polymer is $\bar{v}_2$. Equation 15 is the expansion of the van`t Hoff law expression for the osmotic pressure at infinite dilution. Equation 15 can now be represented in the form of a colligative property measurement in dilute solutions:

$$\frac{\pi}{RT} = \frac{c}{M} + A_2c^2 + A_3c^3 + ... \tag{17}$$

M is the molecular weight of the polymer and c is the polymer mass concentration (weight of polymer per unit volume of solution). In equation 17, A_2 and A_3 are the second and third virial coefficients, and are related to binary and ternary interactions in solution. In dilute solutions of linear polymers, the binary contacts predominate and the value of A_3 is negligible. The second virial coefficient is a measure of the deviation of the solution away from ideal behaviour and the value of the interaction parameter determines this deviation. An ideal polymer solution is obtained when the value of the interaction parameter is 0.5 (A_2 = 0) and the solvent can be described as a θ-solvent for the polymer. Under θ-conditions, the binary polymer-solvent contacts are as thermodynamically favourable as the solvent-solvent contacts and polymer-polymer contacts. In a good solvent, a decrease in χ_1 ($A_2 > 0$) leads to polymer-solvent interactions being thermodynamically more favourable and perturbed polymer dimensions being obtained. Poor solvents have an increase in χ_1 ($A_2 < 0$)

that leads to polymer-polymer contacts being more thermodynamically favourable and the polymers tend to collapse with eventual precipitation.

A disadvantage of the Flory-Huggins lattice theory is that it does not allow for the discontinuous nature of polymer solutions and this led to the development of Flory-Krigbaum theory. This theory considers the solution to consist of clusters of polymers separated by the solvent. In these spherical clusters the polymers are assumed to be Gaussian chains, but the chain segments still occupy a volume where all other chain segments are excluded by long-range interactions. Enthalpy (κ_1) and entropy (ψ_1) of dilution parameters describe these long range interactions in terms of excess partial molar quantities:

$$\Delta H_1 = RT\kappa_1\phi_2^2 \tag{18}$$

and;

$$\Delta S_1 = R\psi_1\phi_2^2 \tag{19}$$

The excess Gibbs free energy of dilution (ΔG_1) is then:

$$\left(\mu_1 - \mu_1^0\right) = \Delta G_1 = RT\left(\kappa_1 - \psi_1\right)\phi_2^2 \tag{20}$$

The comparison of equation 20 to equations 13 and 15 leads to:

$$\left(\frac{1}{2} - \chi_1\right) = \left(\kappa_1 - \psi_1\right) \tag{21}$$

The solution has an ideal thermodynamic state when the value of the interaction parameter of 0.5 is obtained (as seen in equation 16). This leads to κ_1 and ψ_1 to have equal values and the θ-temperature ($\Delta H_1 = T\Delta S_1$) of the solvent can be derived:

$$\theta = T\frac{\kappa_1}{\psi_1} \tag{22}$$

Equation 22 demonstrates the temperature at which ideal thermodynamic state is obtained in a θ-solvent, where excluded volumes interactions disappear ($A_2 = 0$) and the polymer behaves as an ideal Gaussian chain (unperturbed dimensions). Above the θ-temperature the solvent is thermodynamically good ($A_2 > 0$) and the polymer is a non-ideal chain (perturbed dimensions). Below the θ-temperature the solvent is thermodynamically poor ($A_2 < 1$) which leads to a coil to collapsed globule transition. In good solvents the second virial coefficient is positive and is an indicator of how thermodynamically favourable that solvent is for that polymer.[2, 8, 9] Under good thermodynamic conditions, the binary interactions between the polymer are repulsive and the chains cannot freely interpenetrate each other. At the θ-temperature, the opposite occurs and the chains can freely interpenetrate each other. A measure of the interpenetration of polymer chains can be described by the dimensionless interpenetration function (Ψ):

$$\Psi = \frac{A_2 M^2}{4\pi^{3/2} N_A \left\langle R_G^2 \right\rangle^{3/2}} \tag{23}$$

In two-parameter theory, the interpenetration function varies with the excluded volume variable, but reaches an asymptotic value (Ψ^*) in good solvents. This suggests that in good solvents, the polymer chains are behaving as hard spheres and the thermodynamic radius (R_T) of this sphere can be calculated from:

$$R_T = \left(\frac{3}{16\pi N_A} A_2 M^2 \right)^{\frac{1}{3}} \tag{24}$$

The second virial coefficient decreases with increasing molecular weight in a good solvent. This decrease of A_2 is due to the increase in chain length that causes more binary contacts between the polymer units, making the solvent mediated force and the binary excluded volume strength to be lower. The second virial coefficient is found to scale with molecular weight by:

$$A_2 \sim M^{-\delta} \tag{25}$$

If the reduction of molecular weight is small (less than two decades), the exponent δ is usually found in the range of 0.2 to 0.3 for linear polymers At the θ-temperature, the second virial coefficient and the excluded volume strength is zero, so that Ψ is also zero and the polymers can interpenetrate each other easily. In a θ-solvent, the temperature dependence of A_2 is a non-linear decreasing function. The θ-temperature for a polymer solution decreases with increasing molecular weight up to a high molecular weight limit, from where it remains constant.

1.2.3 Molecular Weight Distributions

One of the distinguishing features of polymer science is that the molecular weight of the synthetic macromolecules are not all equal and a range of species exist.[11, 13] This leads to the concept of the polymers having a distribution of molecular weights (Figure 4), with a associated molecular weight average. The number-average molecular weight, $\bar{M}_n$, lies near the peak of the molecular weight distribution and is defined as;

$$\bar{M}_n = \frac{\sum_i N_i M_i}{\sum_i N_i} \tag{26}$$

N_i is the number of molecules of species i having a molecular weight of M_i. A higher molecular weight average is the weight-average molecular weight, $\bar{M}_W$:

$$\bar{M}_W = \frac{\sum_i N_i M_i^2}{\sum_i N_i M_i} \tag{27}$$

Statistically $\bar{M}_n$ is the first moment and $\bar{M}_W$ is the ratio of the second to the first moment of the molecular weight distribution. A higher molecular weight average is the z-average, $\bar{M}_z$, defined as:

$$\bar{M}_z = \frac{\sum_i N_i M_i^3}{\sum_i N_i M_i^2} \tag{28}$$

The width of the molecular weight distribution can be gauged by the polydispersity index, which is the ratio of $\bar{M}_W$ to $\bar{M}_n$. The polydispersity index and the width of the molecular weight distribution is largely affected by the method of polymerisation used. Condensation polymerisations can yield polydispersity indexes of 2 (polydisperse systems), where living anionic polymerisations can yield very narrow molecular weight distributions (monodisperse systems) of polydispersity indexes less than 1.1.

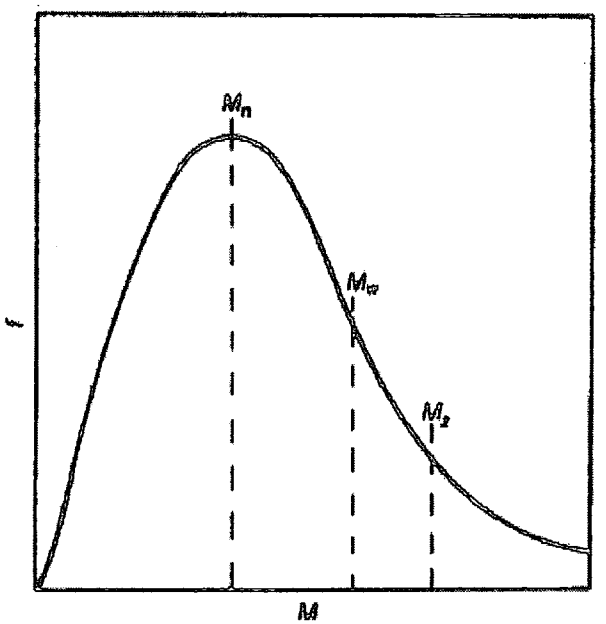

Figure 4: Molecular weight distributions for a polymer showing the $\bar{M}_n$ $\bar{M}_W$ and $\bar{M}_z$, where f is the fraction of polymer with molecular weight M.

1.2.4 Concentrated Solutions and Polymer Melts

Polymer chains in dilute solutions are isolated and only interact with each other during brief times of encounter. The freedom of movement of polymer chains causes density fluctuations of the polymer in this dilute solution to occur. Increasing the concentration of the polymer solution yields a critical concentration value, where the polymer chains start to overlap.[8, 14, 15] This critical concentration is known as the overlap concentration, c^*, determined by;

$$c^* = \frac{M}{(4\pi/3)N_A R_G^3} \tag{29}$$

Above this critical concentration the solution is in the semi-dilute regime with overlapping of the polymer chains. In a semi-dilute solution, density fluctuations no longer take place independently and are correlated. This can be seen in Figure 5, where in the dilute solution the polymer chains are isolated and once the critical concentration is reached they overlap. Equation 29 also demonstrates that the concentration for the onset of overlap decreases with increasing molecular weight. In the semi-dilute solution, the overlapping chains can be segregated into a series of blobs of a correlation length of ξ (Figure 6). Within each blob the polymer still has single chain behaviour.

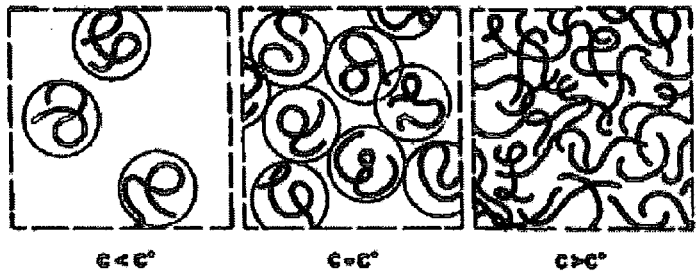

Figure 5: The onset of the semi-dilute regime in polymer solutions above the overlap concentration of c^*.

An increase of the polymer concentration in the semi-dilute solution causes the size of the blobs to decrease, and this is a screening effect because there is a decrease in intrachain interactions caused by chain overlapping. As the concentration is increased further, the highly concentrated regime is reached, where density fluctuations are sufficiently screened and become effective only over distances comparable to the size of a few chain segments. If the concentration of the solution is increased indefinitely, the limiting state of the polymer melt is reached, which is a liquid state composing only of polymer. The concentration of monomer in a polymer melt is constant with the excluded volume interactions being screened out as the monomers experience the same repulsive force throughout. Therefore the polymer in the melt state adopts ideal chain configurations, with a Gaussian distribution of intramolecular distances.

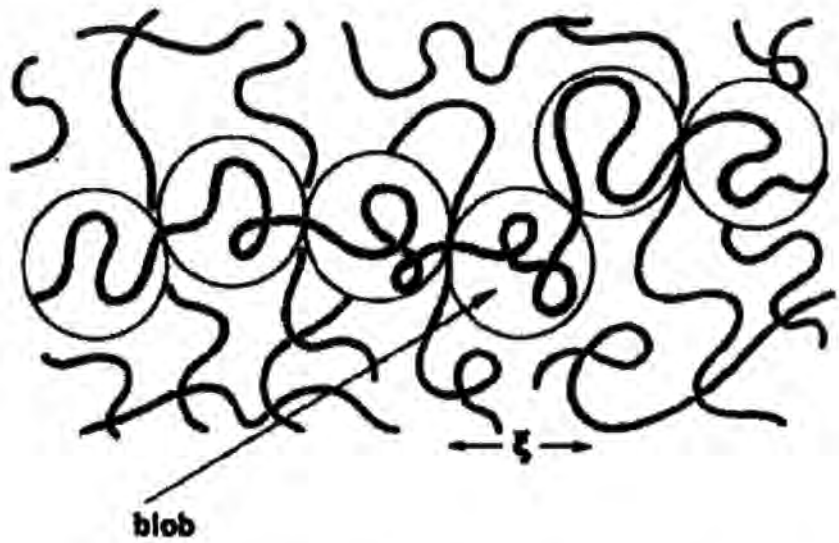

Figure 6: A blob with a correlation length ξ in a semi-dilute solution.

The thermodynamics of mixing of two polymers in the melt state to form a blend depends on obtaining a negative free energy of mixing. Flory-Huggins theory was used to give the first expression for the free-energy of mixing of two polymers, which was dependent on the thermodynamic interaction parameter of χ. Random phase approximation (RPA) theory was used by de Gennes[14] to relate the scattering functions of single phase polymer blends to the interaction parameter. Phase diagrams can be constructed from the temperature dependence of the interaction parameters, including the spinodal and bimodal curves on the phase separation. Inside the binodal curve the two separated phases are in metastable thermodynamic equilibrium with each, but inside the further spinodal curve the two phases are thermodynamically unstable. The bimodal and spinodal curve meet at the critical point where phase separation occurs. The interaction parameters for polymer blends are often linear functions of reciprocal temperature:

$$\chi(T) = A + \frac{B}{T} \tag{30}$$

T is temperature and A and B are constants. If $B > 0$, and the interaction parameter is a linear increasing function of reciprocal temperature, an upper critical solution temperature (UCST) behaviour occurs, and this leads to phase separation as the temperature is decreased. If $B < 0$, the interaction parameter is a linear decreasing function of temperature and lower critical solution temperature dependence occurs (LCST), with phase separation at higher temperatures.

1.2.5 The Dynamics of Polymer Solutions

1.2.5.1 Diffusion Coefficients

The dynamics of polymer molecules in solution depends on the force applied to the macromolecule and the friction experienced due to the presence of the solvent.[3, 8-10] The hydrodynamic property of a polymer in solution, such as the translational diffusion coefficient can be useful in the study of configuration of polymer molecules. The basic approach for the dynamics of polymer solutions is described by Rouse and Rouse-Zimm theories, but the equilibrium averages that involve the forces acting on each of the polymer units can be described by Kirkwood-Riseman theory. The polymer chain is considered as a spring-bead model, with beads experiencing frictional forces with the solvent. In a dilute solution, the velocity (v) of a polymer molecule with a force (F) applied to the centre of its mass, is related to the translational friction coefficient (f) by:

$$F = fv \tag{31}$$

The force applied to the polymer chain is obtained from the sum of the frictional forces (F_i) exerted on the different beads along the chain:

$$F_i = \zeta\left(v_i - v_i^s\right) = \zeta\left(v_i - v_{i,0}^s\right) - \zeta\sum_{i=j}^{N} T_{ij} \tag{32}$$

ζ is the friction coefficient of a bead, v_i is the bead velocity and v_i^s is the solvent velocity. The solvent velocity differs from the bulk solvent velocity ($v_{i,o}^s$) due to the presence of all the beads constituting the polymer chain, and this termed by hydrodynamic interactions represented by the tensor, $\boldsymbol{T_{ij}}$. The hydrodynamic interactions describes the perturbation of a velocity field around the beads due to the presence of the flow fields of the other beads. The hydrodynamic interactions fluctuate with the variation of chain conformation and to overcome this orientational and conformational change, a pre-averaging of the tensor is required ($<\boldsymbol{T_{ij}}>$). The coupling of the hydrodynamic interactions can become so strong that the solvent within the coil region are forced to move together with the chain segments, so that the coil can be essentially be considered as impermeable, and this is known as the non-

draining limit. Therefore the polymers in a solvent can actually be treated as a equivalent-sphere with a hydrodynamic radius (R_H), that can be related to the translational friction coefficient for a sphere by the Navier-Stokes equation:

$$f = 6\pi\eta_S R_H \tag{33}$$

The translational diffusion of polymer chains through a solution is due to a concentration gradient and is represented by Fick's equation which includes the translational diffusion coefficient (D_T). The diffusion coefficient is related to the translational frictional coefficient by the Einstein equation:

$$D_T = \frac{kT}{f} \tag{34}$$

The translational diffusion coefficient is concentration dependent and can be extrapolated to infinite dilution:

$$D_T = D_0(1 + k_D c) \tag{35}$$

D_0 is the translational diffusion coefficient at infinite dilution, c is concentration and k_D is the concentration dependence of the diffusion coefficient. The hydrodynamic radius can be calculated from the Stokes-Einstein equation for an isolated polymer chain in a solvent of viscosity of η_0, by the combination of equations 33 and 34, and by using D_0:

$$R_H = \frac{kT}{6\pi\eta_0 D_0} \tag{36}$$

D_0 decreases with increasing molecular weight of the linear chain, in both good and θ-solvents:

$$D_0 = KM^{-\mu} \tag{37}$$

K and μ are both constants. In a θ-solvent, the exponent μ is 0.5, in good solvent conditions the exponent is in the range 0.5 to 0.6. D_0 is smaller in a good solvent than in a θ-solvent

due to the increase in coil dimensions, and can be represented by the friction expansion factor:

$$\alpha_f = \frac{f}{f_\theta} = \frac{D_{0,\theta}}{D_0} = \frac{R_H}{R_{H,\theta}} \tag{38}$$

The friction expansion factor is a function of the excluded volume variable at small values of z and at the non-draining limit. The concentration dependence coefficient (k_D) of D_0 has thermodynamic and hydrodynamic dependencies:

$$k_D = 2A_2M - k_0\left(\frac{4\pi N_A R_H^3}{3M}\right) - \bar{\nu} \tag{39}$$

The friction constant of the polymer in solution is k_0 and $\bar{\nu}$ is the partial specific volume of the polymer. Pyun and Fixman[16] have calculated k_0 for linear polymers to be 2.23 in θ-solvents and increases up to the hard sphere limit of 7.16 in good solvents.

1.2.5.2 Intrinsic Viscosity

If an external stress is exerted on a fluid, deformation sets in until the stress is removed.[2, 8-10, 17] A steady state can be reached in which the rate of deformation is constant because the deformation process is retarded by internal frictional forces, and results in a velocity gradient within a solution. The higher the internal friction in the fluid, the higher is the stress that must be applied to maintain the velocity gradient. In this case the shear stress is related to the shear rate by the viscosity coefficient (η). The friction of the polymer chain in solution is also described by pre-averaged Kirkwood-Riseman theory. The increase in viscosity for polymer solutions is due to the greater work required to overcome the frictional forces. If the viscosity of a dilute polymer solution and pure solvent are represented by η and η_0 respectively, then the solution viscosity can be expanded in terms of solute concentration (c):

$$\eta = \eta_0\left(1 + a_1c + a_2c^2 + \ldots\right) \tag{40}$$

The coefficient a_1 represents the relative increase in viscosity per solute molecule. This coefficient is called the intrinsic viscosity, $[\eta]$:

$$a_1 \equiv [\eta] = \lim_{c \to 0} \frac{\eta - \eta_0}{\eta_0 c} \tag{41}$$

The intrinsic viscosity is a characteristic function for the single molecule in solution and depends on the molecular weight, structure, configuration, solvent and temperature. It has the dimensions of volume per unit mass and is often termed as the "effective hydrodynamic specific volume" of the polymer in solution. Einstein demonstrated that the excess viscosity of a polymer solution can be directly interpreted using a suspension of spheres, and this excess only depended on the volume fraction of the spheres and not on their relative sizes. This can be envisaged for polymer solutions as impermeable hard spheres in the non-draining limit, with their size determined from the viscometric radius (R_V):

$$R_V = \left(\frac{3}{10\pi N_A} [\eta] M \right)^{\frac{1}{3}} \tag{42}$$

The intrinsic viscosity of a dilute polymer solution increases with molecular weight due to greater frictional forces, and is represented by the Mark-Houwink-Sakurada equation:

$$[\eta] = KM^{a} \tag{43}$$

K and a are parameters for the polymer-solvent system being considered. For flexible linear chains, the exponent a in good solvents is in the range 0.5 to 0.8 and is 0.5 in θ-solvents. Polymers that have exponents greater than 0.8 are semi-flexible. For a polydisperse macromolecule the intrinsic viscosity is related to the viscosity-average molecular weight ($\overline{M}_V$) by the equation:

$$[\eta] = K \frac{\sum N_i M_i^{1+a}}{\sum N_i M_i} = K \overline{M}_V^{a} \tag{44}$$

N_i is the number of molecules of molecular weight M_i. For polymers where $0.5 \leq a \leq 0.8$, $\bar{M}_V$ is closer to $\bar{M}_W$ than $\bar{M}_n$. An expansion factor α_η^3 can also be determined for the intrinsic viscosities in good solvents compared to unperturbed dimensions obtained in θ-conditions:

$$\alpha_\eta^3 = \frac{[\eta]}{[\eta]_\theta} \tag{45}$$

The expansion factor α_η^3 is also a function of the excluded volume variable at small values of z, and at the non-draining limit.

1.3 Properties of Star Polymers in Solution and in the Melt

Studying the global properties of the star polymer in dilute solutions has the benefit of characterising these model species in isolation. Increasing the arm functionalities of the stars caused higher segment densities at the core, and this has been observed to have a remarkable affect on the measured global properties. Changing the solvent condition used also has an effect on the behaviour of these polymers. The global properties of R_G and $[\eta]$ of the stars tended to increase and D_0 decrease with increasing solvent quality. In both good and θ-solvents, R_G and $[\eta]$ both increased with molecular weight for regular star polymers in the same manner as linear polymers. D_0 and A_2 both decreased with molecular weight for the regular stars in good and θ-solvent conditions, also in the same manner as linear polymers. This behaviour has been observed for polybutadiene[18-22], polyisoprene[23-25] and polystyrene[26-28] stars in both solvent conditions.

Parallel molecular weight dependencies have been seen for regular star polymers with varying number of arms. At constant molecular weight, a shift with star functionalities can be seen for R_G, A_2 $[\eta]$ and D_0 from values obtained for linear polymers in both solvent conditions. A decrease in R_G, A_2 and $[\eta]$ and an increase of D_0 with increasing arm functionality from linear polymer values has been noticed.[18-28] These shifts became less pronounced for higher functional stars (f>20), as the insertion of extra arms had no real overall effect on the measured global property. The effect of star functionality can be quantified by calculating branching ratios that compare the star global properties to those of linear polymers of identical molecular weight. Branching ratios g, h and g' have been formulated for R_G, R_H and $[\eta]$ respectively.[1-4] The branching ratio g is defined as:

$$g = \frac{R^2_{G,bra}}{R^2_{G,Lin}} \tag{46}$$

The subscripts *bra* and *lin* correspond to star-branched and linear polymer respectively. The branching ratio g decreases with increasing star functionality from a value of unity for a linear polymer and this has been observed by experimental and theoretical results.[1-4, 18-31] A

theoretical value of g was calculated by Zimm and Stockmayer[29] for a star with monodisperse arms (f), with a Gaussian distribution of intramolecular distances:

$$g = \frac{3f - 2}{f^2} \tag{47}$$

Similar predictions to this Gaussian star have been observed by renormalization group theory[30] and Monte-Carlo simulations.[31] Renormalization group theory predicted similar values to the Gaussian star predictions up to a star functionality of 12. The g-factors obtained experimentally for regular star polymers in good solvents were determined to be similar to the Gaussian predictions of Zimm and Stockmayer.[18-28] This was proposed to be due to the cancellation of the excluded volume effects in the numerator and denominator in equation 46. A different behaviour was observed for regular stars measured under θ-conditions. Regular stars were found to have ideal Gaussian star behaviour up to arm functionality of 6, but above this functionality deviations from ideal behaviour occurred due to the high segment density near the star core. The segment overcrowding caused stretching of the star dimensions, and hence an increase in the branching ratio of g_θ above Gaussian and measured good solvent condition data. This has been observed for polystyrene and polyethylene stars dissolved in a θ-solvent by SANS.[32, 33] The swelling of the dimensions of the polyethylene stars was suggested to be breakdown of two-parameter theory, due to ternary interactions between the arms. The branching ratio h for the hydrodynamic radius is defined as:

$$h = \frac{R_{H,bra}}{R_{H,lin}} \tag{48}$$

The h-ratio also been observed to decrease from the value of unity for a linear polymer with increasing star functionalities, and this has been measured for polybutadiene, polyisoprene and polystyrene stars in both good and θ-solvent conditions.[18-28] Gaussian star predictions of h-ratios were formulated by Stockmayer and Fixman[34] for monodisperse regular arm stars. The branching ratio g' is determined from the intrinsic viscosities of star and linear polymers by:

$$g' = \frac{[\eta]_{bra}}{[\eta]_{lin}} \tag{49}$$

This ratio has similar behaviour to g and h with star functionality in both good and θ-solvents. Zimm and Kilb[35] have calculated Gaussian star predictions of g' for regular star polymers. The g'- and h-ratios were both found to decrease with decreasing solvent quality and this was assumed to be due to the effect of high segment density at the core. These hydrodynamic branching ratios have been found to be sensitive to the extent of solvent draining in the macromolecules. In good and θ-solvents, the h-ratio values were observed to be higher than the Gaussian star predictions of Stockmayer and Fixman, where the g'-ratios were lower than the ideal predictions of Zimm and Kilb. Pre-averaged Kirkwood-Riseman[36] theory gave values of g' for various functional stars similar to the Gaussian data of Zimm and Kilb, but values for h were lower the Gaussian predictions of Stockmayer and Fixman.

The equivalent sphere radii of R_H, R_V and R_T have been calculated for star polymers from D_0, $[\eta]$ and A_2 respectively.[1, 2, 19, 24] R_H and R_V were found to be larger in good solvents than under θ-conditions (assuming the non-draining limit), demonstrating the increase in global dimensions of the stars in a thermodynamically more favourable solvent. The thermodynamic radius disappears at the θ-state. The comparison of the equivalent sphere radii to the directly measurable radius of gyration can be achieved by calculating size ratios. Size ratios of R_H/R_G, R_V/R_G and R_T/R_G have been determined for polybutadiene and polyisoprene star polymers.[19, 24] In good and θ-solvent conditions, the size ratios increased with star functionality from values obtained for linear polymers, up to the hard sphere limit of 1.29.[9] The increase of size ratios with star functionality demonstrated the effect that higher segment densities at the core had on the equivalent sphere radii, and this suggested an increase in the thermodynamic and hydrodynamic interactions experienced by the star polymers in solution. Size ratios for highly branched stars increased above unity showing that the equivalent sphere radii were even greater than the average dimensions of the star.

Regular star polymers have been determined to have lower second virial coefficients than linear polymers of the same molecular weight in good solvent conditions.[1-4, 18-28, 30, 37] The decrease in A_2 for the stars showed that the deviation away from ideal behaviour was reduced, and the solution approached a thermodynamically poorer state due to the presence of the branch point. This decrease in the thermodynamic quality of the solvent was due to

higher segment density at the star core. High segment density would increase the likelihood of ternary contacts and cause the breakdown of the binary cluster approximation. A reduction of second virial coefficient has been noticed with increasing functionality for regular polyisoprene, polybutadiene and polystyrene stars, in good solvent conditions.[18-28]

Interpenetration functions for star polymers in good solvents have been used to characterise polymer branching.[2, 3] In good solvents, an asymptotic value of approximately 0.26 was obtained for high molecular weight linear polymers and this has been observed for linear polybutadienes and polystyrenes, and been predicted by Monte-Carlo simulations and renormalization group theory.[30, 37] An increase in Ψ^* with arm functionality from values for linear polymers has been observed for polybutadiene, polyisoprene and polystyrene stars.[30] Monte-Carlo simulations and renormalization group theory have also predicted an increase of Ψ^* up to values similar to the hard-sphere limit of 1.60. Higher values of this function suggested that increased segment density existing at the star core reduced the likelihood of the interpenetration of two stars in a good solvent, and the stars were effectively behaving as hard spheres.

In thermodynamically poorer solvents, a depression of the θ-temperature has been noticed for regular star polymers from values obtained for linear polymers of the same molecular weight.[38, 39] Ganazzolli and Allegra[40] have predicted the θ-temperature depression for short arm star polymers to increase with arm functionality, with an theoretical free-energy approach using the bead and spring chain model. Increasing the length of the star arms raised the θ-temperature back to asymptotic values obtained for linear polymers. A θ-temperature depression has also been observed experimentally for polyisoprene and polystyrene stars and by Monte-Carlo simulations.[41] Dondos *et al*[42] have predicted an increase for the θ-temperature over linear values for a highly branched star with long arms by the use of a thermal blob theory, and by treating the star core as one overall large blob.

The star polymers may be considered to be isolated species, in dilute solution but different individual regions exist within the star due to the variation of segment density. A quantitative estimation of segment density of regular star polymers was made by Daoud and Cotton[5] for highly functional stars with long arms. In this model, the arms were stretched to minimise repulsive interactions between segments on different arms and was applied to

dilute and semi-dilute solutions. They considered the star consisting of three regions at a radial distance (r) from the star centre, which included an inner melt-like extended core region ($r < r_2$), a intermediate region resembling a concentrated solution ($r_2 < r < r_1$) and a outer semi-dilute region ($r_1 < r < R$) (Figure 7). At the core melt-like region, the number density of the monomers was high and there was an absence of any excluded volume effects. The radius of this region (r_2) is given by the scaling relation:

$$r_2 \sim f^{1/2} a \tag{50}$$

The arm functionality of the star is f and a is the statistical step length of the monomer. From the core region, each of the star arms was divided up into a series of blobs, where inside each blob the arm behaved as an isolated chain. The size of the blobs increased with radial distance, reflecting the decrease in segment density. At a distance greater than r_2, but less than r_1, the density of the polymers was still high and the concentrated solution conditions prevailed. In this region the blobs were unswollen and the portion of the star arm inside these blobs behaved as an ideal chains. The number density ($\rho(r)$) of the monomer varies with radial distance in this region by:

$$\rho(r) \sim \left(\frac{r}{a}\right)^{-1} f^{1/2} \tag{51}$$

The concentrated region persists to a radial distance of r_1:

$$r_1 \sim a f^{1/2} \left(\frac{V}{a^3}\right)^{-1} \tag{52}$$

The excluded volume parameter is V, determined by the polymer-solvent interaction parameter (χ):

$$V = a^3 \left(\frac{1}{2} - \chi\right) \tag{53}$$

At distances greater than r_1 was the semi-dilute region, where the blobs became swollen. The size of the blobs increased with radial distance, reflecting the decrease in segment density. Each blob had a screening length of $\xi(r)$, where the portion of the arm behaved as an ideal chain. In this region the monomer density is:

$$\rho(r) \sim f^{(3\nu-1)/2\nu}\left(\frac{r}{a}\right)^{(1-3\nu)/\nu}\left(\frac{V}{a^3}\right)^{(1-2\nu)/\nu} \tag{54}$$

The term ν is the Flory molecular weight scaling exponent for R_G, as seen in equation 8. For long arm stars, the centre to end distance of the arm (star radius) of R is:

$$R \sim aN^{\nu} f^{(1-\nu)/2}\left(\frac{V}{a^3}\right)^{2\nu-1} \tag{55}$$

In a good solvent the intermediate region disappears, whereas at the θ-temperature the outer swollen region disappears. The different length scales that constitute a Daoud and Cotton star can be investigated by SANS.[43] Scaling dependencies of the scattering cross section with wavevector Q of the star polymers in solution have been investigated, and over the mid-range of Q the length scales of the outer most blobs were obtained. Over this Q-range, the presence of excluded volume or θ-conditions could be determined from scaling dependencies of $Q^{-5/3}$ or Q^{-2}.

Boothroyd and Ball[44] treated the star centre to be an impenetrable core to which all the arms were attached. This model was devised for a star without excluded volume interactions, and was applied to ideal solvent conditions and the melt state. A displaced random walk model was used, calculating the R_G difference between a star with stretched arms to that of a unperturbed star. The star model was proposed to consist of an impenetrable core, with star arms grafted on to the surface of the spherical core (Figure 8). The arms were allowed to take any configuration, apart from re-entry in to the core.

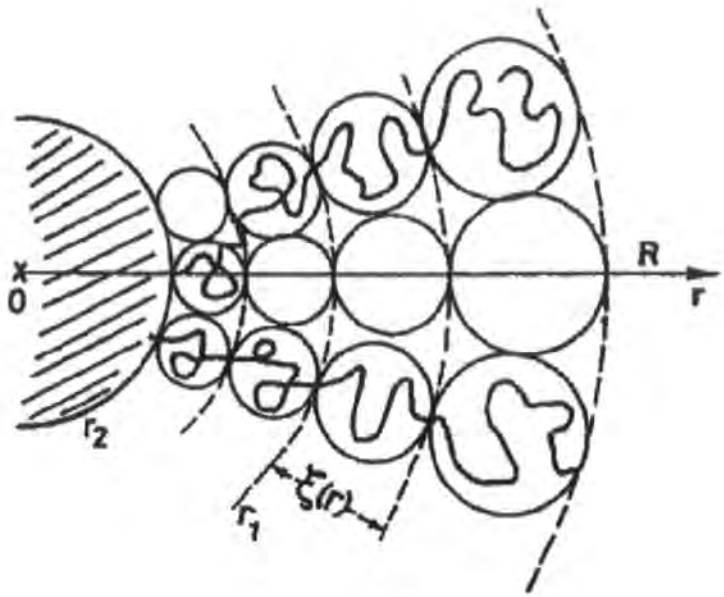

Figure 7: The Daoud and Cotton model demonstrating the melt-like core ($r < r_2$) region, the concentrated solution region ($r_2 < r < r_1$) and the semi-dilute region ($r_1 < r < R$).

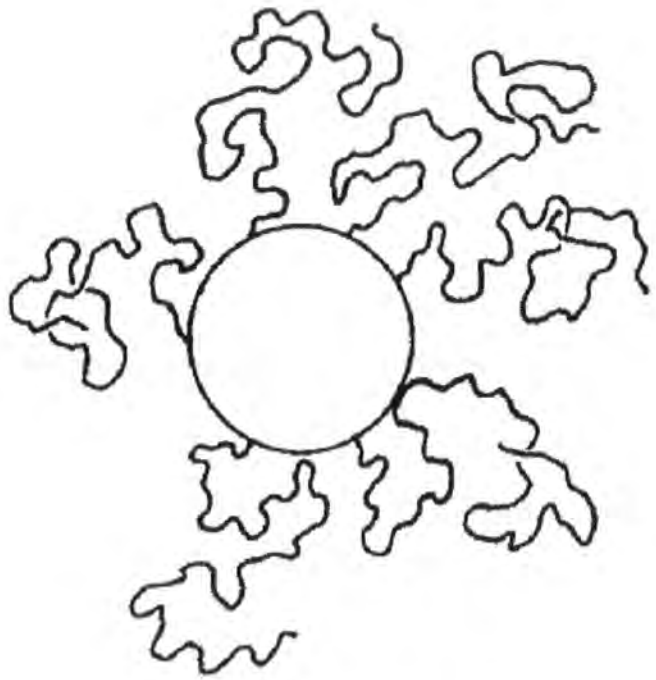

Figure 8: The Boothroyd and Ball impenetrable core model for a star polymer.

Stars can dissolve to form polymer solutions of fairly high concentrations. The high segment densities near the cores cause the overlap concentration for the onset of the semi-dilute regime to be higher than those of linear polymer of the same molecular weight.[1-3] Full interpretation in the semi-dilute region that was assumed for flexible linear polymers cannot be accomplished for star polymers, due to the presence of the branch point. In good solvents, liquid like ordering has been observed at the overlap concentration by regular polystyrene and polyisoprene stars by SANS measurements.[45, 46] The stars behaved as hard spheres up to the overlap concentration in the semi-dilute region and with increasing concentration the hard sphere behaviour diminished with further coil overlap. At the overlap concentration, linear polymers had correlation lengths equal to the end to end distance of the polymer, where for regular star polymers the correlation lengths were equal to the end to end distances for the star arms.

Star polymers continue to have stretched arm dimensions over Gaussian predictions in the melt state. Polyethylene stars with arm functionalities ranging from 3 to18 have been found by SANS to be swollen in the melt with respect to a simple Gaussian dimensions.[47] This has also been seen by SANS for model 3-, 4-, 8- and 12-arm polybutadiene stars, where all the arms were the same molecular weight and one of the arms was deuterated.[7] The stretching of the labelled arm increased with star functionality, and enhanced stretching was noticed between 8- and 12-arms. Intra- and intermolecular interaction parameters of the polymers in the melt state were also obtained using random phase approximation theory. The intramolecular interaction parameter was between the deuterated and hydrogenous arms from the same star, where the intermolecular interaction parameter was between the deuterated arms and other stars in the melt. Stretching of the star arms was believed not to be due to steric crowding at the core, but the failure to screen the excluded volume interactions between the core and corona regions of the star.

Grayce and Schweizer[6] used a liquid state model using PRISM theory to explain this arm stretching, with differential screening of the excluded volume interactions. The excluded volume interactions were assumed to be between the core and corona regions of the same star and between corona regions of different stars. Stretching of the arms was postulated to be due to the arms being pulled out by the excluded volume interactions experienced by the corona regions and not being pushed out by steric crowding at the core. The interaction

parameters obtained by deuterium labelled polybutadiene stars were reflections of this differential screening of the excluded volume interactions between the core and corona regions.[7] Core expansion has been observed for 6-arm polystyrene star block copolymers dissolved in a good solvent by SANS.[48] Two stars were investigated where the inner or outer portions of the star arms were deuterated. The chains were found to be extended near the core, where at the end of the arms they behaved as flexible random coils.

Increasing the length of the star arms reduces the effect of the star core has on the dimensions of the star. A few examples of molecular weight asymmetric stars have been synthesised and characterised. Fetters *et al*[49] produced molecular weight asymmetric polystyrene stars and studied them in dilute solution in good and θ-solvents. Two sets of examples were produced, where one set had the molecular weight of the asymmetric arm double that of the other two arms (LAS), and the second set had the molecular weight of the asymmetric arm half that of the other two (SAS). The branching ratio g' was determined for both sets of stars in the two solvent conditions. In a good solvent, both LAS and SAS had g' a little higher than g' determined for regular 3-arm polystyrene stars. Under θ-solvent conditions, g' for SAS was found to be lower than obtained for LAS, where the latter had a value similar to a regular 3-arm star. Molecular weight asymmetric stars have been synthesised by the divinylbenzene (DVB) route by Mays *et al.*[50] The stars had an equal number of short and long arms, but difficulties of obtaining an average arm functionality were experienced. Characterisation by size exclusion chromatography suggested a complex mixture of isolated and aggregated stars due to the presence of unreactive sites in the divinylbenzene microgel core.

1.4 Motivation

Star polymers have different properties to linear species in solution and in the melt state. These branched polymers have increased segment densities near the star core that can effect their global properties. Stretching of arm dimensions occurs to reduce the overcrowding at the star centre. Increasing the star functionality causes higher segment densities at the core and stretching of the arms becomes enhanced further. Increasing the length of the arms reduces the effect that the star core has on global size and the relative increase in global expansion decreases. In dilute solution, the thermodynamic quality of the solvent has an effect on the global properties of the star polymer. In good solvents, the star polymers experience good polymer-solvent interactions and subsequent swelling to non-ideal dimensions. In θ-solvents, stretched configurations also occur at higher functionalities due to this segment overcrowding at the core. Stretched star dimensions have also been observed for labelled star polymers in the melt state.

The objective of the work reported in this thesis was to investigate the effect of arm length on the configurational properties of star polymers. A series of molecular weight asymmetric stars have been produced by living anionic polymerisation methods. The stars had an arm functionality of 8 to promote high segment densities and stretched configurations in θ-solutions and the pure melt state. The miktoarm stars consisted of seven polybutadiene arms and an eighth polydeuterobutadiene arm that varied in molecular weight. The series of asymmetric stars started with a regular star, up to high molecular weight asymmetric arms, and this star could be envisaged to be like a "branch functionalised linear polymer".

Static and dynamic light scattering and viscometry experiments in dilute solution have been performed on the stars in good and θ-solvents. Cyclohexane and 1,4-dioxane were used as the good and θ-solvents respectively. A temperature range was applied to the dioxane experiments to ascertain the close to θ-point behaviour of these model polymers. Similar experiments were performed on linear polybutadienes as well, with a range of molecular weights. From the global properties obtained, interpenetration functions, equivalent sphere radii, and branching and size ratios have been determined.

SANS experiments were also performed on these materials in the solution and the melt state. The same solvent conditions were used as before and a range of polymer concentrations were investigated. The radii of gyration of the labelled arms are subject to the stretching effect, and this was investigated in the melt and solution. Interaction parameters of the stars in these environments have also been determined. In the melt state, the temperature dependence of the radii of gyration, and the inter- and intramolecular interaction parameters have been obtained.

1.5 References

[1] Grest, G. S.; Fetters, L. J.; Huang, J. S. *Adv. Chem. Phys.* **1996**, Volume XCIV, 67.

[2] Burchard, W *Adv. Polym. Sci.* **1999**, 143, 113.

[3] Freire, J. J. *Adv. Polym. Sci.* **1999**, 143, 34.

[4] Hajichristidis, N: Iatrou, H.; Pispas, S.; Pitsikalis, M.; Vlahos, C.; *Adv. Polym. Sci.* **1999**, 142, 71.

[5] Daoud, M.; Cotton, P. *J. Physique* **1982**, 43, 531.

[6] Grayce, C. J.; Schweizer, K. S. *Macromolecules* **1995**, 28, 7461.

[7] Hutchings, L.R.; Richards, R.W.; *Macromolecules* **1999**, 32, 880.

[8] Fujita, H. *Studies in Polymer Science 9: Polymer Solutions*, Elsevier; Amsterdam, 1990.

[9] Yamakawa, H. *Modern theory of Polymer Solutions*; Harper and Row: New York, 1971.

[10] Strobl, G. *The Physics of Polymers*, Springer: Berlin, 1996.

[11] Cowie, J. M. G. *Polymers: Chemistry and Physics of Modern Materials*, Blackie Academic and Professional: London, 2nd Ed., 1991.

[12] Billmeyer, F. W. *Textbook of Polymer Science*, John Wiley and Sons: New York, 3rd Ed. 1984.

[13] Sperling, L. H. *Introduction to Physical Polymer Science*, John Wiley and Sons: New York, 2nd Ed. 1992.

[14] De Gennes, P. G. *Scaling Concepts in Polymer Physics*, Cornell University Press; Ithaca, 1979.

[15] Doi, M. *Introduction to Polymer Physics*, Clarendon Press: Oxford, 1996.

[16] Pyun, C. W.; Fixman, M.; *J. Chem. Phys.* **1964**, 41, 937.

[17] Bohdanecky, M.; Kovar, J. *Polymer Science Library 2: Viscosity of polymer Solutions*, Ed. Jenkins, A. D.: Elsevier, Amsterdam, 1982.

[18] Toporowski, P. M.; Roovers J. *J. Polym. Sci.: Part A* **1986**, 24, 3009.

[19] Martin, J.E.; Roovers, J. *J. Polym. Sci: Part B* **1989**, 27, 2513.

[20] Zhou, L. L.; Hadjichristidis, N.; Toporowski, P. M.; Roovers, J. *Rubber Chem. Technol.* **1992**, 65, 303.

[21] Roovers, J; Zhou, L. L.; Toporowski, P. M.; van der Zwan, M.; Iatrou, H.; Hadjichristidis, N. *Macromolecules* **1993**, 26, 4324.

[22] Roovers, J.; Toporowski, P. M.; Martin, J. *Macromolecules* **1989**, 22, 1897.

[23] Hajichristidis, N.; Roovers, J. *J. Polym. Sci., Poly. Phys. Ed.* **1974**, 12, 2521.

[24] Bauer, B. J.; Fetters, L. J.; Graessley, W. W.; Hadjichristidis, N.; Quack, G. *Macromolecules* **1989**, 22, 2337.

[25] Adam, M.; Fetters, L. J.; Graessley, W. W.; Witten, T. A. *Macromolecules* **1991**, 24, 2434.

[26] Berry, G. C. *J. Polym. Sci.: Part A-2* **1971**, 9, 687.

[27] Roovers, J; Hadjichristidis, N.; Fetters, L. J. *Macromolecules* **1983**, 16, 214.

[28] Okumoto, M.; Nakamura, Y.; Norisuye, T.; Teramoto, A. *Macromolecules* **1998**, 31, 1615.

[29] Zimm, B. H.; Stockmayer, W. H. *J. Chem Phys* **1949**, 17, 1301.

[30] Douglas, J. F.; Roovers, J.; Freed, K. F. *Macromolecules* **1990**, 23, 4168.

[31] Barrett, A. J.; Tremain, D. L. *Macromolecules* **1987**, 20, 1687.

[32] Huber, K.; Burchard, W.; Bantle, S.; Fetters, L. J. *Polymer* **1987**, 28, 1990.

[33] Boothroyd, A. T.; Squires, G. L.; Fetters, L. J.; Rennie, A. R.; Horton, J. C.; de Vallera, A. M. B. G. *Macromolecules* **1989**, 22, 3130.

[34] Stockmayer, W.; Fixman, M. *Ann. N.Y. Acad. Sci.* **1953**, 57, 334.

[35] Zimm, B. H.; Kilb, R. W. *J. Polym Sci.* **1959**, 37, 19.

[36] Prats, R.; Pla, J.; Freire, J. J. *Macromolecules* **1983**, 16, 1701.

[37] Douglas, J. F.; Freed, K. L.; *Macromolecules* **1984**, 17, 2344.

[38] Bauer, B. J.; Hajichristidis, N.; Fetters, L. J.; Roovers, J. E. L. *J. Am. Chem. Soc* **1980**, 102, 2410.

[39] Striolo, A.; Prausnitz, J. M.; Bertucco, A. *Macromolecules* **2000**, 33, 9583.

[40] Ganazzoli, F.; Allegra, G. *Macromolecules* **1990**, 23, 262.

[41] Bruns, W.; Carl, W. *Macromolecules* **1991**, 24, 209.

[42] Dondos, A.; Papanagopoulos, D. *Polymer* **1997**, 38, 6255.

[43] Hutchings, L. R.; Richards, R. W.; Reynolds, S. W.; Thompson, R. L. unpublished.

[44] Boothroyd, A. T.; Ball, R. C. *Macromolecules* **1990**, 23, 1729.

[45] Bantle, S.; Burchard, W.; Fetters, L. J.; Huber, K. *Macromolecules* **1986**, 19, 1401.

[46] Farago, B.; Fetters, L. J.; Huang, J. S.; Jucknischke, O.; Richter, D.; Willner. L *Europhys. Lett.* **1992**, 19, 297.

[47] Boothroyd, A. T.; Fetters, L. J.; Glinka, C. J.; Horton, J. C.; Squires, G. L.; Rennie, A. R.; Robinson, R. A. *Macromolecules* **1989**, 22, 681.

[48] Lantman, C. W.; MacKnight, W. J.; Rennie, A. R.; Tassin, J. F.; Monnerie, L.; Fetters, L. J. *Macromolecules* **1990**, 23, 836.

[49] Fetters, L. J.; Khasat, N.; Hajichristidis, N.; Pennisi, R. W. *Macromolecules* **1988**, 21, 1100.

[50] Frater, D.J.; Mays, J. W.; Jackson, C. J. *J. Polym. Sci., Part B* **1997**, 35, 141.

Chapter 2

Synthesis of Polybutadiene Miktoarm Stars

2.1 Introduction

This chapter outlines the synthesis of miktoarm star polymers and is divided into three sections. The first section (2.2) reviews the synthesis of star polymers within the literature. The synthetic procedures for regular and asymmetric star polymers are discussed, describing the use of different coupling agents to link polymer arms to form stars with various functionalities. The literature review for asymmetric stars is divided into the three topics of stars with molecular weight, chemical and topological asymmetry. A method chosen from the literature is highlighted for the synthesis of the stars for this research. The second section (2.3) discusses the synthesis performed as part of this project, and covers the synthesis of butadiene-d_6 by the reductive dechlorination of hexachlorobutadiene, the anionic polymerisation of butadiene monomers, hydrosilylation reactions to form chlorosilane coupling agents and the synthesis of polybutadiene miktoarm stars. The final experimental section (2.4) outlines the synthetic procedures, apparatus and materials used.

2.2 Synthesis of Star Polymers

2.2.1 Synthesis of Regular Stars

Scientists have been producing star polymers over the last fifty years as they represent the simplest form of polymer branching. The first attempt at the synthesis of a star polymer was that of Schaefgen and Flory[1] in 1948. They polymerised ε-caprolactam in the presence of either cyclohexanonetetrapropionic acid or dicyclohexanoneoctacarboxylic acid to obtain tetra- and octachain star shaped polyamides. Morton *et al*[2] in 1962, first used anionic polymerised living polystyrene chains that were terminated by tetrachlorosilane to synthesise 3- or 4-arm stars. In 1963, Orofino and Wenger[3] used tri(chloromethyl)benzene as a linking agent to yield 3 arm polystyrene stars. Mayer[4] used 1,2,4,5-tetra(chloromethyl)benzene to prepare 4-arm star di- and tri-block copolymers of styrene and isoprene, but it was found that it was difficult to extend the star functionality further than 6 with chloromethylbenzene derivatives.[5]

Polystyrene stars with 6- to 15-arms have been prepared by Decker and Rempp who used divinylbenzene (DVB) as the coupling agent.[6] The disadvantage of the DVB technique is that the number of arms of the star can not be accurately predicted and this subsequently led to the use of chlorosilanes as the linking agents of choice. In 1965, Zelinski *et al*[7] produced low molecular weight 3- and 4-arm polybutadiene stars by coupling linear poly(butadienyl)lithium chains formed by anionic polymerisation with stoichiometric amounts of trichlorosilane and tetrachlorosilane respectively. In the early seventies, Roovers and Bywater[8,9] produced 4- and 6-arm polystyrene stars using 1,2-bis(dichloromethylsilyl)- and 1,2-bis(trichloromethylsilyl)ethane respectively. Hadjichristidis *et al*[10,11,12] produced polyisoprene stars with 4-, 6-, 8-, 12- and 18-arms. The linking agents for the 8- and 12-arm stars were tetra(methyldichlorosilylethane)silane and tetra(trichlorosilylethane)silane respectively and were synthesised via the hydrosilylation reaction of tetravinylsilane with either dichloromethysilane or trichlorosilane, with the aid of chloroplatinic acid. An octadecachlorosilane was prepared for the 18-arm polyisoprene star.[12] In 1983, polystyrene star polymers of 12- and 18-arms were prepared by Roovers *et al.*[13] This subsequently led to high molecular weight 18-arm styrene and isoprene block

copolymers being developed.[14] Toporowski *et al*[15] synthesised 18-arm polybutadiene stars with an octadecachlorosilane core, with the star arms having a range of molecular weight.

By the early nineties, methods for the synthesis of polybutadiene stars with 32-, 64- and 128-arms had been developed.[16,17] Multifunctional linking agents were prepared for these stars by the hydrosilylation reaction of tetravinylsilane with methyldichlorosilane in the presence of Pt catalyst and the nucleophilic replacement of silicon chloride by vinylmagnesium bromide.[18] This lead to the 1st generation core with 8-terminal vinyl groups, which on further hydrosilylation with dichlormethylsilane led to the hexadecachlorosilane. The hydrosilylation reaction of the 2nd, 3rd and 4th generation dendrimers with dichloromethysilane produced the chlorosilane cores for the 32-, 64- and 128-arm stars respectively. Polybutadiene stars of up to 270 arms have been synthesised using a novel coupling centre.[19] The star core was produced by the hydrosilylation of poly(1,2-butadiene) with methyldichlorosilane. The linking agent of an 18 arm poly(1,2-butadiene) star core has led to a 200-arm poly(1,4-butadiene) star being produced.

2.2.2 Synthesis of Asymmetric Star Polymers

Asymmetry in stars can be grouped into 3 categories: molecular weight asymmetry; chemical asymmetry; and topological asymmetry. Stars with molecular weight asymmetry have chemically identical arms that differ only in molecular weight. Stars with chemical asymmetry have arms that are different in chemical nature. Chemically asymmetric stars are known as miktoarm stars (coming from the Greek word μικτός, meaning mixed). Stars that have arms of the same chemical nature and chain length, but have different end groups are also in this category. Topological asymmetric stars have block copolymer arms that are attached to the central core by a different polymeric block.

2.2.2.1 Stars with Molecular Weight Asymmetry

Three arm polystyrene (PS) stars have been synthesised with molecular weight asymmetry by Pennisi and Fetters.[20] Two types of star were developed where the asymmetric arm was either twice or half as long as the other two arms. Their synthetic procedure involved the reaction of living poly(styryl)lithium chains, prepared by anionic polymerisation, with a 10-fold excess of trichloromethylsilane (Figure 1) to form a star precursor of a poly(styryl) chain, end-capped with dichloromethylsilane. This precursor star was prepared by addition of trichloromethylsilane to a dilute solution of living polymer under vigorous stirring, with no 2-arm star precursor formed. Any unreacted silane was removed by freeze-drying the polymer solution under high vacuum and heating the resulting porous material for 72 hours at 323 K. Benzene was re-introduced into the reaction vessel to re-dissolve the polymer.

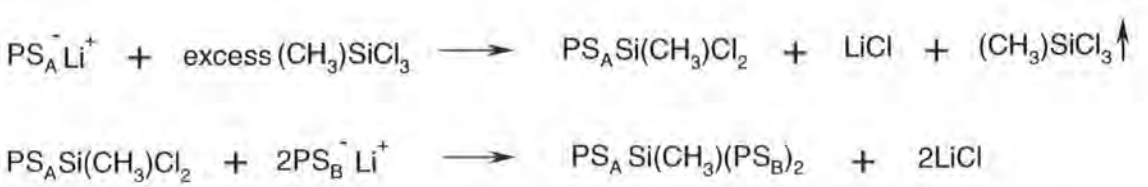

Figure 1: The formation of 3-arm polystyrene star by end capping one arm with dichloromethylsilane.

The next stage was to couple the two living poly(styryl)lithium chains that have either twice or half the molecular weight of the initial asymmetric arm. It was noted the poly(styryl)lithium did not react to full completion with dichloromethylsilane due to steric hindrance of the poly(styryl)lithium anions. Full coupling of the arms was achieved by reducing the steric hindrance by end capping the living chains with a few units of butadiene. The linking of low molecular weight ($<4 \times 10^4$ g mol^{-1}) arms to the end-capped asymmetric chain can also be achieved by the addition of small amounts (2-10 % (w/v)) of triethylamine, instead of using the butadiene approach.

Molecular weight asymmetric 3-arm polybutadiene (PB) stars were also prepared by the same procedure of Pennisi and Fetters[20]. The only alteration was that the living poly(butadienyl)lithium chains were added to an excess of trichloromethylsilane linking agent, to suppress the formation of 2-arm precursor star. Asymmetric polyisoprene (PI) stars have also been prepared.[21] The formation of the 2-arm precursor was suppressed by reacting the living poly(isoprenyl)lithium chains and methyltrichlorosilane at a temperature of 278 K.

Polystyrene stars of the type $A_nA'_n$, where A and A´ are polystyrenes of different molecular weight have been prepared by the divinylbenzene (DVB) method.[22] The living poly(styryl)lithium chains A were reacted with the DVB to form star homopolymers. The ratio of DVB to poly(styryl)lithium chains determined the functionality of the star as the DVB core contains the same number of active anions as the linked arms (assuming no accidental deactivation). These active anions then polymerise further styrene monomer to form asymmetric arms A´. This method suffered from disadvantage of broad molecular weight distributions, molecular heterogeneity (n is an average value) and absence of control of the final product. Crosslinking between stars also occurred during the process, due to the active living arms reacting with DVB cores belonging to other stars.

Asymmetric polystyrene (PS) stars possessing chains of different molecular weights were prepared by Quirk and Yoo[23], using 1,4-bis(1-phenylethenyl)benzene (PDDPE) as the linking agent. PDDPE linking agent was reacted with a poly(styryl)lithium chain in THF to produce a monoadduct product, that was formed due to the delocalisation of the negative charge within the phenyl rings and vinyl groups (Figure 2). The monoadduct was then

reacted with a second poly(styryl)lithium chain to produce the final coupled product, with stoichiometry of reactants determining the linking efficiency. Finally, styrene monomer was introduced to form the 3-arm star. A disadvantage of this reaction was that incomplete linking reactions led to unreacted monoadduct and uncoupled PS_B arms.

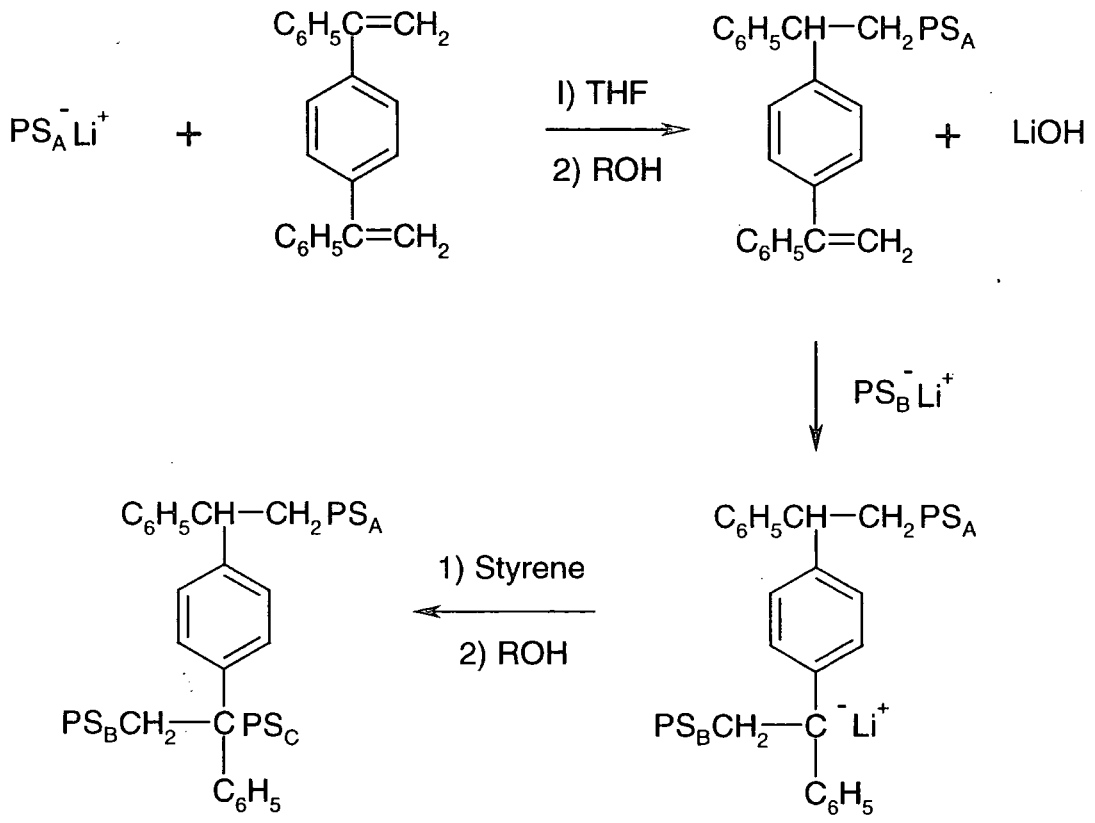

Figure 2: Synthesis of an asymmetric polystyrene star using PDDPE.

2.2.2.2 Stars with Chemical Asymmetry

A 3-arm star polymer of the type A_2B, where A is polyisoprene (PI) and B is polystyrene (PS) has been prepared by Mays *et al.*[24] Living anionic polymerisation techniques were used to prepare the poly(styryl)lithium arms and these were added to an excess of trichloromethylsilane (CH_3SiCl_3) to produce a 1-arm precursor. The addition of excess polyisoprene arms completed the star (Figure 3). The steric hindrance of the poly(styryl)lithium chains allows the formation of the 1-arm precursor. Eisenberg *et al*[25] have prepared an A_2B star where A is PS and B is poly(2-vinylpyridine) (P2VP). A different approach was used, where the PS chains were linked to dichloromethylsilane to obtain the 2-arm precursor star. In another reactor, poly(2-vinylpyridine) was reacted with allyl bromide and then the hydrosilylation reaction between the Si-H group on the 2-arm PS precursor star to the vinyl group of the end functionalised P2VP linked the final third arm.

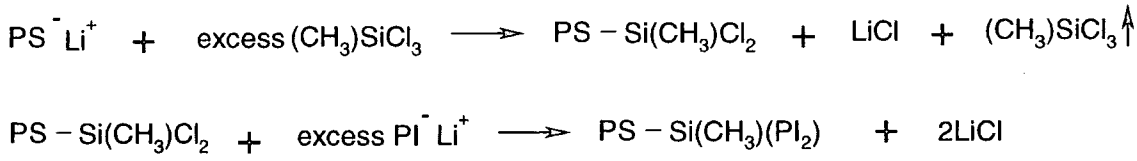

Figure 3: AB_2 star using trichloromethylsilane coupling agent.

Tetrachlorosilane ($SiCl_4$) has been used[26] as the core for 4-arm stars of type A_3B, where A is PI and B is PS. They were prepared by the same route as the trichlorosilane based 3-arm star. The first step was to end cap polystyrene with an excess of tetrachlorosilane. Any remaining tetrachlorosilane was then removed by vacuum transfer and the star completed by the addition of excess living polyisoprene chains. An ABC miktoarm star terpolymer, where A is PS, B is PI and C is PB was synthesised by Iatrou *et al.*[27] The synthetic difficulties of selecting and displacing two chlorine atoms were experienced. The PI arm was coupled first with an simple excess of trichlorosilane. The second arm of polystyrene was added by titration, as it is the most sterically hindered, and a simple excess of PB completed the star (Figure 4). A star terpolymer of PS, PI and poly(methyl methacrylate) (PMMA) has been synthesised using a trichlosilane linking agent.[28] The difficulties of linking the final polymethacrylate arm was overcome by transforming the Si-Cl group to $SiC(Ph_2)(CH_2)_2C^-(Ph_2)Li^+$ (Ph is phenyl) using diphenylethylene (DPE) and lithium, and

then polymerising the methyl methacrylate monomer *in-situ*. These methods lead to a star tetrapolymer ABCD of PS, poly(4-methylstyrene) (P4MeS), PI and PB, where two of the arms were coupled by titration.[29] The PS arm was added first to excess tetrachlorosilane and then the P4MeS and PI arms were coupled consecutively by titration. The star was completed by the addition of an excess of PB. The P4MeS arm was titrated before the PI arm as it has greater steric hindrance.

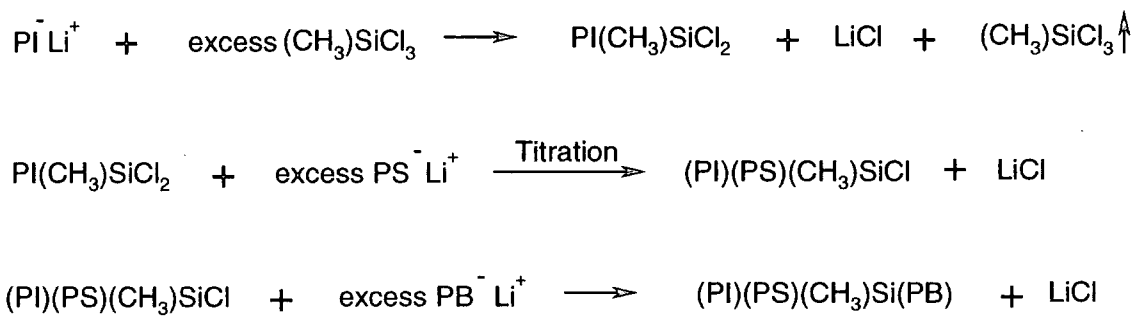

Figure 4: Synthesis of an ABC star terpolymer.

Divinylbenzene (DVB) has been used with anionic polymerisation to synthesise miktoarm stars. The technique was first exploited by Eschwey and Burchard[30], but mainly developed by Rempp and co-workers.[31, 32] The synthesis of a star of the type A_nB_n was a three step procedure with divinylbenzene (figure 5). The first step was the preparation of the living arms of polymer A by anionic polymerisation. The next stage was to react the living arms with divinylbenzene to produce a star polymer with a core (microgel nodule of DVB) that theoretically has the same number of active sites as the number of incorporated arms (Figure 5). This precursor star acts as multifunctional initiator with the addition of monomer B, to form the star polymer A_nB_n. Further addition of electrophilic compounds or other monomers can lead to end functionalised arms or star-block copolymers. The DVB method has been used to synthesise A_nB_n stars where the A-arm was polystyrene and the B-arm was either poly(*tert*-butyl methacrylate),[23] poly(*tert*-butyl acrylate),[32] poly(ethylene oxide)[33] or poly(vinylpyridine).[34] For these stars n was found to vary between 6 to 20.

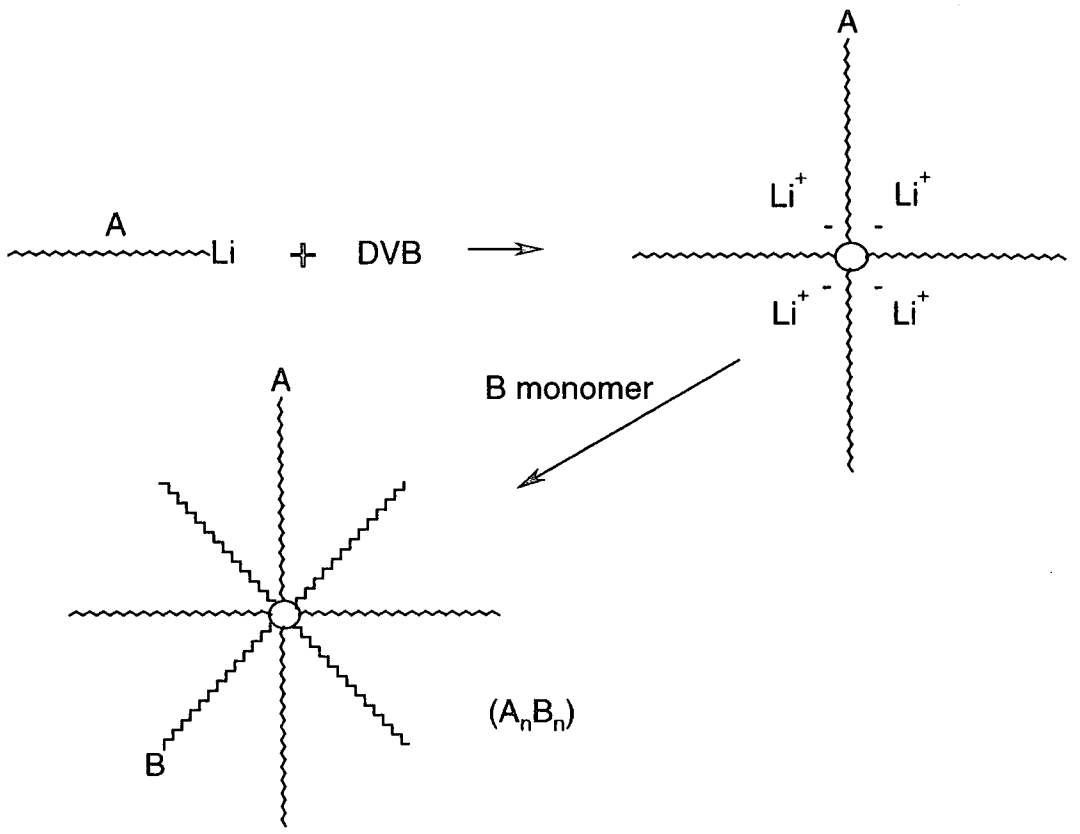

Figure 5: Preparation of A_4B_4 stars using divinylbenzene.

Disadvantages of the DVB method included that only stars with two types of arms (A_nB_n) can be prepared, an average value of n was obtained, the B-arms cannot be isolated and characterised separately, and the vinyl groups within the core can lead to the formation of loops (intramolecular coupling) or networks (intermolecular coupling). Another limitation of this synthetic procedure was that not all of the living A-arms were incorporated into the microgel core and can act as a source of initiation when monomer B was introduced. The average value of n was increased by decreasing the molecular weight of the A-arms or by increasing the molar ratio of DVB to living chains. The advantage of this method is that it can be performed under nitrogen at atmospheric pressure and therefore without the use of rigorous high vacuum techniques.

A star-shaped polymer consisting of vinyl ether arms with a microgel core of divinyl ether has been devised by Higashimura and coworkers.[35] The vinyl ether arms were prepared by cationic polymerisation with a HI/ZnI_2 initiator system. The reaction of a macrocation

$A^+ I^- ZnI_2$ with a small amount of divinyl ether can leave living sites within the core that can polymerise further vinyl ether monomer. Divinyl ethers with long rigid spacers were found to be more efficient linking agents.

Addition of living anionic chains to non-homopolymerisable divinyl compounds has been used to obtain stars of the A_2B, ABC and A_2B_2 variety.[36] Double diphenylethylenes such as *para*-double diphenylethylene (PDDPE), 1,4-bis(1-phenyl-ethenyl)benzene and *meta*-double diphenylethylene (MDDPE), 1,3-bis(1-phenyl-ethenyl)benzene have been used. PDDPE and MDDPE differ in the rates of addition of the 1st and 2nd arms and hence PDDPE was used to synthesise A_2B and ABC type stars (Figure 6) and MDDPE was used for A_2B_2 type stars (Figure 7). Excellent control over the stoichiometry between the A-arms and the DDPE was the key to the synthesis, otherwise a mixture of star and living polymer was produced. Quirk *et al*[37] have prepared PS_2PB_2 stars by using MDDPE.

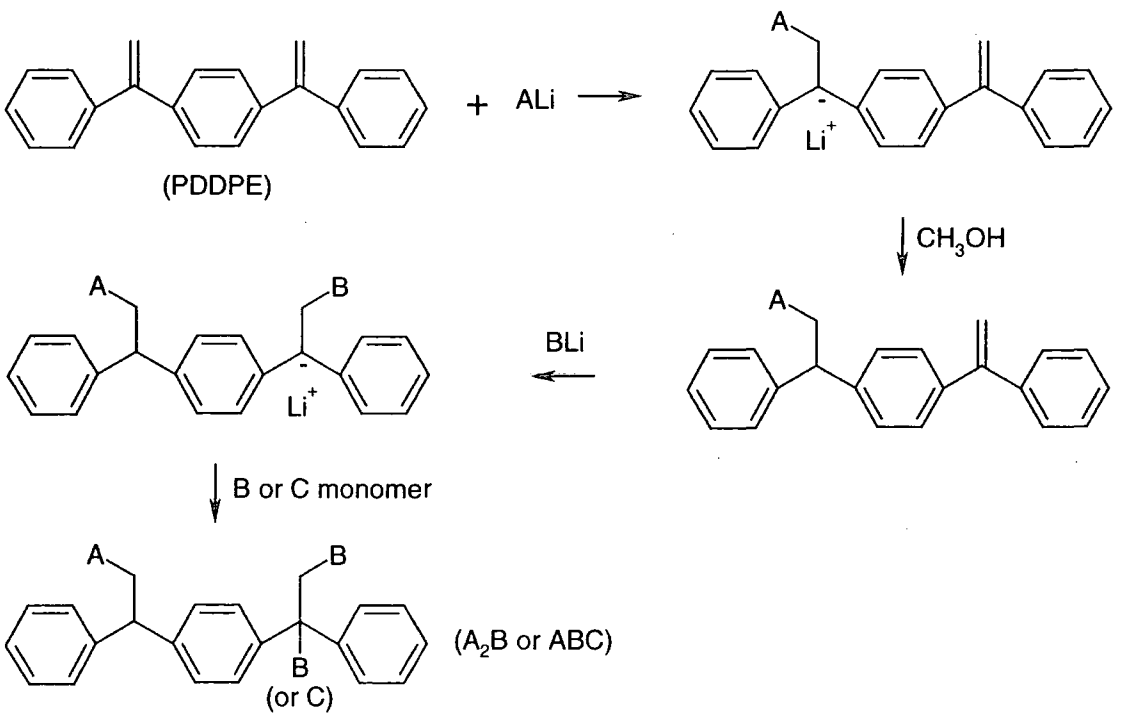

Figure 6: A_2B and ABC type stars synthesised using a PDDPE core.

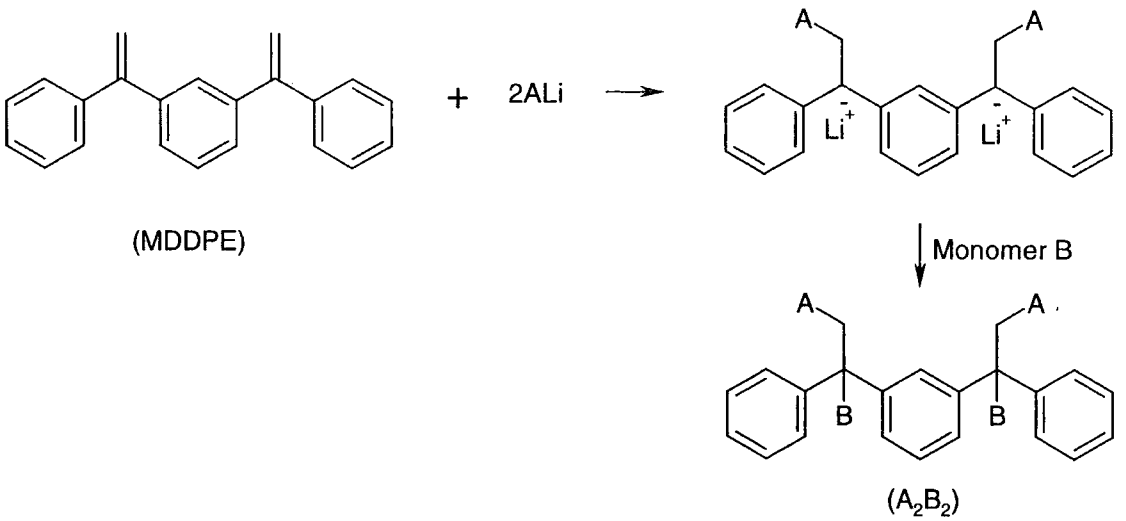

Figure 7: A_2B_2 type star synthesised using an MDDPE core.

Faust *et al*[38] have used cationic polymerisation to couple polyisobutylenes (PIB) to MDDPE, 2,2-bis(diphenylethenyl)propane (BDPEP) and 2,2-bis(ditolylethenyl)propane (BDTEP). BDPEP and BDTEP both have two diphenyl ethane moieties separated by an electro donating spacer, so that a rapid coupling reaction occurred that was independent of molecular weight of precursor polyisobutylene. The reaction with BDTEP was more rapid than BDPEP due to the presence of electron donating methyl groups. A $(PIB)_2(PMeVE)_2$ star has been prepared, where PMeVE is poly(methyl vinyl ether)[39].

An ABC terpolymer of PS, PB, PMMA has been prepared by Huckstadt *et al*[40] with the use of diphenylethylene (DPE) and 1-(4-bromomethylphenyl)-1-phenyl-ethylene (BrMDPE). Anionic polymerisation was used to prepare the living polymer chains. The poly(styryl)lithium chains were prepared and coupled first to DPE, to reduce the reactivity of the polystyryl anion and then BrMDPE by nucleophilic displacement of the bromide (Figure 8). Then a living PB chain was coupled to the terminal DPE unit and the anion formed was used to polymerise the methyl methacrylate monomer for the final third arm.

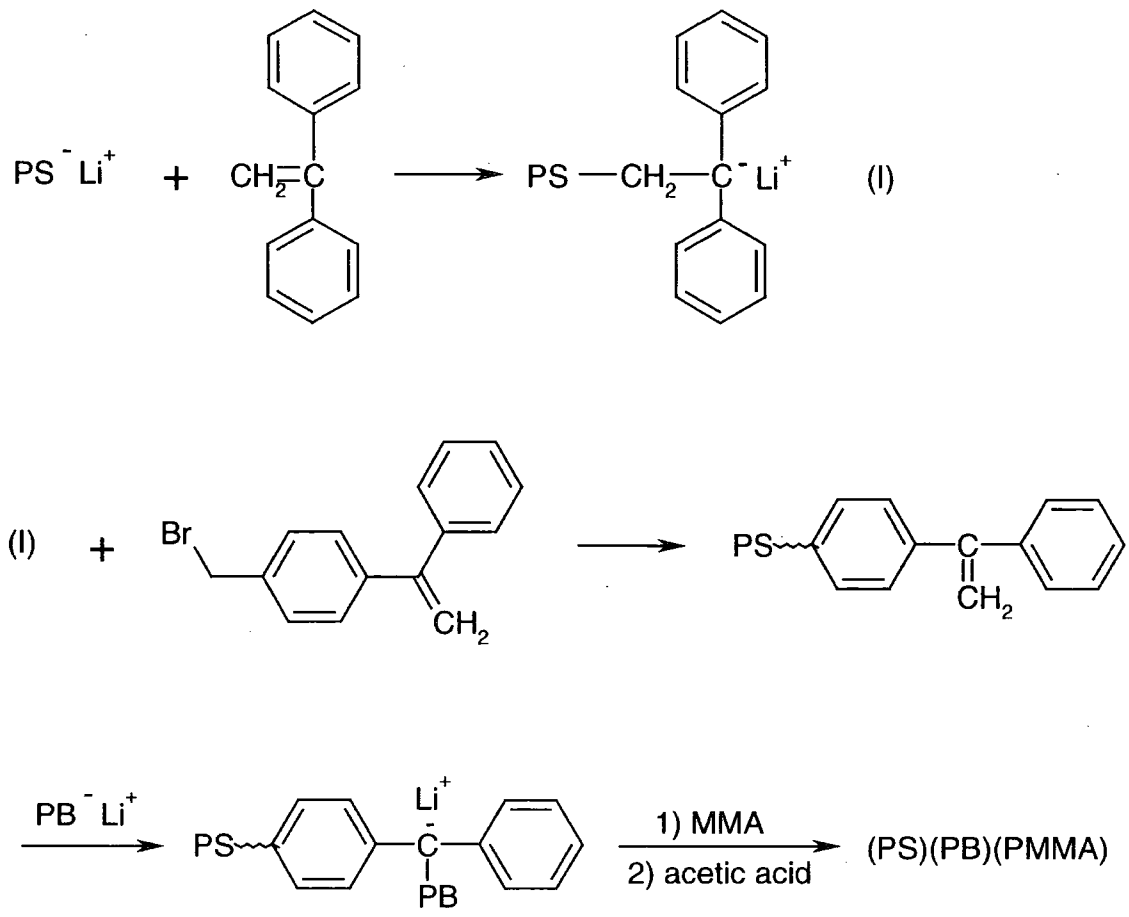

Figure 8: An ABC star by end capping with DPE.

Star polymers of the type A_2B_2 using a tetrachlorosilane core were reported by Xie and Xia.[41] They used anionic polymerisation and the chlorosilane method to synthesise a PS_2PEO_2 star, where PEO is poly(ethylene oxide). The living polystyrene chains were reacted in a molar ratio of 2:1 to form the 2-arm product and the remaining silicon- chloride bonds were used to link the PEO arms (Figure 9). This method utilised the steric hindrance of the PS chains for the formation of the star intermediate and therefore reduced the importance of stoichiometry of the reactants. A PS_2PI_2 star was synthesised by a similar method by Young *et al.*[42] Hajichristidis *et al*[43] used a different approach to form a PS_2PB_2 star where the second PS arm was coupled by titration. A PI_2PB_2 stars have been prepared by two different methods.[44] The first method was to end cap the living poly(isoprenyl)lithium chains with a couple of units of styrene and titrate with tetrachlorosilane. The second method was to react the living PI arms with $SiCl_4$ in the molar ratio of 2:1 at a temperature of 233 K. The low temperature was used to reduce the

reactivity of the living chain end to produce the desired star precursor. A PI_2PMMA_2 star has been achieved using a divinyl coupling agent.[45] Poly(isoprenyl)lithium chain were prepared by anionic polymerisation and then linked to 1,1-(1,2-ethandiyl)bis(4-(1-phenylethenyl)benzene) (EPEB), to create a dianion that polymerised the methyl methacrylate monomer for the other two arms.

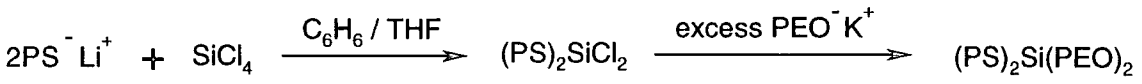

Figure 9: An A_2B_2 star using a $SiCl_4$ core.

Diblock copolymer arms have been incorporated into 3- and 4-arm stars.[43, 46] Hadjichristidis *et al*[43] prepared B(A-b-B)$_2$ and B(A-b-B)$_3$ stars, where A is PI and B is PS. The 3- and 4-miktoarm stars were prepared by the addition of an excess of either dichloromethylsilane or tetrachlorosilane to the living poly(styryl)lithium, removal of excess chlorosilane and finally with subsequent coupling of the diblock copolymer arms. A (PS-b-PB)PB_3 star was prepared by Tsiang *et al.*[47] This star was achieved by the addition of PB to $SiCl_4$ in the molar ratio of 3:1, followed by the diblock copolymer arm. The product was found to be hard to fractionate, due to the range of PB arms attached to the core.

The linking agent of 1,2-bis(trichlorosilyl)ethane[48] ($SiCl_6$) has been used to prepare an A_5B type star, where A is PI and B is PS. The PS arm was coupled to the core by titration in the molar ratio of lithium to silicon of 1:6, to prepare the formation of the monosubstituted product and the avoidance of the disubstituted product. The star was completed by the addition of the pentachlorosilane capped PS to excess PI. The disadvantage of this reaction was that the hexachlorosilane could not be removed by vacuum transfer and therefore a range of coupled products were formed, that would require fractionation. An A_8B_8 star copolymer[49] has been synthesised with a dendritic carbosilane with 16 Si-Cl groups, where A is PS and B is PI. The PS chains were added to the hexadecachlorosilane in the molar ratio of 8:1 to prepare $(PS)_8$-Si-Cl_8 precursor. Excess PI was coupled to the core to complete the star. Miktoarm polybutadiene stars of the type AB_2, AB_3, AB_7 and AB_{11} have been prepared by Hutchings *et al,*[50,51] where the A arm was deuterium labelled. An excess of the appropriate chlorosilane core was used to link the deuterated arm and after the removal of

any unreacted chlorosilane, an excess of hydrogenous arms was used to obtain the desired star. Fractionation was required to isolate the stars.

Naphthalene chemistry has been utilised[52] to prepare A_2B stars, where A is poly(ethylene oxide) PEO and B is PS, PI, poly(α-methyl styrene) or poly(*tert*-butyl styrene). The living polymer chains were reacted with bromomethyl naphthalene to form the mono-substituted star precursor (Figure 10). The prevention of formation of a coupled precursor was achieved by the use of Grignard reagents. The addition of the final monomer B, completes the star. An "umbrella" type star polymer of $PS(PB)_n$ has been prepared by Wang *et al.*[53] Anionic polymerisation in the presence of dipiperidinoethane synthesised a small block of poly(1,2-butadiene), followed by the addition of styrene monomer to yield an poly(1,2-butadiene) end capped polystyrene arm. Hydrosilylation of the 1,2-butadiene double bonds with dichlormethylsilane left active sites available for coupling of the poly(1,4-butadiene) arms to form the "umbrella" star. Limited control over the hydrosilylation reaction results in an inaccurate prediction of the number of arms. A similar method was performed by Takano and co-workers,[54] where anionic polymerisation was used to synthesise poly(2-vinylnapthalene) arm with a few end units of 4-(vinylphenyl)dimethylvinylsilane (VS). The remaining vinyl groups of the VS were the active sites for coupling poly(styryl)lithium chains. Star polymers with 13 polystyrene arms have been prepared.

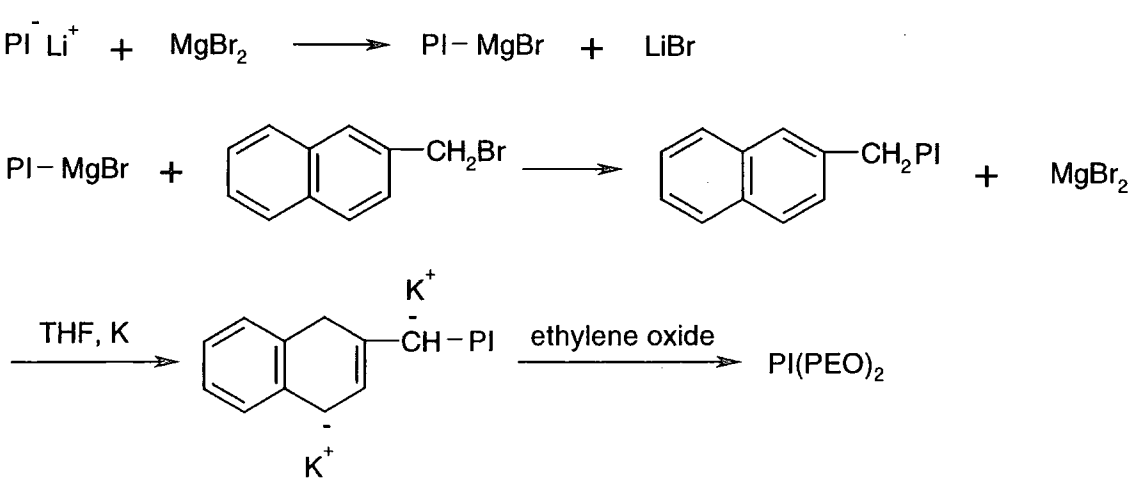

Figure 10: AB_2 stars using bromomethyl naphalene and a Grignard reagent.

Well defined ABC_2 and AB_4 type stars have been produced using anionic polymerisation, with functional group transformation.[55] The stars were synthesised by functionalising the first arm with a defined number of anion stable methoxymethylphenyl groups (MOM). The MOM groups are transformed into the reactive chloromethylphenyl groups to link the remaining arms. An ABC_2 star where A is PS, B is poly(α-methylstyrene) and C is PI was synthesised by functionalising the PS arm with two MOM groups and an iodopropyl group. The iodopropyl group was used to link the poly(α-methylstyrene) arm and the two MOM groups were transformed into reactive chloromethylphenyl groups to link the PI arms. The AB_4 star where A is PS and B is PI was formed in a similar way, but now the PS arm had four MOM groups that after transformation to the reactive chloromethylphenyl groups, allowed the linking of the PI arms.

Asymmetric ω-functionalised polybutadiene stars have been prepared by Pitisikalis *et al.*[56] The stars contain either one, two or three functionalised end groups of either dimethylamine or sulfobetamine. The dimethylamine groups were introduced using the functional 3-dimethylaminopropyllithium initiator. Reaction of the dimethylamine end group with cyclopropane sultone, yielded the sulfobetamine zwitterions. Trichlorosilane was used as the linking agent and the technique of anionic polymerisation to synthesise the arms.

2.2.2.3 Stars with Topological Asymmetry

Inverse star block copolymers have been prepared by Tselikas et al.[57] These stars have 4 diblock copolymer arms of isoprene and styrene, where two of the arms have been attached to the star core by the isoprene end and the other two are attached by the styrene end. The star asymmetry was due to the different topology of the arms. The living PI-b-PS and PS-b-PI diblocks were prepared by anionic polymerisation and sequential addition of monomer (Figure 11). The PI-b-PS diblock was added drop wise to a stoichiometric amount of tetrachlorosilane, until the formation of a small quantity of trimer was seen by SEC. An excess of living diblock PS-b-PI was then reacted to complete the star. The PI-b-PS block was coupled first, as the steric hindrance of the poly(styryl) anion allowed for easier control. A PS-b-PI diblock was end capped with a few units of butadiene to help facilitate the linking reaction.

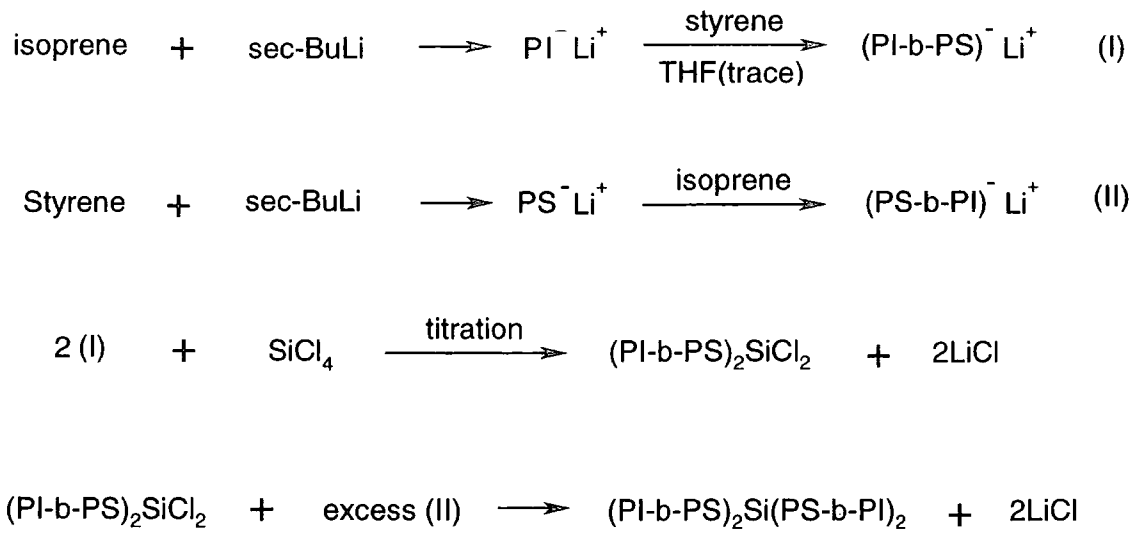

Figure 11: Reaction sequence for a reverse diblock star copolymer.

2.2.3 Summary and Aim of Synthesis

One of the aims of this research, is to synthesise a series of 8-miktoarm star polymers, where one arm has variable chain length. The stars will consist of 7 regular polybutadiene arms and a single deuterated asymmetric arm. Important characteristics of these stars such as the number of arms attached to the core and the molecular weight of each arm need to be known. A synthetic procedure must be devised that allow these characteristics to be to acquired. The use of living anionic polymerisation techniques allow good control over the molecular weight of the uncoupled arms and yield monodisperse molecular weight distributions. A coupling agent needs to be chosen for the core of the star.

The use of divinylbenzene DVB to couple the arms was too unpredictable for the determination of star functionality and has no control over molecular weight of the secondary arms emanating from the microgel core.[30-32] Stars of A_nB_n type can only be synthesised by the DVB method and were subject to inter- and intramolecular coupling. Diphenylethylenes (DPE) and double diphenylethylenes (PDDPE and MDDPE) allow a greater prediction of the number of arms attached to the core, but the molecular weight of the final arm could not be characterised separately and only low functional stars had been produced.[36, 37, 40] This was the same for using naphthalene chemistry, where only 3-arm stars have been produced and the final arms cannot be characterised separately.[52]

Umbrella type stars can lead to the inclusion of asymmetric arms and characterisation of the molecular weight of the arms, but no prediction over the star functionality. The star functionality was dependent on the number of end-capped 1,2-butadiene units and the extent of the hydrosilylation reaction with dichloromethylsilane to form the multi-functional chlorosilane.[53] Similar problems were associated with end-capping with 4-(vinylphenyl)dimethylvinylsilane.[54] Producing coupling agents with a series of methoxyphenyl groups that can be transformed into reactive chlorophenyl groups allows the formation of asymmetric stars.[55] The molecular weight of the arms were characterised and the number of arms be predicted. This technique was only used for stars for up to 5 arms and difficulties arose for synthesising cores for up to 8 arms.

An 8-functional chlorosilane, tetra(methyldichlorosilylethane)silane was the coupling agent of choice to synthesise the 8-miktoarm stars. Chlorosilanes allow a good prediction of the number of arms of each star and the molecular weight of the arms can be characterised easily. The only disadvantages of using higher functional chlorosilanes is that they cannot be removed by vacuum transfer and must be removed in solution by cannulation. The synthetic methods developed by Hutchings *et al*[50,51] were used, where an excess of chlorosilane can be used for preferential coupling of a single asymmetric arm to the core and an excess of regular arms added to complete the star. An *insitu*-fractionation will have to be performed on the star precursor solution, to isolate only the precursor species with one asymmetric arm attached to the chlorosilane, as 2- and 3- arm star precursors may form as well.

2.3 Synthesis of Linear and Asymmetric Star Polymers

2.3.1 Introduction

The synthetic procedures followed to obtain linear polybutadienes and polydeuterobutadienes with a range of molecular weights and a series of 8-miktoarm polybutadiene stars are outlined. The synthesis of the deuterobutadiene monomer by reductive dechlorination of hexabutadiene will be discussed first. This is followed by a description of the technique of anionic polymerisation of butadiene monomers and the factors involved to obtain polybutadienes with the right molecular weight and microstructure. Hydrosilylation of dichloromethylsilane with tetravinylsilane for the synthesis of octachlorosilane coupling agents is then reviewed. Finally the synthesis of a series 8-miktoarm polybutadiene stars is discussed, where the molecular weight of the deuterated asymmetric arm was varied.

2.3.2 Synthesis of Deuterobutadiene Monomer

Deuterobutadiene was synthesised by the reductive dechlorination of hexachlorobutadiene following the procedure first outlined the Craig and Fowler.[58] The reaction depends upon the displacement of chlorine by deuterium in hexachlorobutadiene and so it is important to exclude any hydrogen (especially in the form of water). The deuterated monomer was prepared by the reaction of hexachlorobutadiene with deuterium oxide in the presence zinc dust, sodium iodide and cupric chloride (Figure 12). Anhydrous dioxane was used as a diluent for the reactants. The hexachlorobutadiene was added slowly to the deuterium oxide, dioxane and zinc slurry as the reaction was highly exothermic.

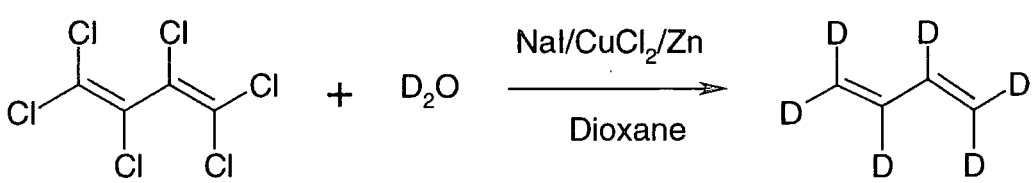

Figure 12: Synthesis of 1,3-butadiene-d_6

The gaseous product obtained contains not only the required 1,3-butadiene- d_6, but also by-products of 1-buten-3-yne-d_4 and 1,3-butadiyne-d_2. To purify the desired 1,3-butadiene-d_6, the gaseous products were heated to 373 K with sulphur dioxide (approximately 50% excess with respect to butadiene) inside a high pressure autoclave. The 1,3-butadiene reacted with SO_2 to form 1,3-butadiene-d_6 sulfone (Figure 13), with the impurities remaining unreacted. The 1,3-butadiene-d_6 sulfone was collected as light yellow to dark brown liquid/crystals, the colour depending on the quantity of impurities. The crystals were purified by recrystallisation from hot methanol and dried in a vacuum oven. The 1,3-butadiene-d_6 was regenerated by thermal decomposition of the sulfone, and the gaseous product was stored inside a gas cylinder with hydroquinone (anti-oxidant) and phenyl-2-naphthylamine (inhibitor). The decomposed sulfone gave deutero-1,3-butadiene with yields between 40 % to 80 %, depending on the purity of the crystals.

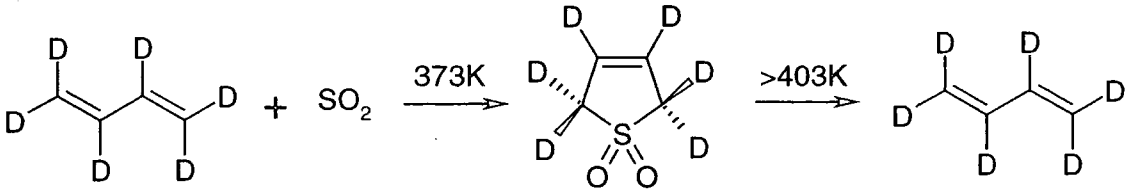

Figure 13: Synthesis of 1,3-butadiene-d_6 sulfone

The degree of deuteration was ascertained by ^{1}H-NMR. A sample of the 1,3-butadiene-d_6 sulfone was dissolved in deuterated chloroform ($CDCl_3$) with an accurately weighed small amount of benzene, as an internal reference A quantity of benzene equivalent to 1-2% of sulfone was used based on the assumption that the percentage deuteration is high. All 6 benzene protons are equivalent and gave a singlet peak at a chemical shift of 7.25 ppm. Butadiene sulfone yields two peaks at chemical shifts of 3.62 ppm and 5.97 ppm, corresponding to the 4 methylene and 2 alkene protons respectively. The percentage deuteration was determined by comparing the integration of the benzene protons to either the integration of the methylene or alkene protons. The percentage deuteration determined for a sample of 1,3-butadiene-d_6 sulfone by using the methylene and alkene protons were 98.7 % and 98.6 % respectively. The degree of deuteration may be higher than indicated as the benzene peak was overlapped by a peak resulting from chloroform ($CHCl_3$) and this will yield a higher than expected integration value.

2.3.3 *Anionic Polymerisation of 1,3-Butadiene and Deutero-1,3-Butadiene*

Anionic polymerisation was employed to synthesise polybutadiene and polydeuterobutadiene from 1,3-butadiene and deutero-1,3-butadiene monomer respectively (Figure 14). Highly reactive initiators reacted with the monomer to form propagating carbanions, which inturn react with further monomer. These addition reactions were called "living polymerisations" as they proceeded in the absence of chain termination and/or chain transfer of the propagating carbanions[59]. The anionic polymerisation of butadiene was performed using standard high vacuum techniques and all monomers and solvents were rigorously purified to prevent termination of initiator or growing chains by adventitious impurities (see experimental section 2.4). Advantages of using this technique included a high level of control over the molecular weight, a narrow molecular weight distribution and good control over the microstructure, tacticity and architecture of the polymers formed. The molecular weight was controlled by the ratio of monomer to initiator. Polymers with narrow molecular weight distributions (Poisson distribution) are obtained when the rate of initiation was competitive with the rate of propagation. Broader molecular weight distributions can be obtained by using less reactive initiators or by the sequential addition of initiator.

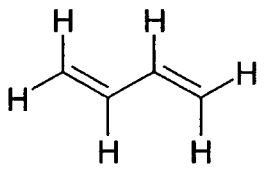

1,3-Butadiene

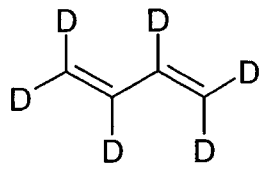

1,3-Butadiene-d_6

Figure 14: The structures of butadiene and butadiene-d_6 monomer.

Organoalkali compounds were used as initiators for these living polymerisations and these form the subsequent propagating carboanions. The initiators of choice are alkyllithium compounds as they have unique properties compared to the other organoalkali compounds (Figure 15). Simple alkyllitihiums compounds tend to be aggregated species in solid state, in solution and in the gas phase. The other organoalkali compounds also form aggregated species in the solid state, but they tend to be insoluble in hydrocarbon solvents. The solubility of alkyllithium compounds in hydrocarbon media is linked to their degree of

aggregation and this is determined by the steric hindrance of the alkyl group. The straight chain alkyllithiums, such as n-butyllithium (Figure 15) and ethyllithium are hexamers in hydrocarbon media. Alkyllithiums with branching in the α- and β-carbon, such as s-butyllithium and t-butyllithium (Figure 15) tend to associate into tetramers. Benzyllithium exists as a dimeric species.

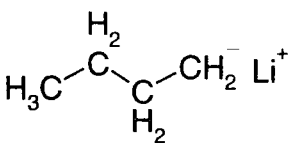

n-Butyllithium

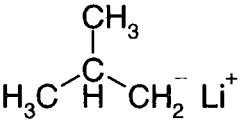

s-Butyllithium

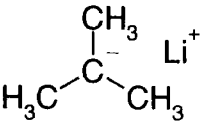

t-Butyllithium

Figure 15: Alkyllithium compounds of n-butyllithium, s-butyllithium and t-butyllithium.

Rates of initiation depend on solvent and the alkyl group attached to the lithium. Dissociated initiators in solution are more reactive initiating species. The alkyllithium aggregates are dissociated better in aromatic solvents than in aliphatic solvents. Different kinetic orders result from this variation in initiator reactivity. Fractional kinetic orders are found using aromatic solvents suggesting initiation via dissociated species, whereas inhibition in aliphatic solvents yield kinetic orders close to unity, due to aggregation. Bulky alkyl groups, such as s-butyl and t-butyl tended to be less aggregated and therefore more reactive than the straight chain alkyl groups, such as n-butyl and ethyl. One of the requirements of living polymerisation is that all active centres are introduced at the start and this is achieved with fast initiation rates. Efficient initiators such as s-butyllithium help to complete initiation within 10-15% consumption of the monomer. Some of the straight chain alkyllithiums in aliphatic solvents can be such poor initiator systems in that amounts of them still remain unreacted, after all the monomer has been consumed. This obviously has a detrimental affect on the molecular weight control over the polymers.

For vinyl monomers that are deemed anionically polymerisable, there must be substituents that stabilise the negative charge formed on the double bond. Substituents such as aromatic rings and double bonds stabilise the anionic charge by charge delocalisation. Butadiene and

deuterobutadiene form stable anions due to the conjugated double bonds. Monomers that form the least stable anions (i.e. have the largest values of pk_A for the corresponding conjugate acids) are the least reactive monomers and require more reactive initiators. For the anionic polymerisation of butadiene and deuterobutadiene, the choice of initiator was s-butyllithium (dissolved in cyclohexane in a 1.4 molar solution) for its fast initiation rates. The monomer was dissolved in an aromatic solvent (benzene) in a 10% (w/v) solution. The initiator was injected into the monomer solution by a gas tight syringe.

A carbanion is defined as the conjugate base of a carbon acid. These species are obtained from the heterolytic fission of a carbon-hydrogen bond. To comprehend the kinetics and mechanisms of living anionic polymerisations, it is important to understand the stability and reactivity of these carbanions. Allylic carbanions are formed by the nucleophilic insertion of the s-butyl carbanion into the vinyl monomer. The allylic anions are highly delocalised and presumed to be planar, sp^2 hybridised π-system. These propagating active centres in anionic polymerisation are essentially ion pairs. They can exist as either ion pair aggregates, contact ion pairs, solvent separated ion pairs or as free ions (Figure 16). Ion pairs with weak interactions to the solvent tend to form contact ion pairs. Kinetics of propagation are more complicated due to the participation of more than one type of intermediate.

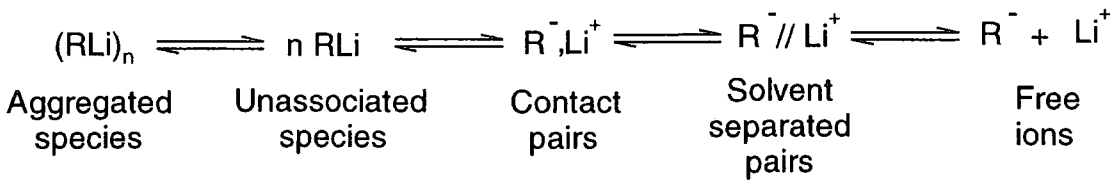

Figure 16: Reactive intermediates of allylic carbanion and counter ion

During living polymerisations, each one of the propagating active centres are as susceptible to further propagation as each other. The kinetics of propagation of dienes have rates that exhibit first order dependence on monomer concentration and fractional dependencies on chain end concentration. These fractional dependencies are due to unreactive aggregated chain ends and only dissociated chain ends propagate. Poly(butadienyl)lithium has been found to aggregate into dimeric and even tetrameric species, and propagation has a one-fourth dependence on chain-end concentration. Polymerisations rates are slow with

monomer half-lives for butadiene at 303 K with millimolar initiator concentrations of 4 hours, but this decreases by a factor of 7 at 323 K. For the synthesis of linear polybutadiene and polydeuterobutadiene here, the reaction mixtures were stirred vigorously and heated to a temperature of 313 K for 15 hours to ensure total conversion of monomer.

The stereochemistry of anionic butadiene polymerisation depends on the counter ion, the solvent, the chain-end concentration, the monomer concentration and temperature. Conjugated 1,3-butadienes can polymerise into 3 constitutional microstructures of cis-1,4-, trans-1,4- and 1,2-polybutadiene (Figure 17). The significance of high 1,4-microstructure for polybutadienes are that they exhibit low glass transition temperatures. The lithium counter ion is unique among the alkali metals for providing polybutadiene with high 1,4-microstructure. Aliphatic solvents tend to give a higher proportion of 1,4-microstructure than aromatic solvents and the highest 1,4 content can be obtained in the absence of solvent. In non-polar solvents, this high 1,4-content is caused by the preference of the lithium to bond to the terminal carbon (α) in the active chain end centre, so that the monomer would add at this position (Figure 18). In polar solvents, more delocalisation of the charge towards the allylic γ-position occurs, with the counter ion in between the α- and γ-positions.

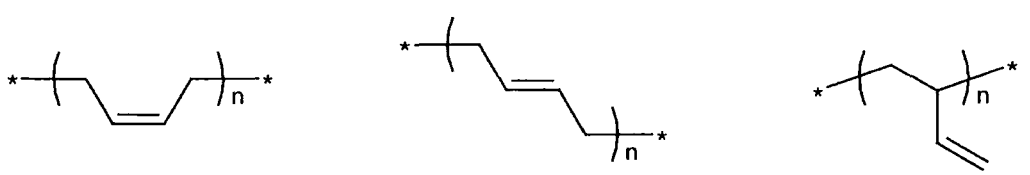

Figure 17: The 3 constitution microstructures for polybutadiene.

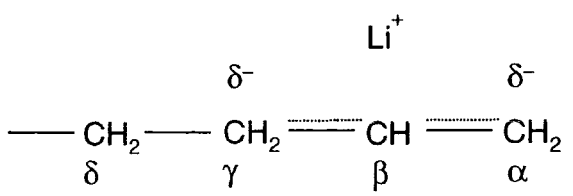

Figure 18: Charge delocalisation of propagating active centre.

The cis/trans content is dependent on the monomer-initiator ratio, where the higher this ratio the greater the cis-content.[60] In hydrocarbon solvents, the equilibrium position of the active centre for the cis/trans isomers is in the trans form. If a monomer is inserted in the cis form, this reacts to form a new cis-formed active centre. The subsequent addition of new monomer to the propagating chain will cause the previous chain addition to be fixed. If addition of the next monomer is rapid then the previous monomer remains in the cis-form, but if the new active centre is left undisturbed it will revert to the trans form. Therefore the rate of addition of new monomer and carboanion active centre isomerism determines the stereochemistry. The higher the monomer-initiator ratio, the greater the number of monomer additions in a given time and therefore the shorter the lifetime of the active centre. As the rate of monomer addition decreases, the trans content will increase. The final trans content will have a limit determined by the fraction of trans content at equilibrium and the relative addition rates of cis and trans centres. If the rate of addition of cis and trans forms are identical, then the trans content of the polymer rises to equal the equilibrium trans content, as the rate of monomer addition rate slows down. For polar solvents the reverse was found, where the active centres tends to be in the cis-form and monomer adds in the trans-form.

In ideal living polymerisations the chains undergo no chain termination or chain transfer reactions. In general, poly(butadienyl)lithium possess good stability in hydrocarbon solvents at ambient temperatures and the solutions are between colourless and light yellow. Degradation of the chains is caused by heating to high temperatures and the solutions change colour to between a dark yellow to amber. The principal mode of decomposition is the loss of lithium hydride to form a double bond at the chain end, with the resulting macromonomer undergoing further reaction with other reactive centres to form coupled products. Chain metalation of the back bone can also occur (Figure 19) with the elimination of lithium hydride. This leads to in-chain diene units that have reactive allylic hydrogens for further metalation-elimination-coupling sequences, that can promote thermal decomposition, branching or colour formation.

Figure 19: Metalation of backbone.

The butadiene polymerisations were terminated with protonating species such as degassed methanol. The methanol was degassed by passing a flow of nitrogen through it to remove any traces of carbon dioxide or oxygen that may cause the formation of carbonyl and peroxide linkages between the polymer chains. A colour change (light yellow to colourless) and a reduction of viscosity was noted as the methanol was injected, due to the disaggregation of poly(butadienyl)lithium chains in solution. The polymers were precipitated out using an excess of non-solvent (methanol) and molecular weights determined by size exclusion chromatography (see table 1). From Table 1, it can be seen that all the polymers have low polydispersities of less than 1.1.

Table 1: Molecular weights determined by size exclusion chromatography of the synthesised linear Polybutadiene and Polydeuterobutadiene samples .

Polybutadiene			
Sample	$\bar{M}_W/10^4$ (g mol^{-1})	$\bar{M}_n/10^4$ (g mol^{-1})	Polydispersity
LH50	5.08	5.02	1.01
LH100	10.1	10.0	1.01
LH300	31.4	30.3	1.04
LH400	44.1	42.7	1.03
LH800	83.2	76.9	1.08
Polydeuterobutadiene			
Sample	$\bar{M}_W/10^4$ (g mol^{-1})	$\bar{M}_n/10^4$ (g mol^{-1})	Polydispersity
LD25	2.47	2.40	1.03
LD100	12.2	12.0	1.02
LD200	21.5	21.1	1.02
LD300	28.5	28.0	1.02

$\bar{M}_w$ = *Weight average molecular weight.*

$\bar{M}_n$ = *Number average molecular weight.*

Polydispersity = $\bar{M}_w / \bar{M}_n$

The percentage of 1,4- and 1,2-microstructure in the polybutadienes was determined by ^{1}H-NMR. The vinyl protons H_A, H_B and H_C (Figure 20) all yielded a peak in the chemical shift region of 5.0 ppm to 5.4 ppm. The vinyl protons H_A and H_B had overlapping peaks at 5.4 ppm and the vinyl proton H_C had a peak at a lower frequency of 5.0 ppm. The H_A and H_C peaks represent 2 equivalent protons each and H_B only represents one proton. The percentage content of 1,4-microstructure ([1,4] %) was calculated by dividing the integration of H_A protons by the sum of the integrations of H_A and H_C protons, by using the equation:

$$[1,4]\% = \frac{I_{H_A}}{I_{H_A} + I_{H_C}} = \frac{I_{5.4} - \frac{I_{5.0}}{2}}{\left(I_{5.4} - \frac{I_{5.0}}{2}\right) + I_{5.0}} \qquad (1)$$

$I_{5.4}$ and $I_{5.0}$ are the integration values at peaks 5.4 ppm and 5.0 ppm respectively. The percentage 1,2-microstructure content was a simple subtraction of 1,4-microstructure percentage content from one. The polybutadienes in table 1 had a 1,4-microstructure content of approximately of 90 % and 1,2-microstructure content of approximately 10 %.

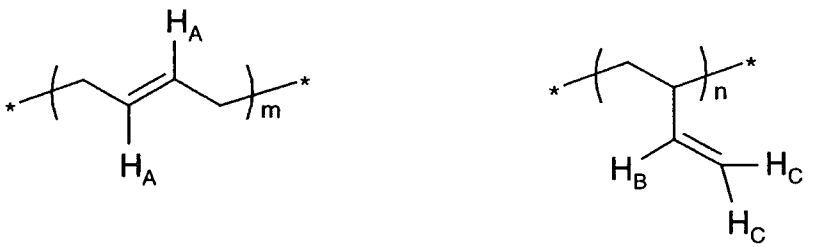

1,4-Microstructure 1,2-Microstructure

Figure 20: The vinyl protons on 1,4- and 1,2-polybutadiene.

2.3.4 *Synthesis of Octachlorosilane*

To link the arms of the star to a central core, chlorosilanes are the coupling agents of choice. An octachlorosilane, tetra(methyldichlorosilylethane)silane was used to prepare an 8-arm star and this was synthesised according to the procedure outlined of Hadjichristidis *et al.*[11] The octachlorosilane was synthesised by the hydrosilylation (Figure 21) of tetravinylsilane with dichloromethylsilane, using chloroplatinic acid as a catalyst (Speiers Catalyst). The electrophilic silicon in the dichloromethylsilane can be easily accessed by the nucleophilic tetravinylsilane. The reaction starts with an slow induction period, but rapidly becomes very exothermic. Temperature control at 313 K was essential, as any increase can lead to an explosion (boiling point of dichloromethylsilane is 314 K) and to prevent any side reactions, such as dehydrogenation and methyl silylation.

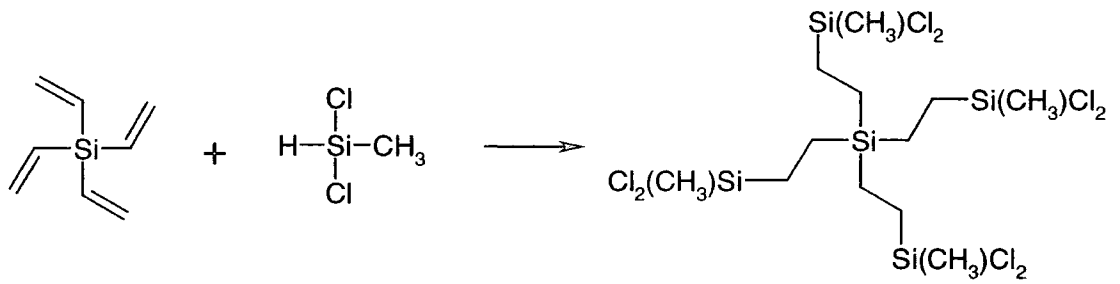

Figure 21: Hydrosilylation reaction to form Octachlorosilane.

At 313 K, the hydrosilylation reaction results in primarily anti-Makownikoff addition to give the desired product (Figure 22). Any excess dichloromethylsilane was removed by distillation and the product was isolated by vacuum distillation to yield a high boiling (471-473 K) clear viscous liquid, which on cooling became a crystalline solid. The coupling agent was dissolved in benzene to a known concentration and stored under nitrogen.

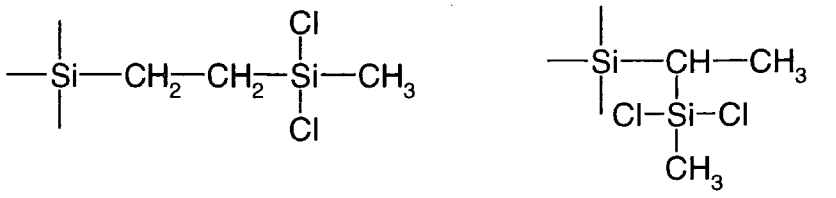

Figure 22: The anti-Markownikoff and Markownikoff additions.

2.3.5 Synthesis of Asymmetric Star Polymers

This section will outline the procedures followed for the synthesis of asymmetric polybutadiene star polymers.[50, 51] A series of 8-arm stars were prepared with a range of molecular weights for the deuterated asymmetric arm. Anionic polymerisation was used to synthesise the arms and octachlorosilanes used as the coupling agent. Rigorous purification of monomers and solvents was necessary (see experimental section 2.4). A specially adapted glass vessel attached to a high vacuum line was utilised, also supplied with dry nitrogen. The glass vessel had two reaction flasks (one tapered) for the separate synthesis of the deuterated and hydrogenous arms (Figure 23). A number of smaller side flasks were attached for the removal of samples for characterisation by size exclusion chromatography (SEC). All impurities inside the reaction vessel were removed by washing the glass with a solution of living poly(styryl)lithium in benzene.

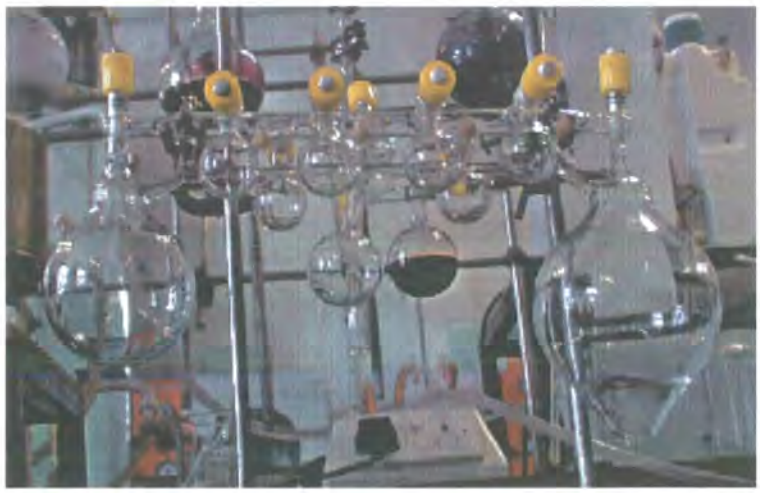

Figure 23: The multi-flask reaction vessel used for star synthesis.

The deuterated arm was synthesised by anionic polymerisation of 1,3-butadiene-d_6 in benzene, using s-butyllithium as the initiator (as outlined in section 2.3.3). A sample of the living poly(deuterobutadienyl)lithium solution was taken (terminated with nitrogen purged methanol) for molecular weight characterisation by SEC. Table 2 lists the molecular weights of the deuterated asymmetric arms. Next an excess of octachlorosilane (silicon to lithium molar ratio of 25:1) was injected into the living polymer solution and the solution was stirred for 5 hours. The nucleophilic insertion of the living carboanion into the octachlorsilane allowed the attachment of one deuterated arm (1-arm star precursor). An

excess of octachlorosilane was required to yield a high proportion of 1-arm precursor stars, but a quantity of 2-arm precursor stars and possibly 3-arm precursor stars existed as well. Fractionation of the polymer solution was performed to remove the stars with a higher number of attached arms. This *insitu*-fractionation required a polymer solution concentration of 1-2% (w/v) and so extra benzene was distilled into the tapered reaction flask. The pressure inside the flask was returned to atmospheric pressure using a flow of dry nitrogen and the solution was stirred vigorously. The flask was then immersed into a water bath to maintain good temperature control. Fractionation began with the injection of dried and distilled methanol drop wise into the flask, until a cloudy suspension appeared. Then the temperature of the water bath was raised a few degrees until the solution clarified. Once this had been achieved, the stirrer was switched off and the temperature of the bath allowed to drop to its original value. Two layers in the solution formed over time, where the lower and much smaller layer was rich in higher molecular weight material (the 2-arm precursor star). The lower layer was removed by cannulation.

Table 2: SEC Data for the Asymmetric Arms of the Star.

Star	$\bar{M}_W/10^4$ (g mol^{-1})	$\bar{M}_n/10^4$ (g mol^{-1})	Polydispersity
S300	32.7	31.1	1.05
S80	8.02	7.91	1.01
S60	6.01	5.84	1.03
S30	2.66	2.58	1.03

A sample of the fractionated upper layer was submitted for a SEC to ascertain the quantity of remaining higher-arm star material. Figure 24 and Figure 25 are SEC chromatogram of the fractionated lower layer after two and six fractionations respectively. On Figure 24, two peaks can be seen at 21.1 ml and 21.9 ml, belonging to 2-arm precursor and 1-arm precursor stars respectively. After a number of fractionations, only the peak belonging to the 1-arm precursor star could be seen, as in the chromatogram in Figure 25. This fractionation procedure was repeated until no higher molecular weight, undesirable material remained.

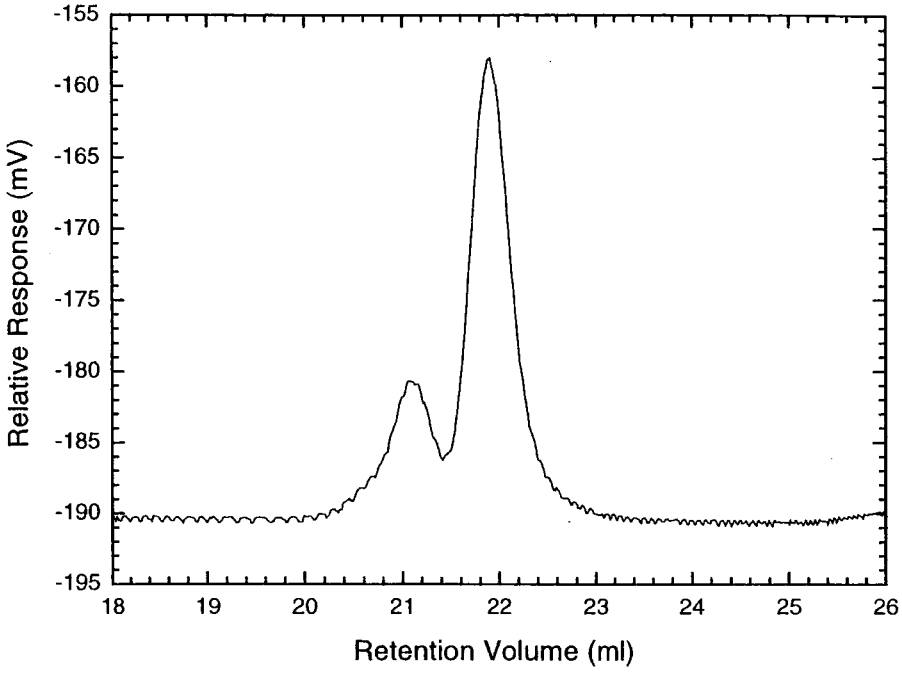

Figure 24: SEC chromatogram after two fractionations

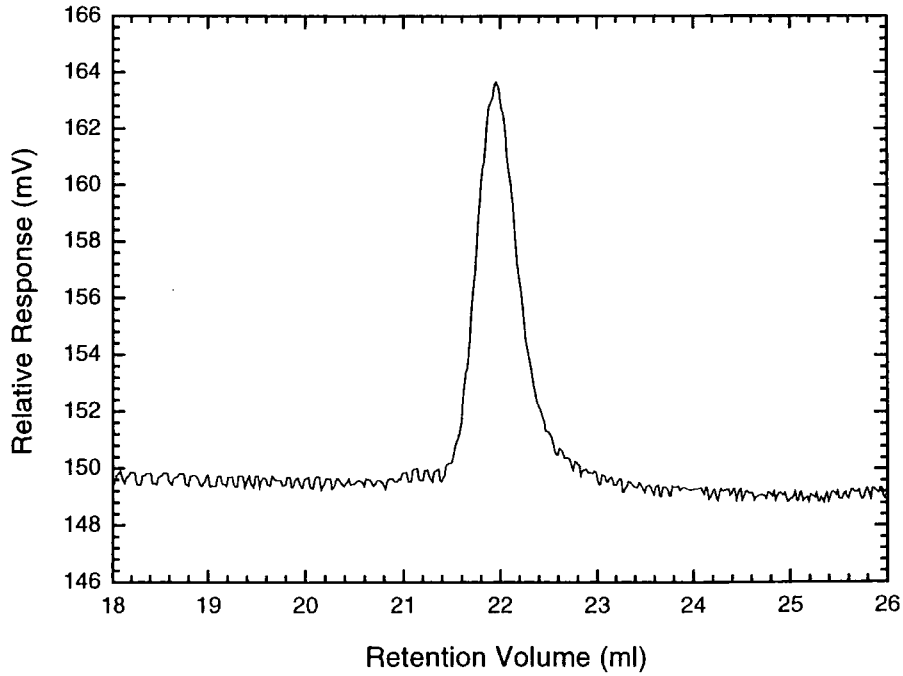

Figure 25: SEC chromatogram after six fractionations.

Since a large excess of octachlorosilane (which on the exposure to methanol has now formed octamethoxysilane) was used to produce the predominantly 1-arm star, any remaining excess needs to be removed. This was achieved by precipitating the polymer out of solution in the reaction flask under a dry nitrogen atmosphere and cannulating the supernatant liquor out into a separate flask. This *insitu*-precipitation was achieved by reducing the volume of benzene solution inside the reaction flask and cannulating in dried and distilled methanol. The polymer was precipitated out slowly to make sure there are no pockets of solution containing octamethoxysilane trapped inside the polymer. The supernatant was analysed by SEC to see whether any traces of octamethoxysilane remained. Figure 26 and Figure 27 show the chromatograms for the supernatant residues dissolved in THF after 4 and 7 precipitations. A reduction of the octamethoxysilane can be seen at 27.6 ml with the number of precipitations. The peak at 26.5 ml is due to other impurities remaining in the supernatant residue. This procedure was repeated until no octamethoxysilane remained.

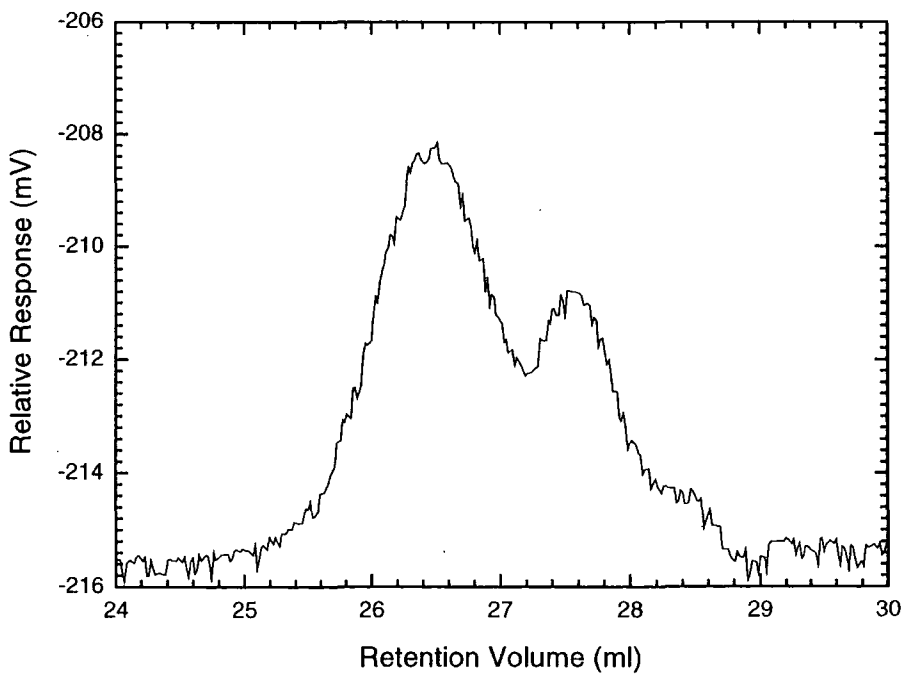

Figure 26: SEC chromatogram of the supernatant residue from the 4th precipitation.

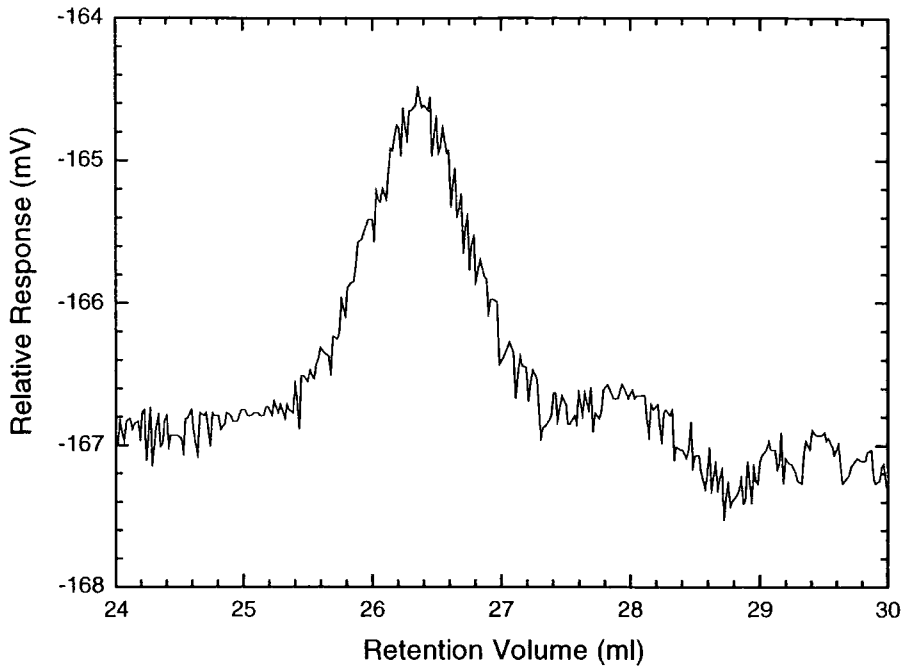

Figure 27: SEC chromatogram of the supernatant residue from the 7th precipitation.

The next stage of star synthesis was to remove any traces of methanol remaining from the precipitations to prevent termination of the living hydrogenous polybutadiene arms, upon their addition to the star precursor. The methanol was removed by distilling benzene into the reaction flask, redissolving the polymer and removing the solvent by distillation. This process was repeated five times. The hydrogenous polybutadiene arms were synthesised in the second reaction flask on the apparatus. Living anionic polymerisation techniques were used with 1,3-butadiene monomer, s-butyllithium initiator and benzene as the solvent. A 25 % excess of polybutadiene arms with respect to the amount required for full coupling was synthesised. A sample of this hydrogenous polymer was taken for molecular weight analysis by SEC. Table 3 shows the molecular weight of the hydrogenous arms for each of the stars synthesised. Completion of the star synthesis was achieved by the addition of the poly(butadienyl)lithium solution to the 1-arm precursor star solution. The coupling of the living poly(butadienyl)lithium chains to the methoxysilane core was carried out at a temperature of 303 K for 7 days. The progress of the coupling reaction was followed by SEC.

Table 3: SEC Data for the Regular Arms of the Star.

Star	$\bar{M}_W/10^4$ (g mol^{-1})	$\bar{M}_n/10^4$ (g mol^{-1})	Polydispersity
S300	3.44	3.43	1.00
S80	3.55	3.47	1.02
S60	3.08	3.03	1.02
S30	3.88	3.81	1.02

Figure 28 and Figure 29 are the chromatograms taken at the start and at the end of the linking reaction and show the coupling of the living poly(butadienyl)lithium chains to the 1-arm precursor star. Three peaks can be seen on both chromatograms at retention volumes 18.5 ml, 20.9 ml and 21.7 ml. The peaks at 18.5 ml and 21.7 ml are the star polymer and uncoupled hydrogenous arms respectively. The peak at 20.9 ml is coupled hydrogenous arms formed by the exposure of the poly(butadienyl)lithium chains to CO_2 or O_2, due to leakage of the glass vessel or insufficient degassed methanol. A reduction in the relative size of the uncoupled arm peak to the star polymer peak can be seen over time as the arms couple to the star polymer.

After 7 days, any remaining living poly(butadienyl)lithium was terminated using degassed methanol. The star polymer was precipitated out into a non-solvent (methanol), with a small amount of anti-oxidant (2,6-butyl-4-methylphenol) and dried in the vacuum oven. Fractionation of the precipitated polymer was required to obtain the star polymer free from any remaining uncoupled polybutadiene. This was achieved by dissolving the polymer in toluene to a concentration of 1-2 % (w/v). The solution was stirred vigorously inside a separating funnel immersed in a water bath. Methanol was added dropwise into the solution until a cloudy suspension formed, the temperature of the water bath was increased until the solution clarified, the stirring ceased and the temperature of the bath was allowed to drop back to its original value. The quantity of non-solvent determines the extent of fractionation. A small lower layer containing higher molecular weight material was obtained with a small addition of methanol. The two layers were separated and precipitated out for analysis by SEC. Analysis of the chromatogram shows the efficiency of fractionation and whether further fractionations are required. The upper layer contained

lower molecular weight material that was due to the uncoupled polybutadiene, the lower layer containing the star polymer.

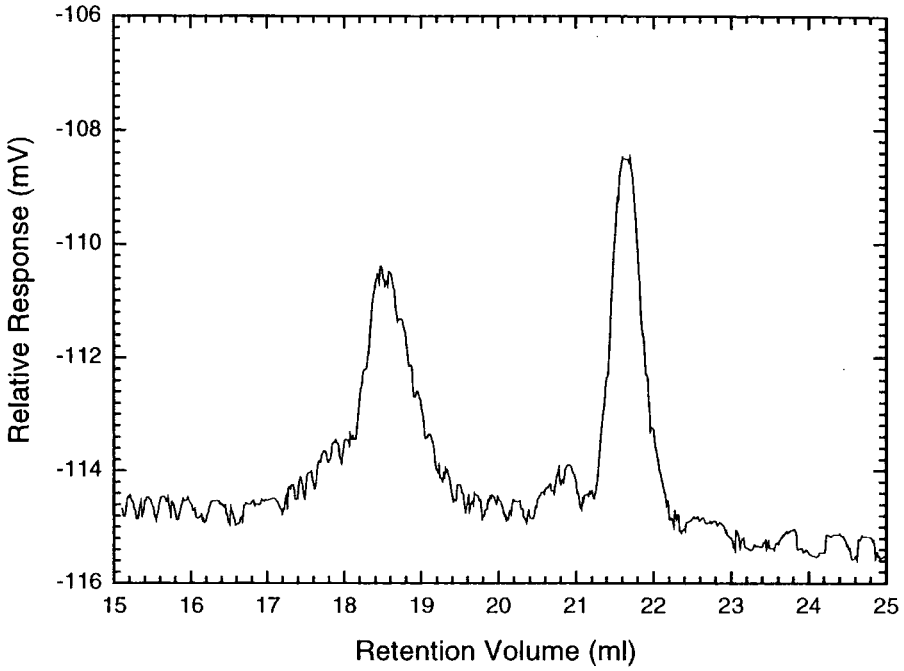

Figure 28: A SEC chromatogram of a sample taken at the start of the coupling reaction.

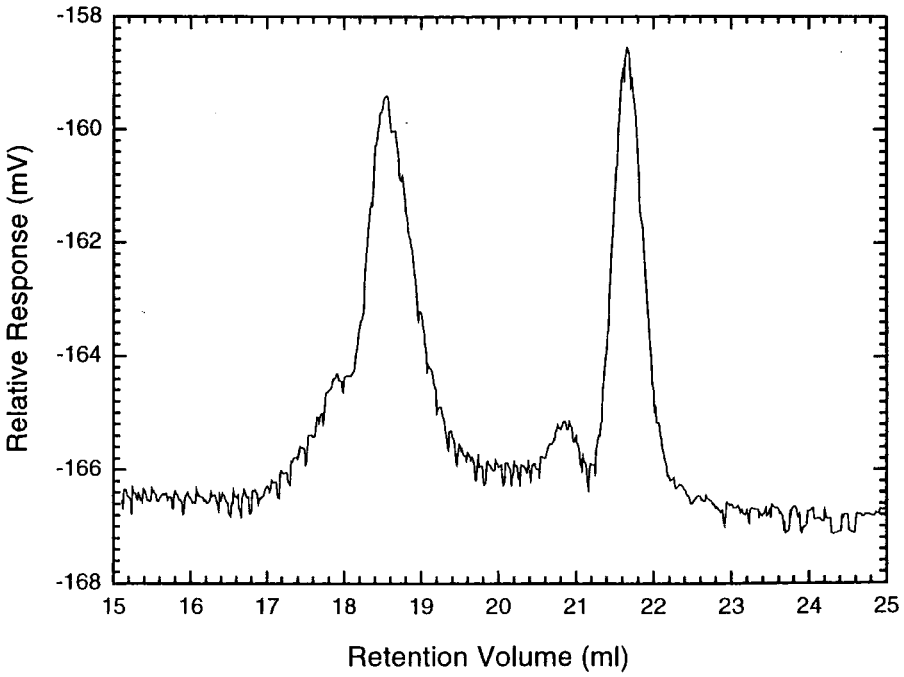

Figure 29: A SEC chromatogram of a sample taken at the end of the coupling reaction.

Table 4: SEC Data for the Fractionated Stars.

Star	$\bar{M}_W/10^5$ (g mol^{-1})	$\bar{M}_n/10^5$ (g mol^{-1})	Polydispersity
S300	5.97	4.94	1.21
S80	3.42	2.73	1.25
S60	2.46	2.28	1.08
S30	3.55	3.04	1.17

Figure 30 and Figure 31 are the SEC chromatograms of a star polymer before and after fractionation. Figure 30 has three peaks at retention volumes of 20.1 ml, 21.2 ml and 22.0 ml, corresponding to unfractionated star, coupled hydrogenous arms and uncoupled hydrogenous arms. The peak corresponding to the isolated miktoarm star polymer is shown in Figure 31 at a retention volume of 20.1 ml. The $\bar{M}_W$, $\bar{M}_n$ and polydispersity index of the fractionated stars are listed in Table 4. The number of arms attached to the central core and hence functionality of the stars were determined using SEC data. A theoretical number average molecular weight, $\bar{M}_n$, was calculated for each star with the knowledge of the $\bar{M}_n$ of the asymmetric and regular arms. This theoretical star $\bar{M}_n$ was compared to the fractionated star $\bar{M}_n$ and the average functionality of the star was determined. The number average molecular weight was used to calculate the star functionality as it is the statistical average molecular weight. Table 5 shows the $\bar{M}_n$ of the theoretical and fractionated stars and the calculated average functionality (*f*). The theoretical $\bar{M}_n$ is calculated from assuming the star has 7 regular arms and a asymmetric arm.

The average number of arms attached to the central core is determined by the star functionality (*f*). As it can be seen from Table 5, not all the stars have an functionality of 8. The asymmetric stars S300, S80, S60 and S30 have an average functionality of 6.3, 6.6, 6.6 and 8.3 respectively. The functionality of star S30 can be assumed to be 8 within the margins of error of the analysis. The star polymers S60, S80 and S300 have a lower average functionalities than 8, suggesting that the stars have a range of arms attached to the core that can be in between 4 to 8. A good indication that a star has a range of the number of arms

attached to the core is given by the polydispersity index. Fractionated stars that have under gone full coupling will be monodisperse and yield a low polydispersity. A range of the number of arms attached to the core will cause a higher polydispersity and a broad fractionated chromatogram peak can be seen. Star polymer S30 with full coupling of the arms to the core has a lower polydispersity than stars S80 and S300, that have a range of number of arms attached (Table 4). The lower polydispersity of S60 compared to S30 could be due to the octachlorosilane synthesised for this star.

There are various factors that can reduce the number of arms on a star. These include termination of the living poly(butadienyl)lithium, steric hindrance, inadequate coupling time and the lower reactivity of the methoxysilane core. A reduction in the excess of living regular arms by termination by impurities leads to a reduction of the number of these arms available to couple to the core. Termination of the living arms could have occurred during transfer across the reaction vessel from one flask to the other or by any remaining methanol not washed out by the benzene. Termination could have happened whilst the stars were coupling due to leaks in the system or by any impurities in the solvent. Steric crowding at the core is likely to hinder the addition of the last couple of arms to the core and hence reduce star functionality.

Table 5: The functionality of the Asymmetric Star Polymers determined by the $\bar{M}_n$ of Asymmetric and Regular Arms and Fractionated Star.

Star	$\bar{M}_n$ /10^4 Asymmetric Arm (g mol^{-1})	$\bar{M}_n$ /10^4 Regular Arm (g mol^{-1})	$\bar{M}_n$ /10^4 Theoretical Star (g mol^{-1})	$\bar{M}_n$ /10^4 Fractionated Star (g mol^{-1})	Functionality (f)
S300	31.1	3.43	55.1	49.4	6.3 ± 0.3
S80	7.91	3.47	32.2	27.3	6.6 ± 0.3
S60	5.84	3.03	27.1	22.8	6.6 ± 0.3
S30	2.58	3.81	29.3	30.4	8.3 ± 0.3

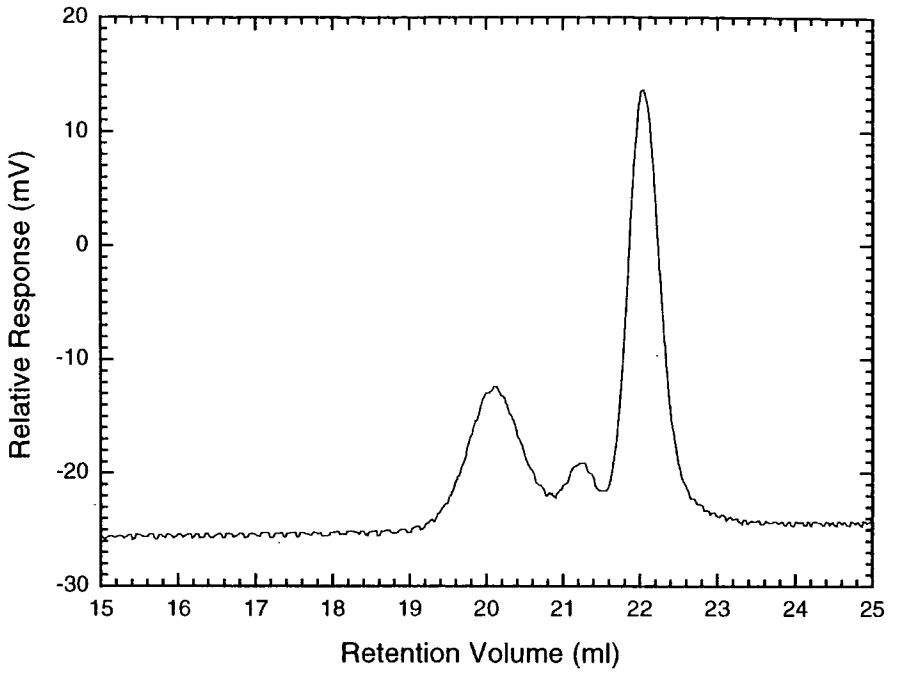

Figure 30: SEC chromatogram for the unfractionated star

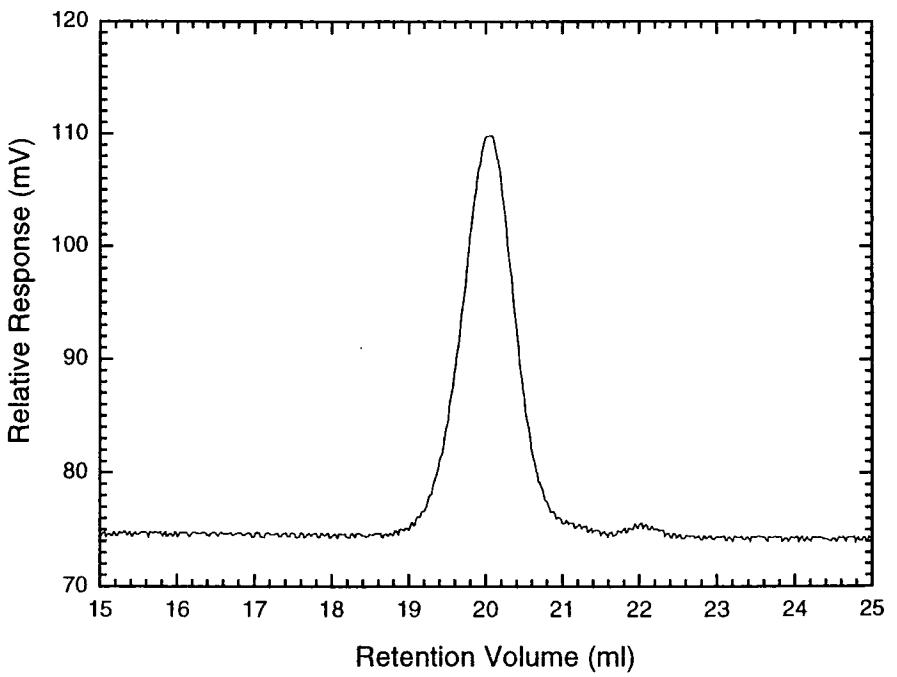

Figure 31: SEC chromatogram for the fractionated star.

2.4 Experimental

2.4.1 Synthesis of Deuterobutadiene Monomer

All glassware was dried in the oven before use. 288 g of zinc dust (purchased from Aldrich), 2.66 g of sodium iodide (Aldrich) and 16 g of cupric chloride (Aldrich) were placed inside a three-neck round bottom flask fitted, with a overhead mechanical stirrer, a double reflux condenser and a supply of dry nitrogen (BOC). To the reflux condenser was attached a calcium chloride (BDH) drying column and then a dry ice/acetone trap (temperature of 195 K), where the product was collected. The apparatus was maintained at a positive pressure of nitrogen at all times. To the reaction flask was added, via a cannular, 380 g of anhydrous 1,4-dioxane (>0.0005% water, Aldrich) and then 88 g of deuterium oxide (99.9% deuteration, Aldrich). The reaction mixture was stirred and quickly heated to reflux (about 359 K). From a side dropping funnel, 174 g of hexachlorobutadiene (Fisher) dissolved in 150 g of anhydrous 1,4-dioxane was added slowly over 2 to 3 hours. Once the hexachlorobutadiene solution had been consumed, then the reaction was maintained at reflux for a further hour. The gaseous product was collected in the dry ice/acetone trap and the yield of condensate was about 75 % based on hexachlorobutadiene.

The crude butadiene-d_6 condensate was vacuum transferred into a high pressure autoclave (volume of 125 ml) containing 1 % (w/w) with respect to butadiene-d_6 of hydroquinone (Aldrich) and phenyl-2-naphthylamine (Aldrich). A 50 % molar excess of sulfur dioxide (Aldrich) with respect to butadiene-d_6 was vacuum transferred in to the autoclave and then the autoclave was heated to a temperature of 373 K for 18 hours, in the high pressure laboratory. After 18 hours, the autoclave was allowed to cool to room temperature and the pressure returned to atmospheric. This was achieved by freezing the contents of the autoclave with liquid air (temperature of 100 K) and attaching to the outlet a bubbler containing potassium hydroxide (BDH) solution. The bubbler was positioned to the autoclave outlet so that when the autoclave was opened up to the atmosphere, air was sucked in and not the potassium hydroxide solution. Once pressure has returned, the bubbler was reversed and the auto clave was allowed to warm up, releasing sulfur dioxide and impurities that are to be removed by the potassium hydroxide solution. The contents of

the bomb are poured into a beaker and the liquid and crystals were dissolved in hot methanol. This solution was filtered still hot through a sinter-funnel and the filtrate cooled inside a ice/water bath to collect crystals of butadiene–d_6 sulfone. The crystals of butadiene-d_6 sulfone were dried inside a vacuum oven.

The butadiene-d_6 was regenerated from the thermal decomposition of the sulfone. This was achieved by placing the sulfone in a two-neck round bottom flask with 1 % (w/w) of p-tert butyl catechol (Aldrich). To this flask was attached a series of bubblers containing potassium hydroxide solution, a column backed with 4A molecular sieve and dry ice/acetone trap to collect the product. The molarity of the potassium hydroxide solution was determined by the moles of SO_2 used. The apparatus was purged with nitrogen and the sulfone heated to a temperature between 403 K to 423 K until no more product can be seen to bubble through the potassium hydroxide solution. A yield of 80 % was usually expected when 10 g or more of butadiene-d_6 sulfone was decomposed. The butadiene-d_6 was vacuum transferred from the trap into a gas cylinder containing 1 % (w/w) of hydroquinone and phenyl-2-naphthylamine. The gas cylinder was stored inside the laboratory freezer.

2.4.2 Purification of Benzene

Benzene (purchased from Aldrich) was purified by washing 3 times with sulphuric acid (Fisher) inside a separating funnel, then was washed once with distilled water, once with concentrated sodium bicarbonate (Aldrich) solution and finally 3 times with distilled water. Any trace water was removed by refluxing with a Dean and Stark apparatus and the remaining benzene was then fractionally distilled and stored in bottles containing 4A molecular sieve (Aldrich). The benzene was then transferred onto the vacuum line in 500 ml round bottom flasks containing calcium hydride (Aldrich), where it was further dried and degassed by a series of freeze, pump, thaw cycles.

2.4.3 Synthesis of Linear Polybutadiene and Polydeuterobutadiene

The polymer was synthesised inside a multi-flask reaction vessel containing a 500 ml reaction flask with a magnetic stirrer bar and a smaller 50 ml side flasks, with one of the flasks containing a living solution of poly(styryl)lithium in benzene. These reactions vessels are attached to a vacuum line so they can be maintained at a pressure of 2×10^6 mbar, by a combined Edwards rotary and diffusion pump. The vessel was cleaned of any impurities by washing the glass with the solution of living poly(styryl)lithium in benzene. Any residue left from this solution was removed by washing the vessel with benzene distilled out from the stock solution and returning the benzene with the poly(styryl)lithium to the side flask.

Benzene was vacuum distilled into the reaction flask from a large stock solution containing poly(styryl)lithium, situated on the vacuum line. The volume of benzene distilled was determined by the mass of monomer to be used to obtain an eventual polymer concentration of 10 % (w/v). The butadiene (or butadiene-d_6) monomer stored inside a gas cylinder was vacuum transferred to a graduated dewar that had been immersed into a dry ice/acetone bath. The dewar was weighed before and after transfer to calculate the weight of the monomer collected. A "sacrificial" polymerisation was performed on the monomer by transfer to a 250 ml round-bottom flask containing a magnetic stirring flea. The flask was immersed inside an ice/methanol bath (temperature of 253 K) and 1 ml of n-butyllithium (purchased from Aldrich) was injected and the monomer stirred for 20 minutes. The monomer was then vacuum transferred into the reaction flask and the mass of monomer determined by weighing the 250 ml round-bottom flask before and after transfer. The volume of s-butyllithium (Aldrich) initiator required to obtain the desired molecular weight of the polymer was determined by the equation:

$$\text{Initiator volume (ml)} = \frac{\text{Mass of monomer (g)}}{\text{Molecular Weight (g mol}^{-1}\text{)}} \times \frac{1000}{\text{Molarity (mol l}^{-1}\text{)}} \qquad (2)$$

The initiator was injected quickly in to the monomer/benzene solution, using a gas tight syringe. The reaction vessel was immersed in a oil bath at a temperature of 313 K and stirred for 12 hours. The polymerisation was terminated with 1 ml of methanol, which was degassed by passing a stream of nitrogen through it for 5 minutes. 1 ml of 10 % (w/v)

solution of 2,6-di-tert-butyl-4-methylphenol (Aldrich) in toluene was injected into the polymer solution. The polymer was precipitated out in an 8-fold excess of a non-solvent (methanol) and dried inside a vacuum oven. The molecular weight of the polymer was characterised using a Viscotek Size Exclusion Chromatograph (SEC), fitted with light scattering, refractive index and viscosity detectors. The elution solvent was THF and the temperature of the column was maintained at a temperature of 308 K. The SEC was calibrated using polystyrene standards (Polymer Laboratories) of a known molecular weight and refractive index increment and samples analysed have molecular weights with an error of less than 5 %. A specific refractive index increment (dn/dc) of 0.124 ml g^{-1} for polybutadiene was used for the light scattering analysis, that was determined using a Abe differential refractomer.

2.4.4 Synthesis of Octachlorosilane

All glassware was dried inside the oven before use and an atmosphere of nitrogen maintained at all times. Into a 250 ml three-neck round bottom flask is added 30.74 g (0.27 mol) of dichloromethylsilane (purchased from Aldrich) and 2 ml of catalyst solution. The catalyst solution was prepared under nitrogen with 1 g of hydrogen hexachloroplatinate (IV) hydrate (Aldrich) in 9 ml of ethylene glycol dimethyl ether (Aldrich) and 1 ml of methanol (dried and distilled). The three-neck flask was fitted with a water condenser, an nitrogen inlet and a rubber septum. 5.0 g (0.037 mol) of tetravinylsilane (Aldrich) was added via a gas tight syringe through the rubber septum over 2 to 3 hours and the temperature was critically maintained at 313 K with a water bath. After complete addition of the tetravinylsilane, the mixture was stirred for a further 30 minutes. Excess dichloromethylsilane (boiling point = 314 K) was removed by distillation and the octachlorosilane was collected by vacuum distillation as a high boiling liquid (temperature = 471 K to 473 K). The product was dissolved in benzene to a known concentration and stored under nitrogen.

2.4.5 Synthesis of Asymmetric Star Polymers

A reaction vessel was used with two 500 ml flasks (one tapered), four 50 ml side sample flasks and a 50 ml flask containing 25 ml of living poly(styryl)lithium in benzene. The vessel was attached to a vacuum line and maintained at a vacuum of 2×10^6 mbar, by a combined Edwards rotary and diffusion pump. The reaction vessel was cleaned with a solution of poly(styryl)lithium and weighed dry. The deuterated asymmetric arm was synthesised first as outlined in section 2.4.3, and a sample of the polymer was taken for molecular weight determination by SEC. An excess of octachlorosilane (a silicon to lithium molar ratio of 25:1) was injected next and the linking reaction was allowed to proceed for 5 hours with vigorous stirring.

The polymer solution was now fractionated to remove any higher arm star precursors. The solution was diluted to a concentration of 1-2 % (w/v) with benzene and the vessel was let down to atmospheric pressure with dry nitrogen. The reaction flask was immersed inside a water bath and the solution stirred. Methanol was used as the non-solvent and was distilled over magnesium (purchased from BDH) and dried with 4A molecular sieve (Aldrich). The methanol was added drop wise from a gas tight syringe until the solution became cloudy and then the temperature of the water bath was raised a few degrees. Once the solution clarified, stirring was halted and the temperature of the water bath was returned to its original value. Over time the polymer solution fractionated into two layers and the lower and smaller layer was removed to a 250 ml reaction flask, via a cannula, under a stream of nitrogen. A sample was prepared for SEC from this lower fraction by injecting 1 ml of n-butyllithium and allowing it to stir for 2 hours. Then 1 ml of degassed methanol was injected to terminate the n-butyllithium and the polymer was precipitated into a non-solvent (methanol), dried inside a vacuum oven, and characterised by SEC. This *insitu*-fractionation continued until only one peak belonging to the asymmetric arm could be seen on the chromatogram.

The excess octamethoxysilane was removed next by reducing the volume of the solvent inside the reaction flask to about 20-30 ml by vacuum transfer and returning the flask to a nitrogen environment. Methanol was added slowly via a cannula, under a stream of nitrogen to precipitate out the polymer. Then the supernatant liquor was removed via the

cannula to a 250 ml reaction flask, the solvent removed by vacuum transfer and replaced with 10 ml of benzene from the vacuum line. The residue was allowed to redissolve with stirring and 1 ml of n-butyllithium was injected into the stirring solution and left for 2 hours to be finally terminated with 1 ml of degassed methanol. The solvent was removed again by vacuum transfer and a sample of the residue was dissolved in THF for SEC analysis. The precipitation procedure was continued until no peak for octamethoxysilane could be seen by SEC. The next stage was to remove the solvent from the reaction flask so that it can be replaced by 50 ml of benzene. The polymer was redissolved in this solvent with stirring and the solvent removed again by vacuum transfer. This process was repeated five times to ensure total removal of any trace methanol. A dry ice/acetone bath was used instead of liquid air to prevent fracturing of the glass as the polybutadiene passes through its glass transition temperature. The reaction flask is weighed "dry" to determine mass of polymer inside the flask and then redissolved in 30 ml of benzene.

Inside the other reaction flask on the vessel, a 10% (w/v) solution of living poly(butadienyl)lithium in benzene was synthesised as described in section 2.4.3. An 25 % excess of arms were prepared and a sample was taken for molecular weight determination by SEC. The living polymer solution was transferred to the asymmetric arm solution and was allowed to react with stirring for 7 days. The reaction flask was immersed into a oil bath and maintained at a temperature of 303 K. Samples can be taken during this time to follow the coupling reaction. After 7 days, 1 ml of degassed methanol was injected, stirred and then 1 ml of a 10 % (w/v) concentration of 2,6-di-tert-butyl-4-methylphenol in toluene was injected as well. The star polymer was precipitated into an 8-fold excess of non-solvent (methanol) and dried inside a vacuum oven. A sample of this material was dissolved in THF for analysis by SEC.

Fractionation of the star polymer was performed inside a 3 L separating funnel, fitted with overhead mechanical stirrer and a 250 ml dropping funnel. The separating funnel was immersed inside a water bath. Into the separating funnel was a solution of star polymer in toluene at a concentration of 1-2 % (w/v). The solution was stirred vigorously and methanol was added drop wise until a cloudy suspension forms. The temperature of the bath was raised a few degrees until the solution clarifies and the stirrer was switched off and the temperature lowered to its original value. Two layers were formed were separated and

precipitated out into non-solvent, dried in the vacuum oven and molecular weights characterised by SEC. Further fractionation of the layers were required until the star polymer was isolated on the chromatogram.

2.5 References

[1] Schaefgen, J. R.; Flory, P. J. *J. Am. Chem. Soc.* **1948**, 70, 2709.

[2] Morton, M.; Helminiak, T. E.; Gadkary, S. D.; Bueche, F. *J. Polym. Sci.* **1962**, 57, 471.

[3] Orofino, T. A.; Wenger, F. *J. Phys. Chem.* **1963**, 67, 566.

[4] Mayer, R. *Polymer* **1974**, 15 137.

[5] Meunier, J. C.; Van Leemput, R. *Makromol. Chem.* **1971**, 142, 1.

[6] Decker, D; Rempp, P. *CR Acad. Sci.* **1965**, 261, 1977.

[7] Zelinski, R. P. ; Wofford, C. F. J. *Polym. Sci., Part A.* **1965**, 3, 93.

[8] Roovers, J.; Bywater, S. *Macromolecules* **1972**, 5, 384.

[9] Roovers, J.; Bywater, S. *Macromolecules* **1974**, 7, 443

[10] Hadjichristidis, N.; Roovers, J. *J. Polym. Sci., Polym. Phys. Ed.* **1974**, 12, 2521.

[11] Hadjichristidis, N.; Guyot, A; Fetters, L. J. *Macromolecules* **1978**, 11, 668.

[12] Hadjichristidis, N.; Fetters, L. J. *Macromolecules* **1980**, 13, 191.

[13] Roovers, J.; Hadjichristidis, N.; Fetters, L. J. *Macromolecules* **1983**, 16, 214.

[14] Nguyen, A. B.; Hadjichristidis, N.; Fetters, L. J. *Macromolecules* **1986**, 19, 768.

[15] Roovers, J; Toporowski, P. M.; *J. Polym. Sci., Part A.* **1986**, 24, 3009.

[16] Zhou, L. L.; Hadjichristidis, N.; Toporowski, P. M.; Roovers, J. *Rubber Chem. Technol.* **1992**, 65, 303.

[17] Roovers, J; Zhou, L. L.; Toporowski, P. M.; van der Zwan, M.; Iatrou, H.; Hadjichristidis, N. *Macromolecules* **1993**, 26, 4324.

[18] Zhou, L. L.; Roovers, J *Macromolecules* **1993**, 26, 963.

[19] Roovers, J; Toporowski, P. M.; Martin, J. *Macromolecules* **1989**, 22, 1897.

[20] Pennisi, R. W.; Fetters, L. J. *Macromolecules* **1988**, 21, 1094.

[21] Gell, C. B., Graessley, W. W.; Efstratiadis, V.; Pitsikalis, M.; Hadjichristidis, N. *J. Polym. Sci., Part B* **1997**, 35, 1943.

[22] Frater, D.J.; Mays, J. W.; Jackson, C. J. *J. Polym. Sci., Part B* **1997**, 35, 141.

[23] Quirk, R.P.; Yoo, T. *Polym. Bull.* **1993**, 31, 29.

[24] Mays, J. W. *Polym Bull* **1990**, 23, 247.

[25] Khan, I. M.; Gao, Z.; Khougaz, K.; Eisenberg, A.; *Macromolecules* **1992**, 25, 3002.

[26] Tselikas, Y.; Hadjichristidis, N.; Iatrou, H.; Liang, K. S.; Lohse, D. J. *J. Chem. Phys.* **1996**, 105, 2456.

[27] Iatrou, H. Hajichristidis, N. *Macromolecules* **1992**, 25, 4649.

[28] Sioula, S.; Tselikas, Y.; Hajichristidis, N.; *Macromolecules* **1997**, 30, 1518.

[29] Iatrou, H.; Hajichristidis, N. *Macromolecules* **1993**, 26, 2479.

[30] Eschwey, H.; Burchard, W. *Polymer* **1975**, 16, 180.

[31] Tsitsilianis, C; Graff, S.; Rempp, P. *Eur. Polym. J.* **1990**, 27, 243.

[32] Tsitsilianis, C; Lutz, P.; Graff, S.; Lamps, J-P.; Rempp, P. *Macromolecules* **1991**, 24, 5897.

[33] Tsitsilianis, C; Panagopoulos, D.; Lutz, P. *Polymer* **1995**, 36, 3745.

[34] Tsitsilianis, C; Voulgaris, D. *Macromol. Chem. Phys.* **1997**, 198, 997.

[35] Kanaoka, S.; Swamoto, M.; Higashimura, T.; *Macromolecules* **1993**, 26, 254.

[36] Quirk, R. P.; Yoo, T.; Lee, B. *JMS Pure Appl. Chem.* **1994**, A31(8), 911.

[37] Quirk, R.P.; Lee, B.; Schock, L.E. *Macromol. Symp.* **1992**, 53, 201.

[38] Bae, Y. C; Fodor, Z; Faust, R. *Macromolecules* **1997**, 30, 198.

[39] Bae, Y. C; Faust, R. *Macromolecules* **1998**, 31, 240.

[40] Huckstadt, H.; Abetz, V.; Stadler, R.; *Macromol. Rapid Commun.* **1996**, 17, 599.

[41] Xie, H.; Xia, J. *Makromol. Chem.* **1987**, 188, 2543.

[42] Wright, S.J.; Young, R.N. Croucher, T. G. *Polymer International* **1994**, 33, 123.

[43] Iatrou, I.; Hajichristidis, N. *Macromolecules* **1993**, 26, 2479.

[44] Allgaier, J.; Young, R.N., Esttratiadis, V.; Hajichristidis, N. *Macromolecules* **1996**, 29, 1794.

[45] Fernyhough, C.M.; Young, R.N.; Tack, R.D. *Macromolecules* **1999**, 32, 5760.

[46] Averopoulos, A.; Hadjichristidis, N.; *J. Polym. Sci., Polym. Chem. Ed.* **1997**, 35, 813.

[47] Tsiang, R. C. C. *Macromolecules* **1994**, 27, 4399.

[48] Velis, G.; Hajichristidis, N. *Macromolecules* **1999**, 32

[49] Averopoulos, A.; Poulos, Y.; Hadjichristidis, N.; Roovers, J. *Macromolecules* **1996**, 29, 6076.

[50] Hutchings, L.R.; Richards, R.W.; *Polym. Bull.* **1998**, 41, 283.

[51] Hutchings, L.R.; Richards, R.W.; *Macromolecules* **1999**, 32, 880.

[52] Ba-Gia, H.; Jerome, T.;Teyssié, P. *J. Polym. Sci., Polym. Chem. Ed.* **1980**, 18, 3483.

[53] Wang, F.; Roovers, J.; Toporowski, P. M. *Macromol. Symp.* **1995**, 95, 255.

[54] Takano, A.; Okada, M.; Nose, T.; Fujimoto, T.; *Macromolecules* **1992**, 25, 3596.

[55] Hayashi, M.; Kojima, K.; Hirao, A.; *Macromolecules* **1999**, 32, 2425.

[56] Pitsikalis, M.; Hajichristidis, N. *Macromolecules* **1995**, 28, 3904.

[57] Tselikas, Y.; Hajichristidis, N.; Lescanec, R.L.; Honeker, C.C.; Wohlgemuth, M.; Thomas, E. L. *Macromolecules* **1996**, 29, 3390.

[58] Craig, D.; Fowler, R. B. *J. Org. Chem.* **1961**, 26, 713.

[59] Hsieh, H. L.; Quirk, R. P. Anionic Polymerisation: Principals and Practical Applications, Marcel Dekker, New York, 1996.

[60] Bikales, N. M.; Kroschwitz, J. I.; Mark, H. F.; Menges, G.; Overberger, C. G. Anionic Polymerisation; Encyclopaedia of Polymer Science, John Wiley & Sons, New York, 1985, 2nd Ed., Vol. 2, pp 1-43.

Chapter 3

Dilute Solution Characterisation of Miktoarm Star-Branched Polymers

3.1 Introduction

This chapter outlines the dilute solution characterisation of miktoarm star-branched and linear polymers in good and θ-solvents. The characterisation techniques of static and dynamic light scattering and viscometry were used and have been reviewed in section 3.2. These techniques allow the measurement of global properties of the polymers, such as the weight-average molecular weight, the radius of gyration, the second virial coefficient, the diffusion coefficients and the intrinsic viscosity. Section 3.3 describes the experimental procedures to obtain the these global properties from the characterisation techniques. The final section, section 3.4 outlines the dilute solution characterisation of linear and miktoarm star polybutadienes that were synthesised in chapter 2. The miktoarm star polymers have asymmetric arms with varying chain length. The solvents used for good and θ-solvents conditions were cyclohexane and 1,4-dioxane respectively. The global properties obtained were used to characterise the star polymers in solution, by calculating equivalent sphere radii, size ratios, interpenetration functions and branching ratios.

3.2 Dilute Solution Characterisation Techniques

3.2.1 Static Light Scattering

3.2.1.1 Introduction

The interaction of electromagnetic radiation with atoms or molecules in the absence of absorption, induces oscillations in their electronic density.[1,2] These atoms or molecules then have oscillating electronic dipoles that irradiate in all directions. If the incident and scattered radiation are of the same frequency (equal energy), then an elastic scattering process occurs. If an energy exchange and hence frequency shift in radiation is observed, then the scattering process is non-elastic and this has been utilised by Raman spectroscopy. The elastic part of the scattering spectrum may be broadened by concentration fluctuations and also by weak frequency displacements caused by Brownian motion of the scatterers (see section 3.2.2 on dynamic light scattering).

Static light scattering is an elastic process and can be classified into three types, Rayleigh, Debye and Mie, that depending on the size of the independent scattering particles. Rayleigh scattering is obtained from particles that are much smaller (less than $\lambda/20$) than the incident radiation wavelength and have a refractive index similar to the medium. Debye scattering occurs when the incident radiation wavelength is approximately the same size of the scattering particle and has a refractive index similar to that of the medium. Mie scattering is a complex process and is obtained when large particles are present that have a refractive index significantly different to that of the medium. This type of scattering can no longer be considered as a result of induced dipoles fluctuating in a electromagnetic field.

3.2.1.2 Light Scattering from Gas Particles

Lord Rayleigh developed the simplest theory of light scattering for dilute ideal gasses, where there are no thermodynamic interactions between the gas molecules. In this theory, the system has a large number of scattering particles, smaller than the wavelength (λ_0) of the incident radiation in a vacuum, that are well separated and move in a random fashion. A

plane polarised incident electromagnetic wave is considered, whose associated electric field varies sinusoidally in the plane perpendicular to the direction of propagation. The electromagnetic wave is vertically polarised and the electromagnetic field is parallel to the *z*-axis (see Figure 1). The electric field associated with the propagating wave in the x-axis direction through the vacuum is:

$$E = E_0 \exp[i(\omega t - \boldsymbol{k}_0)r)] \tag{1}$$

E_0 is the incident electric vector, ω is the angular frequency, t is time, $\boldsymbol{k}_0$ is the vectorial wave number and r is any position referred to the coordinate origin. At the origin position, the gas molecule has an oscillating electronic density that is in phase with the local electric field, that induces an electric dipole with a dipole moment (μ) given by the product of the polarisability and the electric field strength:

$$\mu = \alpha E = \alpha E_0 \exp(i\omega t) \tag{2}$$

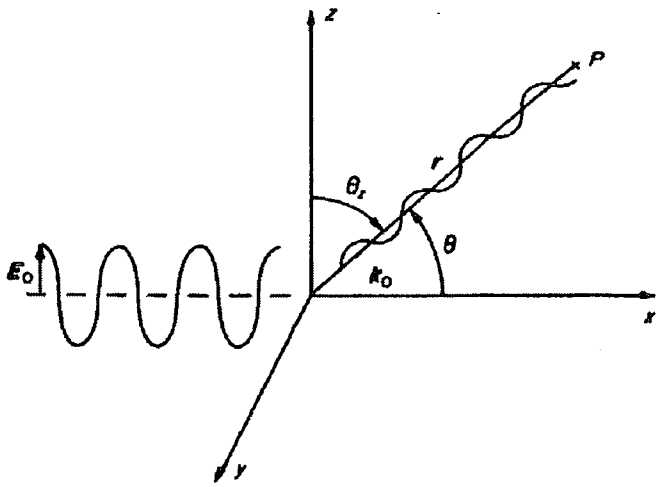

Figure 1: Scattering of vertically polarised light radiation by an isotropic small particle.

The induced oscillating dipole moment acts as a secondary radiating source and the gas molecule emits plane polarised radiation in all directions that is identical in frequency to the incident source. The electric field amplitude of the scattered wave is dependent on the dipole-moment component perpendicular to the scattering direction. The electric field of the scattered wave (E_S) at a point P that is at a distance r from the dipole (now considered a

point source) will be perpendicular to r and will be situated on the zr plane. The modulus of the scattered electric field is;

$$E_S = \frac{1}{rc^2}\frac{\partial \mu}{\partial t^2}\sin\theta_z \tag{3}$$

The speed of light in a vacuum is c and θ_z is the angle between the scattering direction r and the z-axis. Equations 2 and 3 lead to a scattered electric field modulus of:

$$E_S = \frac{k_0^2 \alpha E_o}{r}\sin\theta_z \exp[i(\omega t - k_0 r)] \tag{4}$$

The phase displacement of the electric field between the gas particle and point P is $k_0 r$. The intensity of the scattered wave at P is calculated by the square of the amplitude electric field by ($k_0 = 2\pi/\lambda_0$);

$$I = \frac{16\pi^4 \alpha^2 I_0}{r^2 \lambda_0^4}\sin^2\theta_z \tag{5}$$

The wavelength of the electromagnetic wave in the vacuum being λ_0. Equation 5 also shows that the intensity of scattered light is dependent on the wavelength and for vertically polarised incident light, has no intensity in the z-direction. The intensity of scattered light in the xy plane, that is perpendicular to the plane of polarisation of the incident light is;

$$I = \frac{16\pi^4 \alpha^2}{r^2 \lambda_0^4} I_0 \tag{6}$$

If the system contains N gas molecules, then the scattered intensity for incident vertically polarised light is:

$$I = \frac{16\pi^4 \alpha^2 N}{r^2 \lambda_0^4} I_0 \tag{7}$$

The polarisability α is not easy to obtain experimentally, but is related to the gas refractive index (n) through its dielectric constant ($n^2 = \varepsilon$) by:

$$\left(n^2-1\right)=\left(\varepsilon-1\right)=4\pi N\alpha \tag{8}$$

In a vacuum, the refractive index is close to unity and can be expressed as a Taylor expansion, being truncated at the 2nd term:

$$n^2=1+2(dn/dc)c \tag{9}$$

The concentration of the gas is c and dn/dc is the specific refractive index increment. Allowing for the number of molecules per unit volume of the gas being expressed as N_Ac/M, then the intensity of scattered radiation is:

$$I=\frac{4\pi^2M}{r^2\lambda_0^4N_A}I_0\left(\frac{dn}{dc}\right)^2 \tag{10}$$

M is the molecular weight of the gas molecule and N_A is Avogadro's constant. To remove the dependence of scattered light intensity on the distance r from the scatterer and the measurement of incident light intensity, the Rayleigh ratio is used:

$$R_\theta=\frac{Ir^2}{I_0} \tag{11}$$

This leads to the final equation of light scattering of gas molecules using incident vertically polarised light:

$$R_\theta=\frac{4\pi^2Mc}{\lambda_0^4N_A}\left(\frac{dn}{dc}\right)^2 \tag{12}$$

3.2.1.3 Light Scattering from Pure Liquids

A thermodynamic approach is used to study light scattering from a pure liquid. For a liquid, the molecules are not distributed randomly like a gas and a reduction of intensity is experienced due to interference of the scattered waves. If the medium is completely ordered and incompressible, then for any given direction apart from the incident direction, the liquid

can be associated into paired volumes of very small dimensions, compared to the incident radiation. This causes the distances covered by the scattering waves over the paired volume to the observation point to differ by half a wavelength. The electric fields for the scattered waves will be totally out of phase and therefore the scattered light intensity for any direction will be zero. In real liquids, there is no perfect ordering of molecules and the liquid density inside the volume elements only remains constant when averaged over time. At any given point of time, fluctuations of liquid density will occur inside the volume elements. This leads to a fluctuation in scattering amplitudes from the volumes, that will be not cancelled by interference. As the density of a liquid is much greater than a gas, then the fraction of liquid molecules scattering coherently inside the volume elements is far greater than for the same volume of gas and therefore a greater intensity of scattering is observed. Each scattering particle is now represented by a volume element (δV), that is small compared to the wavelength of incident radiation. The volume elements contain enough molecules to allow for density fluctuations, which act independently of each other. Each volume element will have a polarisability (α) that will fluctuate by a small amount ($\Delta\alpha$) about an average polarisability ($\bar{\alpha}$) of the system:

$$\alpha^2 = (\bar{\alpha} + \Delta\alpha)^2 = \bar{\alpha}^2 + 2\bar{\alpha}\Delta\alpha + \Delta\alpha^2 \tag{13}$$

If there are N scattering volumes inside a unit volume, the value of $\bar{\alpha}$ is the same within each scattering volume. Then the terms in $\bar{\alpha}$ will cancel out, due to the same reason for the scattered light in an ordered system being of zero intensity. The average value of $2\,\bar{\alpha}\Delta\alpha$ will also be zero, because $\Delta\alpha$ can take equally positive and negative values. Then the Rayleigh ratio for a liquid using vertically polarised light is:

$$R_\theta = \frac{16\pi^4 \overline{\Delta\alpha^2}}{\lambda_0^4 \delta V} \tag{14}$$

The term of $1/\delta V$ represents the number of volume elements present in the system. Using the relationship between polarisability and dielectric constant, the polarisability fluctuation can be represented as:

$$\Delta\alpha = \frac{\delta V \Delta\varepsilon}{4\pi} \tag{15}$$

The insertion of equation 15 into equation 14, leads to:

$$R_\theta = \frac{\pi^2 \delta V \overline{\Delta\varepsilon^2}}{\lambda_0^4} \tag{16}$$

The fluctuations of the dielectric constant in a pure liquid are due to fluctuations in density (ρ) and temperature. The effect of temperature fluctuations are usually negligible and therefore:

$$\overline{\Delta\varepsilon^2} = \left(\frac{\partial\varepsilon}{\partial\rho}\right)^2 \overline{\Delta\rho^2} \tag{17}$$

The fluctuations of solution density is given by the general theory of fluctuations:

$$\overline{\Delta\rho^2} = \frac{kT}{\partial^2 F / \partial\rho^2} \tag{18}$$

The Boltzmann constant is k, T is the absolute temperature and F is the Helmholtz free energy of the system. Thermodynamic arguments lead to:

$$\left(\frac{\partial^2 F}{\partial\rho^2}\right) = \frac{\delta V}{\rho^2}\left(\frac{1}{\beta} - 2p\right) \tag{19}$$

The isothermal compressibility of the system is β and p is the pressure. Under normal experimental conditions $1/\beta > 2p$, making the 2nd term on the right hand side of equation 19 negligible and combining equations 16 to 19 yields:

$$R_\theta = \frac{\pi^2 kT\rho^2\beta}{\lambda_0^4}\left(\frac{\partial\varepsilon}{\partial\rho}\right)_T \tag{20}$$

3.2.1.4 Light Scattering from Solutions of Small Solute Molecules

The introduction of small solute molecules (sizes less than $\lambda/20$) into the solvent, causes the increment of the dielectric constant ($\Delta\varepsilon$) to depend on the number of solute and solvent molecules inside the volume elements (density fluctuations) and the interchange between each type of molecule (concentration fluctuations). The solute and solvent molecules have different polarisabilities and $\Delta\varepsilon$ is now:

$$\Delta\varepsilon = \left(\frac{\partial\varepsilon}{\partial\rho}\right)\Delta\rho + \left(\frac{\partial\varepsilon}{\partial c}\right)\Delta c \tag{21}$$

The solute concentration being c. If the density and concentration fluctuations are independent of each other, then the average dielectric constant fluctuation is:

$$\overline{\Delta\varepsilon^2} = \left(\frac{\partial\varepsilon}{\partial\rho}\right)^2\overline{\Delta\rho^2} + \left(\frac{\partial\varepsilon}{\partial c}\right)^2\overline{\Delta c^2} \tag{22}$$

For a dilute solution, the density fluctuations are nearly identical to those of the pure solvent. The excess scattering arising from the introduction of a solute therefore only due to the concentration fluctuations. The excess Rayleigh ratio being:

$$\Delta R_\theta = R_{\theta,solution} - R_{\theta,solvent} = \frac{\pi^2 \partial V}{\lambda_0^4}\left(\frac{\partial\varepsilon}{\partial c}\right)^2\overline{\Delta c^2} \tag{23}$$

In Rayleigh scattering, the refractive index of the solute is similar to the solvent. The refractive index of the dilute solution can be expressed as a concentration series that is truncated at the 2nd term and squared:

$$n^2 = n_1^2 + 2n_1\left(\frac{\partial n}{\partial c}\right)c + \left(\frac{\partial n}{\partial c}\right)^2 c^2 \tag{24}$$

The refractive index of the solvent is n_1. The 3rd term on the right hand side of equation 24 is negligible and with the use of the Maxwell equation for refractive index ($n^2 = \varepsilon$) leads to:

$$\left(\frac{\partial \varepsilon}{\partial c}\right)^2 = 4n_1^2\left(\frac{\partial n}{\partial c}\right)^2 \tag{25}$$

The $\partial n/\partial c$ term is the specific refractive index increment of solute in solution. If the general theory of fluctuations is applied, then the mean-squared average concentration fluctuations are given by:

$$\overline{\Delta c^2} = \frac{kT}{\left(\partial^2 F/\partial c^2\right)_T} \tag{26}$$

From thermodynamic arguments, this lead to:

$$\left(\frac{\partial^2 F}{\partial c^2}\right) = -\frac{\delta V}{\overline{V}_1 c}\frac{\partial \mu_1}{\partial c} \tag{27}$$

The chemical potential and partial molar volume of the solvent in the solution are represented by μ_1 and $\overline{V}_1$ respectively. The combination of equations 23 and 25-27 lead to the value of the excess Rayleigh ratio of:

$$\Delta R_\theta = \frac{4\pi^2 n_1^2 kT\left(\partial n/\partial c\right)^2 \overline{V}_1 c}{\lambda_0^4\left(\partial \mu_1/\partial c\right)_T} \tag{28}$$

The chemical potential of the solvent is related to the osmotic pressure (π) by:

$$\pi \overline{V}_1 = -\left(\mu_1 - \mu_1^0\right) \tag{29}$$

The value $\mu_1{}^0$ is the chemical potential of the pure solvent. The insertion of equation 29 into 28 yields:

$$\Delta R_\theta = K\frac{RTc}{\partial \Pi/\partial c} \tag{30}$$

Where the optical constant K is;

$$K = \frac{4\pi^2 n_1^2}{\lambda_0^4 N_A}\left(\frac{\partial n}{\partial c}\right)^2 \tag{31}$$

The osmotic pressure can be expressed as a virial expansion in concentration:

$$\frac{\Pi}{c} = RT\left(\frac{1}{M} + A_2 c^2 + A_3 c^3 + ...\right) \tag{32}$$

Where A_2 and A_3 are the 2nd and 3rd virial coefficients. Insertion of equation 32 into equation 30 yields the final expression for the excess Rayleigh ratio:

$$\frac{Kc}{\Delta R_\theta} = \frac{1}{M} + 2A_2 c + 3A_3 c^2 + ... \tag{33}$$

This is the general equation of light scattering of vertically polarised light from a dilute solution. The equation yields the molar mass of the solute and the thermodynamic 2nd and 3rd virial coefficients. In a very dilute solution the 3rd virial coefficients can be ignored due to the negligible number of ternary contacts.

3.2.1.5 Light Scattering from Polymer Solutions

When the size of the solute molecules are greater than one twentieth of the incident light, then Debye scattering occurs. The angular distribution of the scattered light intensity is no longer symmetrical around the *zy* plane and the scattering intensity decreases as the angle increases from the incident direction. The lack of symmetry in the angular distribution of scattered light for large molecules, such as macromolecules, is due to intramolecular interference. Macromolecules can no longer be considered as a single point scatterer, but a series of point scatterers. Angular dissymmetry is described by the particle scattering factor $P(\theta)$, a function which is the ratio of real observed intensity of scattered light at a given angle to a theoretical intensity that would occur at the same angle without intramolecular interference. As intensity is related to the Rayleigh ratio, then the particle scattering factor is calculated by:

$$P(\theta)=\frac{\Delta R_\theta(Observed\ \ Intensity)}{\Delta R_\theta(Theoretical\ \ Intensity)} \tag{34}$$

The theoretical intensity is obtained by using equation 33. The function $P(\theta)$ has a value of unity at zero angle and decreases as angle increases. This behaviour necessitates the extrapolation of data back to zero angle for the determination of molecular weight, but also the geometry of the macromolecule. To determine an expression for $P(\theta)$ that is related to the geometric parameters of the macromolecule, the incident electromagnetic radiation is assumed to be uniform over the whole scattering particle and the molecule is represented by a set of dipoles. If one of these dipoles a distance r from the origin is considered (Figure 2), the electric field at this point is then:

$$E = E_0 \exp[i(\omega t - \boldsymbol{k}_0 r)] \tag{35}$$

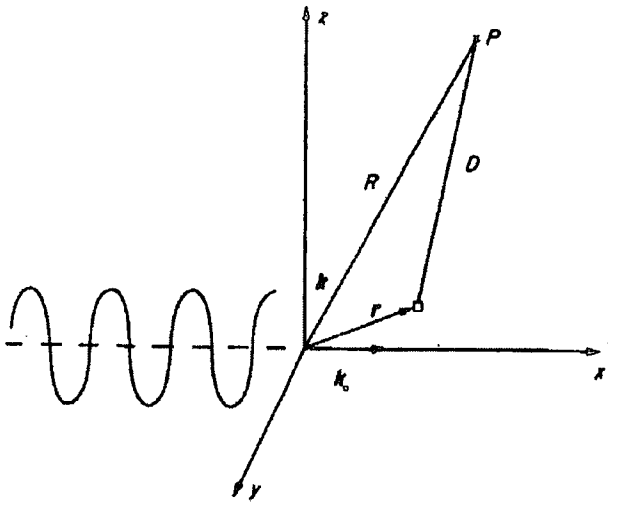

Figure 2: The scattering of vertically polarised radiation from a large scattering particle.

The wave vector of propagation of incident wave is $\boldsymbol{k}_0$. The scattered radiation at point P situated a distance D form the scattering centre has a electric field determined by the equation:

$$E_S \propto \frac{\exp(i\omega t)}{D}\exp[i(\boldsymbol{k}_0 r - k_0 D)] \tag{36}$$

The phase displacement of the electromagnetic wave at the scattering point with regards to the wave front at the origin is $\boldsymbol{k_0 r}$. As the function for $P(\theta)$ is only being determined, then constants can be ignored. As the distance D is far greater than distance r, then:

$$k_0 D = k_0 R - \boldsymbol{kr} \tag{37}$$

The value $\boldsymbol{k}$ is the wave vector in the direction P. Insertion of equation 37 into equation 36 yields:

$$E_s \propto \frac{\exp(i\omega t)}{R}\exp[-i(\boldsymbol{k_0} + k_0 R - \boldsymbol{kr})] \tag{38}$$

The modulus of the vector $q = |\boldsymbol{q}| = \boldsymbol{k_0} - \boldsymbol{k}$ is given by:

$$q = \frac{4\pi n}{\lambda_0}\sin\left(\frac{\theta}{2}\right) \tag{39}$$

This leads to equation 38 becoming:

$$E_S \propto \frac{\exp[i(\omega t - k_0 r)]}{R}\exp(i\boldsymbol{qr}) \tag{40}$$

The first term on the right hand side of equation 40 represents the light scattered from the origin and the second term ($exp(i\boldsymbol{qr})$) is the phase factor related to the interference effects between the emitted radiation from the two different dipoles. If m scattering centres are present, the electric field of the scattered radiation is given by:

$$E_S \propto \frac{\exp[i(\omega t - k_0 R)]}{R}\sum_{a=1}^{m}\exp(i\boldsymbol{qr}_a) \tag{41}$$

The intensity of the scattered radiation is the product of the electric field amplitude and its complex conjugate:

$$I \propto \sum_{a=1}^{m}\sum_{b=1}^{m}\exp[-i\boldsymbol{q}(\boldsymbol{r}_a - \boldsymbol{r}_b)] \tag{42}$$

In the absence of intramolecular interference at zero scattering angle, all the exponents in the equation 42 are zero, then

$$I \propto \sum_{a=1}^{m}\sum_{b=1}^{m} 1 = m^2 \tag{43}$$

Utilising the definition of $P(\theta)$ in equation 34, this leads to:

$$P(\theta) = \frac{1}{m^2}\sum_{a=1}^{m}\sum_{b=1}^{m} \exp[-iq(r_a - r_b)] = \frac{1}{m^2}\sum_{a=1}^{m}\sum_{b=1}^{m} \exp(-iqr_{ab}) \tag{44}$$

Equation 44 is the particle scattering factor for a molecule in fixed space. If the solution is isotropic, the particle will be free to choose any direction and the measured intensity will be average over all orientations. The Debye equation of $P(\theta)$ for a molecule averaged over all orientations is:

$$P(\theta) = \frac{1}{m^2}\sum_{a=1}^{m}\sum_{b=1}^{m} \frac{\sin qr_{ab}}{qr_{ab}} \tag{45}$$

Flexible macromolecules can vary their shape over time, with a change in distance r_{ab} and therefore a second average is required. From equation 45, the P(θ) will depend on the average conformation of the macromolecule and this dependence decreases as the distance qr_{ab} approaches zero. The use of the MacLaurin series for $qr_{ab} < 1$ leads to:

$$P(\theta) = \frac{1}{m^2}\sum_{a=1}^{m}\sum_{b=1}^{m}\left(1 - \frac{q^2 r_{ab}^2}{3!} + \frac{q^4 r_{ab}^4}{5!} - \cdots\right) \tag{46}$$

Considering only the first two terms, then:

$$P(\theta) = 1 - \frac{q^2}{6m^2}\sum_{a=1}^{m}\sum_{b=1}^{m} r_{ab}^2 \tag{47}$$

For a flexible macromolecule chain, the mean-square average radius of gyration $\langle R_G^2 \rangle$ is given by:

$$\left\langle R_G^2 \right\rangle = \frac{1}{2m^2} \sum_{a=1}^{m} \sum_{b=1}^{m} \left\langle r_{ab}^2 \right\rangle \tag{48}$$

Equations 39, 47 and 48 lead to $P(\theta)$ being expressed as:

$$P(\theta) = 1 - \frac{q^2 \left\langle R_G^2 \right\rangle}{3} = 1 - \frac{16\pi^2}{3\lambda_0^2} \left\langle R_G^2 \right\rangle \sin^2\left(\frac{\theta}{2}\right) \tag{49}$$

For this condition of $qR_G<1$, the mean-square average radius of gyration of a macromolecule is independent of molecular shape. The limiting slope of a line of $P(\theta)$ versus $sin^2(\theta/2)$ is $-16\pi^2<R_G^2>/3\lambda_0^2$, enabling calculation of $<R_G^2>$. This method can only be used when the dimensions of the macromolecule are similar to or greater than $\lambda/20$. Increasing the dimensions of the particles in such that the condition $qR_G < 1$ no longer applies, making equation 49 is no longer valid to calculate R_G. The function $P(\theta)^{-1}$ is a non-linear in $q^2<R_G^2>$ and has a curvature characteristic of the scattering particle shape. Debye's general formula (equation 45) can be used to calculate $P(\theta)$ for all general particle types. Three common derived $P(\theta)$ functions are for monodisperse linear random coils (Gaussian chains), infinitely thin rods, and homogeneous spheres. Figure 3 represents the $P(\theta)^{-1}$ versus $q^2<R_G^2>$ for the three particle types. All functions have a common tangent at $q^2<R_G^2> < 1$, with a slope of 1/3. Asymptotic behaviour is observed for these functions at large values of $q^2<R_G^2>$. For homogeneous spheres of radius R, then the particle scattering function is (curve 1):

$$P(\theta) = \frac{9}{q^6 R^6} (\sin qR - qR\cos qR)^2 \tag{50}$$

The particle scattering function for a random (Gaussian) coils (curve 2) is:

$$P(\theta) = \frac{2}{\left(q^2 \left\langle R_G^2 \right\rangle\right)^2} \left[q^2 \left\langle R_G^2 \right\rangle - 1 + \exp\left(-q^2 \left\langle R_G^2 \right\rangle\right)\right] \tag{51}$$

The particle scattering function for a rigid rod (curve 3) is:

$$P(\theta)=\frac{2}{qL}\int_0^{qL}\frac{\sin u}{u}\partial u-\left[\frac{\sin(qL/2)}{qL/2}\right]^2 \qquad (52)$$

L is the contour length of the rod. The term $u = qkl$, where l and k are the distance between and the number of scattering centres respectively. The integral of equation 52 cannot be solved in an analytical way, but values have been tabulated.

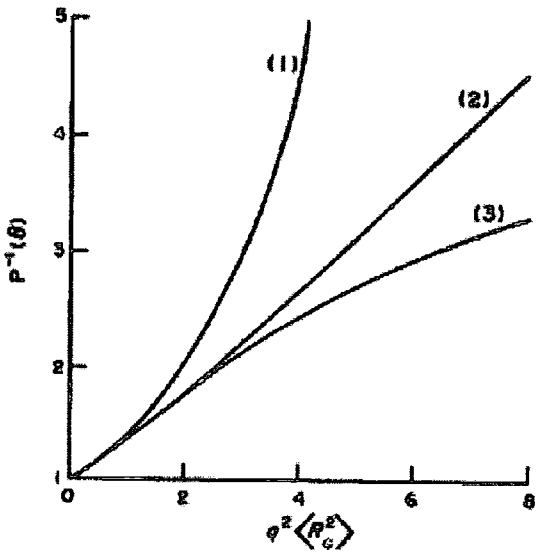

Figure 3: $P^{-1}(\theta)$ as a function of $q^2<R_G^2>$ for basic particle shapes of sphere (1), random coils (2) and rod (3).

Branching in macromolecules affect the size and shape of the particles in solution compared to a linear polymer of equal molecular weight. Highly branched polymer molecules can be approximately described as spherical particles. The particle scattering function for branched polymers is characterised by an upward curve in Figure 3. The curve is found in-between linear coils and spherical particles. Branching in polymer chains can produce polydisperse systems, which causes the $P(\theta)^{-1}$ function to bend downwards a random coil. The coupled effects of branching and polydispersity obscures the interpretation of $P(\theta)$. To limit the degree of branching and reduce the effects of polydispersity, star polymers have been developed with monodisperse arms attached to a single branch point. A particle scattering function was derived by Benoit[3] for a regular star polymer with f monodisperse arms, which obeys unperturbed Gaussian statistics:

$$P(\theta)=\frac{2}{fV^2}\left[V-(1-\exp(-V))+\frac{f-1}{2}(1-\exp(-V))^2\right] \quad (53)$$

The term V in equation 53, where $U = q^2<R_G^2>$, is:

$$V=\frac{f}{3f-2}U^2 \quad (54)$$

Most polymeric systems are disperse and this produces average values for molecular weight and radius of gyration obtained from light scattering studies. The intensity of light scattered from a polydisperse system is the sum of the intensities scattered from the molecular weight species (i):

$$\Delta R_\theta = K\sum_i c_i M_i P_i(\theta) \quad (55)$$

$P_i(\theta)$ is the particle scattering factor for the isomolecular species i. K is the optical constant of the scattering system. Equation 55 can be rewritten as:

$$\Delta R_\theta = K\sum c_i \frac{\sum c_i M_i}{\sum c_i}\frac{\sum c_i M_i P_i(\theta)}{\sum c_i M_i} \quad (56)$$

This leads to equation 56 being represented as:

$$\Delta R_\theta = Kc\bar{M}_W \overline{P(\theta)}_z \quad (57)$$

Equation 56 has a term for the weight average molecular weight ($\bar{M}_W$) of the polymer and the z-average particle scattering factor:

$$\overline{P(\theta)}_z = \frac{\sum_i c_i M_i P_i(\theta)}{\sum_i c_i M_i} \quad (58)$$

Substituting for $P_i(\theta)$ from equation 49 yields:

$$\overline{P(\theta)_z} = 1 - \frac{q^2}{3}\frac{\sum_i c_i M_i \left\langle R_G^2 \right\rangle_i}{\sum_i c_i M_i} \tag{59}$$

The final equation for Debye scattering of vertically polarised light for polydisperse macromolecules is:

$$\frac{Kc}{\Delta R_\theta} = \frac{1}{\overline{M}_W}\left(1 + \frac{16\pi^2}{\lambda^2}\overline{\left\langle R_G^2 \right\rangle}_z \sin^2\left(\frac{\theta}{2}\right)\right) + 2A_2 c \tag{60}$$

Equation 60 allows the determination of the weight average molecular weight and the mean-square z-average of the radius of gyration of the polymers dissolved in solution. To ascertain the $\overline{M}_W$, $\langle R_G^2 \rangle_z$ and A_2, a Zimm plot is used. The Zimm plot is a graphical representation of the light scattering data obtained from the standard light scattering equation:

$$\frac{Kc}{\Delta R_\theta} = \frac{1}{\overline{M}_W P(\theta)} + 2A_2 c \tag{61}$$

The second virial coefficient is obtained by plotting the scattering data for each concentration and extrapolating back to zero angle:

$$\left(\frac{Kc}{\Delta R_\theta}\right)_{\theta=0} = \frac{1}{\overline{M}_W} + 2A_2 c \tag{62}$$

The radius of gyration is obtained by plotting the light scattering data for each angle and extrapolating back to zero concentration:

$$\left(\frac{Kc}{\Delta R_\theta}\right)_{c=0} = \frac{1}{\overline{M}_W} P(\theta)^{-1} \tag{63}$$

The common intercept of the two plots yields the weight average molecular weight. The two plots can be represented on the same graph, where $Kc/\Delta R_\theta$ values are plotted against $kc + sin^2(\theta/2)$ values (k is an arbitrary constant to yield a spread of data points).

3.2.1.6 Effects of Optical Anisotropy

Up to now, all the scattering particles have been considered to be optically isotropic. Optical anisotropy occurs when the particles have fluctuating orientations that lead to additional scattering. The expression for the Rayleigh ratio that allows for these anisotropic particles is:

$$R_\theta = R_\theta^{iso} C(\theta) \tag{64}$$

R_θ^{iso} is the Rayleigh ratio for scattering from isotropic particles and $C(\theta)$ is a factor depending upon the depolarisation ratio. The depolarisation ratio for vertically polarised light is defined as the ratio of the horizontally polarised component (H_V) to the vertically polarised component (V_V) of the scattered radiation:

$$\rho_V = \frac{H_V}{V_V} \tag{65}$$

The depolarisation ratio can be measured at any angle, but it is usually at 90°. The Rayleigh ratio for system of anisotropic particles is given by:

$$R_{\theta,V} = R_{\theta,V}^{iso} \frac{3+3\rho_V}{3-(4+7\cos^2\theta)\rho_V} \tag{66}$$

For observation angle of 90°, the Rayleigh ratio is:

$$R_{90,V} = R_{90} \frac{3+3\rho_V}{3-4\rho_V} \tag{67}$$

This correction factor is known as the Carbannés factor. Many solvents, particularly aromatic solvents are anisotropic, but their effect on optical anisotropy is reduced due to the subtraction of scattering of pure solvent from the solution to obtain the excess Rayleigh ratio (ΔR_θ). The anisotropy of the repeating units can lead to the anisotropy of the polymer as a whole. The more anisotropic the repeating unit, the greater the anisotropy of the resultant polymers. Rod like and highly stereoregular polymers have high levels of anisotropy. The majority of synthetic polymers tend to assume coil formations in solution, the optical anisotropy of these species are quite low and the Carbannés factor is close to unity. The effect of optical anisotropy can be ignored for most polymers, except when very precise molecular weights are required.

3.2.1.7 Specific Refractive Index Increment.

The specific refractive index increment (*dn/dc*) is an important characteristic of the polymer-solvent system being used at a given temperature. The optical constant K is related to the square of the refractive index increment and a high value yields greater intensity of scattered light for a given polymer concentration. The *dn/dc* is the slope of the dependence of the refractive index of the solution on the polymer concentration at a given concentration. In dilute solutions, it is a constant approximated by the ratio $\Delta n/c$, where Δn is the difference of the refractive index values of solution and pure solvent. The value of Δn can be determined by using the technique of differential refractometry, by using the equation:

$$\Delta n = k\Delta d \tag{68}$$

The measured different displacements by the refractometer between solution and solvent is Δd and k is a constant for the apparatus for a particular wavelength. A range of Δn values with concentration leads to the determination of *dn/dc*. The specific refractive index increment is dependent on the wavelength of light used. A decrease in wavelength causes an increase in specific refractive index increment. Temperature also plays a role, where as a rule *dn/dc* increases with temperature. A molecular weight dependence of *dn/dc* is often observed, but for molecular weights of *circa* 2×10^4 g mol^{-1}and above, the values of *dn/dc* are constant.

3.2.2 Dynamic Light Scattering

3.2.2.1 Introduction

The measurement of the angular light intensity from scattering molecules within solution, can lead to the determination of global properties such as the $\bar{M}_W$, R_G and A_2. The detected light intensity is an average over all the particles within the scattering volume and is a measurement of a steady state or static phenomenon. Dynamical motion of the molecules in solution cause a small frequency broadening of the spectrum of scattered light. Frequency broadening is due to small intensity fluctuations that can be analysed by the technique of dynamic light scattering.[4,5] Dynamic properties of the scattering particles such as the translational diffusion coefficient and hydrodynamic radius can be obtained. This type of light scattering is a quasi-elastic process as it measures the small frequency changes of the incident to the scattered electromagnetic radiation. Inelastic light scattering techniques of Raman spectroscopy, fluorescence and phosphorescence have frequency shifts in the range of GHz to PHz, where quasi-elastic scattering has frequency shifts in the range of Hz to MHz. The technique of dynamic light scattering is also known as quasi-elastic light scattering and photon correlation spectroscopy.

Intensity fluctuations arise due to the interference of scattered electromagnetic radiation from moving particles. The intensity of the scattered radiation is not only obtained by the summation of the electric field amplitudes and hence intensity of each wave, but also by the relative phase of the waves to each other. The combination of two scattered waves of equal electric field amplitude and phase leads to constructive interference and enhanced intensity. On the other hand, if the two waves are totally out of phase with each other, total destructive interference occurs and no intensity is measured. The addition of two waves with a phase difference between these two extremes, can lead to a range of intensities. If the electromagnetic radiation originates from a source (usually a laser) at the speed of light, a series of parallel planes of equal phase can be imagined (see Figure 4). These planes transverse from source (S) to particles to detector (D) by different paths, so when the electromagnetic radiation reaches the detector with phase differences, then interference is evident. When the scattering particles lie exactly on the planes of equal phase, this yields total constructive interference. If the particles are near or midway between the planes, then

destructive interference occurs. The translational motion of the particles between the planes causes intensity fluctuations to be measured at the detector. The orientation and spacing of the planes is determined by the geometry and the wavelength of incident light. The planes are orientated so that the incident and scattered light make equal angles with them. If the planes are viewed as maxima of a cosine wave, the wavevector ($q = |\mathbf{q}|$) of that wave has a magnitude of:

$$q = \frac{4\pi n}{\lambda_0} \sin\left(\frac{\theta}{2}\right) \tag{69}$$

The refractive index of the solution is n, λ_0 is the wavelength of the incident light in a vacuum and θ is the scattering angle measured from the incident direction.

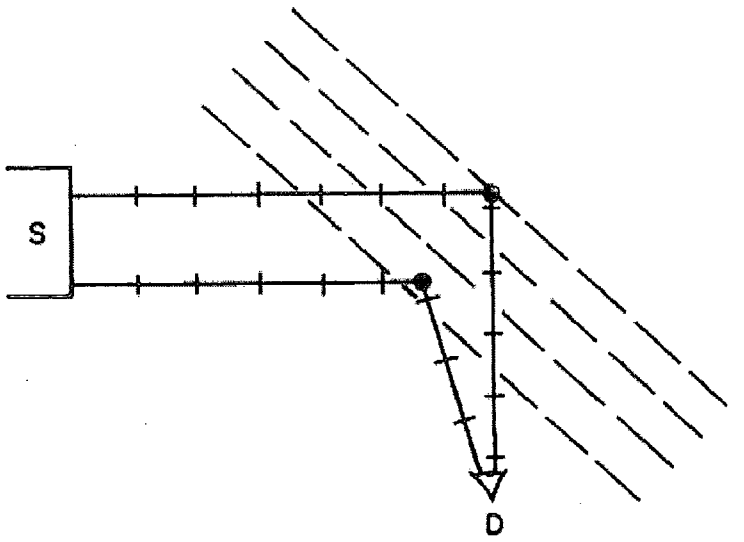

Figure 4: Phase of light along different paths in a light scattering experiment.

The count of the total number of particles on the planes of constant phase relative to the total number of particles midway between the planes, corresponds mathematically to a spatial Fourier transform of the particle number intensity with wave vector q. The scattering intensity is proportional to the q^{th} spatial Fourier component of the particle concentration. The scattering solution macroscopically appears homogeneous, but microscopically inhomogeneous due to concentration fluctuations. These concentration fluctuations are due to random Brownian motion of the molecules, with a rate of motion determined by the diffusion coefficient. The scattering particles exist in a concentration gradient caused either

by thermal fluctuations or external interventions, which if they are of equal size, relax in the same way. A solution with a concentration fluctuation at one value of $\boldsymbol{q}$ has the form:

$$c(\boldsymbol{r},t) = c_0 + a_q(t)\cos(\boldsymbol{q}\cdot\boldsymbol{r}) \tag{70}$$

The value $c(\boldsymbol{r},t)$ is the concentration at position $(\boldsymbol{r},t)$ and $a_q(t)$ is the amplitude of the $\boldsymbol{q}^{th}$ spatial Fourier component of the concentration. On the average, $c(\boldsymbol{r},t)$ relaxes over time according to Ficks Law:

$$\boldsymbol{J}(\boldsymbol{r},t) = -D_T \nabla c(\boldsymbol{r},t) \tag{71}$$

D_T is the translational diffusion coefficient, $\boldsymbol{J}$ being the diffusion current and ∇ is nabla function related to the diffusion of a substance of concentration, c, through a volume element defined by x, y and z coordinates:

$$\nabla = \frac{\partial^2 c}{\partial x^2} + \frac{\partial^2 c}{\partial y^2} + \frac{\partial^2 c}{\partial z^2} \tag{72}$$

Combining Ficks Law with the continuity equation yields:

$$\frac{\partial c(\boldsymbol{r},t)}{\partial t} = -\nabla \cdot \boldsymbol{J}(r,t) \tag{73}$$

This yields for $a_q(t)$:

$$\frac{\partial a_q(t)}{\partial t} = -D_T q^2 a_q(t) \tag{74}$$

The solution of equation 74 is:

$$a_q(t) = a_q(0)\exp(-D_T q^2 t) \tag{75}$$

The scattered field simply tracks $a_q(t)$ and if the scattered intensity is initially bright then I(t) decays exponentially with a decay constant $2D_T q^2$.

3.2.2.2 Correlation Functions

Correlation functions provide a concise method for expressing the degree in which two dynamical properties, such as the motion of two scattering particles are correlated over time.[6] A property A is considered that is dependent on the positions and momenta of all the particles in the system. The particles are in random motion due to thermal fluctuations and their positions and momenta are changing over time. This causes a variation in property A and the time dependence will resemble a noise pattern. The measurement of the bulk property of a equilibrium system is simply a time average:

$$\overline{A}(t_0,T)=\frac{1}{T}\int_{t_0}^{t_0+T}\partial tA(t) \tag{76}$$

The initial time of measurement is t_0 and T is the total time the measurement is made. The time average only becomes meaningful when the period of fluctuation is much smaller than the total time of measurement. If the time average is measured over a infinite length of time and independent of t_0, then:

$$\langle A\rangle=\lim_{T\to\infty}\frac{1}{T}\int_{0}^{T}\partial tA(t) \tag{77}$$

If property A is measured at two separate times of t and $t + \tau$, then A will have two different properties. If τ is very small compared to the times typifying the fluctuations in property A, then the property $A(t)$ will be close to $A(t + \tau)$. As τ increases, the deviation between these two properties is more likely to be non-zero and will become more out of phase with each other. Overall, the property $A(t + \tau)$ is correlated to property $A(t)$ when τ is small, but this correlation is lost when τ becomes large relative to the period of fluctuation. The measure of this correlation of property A is the autocorrelation function, which is defined as:

$$\langle A(0)A(\tau)\rangle=\lim_{T\to\infty}\frac{1}{T}\int_{0}^{T}\partial tA(t)A(t+\tau) \tag{78}$$

The measurement time can be divided into discrete intervals Δt, so that $t = j\Delta t$, $\tau = n\Delta t$, total time $T = N\Delta t$ and $t+\tau = (j+n)\Delta t$. If property A varies little over the discrete time interval, then equations 77 and 78 can be represented by:

$$\langle A \rangle \cong \lim_{N\to\infty} \frac{1}{N} \sum_{j=1}^{N} A_j \tag{79}$$

and;

$$\langle A(0)A(\tau) \rangle \cong \lim_{N\to\infty} \frac{1}{N} \sum_{j=1}^{N} A_j A_{j+n} \tag{80}$$

A_j is the value of the property in the j^{th} interval. During dynamic light scattering experiments, a correlator computes the autocorrelation functions of the scattered field by using discrete time intervals. For the dependence of the correlation function with time, the property is measured initially at time zero, i.e. $<A(0)A(0)>$. At this point, the sum of the properties will be large ($A_j^2 > 0$) and therefore:

$$\sum_{j=1}^{N} A_j^2 \geq \sum_{j=1}^{N} A_j A_{j+n} \tag{81}$$

or;

$$\langle A(0)^2 \rangle \geq \langle A(0)A(\tau) \rangle \tag{82}$$

At time zero, the two properties are in phase with each and the autocorrelation function has a maximum value. For a non-conserved non-periodic property, the two properties start to have a phase difference and the autocorrelation function decays from its initial value $<A^2>$. For times τ greater than the characteristic time of the fluctuation of A, $A(t)$ and $A(t + \tau)$ become totally uncorrelated and out of phase, so that:

$$\lim_{\tau\to\infty} \langle A(0)A(\tau) \rangle = \langle A(0) \rangle \langle A(\tau) \rangle = \langle A \rangle^2 \tag{83}$$

The time-correlation function of a non-periodic property decays from $<A^2>$ to $<A>^2$ over time (see Figure 5). The autocorrelation function decays like a single exponential so that:

$$\langle A(0)A(\tau)\rangle = \langle A\rangle^2 + \left\{\langle A^2\rangle - \langle A\rangle^2\right\}\exp\frac{-\tau}{\tau_r} \tag{84}$$

The relaxation time or correlation time of the property is τ_r.

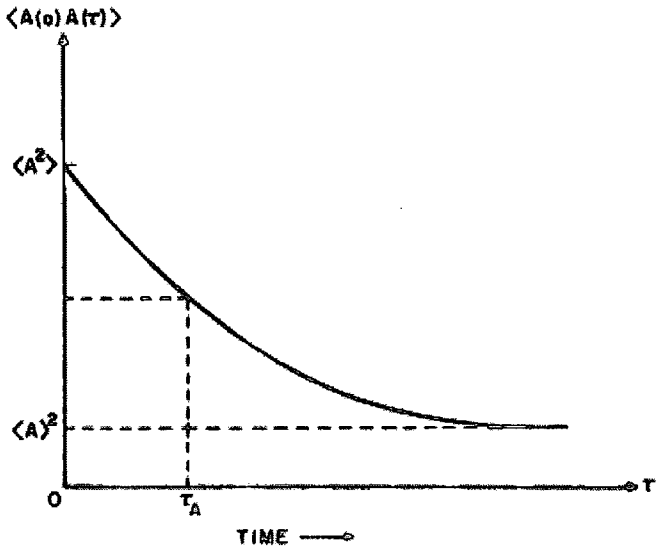

Figure 5: The time correlation function, <A(0) A(τ)>.

3.2.2.3 Measurement of Intensity Fluctuations by Correlation Functions

The dynamical motion of scattering particles can be ascertained by measuring the scattered intensity over time using a digital correlator. Two optical mixing techniques of heterodyne and homodyne have been developed.[7] Heterodyne mixing is when the scattered radiation is mixed with an unscattered reference beam, that is shifted or unshifted in frequency from the incident light beam. In homodyne mixing the scattered beam is not mixed with a reference signal but is directly detected Most experimental arrangements use the less complicated homodyne technique. The intensity-intensity autocorrelation function measured using the homodyne technique is:

$$G(\tau) = \lim_{T\to\infty}\frac{1}{2T}\int_{-T}^{T} I(t)I(t+\tau)\partial t \tag{85}$$

Where T is now the integrating time. Dynamic light scattering is intrinsically a two photon experiment, where a non-zero contribution to $I(t)I(t+\tau)$ requires an observation of photons at two times. The critical parameter is the number of photons received during the decay time within a single coherence area. A coherence area is defined as the limiting diffraction area at the detector over which the scattering volume does not change significantly. The coherence area is inversely proportional to the cross-section of the scattering volume. Focussing the light beam into the scattering cell or by using a small aperture on the detector can increase the coherence area.

The low intensity scattered radiation is measured by a photomultiplier and the photon count analysed by a digital correlator. The digital correlator is divided into channels of finite time that is determined by the operator and correlators with up to 1024 channels have been used. The delay times between each of the channels can be spaced linearly or logarithmically. A linear-correlator separates out the channel spacing by equal time, where logarithmic-correlator distributes the channel spacing exponentially in time. The time range of the correlator can be extended further by dividing the correlator up into separate regions, that can have either a linear or logarithmic time scale. Extended channels at high delay time are used to measure the baseline of the correlation function. The digital correlator is a signal comparator with a shift register. The incoming scattered photons are measured by the input counter and the total counts in that sample time are passed into a shift register. All the other counts in the shift register then move along by one and the contents of the last shift channel are discarded. The number of counts in the first shift register channel is then multiplied by the number of counts in each of the other shift register channels in turn and then each product being added to the appropriate store channel. The number of counts at the next sample time is treated the same way and so on to build up a decaying correlation function.

3.2.2.4 Data fits to Correlation functions

The correlograms obtained from the digital correlator are fitted to determine the dynamic properties. For a monodisperse particles undergoing Brownian motion, the single exponential decay correlation function ($G(\tau)$) with delay time (τ) is:

$$G(\tau) = A\left[1 + B\exp\left(-2D_T q^2 \tau\right)\right] \tag{86}$$

D_T is the translational diffusion coefficient of the species and q is the wavevector. A least-squares fit to equation 86 using A as the baseline measurement of the correlation function at infinte time ($G(\infty)$) and B as the intercept of the correlation function. For polydisperse systems such as polymer molecules, single exponential decay can no longer be applied due to the range of diffusing species. This system requires difficult multi-exponential fitting and an alternative method is that of Cumulants[8]. The correlation function is expanded in terms of a power series:

$$\frac{1}{2}\ln[G(\tau)-G(\infty)] = C_0 - K_1\tau + \frac{1}{2!}K_2\tau^2 - \frac{1}{3!}K_3\tau^3 + ... \tag{87}$$

The cumulants of the expansion are K_1, K_2 and K_3, where they represent the average diffusion constant, the distribution of the diffusion constants, the skewness of the distribution, etc. It is difficult to obtain accurate values of the moments greater than the second moment and the expansion is truncated:

$$G(\tau) = A + B\exp\left(-2K_1\tau + K_2\tau^2\right) \tag{88}$$

A is the baseline of the correlation function obtained experimentally and B is a fitting variable. The average translational diffusion coefficient and polydispersity of the system are determined from the cumulant values K_1 and K_2:

$$K_1 = \langle\Gamma\rangle \tag{89}$$

and;

$$K_2 = \left\langle\left(\Gamma - \langle\Gamma\rangle\right)^2\right\rangle \tag{90}$$

The average translational diffusion coefficient is obtained form the decay constant, Γ:

$$\Gamma = D_T q^2 \tag{91}$$

For random-coil polymers, dynamic light scattering is sensitive to internal polymer motions, as well as translational centre of mass motion. Dynamic light scattering only measures the translational diffusion coefficient if $qR_G < 1$.

3.2.3 Solution Viscometry

The viscosity of a polymer solution has the important characteristic of always being greater than the pure solvent. This viscosity difference arises from the greater size of macromolecules compared to solvent molecules and still has significance even at low solute concentrations. The technique of dilute solution viscometry allows the accurate quantitative measurement of the increase in viscosity of a solution from a pure solvent at a given temperature.[9-11] Information can then be obtained on the molecular weight, size of the polymer molecule in solution, the hydrodynamic volume and polymer-solvent interactions.

The viscosity of a fluid is a measure of its resistance to flow when a shearing force is applied. The fluid is considered to be a series of parallel layers, that each have an area A, separated by a distance dz. A force is applied to a single layer that causes it to move with a velocity (v). Frictional forces exist between the fluid molecules and some of the energy supplied by the force is imparted on all the other layers. This causes a viscous drag on the second layer and moves with a velocity, v-dv. If all the layers move in parallel with the velocities below a critical value, the viscous flow is laminar. The variation of the shear strain (γ) with time is known as the shear rate ($\dot{\gamma} = d\gamma/dt$) and is equal to the velocity gradient (dv/dz). For the laminar flow of a Newtonian fluid, the shear rate is proportional to the shear stress ($\tau = F/A$) and the proportionality constant is known as the viscosity (η) of the fluid:

$$\tau = \eta\dot{\gamma} \tag{92}$$

Newtonian behaviour is observed for most dilute polymer solutions, but a reduction in apparent viscosity with increasing shear rate can lead to non-Newtonian behaviour. Absolute measurements of viscosity are not essential in dilute solution viscometry, as it is only necessary to determine the viscosity of a solution relative to the pure solvent. Viscosity measurements are achieved by determining the flow times of each respective fluid through a capillary viscometer. The viscosity of a liquid passing through the capillary under steady laminar flow is described by Poiseuille's equation:

$$\frac{V}{t} = \frac{\pi r^4 P}{8\eta l} \tag{93}$$

Equation 93 describes the flow time (t) of a volume of the liquid (V) flowing through a capillary of specific length (l) and radius (r). The pressure difference across the capillary is P. The velocity profile of the liquid is parabolic across the capillary, with maximum velocity along the axis and zero velocity at the wall. During the flow time measurements, the pressure difference across the capillary varies and is represented as:

$$p = \langle h \rangle \rho g \tag{94}$$

The average pressure head is $<h>$, ρ is the density of the liquid and g is the acceleration due to gravity. Hence Poiseuilles equation can be re-written as:

$$\eta = \frac{\pi r^4 \langle h \rangle g \rho t}{8Vl} \tag{95}$$

Corrections must be applied to equation 95 as it neglects energy dissipated by imparting kinetic energy to the liquid and the flow into and out of the capillary. Equation 95 is re-written, with constants A and B for a particular viscometer:

$$\eta = A\rho t - \frac{B\rho}{t} \tag{96}$$

During dilute solution viscometry experiments, the relative increase of viscosity of solution to solvent is measured. The density of solution and pure solvent are considered to be equal and if the kinetic energy correction is negligible, so that the relative viscosity is:

$$\eta_r = \frac{t}{t_0} \tag{97}$$

The flow times of the solution and pure solvent are t and t_0 respectively. As the relative viscosity approaches unity at infinite dilution, the specific viscosity is usually defined:

$$\eta_{sp} = \eta_r - 1 = \frac{t - t_0}{t_0} \tag{98}$$

The specific viscosity is a measure of the increase of the solution viscosity due to the addition of polymer to pure solvent. The ratio of η_{sp}/c, where c is concentration is the specific capacity of the polymer to increase the relative viscosity. At the limit of infinite dilution, this specific viscosity ratio (the reduced viscosity) is known as the intrinsic viscosity:

$$[\eta] = \left(\frac{\eta_{sp}}{c} \right)_{c \to 0} \tag{99}$$

The concentration dependence of η_{sp}/c can be represented as:

$$\frac{\eta_{sp}}{c} = [\eta] + k_1 [\eta]^2 c + k_2 [\eta]^3 c^2 + ... \tag{100}$$

In polymer solutions where $[\eta]c < 1$, the Huggins equation can be used:

$$\frac{\eta_{sp}}{c} = [\eta] + k_H [\eta]^2 c \tag{101}$$

The Huggins constant (k_H) is related to the size and shape of the polymer molecules and to the hydrodynamic interactions between different segments of the same polymer molecule. The Huggins constant is independent of molecular weight, with values between 0.3 for a good solvent to 0.5 for a poor solvent. Values of k_H greater than 0.5 are usually due to aggregation. The intrinsic viscosity and Huggins constant are obtained by measuring a series of solutions with a range of polymer concentrations and pure solvent as well to obtain the specific viscosity. A plot of η_{sp}/c versus c yields these values. Modified Ubbelohde viscometers are used to obtain the specific viscosity.

3.3 Experimental

3.3.1 Refractive Index Measurements

Refractive indices of the solvents used during static and dynamic light scattering experiments were measured with a ABBE 60 series refractometer. A spectral lamp was used as the light source and wavelengths filters were available of 644 nm, 546 nm and 436 nm. Temperature control over the refractometer prism was maintained by a Grant water bath/circulator. The instrument employs the critical angle effect marked by a demarcation line between dark and light portions of a telescope field, where the demarcation line is generally known as the borderline. The ABBE refractometer consists of a measuring prism that sits on a glass plate. Beneath the glass plate is a rotating mirror that reflects the refracted light from the prism into the field telescope.

A small quantity of liquid was placed in between a glass plate and the calibrated prism. A borderline between the light and dark regions can be seen within the telescope, and the mirror was rotated until the crosshair of the telescope reaches the borderline. The movement of the crosshair yields a scale reading and with the use of calibration tables, the refractive index of the liquid was ascertained. The refractive index for cyclohexane at a temperature of 298 K and at wavelengths of 488 nm and 632.8 nm was 1.429 and 1.422 respectively. Table 1 gives the refractive index values measured for toluene at a laser wavelength of 488 nm, determined over the temperature range of 298 K to 323 K. Table 2 gives the refractive indices measured for 1,4 dioxane over the same temperature range for laser wavelengths of 488 nm and 632.8 nm

Table 1: Refractive indices of toluene and dioxane for a laser wavelength of 488 nm over the temperature range of 298 K to 323 K.

Temperature (K)	Refractive index
298.0	1.509
299.5	1.508
303.0	1.506
308.0	1.504
313.0	1.501
323.0	1.495

Table 2: Refractive indices for 1,4-dioxane for laser wavelengths 488 nm and 632.8 nm over the temperature range of 298 K to 323 K.

Temperature (K)	$\lambda_0 = 488$ nm	$\lambda_0 = 632.8$ nm
298.0	1.431	1.417
299.5	1.430	1.416
303.0	1.429	1.415
308.0	1.427	1.413
313.0	1.425	1.411
323.0	1.421	1.406

3.3.2 Specific Refractive Index Increments

A Brice-Phoenix differential refractometer was used to obtain the specific refactive index increments (*dn/dc*) for the polymers within each solvent. The differential refractometer consisted of a spectral lamp, wavelength filters, an adjustable slit, a sample housing, a projector lens and a microscope, that were all positioned directly on one line. The sample housing contains a split quartz refractometer cell, which can be rotated by 180° for two measurement directions along the light beam. Thermal control over the sample housing was maintained by a Grant water bath/circulator. The wavelength filters available were 436 nm, 488 nm, 546 nm and 633 nm.

The specific refractive index increments (*dn/dc*) were measured for linear and star polymers in dioxane and cyclohexane. Polymer solutions were prepared in the concentration range 0.2 % to 2 % (w/v). The differential refractomer cell has two-compartments, where one was filled with pure solvent and the other with the polymer solution. A microscope reading (d_1) was taken with the cell in the first direction (d_1) and the cell was rotated by 180° for the second reading (d_2). The total displacement (Δd) was calculated by:

$$\Delta d = (d_2 - d_1) - (d_2^0 - d_1^0) \tag{102}$$

The readings d_1^0 and d_2^0 were for the pure solvent only in both cell compartments. The refractive index difference (Δn) was calculated by the total displacement by:

$$\Delta n = k\Delta d \tag{103}$$

The calibration constant k for each wavelength were determined from reported refractive index difference data for aqueous potassium chloride solutions.[12] A linear fit to the plot of Δn versus polymer concentration allows the determination of *dn/dc* form the gradient. The *dn/dc* value used for the linear polybutadienes LH50, LH100 and LH300 in cyclohexane was 0.112 ml g^{-1} and for the miktoarm star polymers S30, S60, S80 and S300 was 0.113 ml g^{-1}. The *dn/dc* values used for the linear and miktoarm star polymers in dioxane over the temperature range are listed in Table 3.

Table 3: Specific refractive index increments for linear and miktoarm star polymers in dioxane for a laser wavelength of 488 nm, over the temperature range 298 K to323 K.

Temperature (K)	LH50, LH100, LH300	S30, S60, S80	S300
	dn/dc (ml g^{-1})	*dn/dc* (ml g^{-1})	*dn/dc* (ml g^{-1})
298.0	0.117	0.093	0.097
299.5	0.117	0.094	0.098
303.0	0.117	0.098	0.100
308.0	0.118	0.103	0.104
313.0	0.119	0.108	0.108
323.0	0.121	0.119	0.115

3.3.3 Static Light Scattering

Static light scattering experiments were performed on a Malvern Instruments 4700c system, as shown in the schematic diagram in Figure 6. The apparatus consists of a goniometer, temperature controller, stepper motor controller, correlator and a computer. An argon-ion laser source was attached to a goniometer base, which housed the sample vat assembly and to this base was also attached a moveable arm with a photomultiplier detector. The argon-ion laser source has a wavelength in a vacuum of 488 nm and was air cooled by a fan to prevent overheating. Attached to the laser source was a lens focusing the monochromatic light beam onto the sample vat assembly. The vat assembly holds the sample cell, which sits inside a quartz trough containing a refractive index matching liquid. Burchard quartz sample cells (supplied by Hellma), with a diameter of 26 mm were used. The beam enters flat optical windows on the trough and the use of a refractive index matching liquid prevents flare within the assembly. Temperature was maintained in the vat assembly by the controller unit to an accuracy of ±0.1 K of the set value. A window within the vat assembly allows the detection of the scattered light by the photomultiplier. The photomultiplier was attached to a goniometer arm and the angle of detection was controlled by the stepper motor. The scattering angle could be accurately measured by the number of steps away from the reference sensor positioned at an angle of 10°. Each step away from the reference

position was 0.1° and this was the accuracy of angle measurement. Attached to the photomultiplier was a focusing lens and aperture selector. For the purpose of static measurements an aperture of 500 microns was selected. Intensity recordings, data analysis and control over experiment was by an computer using Malvern PCS version 1.35 software.

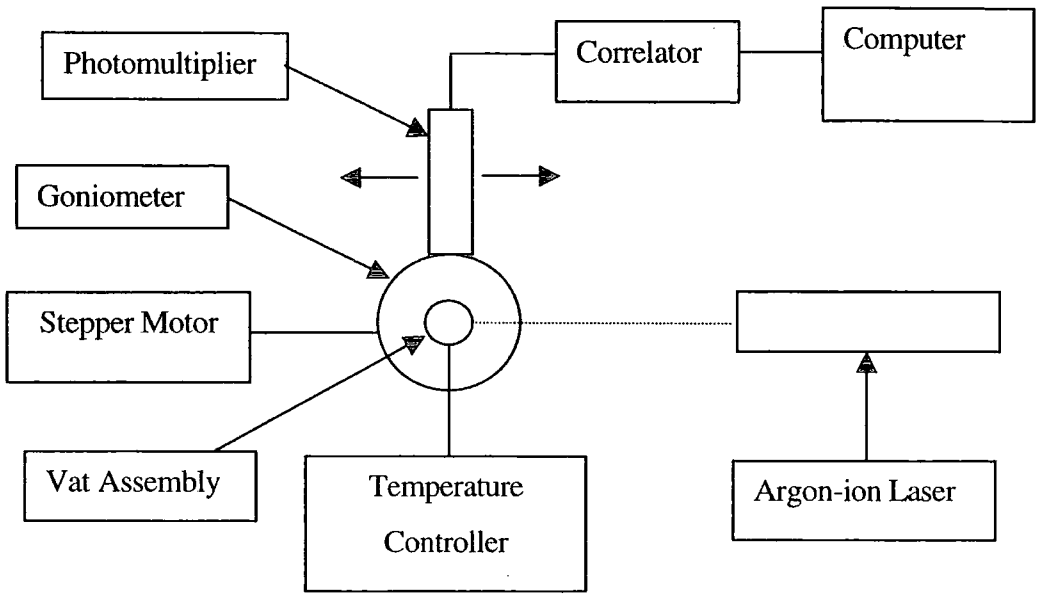

Figure 6: Schematic diagram of the Static Light Scattering Apparatus.

Static light scattering experiments were performed upon dilute polymer solutions of linear polybutadienes LH50, LH100 and LH300 and miktoarm star polymers S30, S60, S80 and S300 in cyclohexane and 1,4-dioxane. The solvents of 99.5 % pure "AnalaR" grade cyclohexane (supplied from BDH) or 99.9 % pure HPLC grade 1,4-dioxane (Aldrich) were used. The solvents were dried with 3A molecular sieve (Aldrich). Light scattering solutions were prepared inside a series of volumetric flasks, that had been cleaned of any dust or impurities. The volumetric flasks were washed with permanganic acid (sulphuric acid/potassium manganate VII), distilled water and dried inside a vacuum oven. Dilute polymer solutions were prepared with concentrations ranging from 0.1 % to 1.0 % (w/v), depending on molecular weight of polymer to be characterised. These solutions were diluted to produce a range of 5 polymer concentrations for each polymer-solvent system. The dioxane solutions were stored inside a water bath that was maintained at a temperature of 50 °C, to prevent precipitation of the polymer.

All light scattering samples were passed through a Millipore filter assembly containing a PVDF-Durapore (supplied by Millipore) filter membrane of pore size of 0.22 μm, into the Burchard light scattering cells. Filtering of samples was repeated until no dust could be seen in the laser beam. The cyclohexane solutions experiments were performed at a temperature of 298 K, measurements in 1,4-dioxane solutions were made over a temperature range of 298 K to 323 K. Spectroscopic grade toluene (Aldrich) was used as the calibrant and the Rayleigh ratio of this solvent at a laser wavelength of 488 nm and at a temperature of 298 K is 4.7×10^{-5} cm^{-1}. The static light scattering experiments were controlled by the computer with the use of Malvern PCS version 1.35 software. Experimental parameters such as the laser wavelength, the Rayleigh ratio, temperature and the refractive index of toluene and solvents could be entered into the software. The "Zimm plot" experiment was followed to obtain the global properties. Angular intensity scans were performed between 30° and 150° at 12° increments on the pure solvent and on the series of polymer concentrations. An intensity scan was also performed on the Rayleigh solvent at an angle of 90°. A background measurement was also taken in this angular range by closing the laser shutter. The Malvern software computed a Zimm plot and the weight-average molecular weight, radius of gyration and second virial coefficients were calculated.

The Malvern software produced values of $\bar{M}_W$, R_G and A_2 from computer generated Zimm plots. This software allowed no control over the spread of data in the Zimm plots and often flat plots were obtained, instead of the usual grid-like type. To facilitate the spread of data points, the $Kc/\Delta R_\theta$ values per scattering angle of each polymer concentration were extracted from the Zimm plot and imported into a Excel spread sheet. The data points were spread out by the alteration of arbitrary constant k. In the spread sheet, each polymer concentration was extrapolated back to zero scattering angle and each scattering angle was extrapolated back to zero concentration. This yielded zero angle and concentration $Kc/\Delta R_\theta$ values, that were extracted into a Microcal Origin work sheet and the Zimm plot was replotted (Figure 7). The zero-angle extrapolated data had $Kc/\Delta R_\theta$ values plotted against kc and a least-squares linear fit yielded $\bar{M}_W$ and A_2. The $\bar{M}_W$ was calculated from the reciprocal of the intercept of the graph and A_2 was from the gradient of the graph, using the equation:

$$A_2 = \frac{1}{2}(gradient)k \qquad (104)$$

The zero-concentration extrapolated data had $Kc/\Delta R_\theta$ values plotted against $sin^2(\theta/2)$ and a least-squares linear fit yielded $\overline{M}_W$ and R_G. The $\overline{M}_W$ was calculated from the reciprocal of the intercept of the graph and the R_G from the gradient of the graph, using the Debye equation:

$$R_G = \frac{\sqrt{3}}{4\pi}\frac{\lambda_0}{n}\left(\frac{(gradient)}{(\overline{M}_W)^{-1}}\right)^{\frac{1}{2}} \tag{105}$$

The $\overline{M}_W$ values from both graphs were identical. As the Rayleigh ratio of toluene used for all experiments was for 298 K, a correction factor was required for higher temperature data and applied to the $\overline{M}_W$ and A_2 values. These correction factors were calculated by the ratio of 90° scattering angle intensities of the Rayleigh solvent at a specific temperature to that obtained at 298 K.

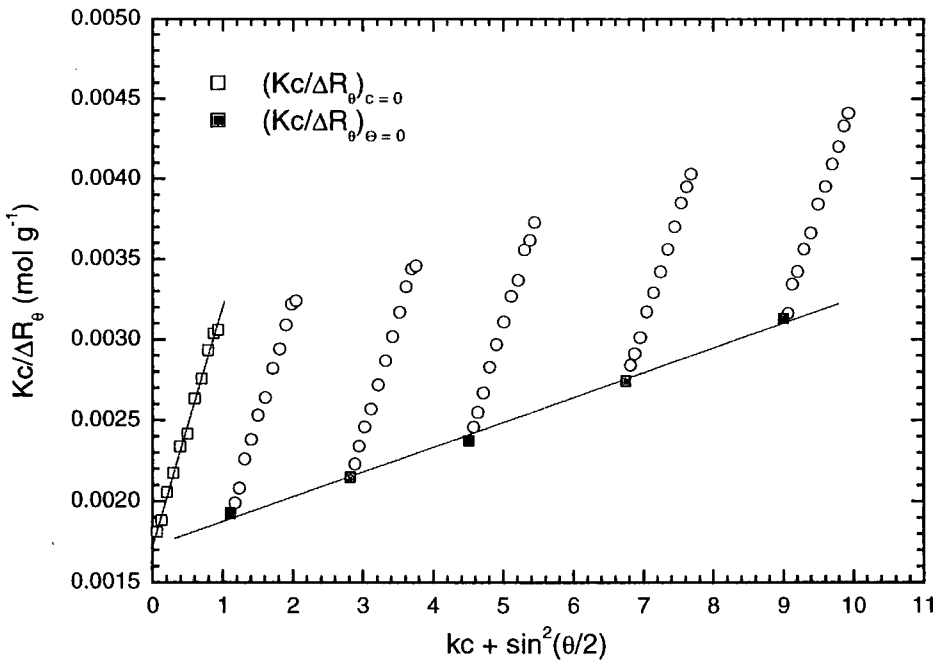

Figure 7: A Zimm Plot a of linear polymer within a good solvent.

3.3.4 Dynamic Light Scattering

Dynamic light scattering experiments were performed on a Brookhaven apparatus, which consisted of a spectrometer, a temperature control unit, a 128-channel digital correlator and a computer. The goniometer was identical to the one used in static light scattering experiments (see section 3.3.1.1), except for a He-Ne laser light source was used (λ_0 = 632.8 nm). The goniometer arm was fixed at a scattering angle of 90° and the photomuliplier had an aperture of 150 microns. Quartz sample cells (supplied from Hellma) of a diameter of 10 mm were used. A model BI-9000AT digital correlator with 128-channels was used to count intensity fluctuations and data were recorded on the computer. Brookhaven software was used to configure the correlator.

Dynamic light scattering experiments were performed on linear polybutadienes LH50, LH100 and LH300 and miktoarm star polybutadienes S30, S60, S80 and S300 in cyclohexane and dioxane. For cyclohexane a temperature of 298 K was used and for dioxane a temperature range of 298 K to 323 K was performed. Polymer solutions were prepared in volumetric flasks (cleaned as in section 3.3.3) and allowed to stand overnight. Dilute solutions were prepared in the concentration range of 0.1 % to 1.0 % (w/v), depending on molecular weight of polymer. The dioxane solutions were immersed in a water bath at a temperature of 50°C to prevent precipitation of the polymer. Polymer solutions were passed through a Millipore filter assembly containing a PVDF-Durapore (supplied by Millipore) membrane with a pore size of 0.22 μm, into the light scattering cells to remove any dust from the system. Repeated filtering was required if speckle from dust scattering could still be seen.

The 128-channel digital correlator was set up in linear mode and the delay time selected to produce an exponentially decaying correlation function with extended base line. Medium speed circuits were used and delay times of 5, 10 and 20 μs were applied, with final delay times of 640 μs, 1.28 ms and 2.56 ms, to produce correlation functions with flat baselines. Measured and calculated baselines (calculated from scattering intensity) were within >1% of each other. Total counts per channel were recorded and the data extracted from the computer. The total counts ($G(\tau)$) per sample time (τ) were measured and the data were imported into a Microcal Origin worksheet. The correlation function was fitted by

cumulants analysis (Figure 8) by using the non-linear-least squares curve fitting function of the worksheet. The cumulants equation applied to the curve fitting option was:

$$G(\tau) = A + B\exp\left(-2K_1\tau + K_2\tau^2\right) \tag{106}$$

The fitting parameters of the function were K_1, K_2 and B. The obtained baseline of the correlation function was A and was obtained during the measurement. The values K_1 and K_2 are the first and second cumulants of the function, where K_1 is related to the translational diffusion coefficient (D_T) of the polymer molecules in solution by:

$$K_1 = D_T q^2 \tag{107}$$

The wavevector q was calculated by equation 69.

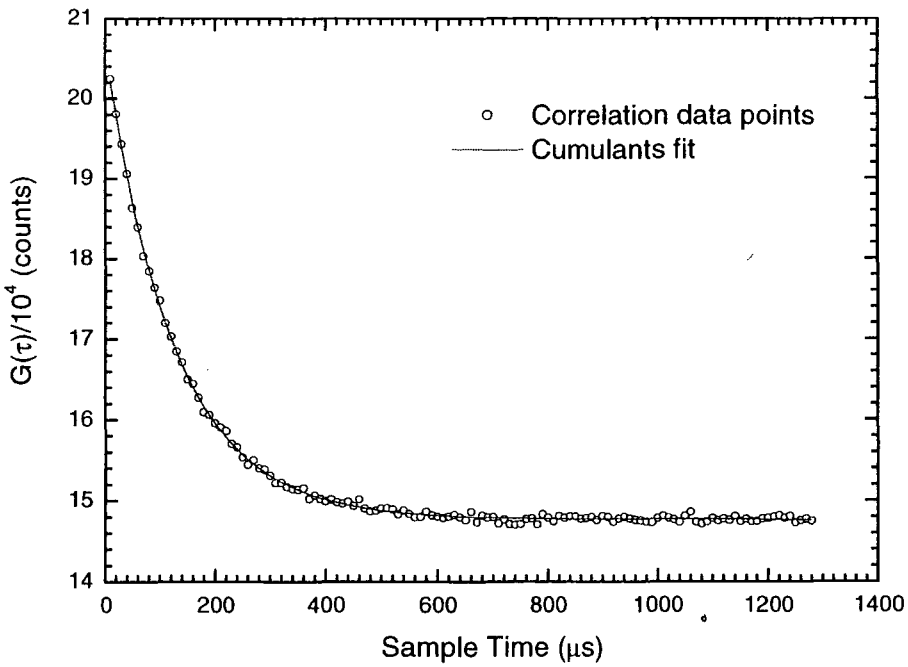

Figure 8: Correlation function and with a cumulants fit.

3.3.5 Solution Viscometry

Dilute solution viscometry experiments were performed on an automatic viscometer system, supplied by Schott. The apparatus consisted of a modified Ubbelohde viscometer, housed inside a temperature controlled water bath, with a viscosity measuring unit and an automatic burette attached to the viscometer. The glass Ubbelohde viscometer (see Figure 9) consisted of a capillary tube fixed above the reservoir vessel, with a venting tube positioned just below the capillary and a filling tube attached to the reservoir vessel. Above the capillary was a measuring sphere and a pre-run sphere.

The Ubbelohde viscometer I was used during these experiments with a capillary of diameter of 0.63 mm. The viscometer was housed vertically within a stand and the stand contained two photodiodes positioned above and below the measuring sphere. As the liquid was allowed to flow down the capillary, the timer of the viscosity measuring unit was started and stopped as the liquid meniscus passed the photodiodes. This yielded flow times of the liquid through the capillary. Polymer solutions within the reservoir vessel were diluted *in-situ* by use of an automatic burette. Polymer solutions were mixed thoroughly by the use of a magnetic stirrer contained within the water bath. The automatic viscometer can be programmed for initial solution concentration, the number of dilutions, volume of dilution and number of flow time measurements per concentration for each experiment. At the end of the experiment a print out of flow times per concentration was produced.

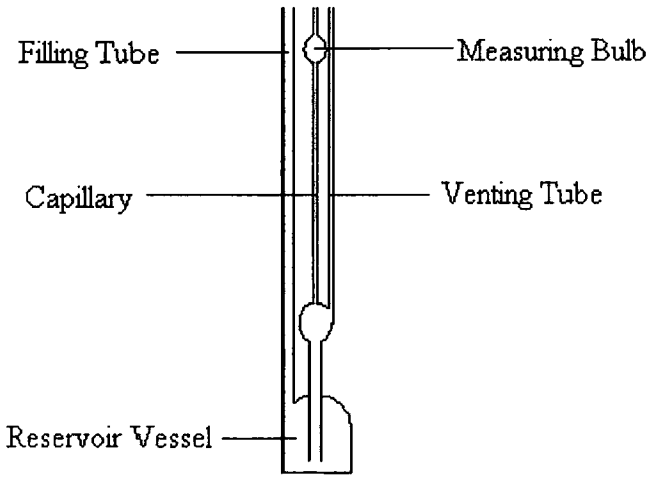

Figure 9: An UbbelohdeViscometer.

Dilute solution viscometry experiments were performed on linear polybutadienes LH50, LH100 and LH300 and miktoarm star polybutadienes S30, S60, S80 and S300 in cyclohexane (supplied by BDH) and 1,4-dioxane (Aldrich). The range of polymer concentrations for each experiment were tailored so that the highest concentration did not exceed a relative viscosity of 1.6. Samples were prepared in volumetric flasks (cleaned by permanganic acid) and the dioxane solutions were stored in a water bath, set at a temperature of 323 K. All solutions and solvents were passed through a Millipore filter assembly containing a PTFE-Fluoropore filter membrane of pore size of 0.5 μm, to remove any dust. The Ubbelohde viscometer was cleaned by passing permanganic acid, distilled water and methanol through the capillary and then dried under a flow of nitrogen.

The viscometer was placed inside the waterbath, set at the desired temperature and time was allowed for all solvents and solutions to reach thermal equilibration. The solution viscometry experiment began by the measurement of the flow times of the pure solvent. Flow times with a precision of 0.1 s were obtained. The viscometer capillary was dried again by a flow of nitrogen, a accurate volume of 15 ml of polymer solution was introduced into the viscometer reservoir vessel via a volumetric pipette and the viscometer was placed back into the waterbath. Experimental parameters were programmed into the automatic viscometer. During the experiment the polymer solution was diluted 5 times by 5 ml of pure solvent via the automatic burette. A delay time of 20 minutes was used after each dilution to allow for thorough mixing and coating of viscometer capillary with the solution. Flow times through the capillary were measured 10 times for each polymer concentration. At the end of all measurements, a print out of flow time per concentration was produced.

Viscometry flow time data were analysed with the use of a Microsoft Excel spreadsheet. Average flow times were calculated per concentration and flow times were omitted if they were double the standard deviation away from the mean. The relative (η_r), specific (η_{sp}) and reduced (η_{sp}/c) viscosities were determined per concentration (c). Values of the reduced viscosity were plotted against concentration using a Microcal Origin worksheet. A linear least-square fit to the data points yielded the intrinsic viscosity ($[\eta]$) and the Huggins constant (k_H) for each polymer-solvent system.

3.4 Dilute Solution Characterisation of Linear and Miktoarm Star Polybutadienes

3.4.1 Dilute Solutions in Cyclohexane

Static and dynamic light scattering and viscometry experiments were performed on dilute solutions of linear and miktoarm star polybutadienes. Linear polybutadienes LH50, LH100 and LH300 and miktoarm star polybutadienes S30, S60, S80 and S300 were dissolved in the good solvent of cyclohexane (A_2>0) and measurements were performed at a temperature of 298 K. Table 4 lists the weight-average molecular weight ($\bar{M}_W$), radius of gyration (R_G), second virial coefficient (A_2), translational diffusion coefficient at infinite dilution (D_0) and the concentration dependence of the translational diffusion coefficient (k_D) for all the polymers, obtained from light scattering. The solution viscometry results of the intrinsic viscosity ($[\eta]$) and the Huggins constant (k_H) for each polymer are shown in Table 5. No dynamic light scattering data is available for S300, as all the polymer available was used for other experiments.

Table 4: Static and dynamic light scattering results for linear and miktoarm star polybutadienes in cyclohexane at 298 K.

Sample	$\bar{M}_W/10^4$ (g mol^{-1})	R_G (nm)	$A_2/10^{-4}$ (mol ml g^{-2})	D_0 / 10^{-7} (cm^2 s^{-1})	k_D (cm^3 g^{-1})
LH50	5.8 ± 0.2	11.9 ± 1.2	15.2 ± 0.6	3.69 ± 0.44	33.9 ± 30.3
LH100	11.8 ± 0.2	17.1 ± 0.5	12.5 ± 0.4	2.72 ± 0.35	23.0 ± 20.5
LH300	36.9 ± 0.3	32.5 ± 0.5	10.5 ± 0.1	1.27 ± 0.08	124.4 ± 26.5
S30	37.5 ± 0.7	18.8 ± 0.4	4.3 ± 0.3	1.29 ± 0.10	91.6 ± 33.2
S60	23.9 ± 0.3	16.4 ± 0.5	7.3 ± 0.2	1.58 ± 0.12	84.8 ± 29.4
S80	35.8 ± 0.4	24.4 ± 0.7	6.8 ± 0.1	1.27 ± 0.05	106.4 ± 17.0
S300	58.1 ± 0.1	43.7 ± 0.5	7.6 ± 0.3	-	-

The weight-average molecular weights obtained by light scattering from cyclohexane solutions of linear and star polybutadienes are in close agreement to those ascertained by size exclusion chromatography (SEC) in THF (see Tables 1 and 4 in chapter 2). For the linear polybutadienes LH50, LH100 and LH300, $\bar{M}_W$ values from SEC were 5.08×10^4 g mol^{-1}, 10.1×10^4 g mol^{-1} and 31.4×10^4 g mol^{-1} respectively. The star polybutadienes S30, S60, S80 and S300 had $\bar{M}_W$ measured by SEC to be 35.5×10^4 g mol^{-1}, 24.6×10^4 g mol^{-1}, 34.2×10^4 g mol^{-1} and 59.7×10^4 g mol^{-1} respectively.

Table 5: Viscometry data for linear and star polybutadienes in cyclohexane at 298 K.

Sample	$[\eta]$ (ml g^{-1})	k_H
LH50	68.7 ± 0.2	0.40 ± 0.01
LH100	113.4 ± 0.3	0.41 ± 0.01
LH300	245.5 ± 0.3	0.41 ± 0.01
S30	112.2 ± 0.1	0.63 ± 0.01
S60	105.8 ± 0.1	0.54 ± 0.01
S80	122.4 ± 0.1	0.58 ± 0.01
S300	299.6 ± 0.6	0.36 ± 0.01

The radius of gyration (R_G) for each linear and miktoarm star polybutadiene sample are plotted against their respective $\bar{M}_W$ in Figure 10. The R_G increased with molecular weight for both linear and star polybutadienes.[13] Star polymers had a lower R_G compared to a linear polymers of the same molecular weight and this reduction increases with star functionality. This has been observed for polybutadiene stars[14-18], polyisoprene stars[19-21] and polystyrene stars.[22-24] The stars S30, S60 and S80 had R_G values that appear to be lower than for a linear polymer, where S300 with the longest asymmetric arm and the highest molecular weight had an R_G comparable to that of a linear polymer. A double logarithmic plot of R_G versus $\bar{M}_W$ for the linear polybutadienes can be seen in Figure 11 and molecular weight dependence for R_G was calculated:

$$R_G = 3.0 \times 10^{-2} \bar{M}_W^{0.54} \qquad (108)$$

The exponent in equation 108 is greater than the Flory exponent ν of 1/2 expected for linear polymers in θ-conditions, but it was less than 3/5 predicted for good solvent conditions.[25] A log-log plot of radius of gyration versus the normalised weight average molecular weight for the miktoarm star polymers is plotted in Figure 12. These normalised molecular weights were calculated by dividing the $\overline{M}_W$ by the average functionality (*f*) for each star. In Figure 12, the increase of R_G with normalised molecular weight, follows an overall steady increase with asymmetric arm length. Star polymer S30 had a greater R_G than for S60, as the molecular weight for the regular arms and star functionality were higher, that would lead to a more stretched configuration. A linear fit to the data in Figure 12 yielded an R_G dependence on normalised molecular weight:

$$R_G = 1.69\times10^{-4}\left(\frac{\overline{M}_W}{f}\right)^{1.09} \qquad (109)$$

The exponent of 1.09 in equation 109 is greater than the exponent of 0.54 obtained in equation 108 for linear polymers. This suggested that with increasing molecular weight of the asymmetric arm, the star polymers had values of R_G for the asymmetric arms of these stars approach those similar to linear polymers of the same molecular weight. An increase in asymmetric arm length produces R_G values to appear more "linear-like" in nature.

Figure 13 is a plot of A_2 versus $\overline{M}_W$ for the linear and star polybutadienes. The second virial coefficient for linear polybutadienes have been found to decrease with molecular weight in cyclohexane at 298 K by Roovers *et al.*[16] The linear polybutadienes in Figure 13 and Table 4 have A_2 decreasing with molecular weight. Star polymers have lower values of A_2 compared to the linear polymers of the same molecular weight, due to the presence of the single branch point and the greater segment density at the core. At constant molecular weight, star polymers show a decrease in A_2 with arm functionality, from that of a linear polymer. Regular star polymers also have a decrease in A_2 with an increase in arm molecular weight. This has been observed with polybutadiene stars[15-19], polyisoprene stars[20-22] and polystyrene stars.[23-25] In Figure 13, the regular star polymer S30 has a lower A_2 compared to the asymmetric star polymers, but this is due to the higher average functionality and hence greater segment density near the core. Star polymers S60, S80 and

S300 with approximately identical star arm functionalities, seemed to have values of A_2 approaching those of linear polymers with the increase of the asymmetric arm length. The double logarithmic plot of A_2 versus $\overline{M}_W$ for the linear polybutadienes can be seen in Figure 14 and the molecular weight dependence of A_2 was:

$$A_2 = 1.27\times10^{-2}\,\overline{M}_W^{-0.20} \tag{110}$$

The exponent of -0.2 obtained in equation 110 corresponds to the behaviour expected for linear polymers under good solvent conditions[14] and shows the decrease in A_2 with increasing molecular weight. Roovers[16] obtained a similar exponent of -0.21 for linear polybutadienes in cyclohexane at a temperature of 298 K. A log-log plot of A_2 versus $\overline{M}_W/f$ (normalised molecular weight) for the miktoarm star polymers is shown in Figure 15. A small positive dependence of A_2 with increasing asymmetric arm length can be seen on A_2, but this could be due to the presence of the higher functional S30 star which would reduce A_2:

$$A_2 = 6.74\times10^{-5}\left(\frac{\overline{M}_W}{f}\right)^{0.21} \tag{111}$$

The positive increase of A_2 with asymmetric arm length and hence molecular weight is contrary to that for regular stars and linear polymers.[14] If the datum point for the star polymer S30 is ignored in Figure 15, then a small positive dependence for A_2 with asymmetric arm length can still be seen, as these stars have approximately identical arm functionalities. Therefore, an increase of asymmetric arm length for these stars will eventually lead to a second virial coefficient similar to those obtained for linear polymers of equal molecular weight.

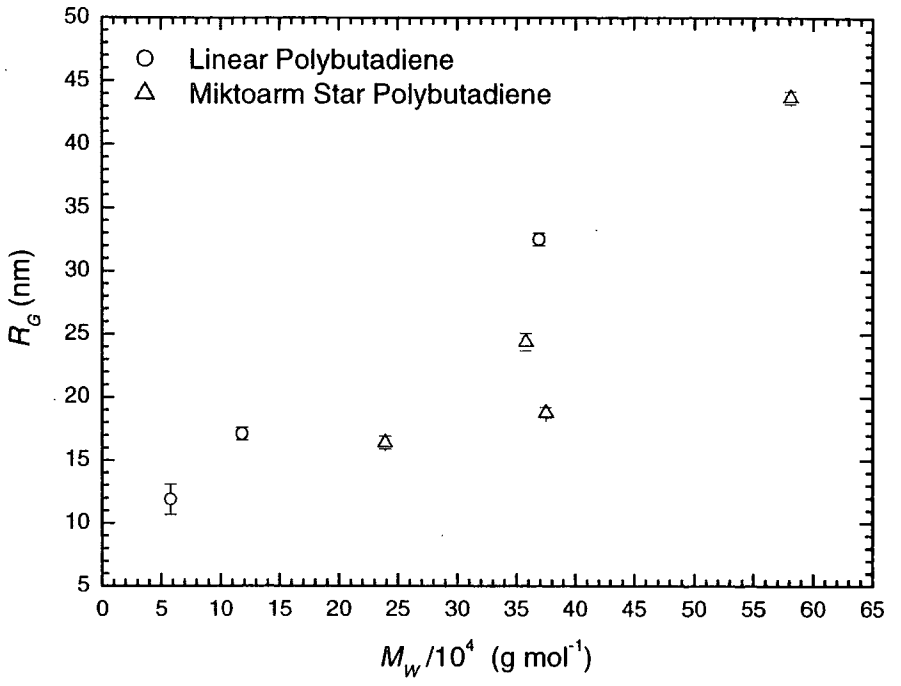

Figure 10: A graph of R_G versus $\bar{M}_W$ for the linear and miktoarm star polybutadienes in cyclohexane at a temperature of 298 K.

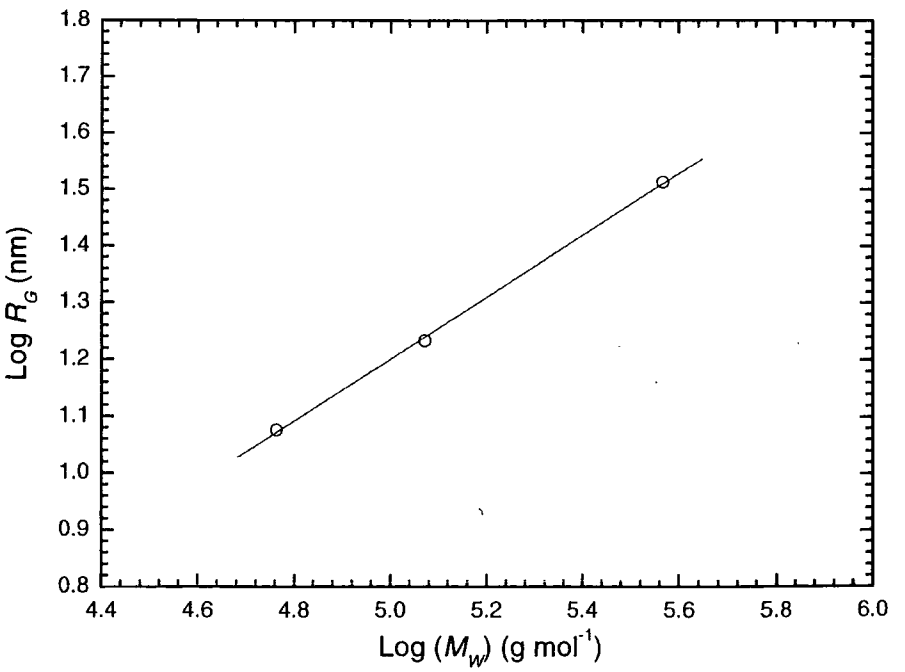

Figure 11: A log-log plot of R_G versus $\bar{M}_W$ for linear polybutadienes in cyclohexane at a temperature of 298 K.

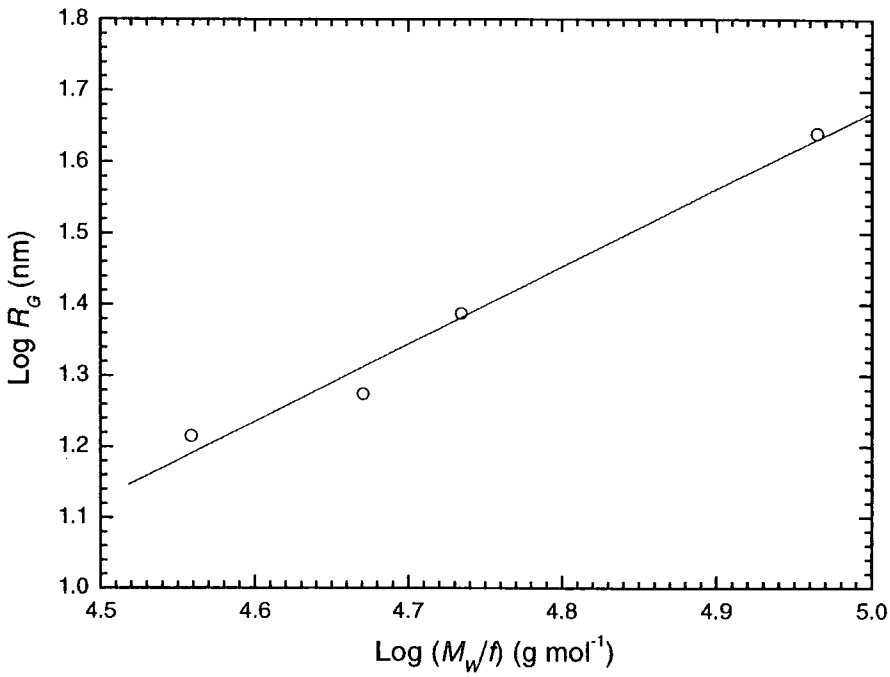

Figure 12: A log-log plot of R_G versus $\bar{M}_W/f$ for the miktoarm star polybutadienes in cyclohexane at a temperature of 298 K.

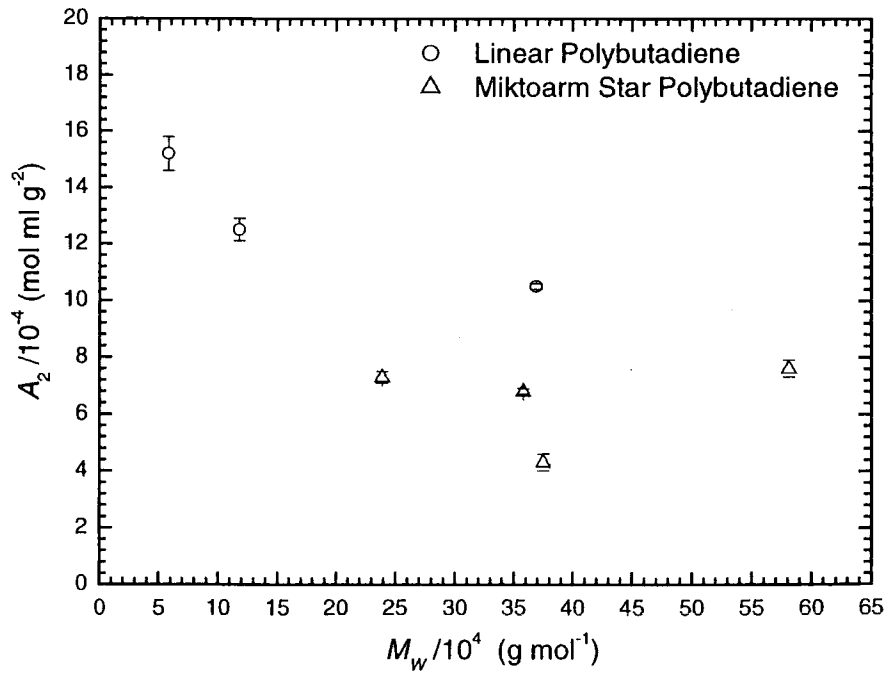

Figure 13: A plot of A_2 versus $\bar{M}_W$ for linear and miktoarm star polybutadienes in cyclohexane at a temperature of 298 K.

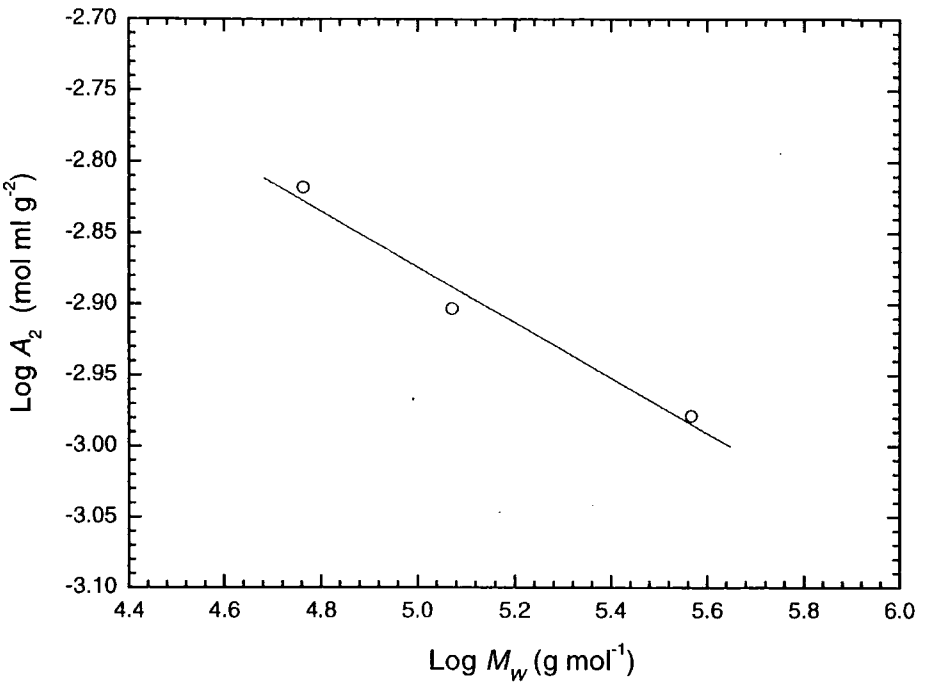

Figure 14: A log-log plot of A_2 versus $\bar{M}_W$ for linear polybutadienes in cyclohexane at a temperature of 298 K.

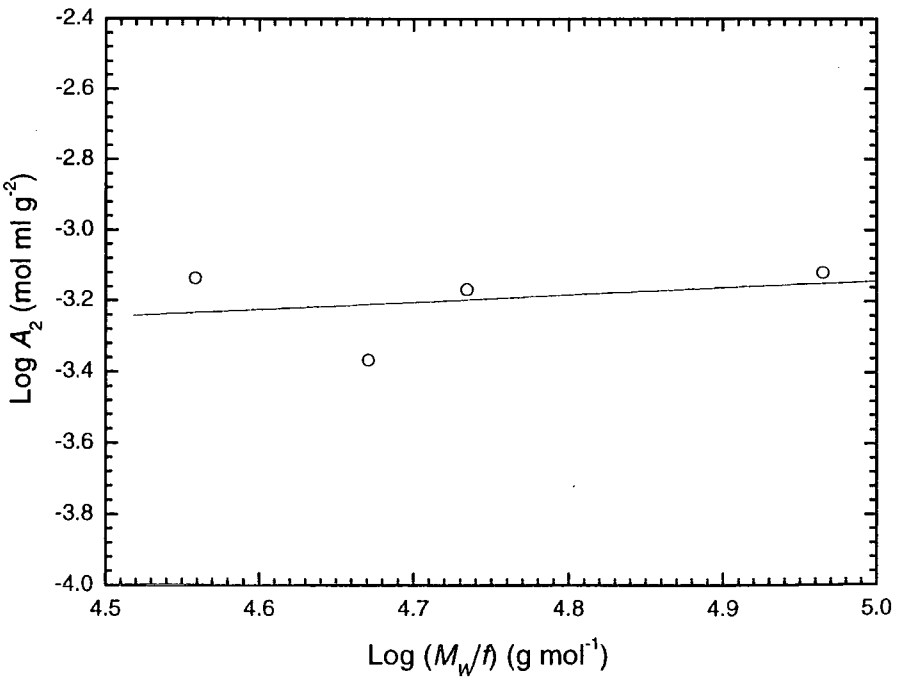

Figure 15: A log-log plot of A_2 versus $\bar{M}_W/f$ for miktoarm star polybutadienes in cyclohexane at a temperature of 298 K.

Figure 16 shows the translational diffusion coefficient at infinite dilution (D_0) versus $\overline{M}_W$ for the linear and miktoarm star polybutadienes. D_0 decreases with increasing molecular weight for both linear and regular star polymers. The increase in arm functionality of regular stars causes D_0 to increase away from values obtained for linear polybutadienes, at constant molecular weight.[14] This has been observed with polybutadiene stars[15-19], polyisoprene stars[20-22] and polystyrene stars.[23-25] D_0 decreases with increasing molecular weight for the linear polybutadienes and this can be observed in Figure 16. A slight decrease in diffusion coefficients for the star polymers can be seen with molecular weight. The stars S30 and S80 have comparable diffusion coefficient, that could be due to the effects of the differing star functionalities and asymmetric arm lengths on D_0. The D_0 values for the miktoarm star polymers are approximately the same for linear polybutadienes at equivalent molecular weight, which is contrary to data within the literature.[14] The size of the error bars in Figure 16 could lead to D_0 values lower than for star polymers at the same molecular weight and comply with the data reported in the literature. Figure 17 is the double logarithmic plot of D_0 versus $\overline{M}_W$ for the linear polybutadienes LH50, LH100 and LH300, with a molecular weight dependence of:

$$D_0 = 2.36\times10^{-4}\,\overline{M}_W^{-0.59} \qquad (112)$$

The exponent in equation 112 is in close agreement with the value of -0.56 obtained by Roovers *et al*[16] for linear polybutadienes in cyclohexane at 298 K. Figure 18 is the double logarithmic plot of D_0 versus $\overline{M}_W/f$ (normalised molecular weight) for the miktoarm stars. The molecular weight dependence of the these stars is:

$$D_0 = 6.10\times10^{-5}\left(\frac{\overline{M}_W}{f}\right)^{-0.57} \qquad (113)$$

The exponent in equation 113 is similar to the exponent obtained for linear polymers in equation 112 and shows that D_0 decreases with increasing molecular weight. No evidence suggests that D_0 will approach values similar to those of linear polymers with increasing arm length. The concentration dependence coefficients were found to be lower for the star polymers, when compared to linear polymers of the same molecular weight. Roovers[16]

obtained lower values of k_D for 18-arm polybutadiene stars in cyclohexane, than for linear polymers of comparable molecular weight. This reflects the smaller values of the second virial coefficient obtained for star-branched materials. Roovers[16] found an increase in k_D with molecular weight for both linear and star polymers. An increase in k_D can be seen from linear polybutadienes LH50 and LH100 to the higher molecular weight LH300, but no molecular weight dependence was noticed for the star polymers. Figure 19 is the plot of $[\eta]$ versus $\overline{M}_W$ for the linear and star polybutadienes in cyclohexane at a temperature of 298 K. Linear and regular star polymers have an increase in intrinsic viscosity with increasing molecular weight, and the molecular weight dependencies are approximately parallel. Regular stars have an decrease in $[\eta]$ with arm functionality at constant molecular weight, and this has been demonstrated by model polybutadiene stars[15-18], polyisoprene stars[19-21] and polystyrene stars.[22-24] In Figure 19 the miktoarm star polymers have a lower $[\eta]$ than for the linear polymers with approximately the same molecular weight. An increase in $[\eta]$ with molecular weight could be seen for the linear polybutadienes. Star polymer S300 with the longest asymmetric arm seemed to have a $[\eta]$ that approach a value similar to a linear polymer with the same molecular weight. A log-log plot of $[\eta]$ versus $\overline{M}_W$ for linear polybutadienes is shown in Figure 20, and yields a molecular weight dependence of:

$$[\eta] = 3.67 \times 10^{-2} \overline{M}_W^{0.69} \tag{114}$$

The exponent in equation 114 of 0.69 is in close agreement to an exponent of 0.70 obtained for linear polybutadienes in cyclohexane by Roovers *et al.*[16] The exponent in equation 114 is greater than 0.54 obtained in equation 112 for R_G and the Flory scaling exponent of 3/5 predicted for good solvent conditions. Ioan *et al*[26] developed a correlation equation between the star functionality and the Mark-Houwink-Sakaruda (MHS) exponent to calculate the constant K in equation 43, chapter 1, for polybutadiene stars under various solvent conditions. For a linear polybutadiene (f=2) and using a MHS exponent of 0.70, a value of K of 3.67×10^{-2} ml g^{-1} was obtained, which is in exact agreement with the value in equation 114. A log-log plot of $[\eta]$ versus normalised $\overline{M}_W/f$ for the miktoarm star polymers is shown in Figure 21 and a linear fit to this data yields:

$$[\eta] = 3.78 \times 10^{-4} \left(\frac{\overline{M}_w}{f} \right)^{1.18} \quad (115)$$

An increase in $[\eta]$ with normalised molecular weight can be seen in Figure 21, for these asymmetric stars. This increase in $[\eta]$ with molecular weight is similar to the behaviour of linear and regular star polymers. The greater exponent of 1.18 in equation 115 compared to the exponent of 0.69 obtained for linear polybutadienes in equation 114, suggests that $[\eta]$ will increase with the molecular weight of the asymmetric arm and eventually yield values similar to those of linear polymers at the same molecular weight.

Linear polymers dissolved in good solvents have Huggins constants between 0.3 to 0.5 depending on size and shape of the polymer, but independent of molecular weight.[11] In Table 5, the linear polybutadienes LH50, LH100 and LH300 had k_H values of 0.40, 0.41 and 0.41 respectively, showing good polymer-solvent pair interactions. Branched polymers have a greater segment density than linear polymers of the same molecular weight and are assumed to have a larger k_H. An increase in k_H with arm functionality has been noticed for polyisoprene stars.[21] The star polymers S30, S60 and S80 had Huggins constants greater than 0.5, reflecting the higher segment density and more polymer-polymer contacts. The highest value of k_H of 0.63 was for the regular star S30, which had the largest average functionality (f = 8) and therefore greater segment density. The star polymers S60 and S80, with equal average functionalities (f = 6.6), had similar Huggins constants of 0.54 and 0.58 respectively. A much lower value for k_H of 0.36 was obtained for star polymer S300 when compared to S80 and S60. Star S300 had a similar average functionality (f = 6.3) to stars S60 and S80, but a much longer asymmetric arm length. The star S300 had a Huggins constant similar to those ascertained for linear polybutadienes.

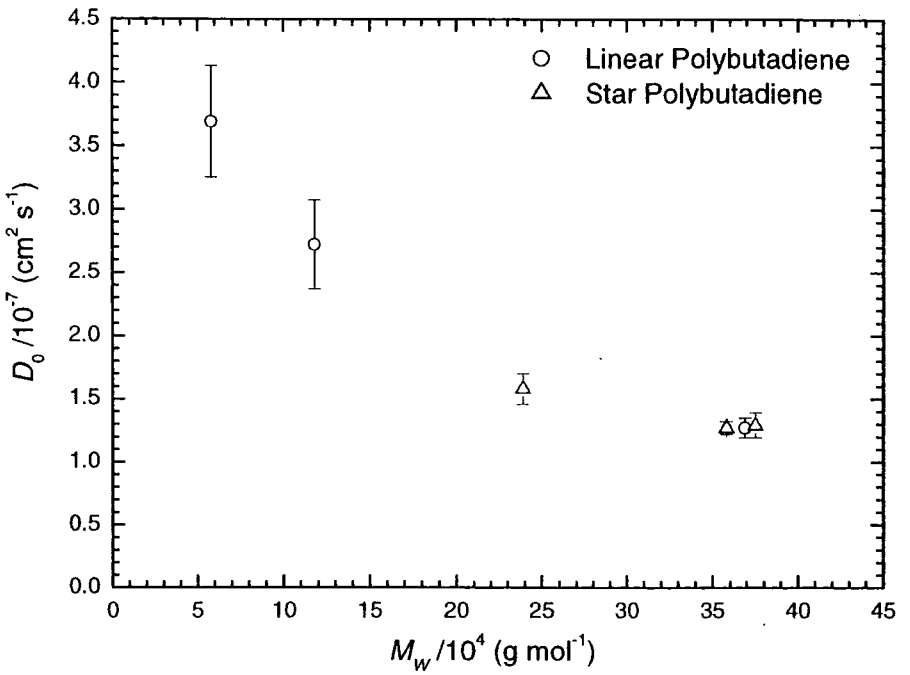

Figure 16: *A plot of D_0 versus $\bar{M}_W$ for the linear and miktoarm star polybutadienes in cyclohexane at a temperature of 298 K.*

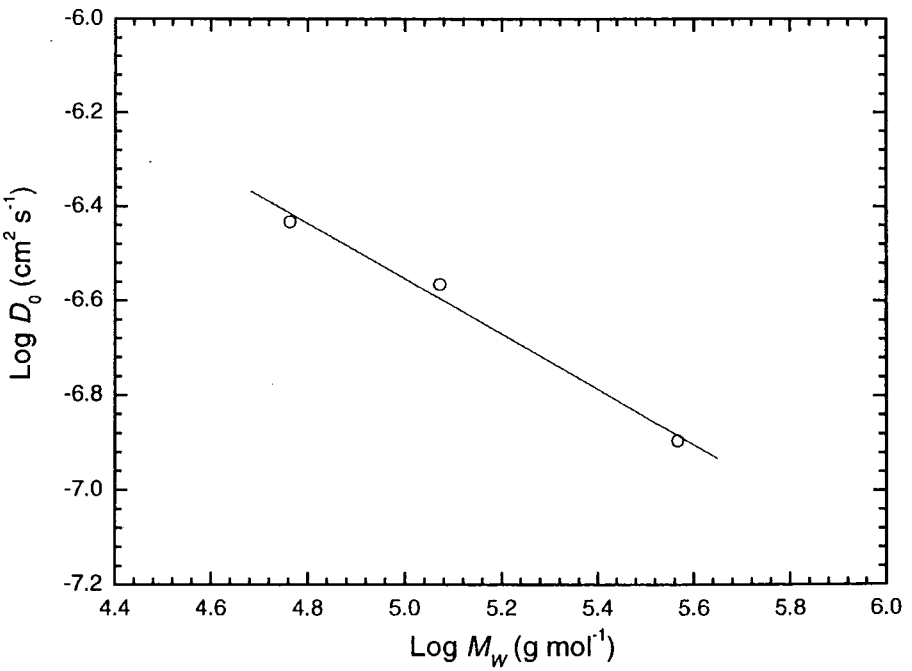

Figure 17: A log-log plot of D_0 versus $\bar{M}_W$ for linear polybutadienes in cyclohexane at a temperature of 298 K.

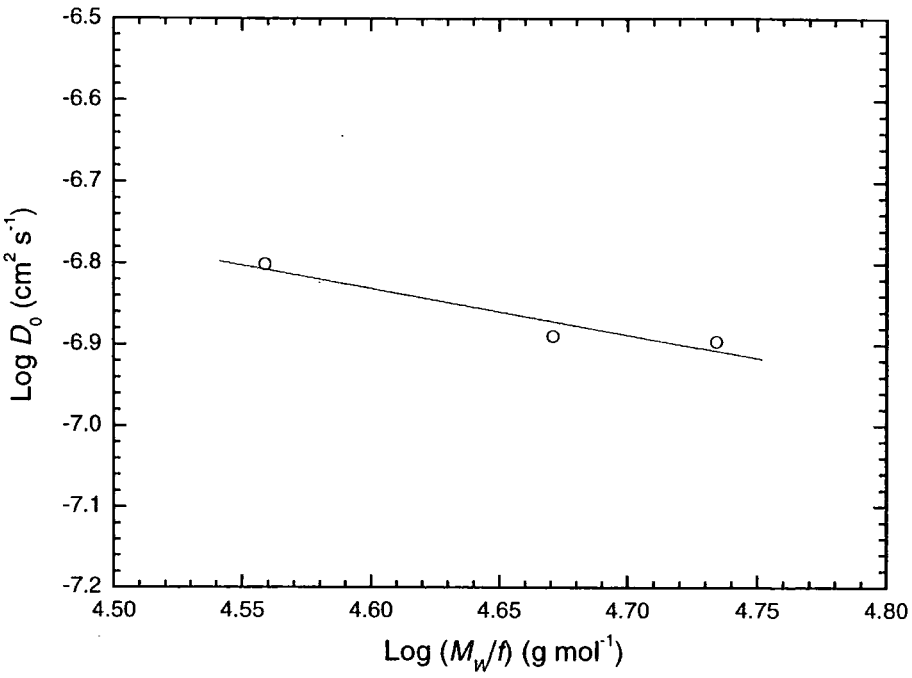

Figure 18: A log-log plot of D_0 versus $\bar{M}_W/f$ for miktoarm star polybutadienes in cyclohexane at a temperature of 298 K.

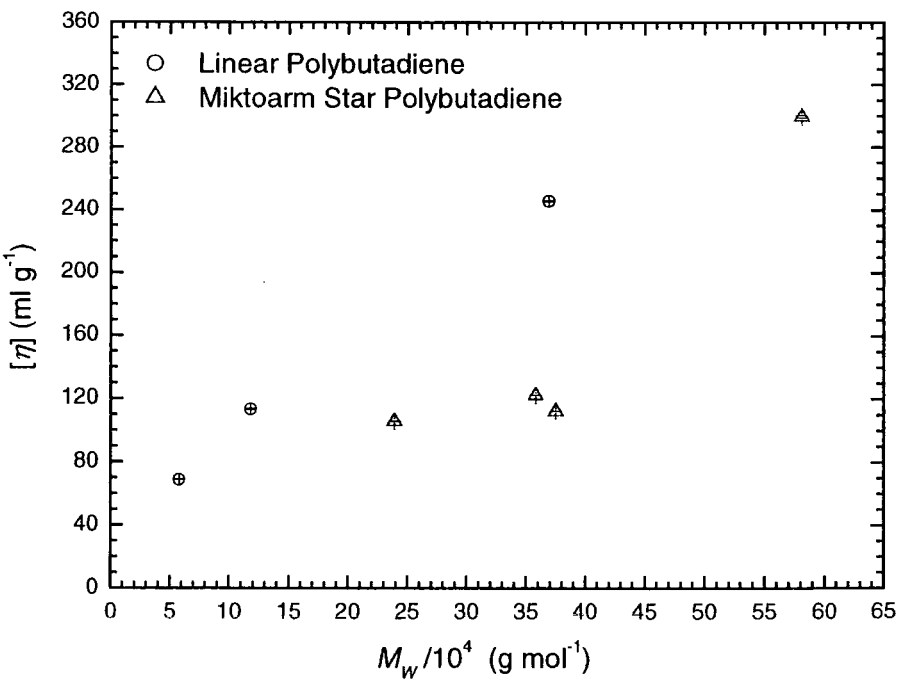

Figure 19: A plot of $[\eta]$ versus $\bar{M}_W$ for linear and miktoarm star polybutadienes in cyclohexane at a temperature of 298 K.

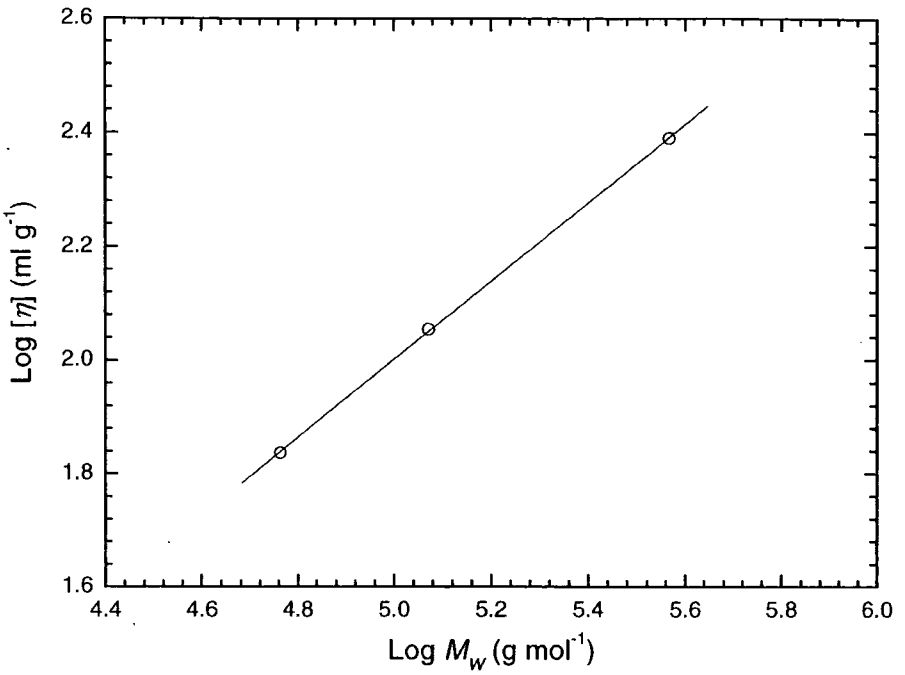

Figure 20: A log-log plot of [η] versus $\bar{M}_W$ for linear polybutadienes in cyclohexane at a temperature of 298 K.

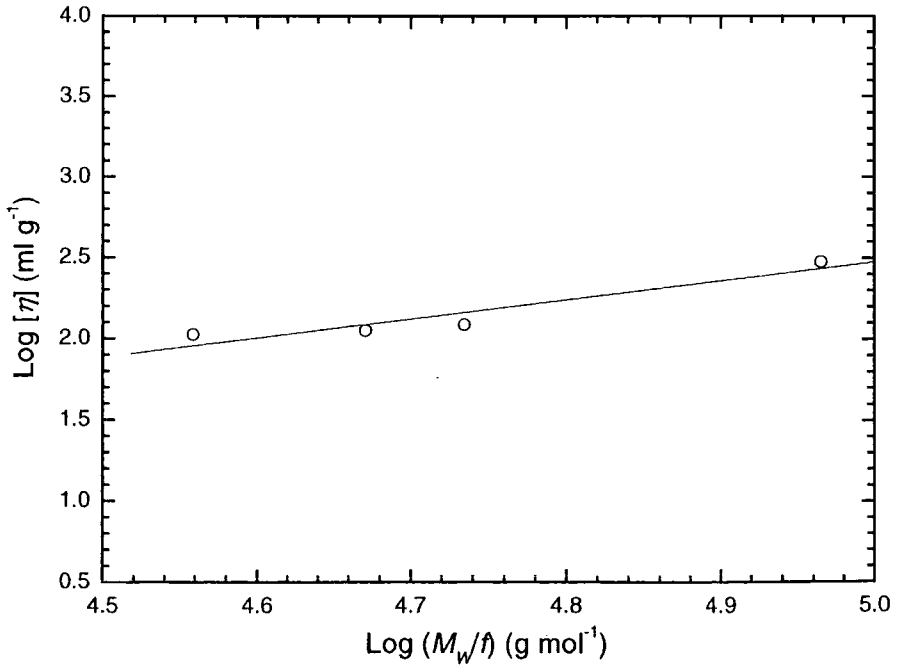

Figure 21: A log-log plot of [η] versus $\bar{M}_W/f$ of the miktoarm star polymers in cyclohexane at a temperature of 298 K.

The thermodynamic (R_T), hydrodynamic (R_H) and viscometric (R_V) radii are the equivalent sphere radii for the polymers in dilute solution, which can be calculated from the global properties listed in Table 4 and Table 5, by equations 24, 36 and 42 (chapter 1) respectively. R_T, R_H and R_V are the equivalent sphere radii evaluated from A_2, D_0 and $[\eta]$ respectively, and are listed with R_G for each linear and miktoarm star polybutadiene in Table 6. For regular star and linear polymers, the equivalent sphere radii increased with increasing molecular weight.[16, 20] At constant molecular weight, the equivalent sphere radii become smaller with increasing arm functionality for regular star polymers. For monodisperse hard spheres, the equivalent sphere radii are equal and are smaller than R_G by approximately:

$$R_T = R_V = R_H = \sqrt{\left(\frac{3}{5}\right)} R_G \qquad (116)$$

Regular star polymers have greater segment densities when compared to linear polymers. Highly functional stars have high segment densities near the core that cause the equivalent sphere radii to become greater than the radius of gyration and above the hard sphere limit.[16] Figure 22 is a plot of the equivalent sphere radii and radius of gyration versus $\bar{M}_W$ for the linear polybutadienes. The thermodynamic and viscometric equivalent radii were approximately identical over the molecular weight range, but the hydrodynamic radii were lower than expected. The equivalent radii were constantly lower than the radius of gyration for the linear polymers over this molecular weight range.[27]

Figure 23 is a plot of the equivalent sphere radii and radius of gyration versus $\bar{M}_W/f$ for the miktoarm star polybutadienes, and the data points are labelled by the star they represent. The equivalent sphere radii for the stars are approximately identical over the molecular weight range. A steady increase between the equivalent sphere radii and R_G can be seen with increasing asymmetric arm length in Figure 23. The regular star polymer S30 has equivalent radii equal to the radius of gyration, reflecting the high segment density and greater spherical shape of this star. The star polymer with the longest asymmetric arm, S300, has a large difference between the equivalent sphere radii and R_G. The increase in the difference between the equivalent sphere radii and the radii of gyration with asymmetric arm length was due to a decrease in segment density near the star core.

Table 6: Equivalent sphere radii and R_G for linear and miktoarm star polybutadienes in cyclohexane at 298 K.

Sample	R_T (nm)	R_H (nm)	R_V (nm)	R_G (nm)
L50	8.0 ± 0.3	6.6 ± 0.8	8.6 ± 0.1	11.9 ± 1.2
L100	12.0 ± 0.3	8.9 ± 1.1	12.9 ± 0.1	17.1 ± 0.5
L300	24.2 ± 0.2	19.1 ± 1.2	24.3 ± 0.1	32.5 ± 0.5
S30	18.2 ± 0.9	18.8 ± 1.5	18.8 ± 0.1	18.8 ± 0.4
S60	16.1 ± 0.4	15.4 ± 1.1	15.9 ± 0.1	16.4 ± 0.5
S80	20.5 ± 0.3	19.1 ± 0.8	19.1 ± 0.1	24.4 ± 0.7
S300	29.4 ± 0.8	-	30.2 ± 0.1	43.7 ± 0.5

The differences between the equivalent sphere radii and the radii of gyration can be seen more clearly by calculating size ratios. The size ratios of R_T/R_G, R_H/R_G and R_V/R_G are listed within Table 7 and are smaller than the hard sphere value of 1.29. R_G was preferred for the basis of comparison of polymer dimensions as it is directly measurable, where the other dimensions are based upon equivalent spheres. For monodisperse hard spheres, the size ratios are identical. Data have been reported for R_T/R_G, R_H/R_G and R_V/R_G of 0.71, 0.72 and 0.84 respectively for linear polybutadienes in cyclohexane by Roovers *et al.*[16] The R_T/R_G and R_V/R_G values for the linear polybutadienes were similar to these reported data. The R_H/R_G ratios for the linear polybutadienes in Table 7 were lower than those determined by Roovers.[16]

R_T/R_G, R_H/R_G and R_V/R_G data of 1.00, 0.99 and 0.99 respectively have been reported in the literature for an 8-arm regular star at the good solvent limit.[28] These are in close agreement with R_T/R_G, R_H/R_G and R_V/R_G data of 0.97, 1.00 and 1.00 respectively for the 8-arm regular star S30 in Table 7. The identical values obtained demonstrate that the stars were behaving as hard spheres with this good solvent. A decrease in these ratios with increasing asymmetric arm length can be seen for the miktoarm stars in Table 7, and are shown in Figure 24 (data points are labelled by the star they represent). The size ratios for the star S300, with the longest asymmetric arm length are close to those obtained for a linear polybutadienes (see Table 7).

Table 7: Size ratios of equivalent sphere radii to the radius of gyration, the interpenetration functions and friction constants for linear and miktoarm star polybutadienes in cyclohexane at 298 K.

Sample	R_T/R_G	R_H/R_G	R_V/R_G	Ψ	k_0
LH50	0.67 ± 0.09	0.55 ± 0.12	0.72 ± 0.08	0.23 ± 0.09	11.30 ± 15.43
LH100	0.70 ± 0.04	0.52 ± 0.08	0.75 ± 0.03	0.26 ± 0.04	17.98 ± 23.88
LH300	0.74 ± 0.02	0.59 ± 0.05	0.75 ± 0.01	0.31 ± 0.02	13.63 ± 18.62
S30	0.97 ± 0.07	1.00 ± 0.10	1.00 ± 0.03	0.68 ± 0.12	5.14 ± 3.64
S60	0.98 ± 0.05	0.94 ± 0.10	0.97 ± 0.04	0.71 ± 0.10	6.82 ± 4.18
S80	0.84 ± 0.04	0.78 ± 0.06	0.78 ± 0.03	0.45 ± 0.06	7.73 ± 2.49
S300	0.67 ± 0.03	-	0.69 ± 0.01	0.23 ± 0.02	-

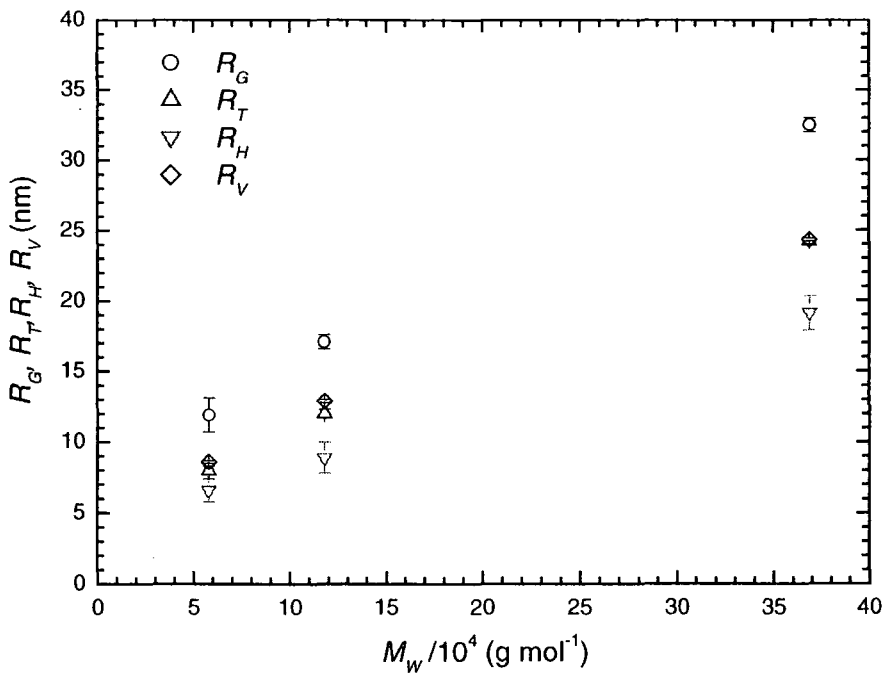

Figure 22: A plot of R_G, R_T, R_H and R_V versus $\overline{M}_W$ for linear polybutadienes in cyclohexane at a temperature of 298 K.

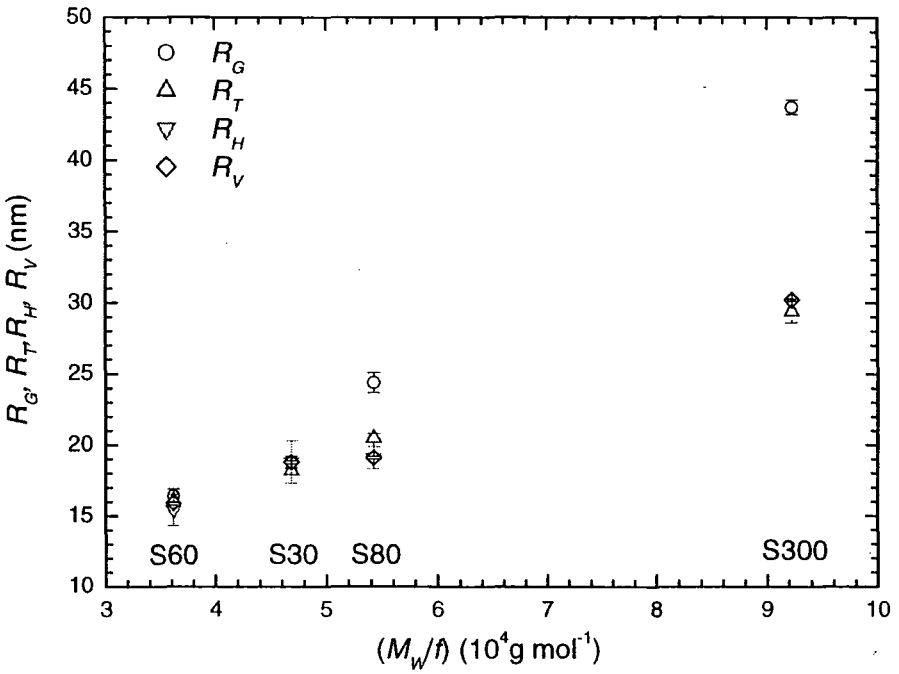

Figure 23: A plot of R_G, R_T, R_H and R_V versus $\bar{M}_W/f$ for miktoarm star polybutadienes in cyclohexane at a temperature of 298 K.

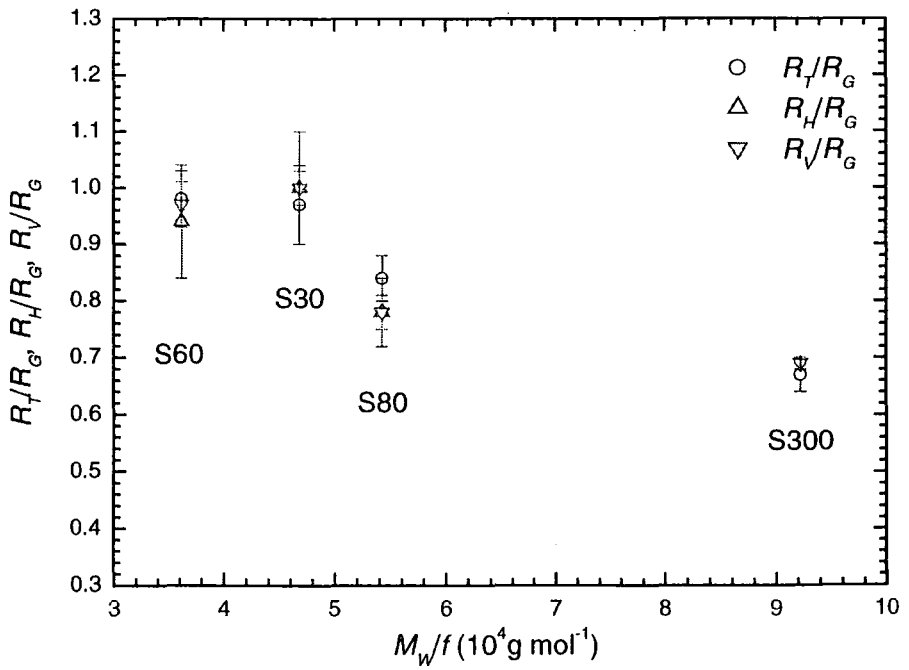

Figure 24: A plot of R_T/R_G, R_H/R_G and R_V/R_G for the miktoarm star polybutadienes in cyclohexane at a temperature of 298 K.

The interpenetration functions (Ψ^*) were calculated from equation 23 (chapter 1), for the linear and star polybutadienes in cyclohexane and are listed in Table 7. The interpenetration function (Ψ) is a dimensionless measurement of the second virial coefficient, and reaches an asymptotic limit (Ψ^*) in good solvents.[17] The changes in interpenetration function are related to the size ratio R_H/R_G. Branching increases the interpenetration function up to the hard sphere value of 1.61, due to the decrease of A_2 with higher segment density at the star core. Literature data for polybutadiene and polystyrene stars and from Renormalisation Group Theory and Monte-Carlo simulations are listed in Table 8. Linear, 4- and 18-arm polybutadiene stars in cyclohexane at 298 K have been found to have Ψ^* in the ranges of 0.24 to 0.29, 0.41 to 0.46 and 1.03 to 1.35 respectively.[29] Linear, 4-, 6- and 12-arm regular polystyrene stars show Ψ^* values of between 0.24 to 0.27, 0.46 to 0.59, 0.65 to 0.67 and 1.10 respectively.[29] Renormalization group theory predicted Ψ^* for linear, 4-, 6- and 12-arm regular stars to be 0.27, 0.52, 0.79 and 1.35 respectively in good solvents.[30] Alternatively, Monte Carlo methods estimated Ψ^* for linear, 4-, 6-, 12- and 18-arm stars to be 0.24, 0.43, 0.62, 1.05 and 1.21 respectively.[31]

The values of Ψ^* for the linear polybutadienes LH50, LH100 and LH300 in Table 7 are 0.23, 0.26 and 0.31 respectively, and are in close approximation to experimental and theoretical data for linear polymers listed in Table 8. The 8-arm regular star S30 had a interpenetration function of 0.68, in between the data for 4- and 18-arm polybutadiene stars and the Monte Carlo data for 6- and 12-arm stars. The star polymer S60 (f = 6.6) had a higher value of Ψ^* of 0.71, that was close to the values obtained for 6-arm polystyrene stars. The interpenetration functions for S80 and S300 were 0.45 and 0.23 respectively. A decrease to lower functionality can be seen for these two stars when comparing these values to the data in Table 8. S80 seems to have an Ψ^* similar to a 4-arm star where S300 has an interpenetration function in close agreement to a linear polymer.

Table 8: Literature data for interpenetration functions, Ψ^*, for polybutadiene and polystyrene stars and from Renormalisation Group Theory and Monte-Carlo Simulations for stars of varying functionality under good solvent conditions.

Functionality (f)	Polybutadiene[a]	Polystyrene[a]	Renormalization Group Theory[b]	Monte-Carlo Simulations[c]
2 (Linear)	0.24 – 0.29	0.24 – 0.27	0.27	0.24
4	0.41 – 0.46	0.46 – 0.59	0.52	0.43
6	-	0.65 – 0.67	0.79	0.62
12	-	1.10	1.35	1.05
18	1.03 – 1.35	-	-	1.21

[a] Reference 29. [b] Reference 30. [c] Reference 31.

The frictional constant (k_0) can be calculated from equation 39, chapter 1, from the concentration dependence of the diffusion coefficient (k_D) and are reported for linear and star polybutadienes in Table 7. The friction constants for the linear polybutadienes LH50, LH100 and LH300 were 11.30, 17.98 and 18.62 respectively. Linear polybutadienes[16] and polyisoprenes[32] have both been found to have k_0 of 5.2 and 4.8 respectively. The friction constants are highly sensitive to measured parameters and the accuracy of the dynamic scattering data will reflect in the calculated values. Roovers[18] reported that k_0 was independent of chain architecture for linear and regular star polybutadienes in cyclohexane. For an 18- and 32-arm polybutadiene stars in cyclohexane, the friction constant were found to be in between 6.4 to 9.3 and 7.1 to 8.4 respectively.[16, 17] Polybutadiene stars with 64- and 128-arms yielded k_0 in between 7.0 and 11.0 in cyclohexane at 298 K.[18] The miktoarm star polymers S30, S60 and S80 had k_0 as 5.1, 6.8 and 7.7 respectively. These values increase with asymmetric arm length and seem to be contrary to Roovers view of architecture independence.

Branching ratios g, h, and g' were calculated for the star polymers and are listed in Table 9. The branching ratios g, h, and g' are the ratio of the R_G^2, R_H and $[\eta]$ for the star polymers to that of a linear polymer of the same molecular weight, as seen in equations 46, 48 and 49 in chapter 1 respectively. The linear analogue values were calculated using the $\bar{M}_W$ dependent equations 108, 112 and 114 for these global properties. The branching ratio g decreases from a value of unity with increasing star functionality.[21, 29] In good solvents, the branching g-ratio of 0.38 was determined for the 8-arm regular star S30, which was in close approximation to the value of 0.35 obtained by Zimm and Stockmayer[33] for a Gaussian star, a value also reported by Renormalisation Group calculations[30] and Monte-Carlo simulations[34]. A value of g of 0.35 has been determined for an 8-arm polyisoprene star under good solvent conditions.[21] Star polymers S60 and S80 both had an average functionality of 6.6 and have g-ratios of 0.46 and 0.67 respectively. These values were greater than the Gaussian star predictions of 0.39 and 0.44 for a 6- and 7-arm regular stars respectively and similar to lower functional stars. The deviation away from the Zimm and Stockmayer[23] predictions was greater for the star S80, with a longer asymmetric arm than S60. Star polymer S300 had a g ratio of 1.26 that was greater than for a linear chain (g = 1.0), which suggested the star was behaving as a linear polymer.

The hydrodynamic radii branching ratio h for the star polymers are listed in Table 9. These branching ratios have been found to decrease from unity for a linear polymer, with increasing star functionality.[29] The regular star S30 had a h-ratio of 0.93, higher than the value calculated by Stockmayer and Fixman[35] of 0.73 for an 8-arm Gaussian star. For a 8-arm polyisoprene star[15] under good solvent conditions a h-ratio of 0.82 was also lower than the value obtained for S30. A Gaussian model determined by pre-averaged Kirkwood-Riseman theory[36] yielded 0.81 for an 8-arm star, similar to that obtained from the 8-arm polyisoprene star. An increase in h can be seen for S60 and S80 from S30 with the decrease in star functionality. Asymmetric star polymers S60 and S80 had h-ratios of 1.00 and 0.90 respectively and both had a lower average star functionality of 6.6 when compared to S30. The h-ratios for S60 and S80 were higher than the values obtained for a 6-arm regular star of 0.80 and 0.86 by Stockmayer and Fixman[36] and preaveraged-Kirkwood and Riseman theory[37] respectively. A h-value of 0.86 has been obtained for a 6-arm polystyrene star under good solvent conditions.[37] The h-ratios obtained for the stars depended on the linear polybutadiene scaling equation 112 for D_0, and the higher than expected h-ratios for these

stars could be due to the D_0 ascertained for the linear polymer analogues. No dependence on asymmetric arm length could be seen for h and the higher values for S60 and S80 are due to the difference in star functionality.

The intrinsic viscosity branching ratio, g', for the star and linear polymer analogues are listed in Table 9. The g'factors have been found to decrease from unity for a linear polymer with increasing star functionality.[29] The regular 8-arm star S30 had a value of $g'$of 0.44, smaller than 0.63 determined by the Gaussian star model of Zimm and Kilb.[38] An 8-arm polyisoprene star under good solvent conditions gave a $g'$of 0.43, similar to the value obtained for S30.[21] Pre-averaged Kirkwood-Riseman theory[37] determined g' to be 0.61 for an 8-arm star, similar to the value of Zimm and Kilb.[39] The asymmetric stars S60, S80 and S300 had g'-ratios of 0.56, 0.49 and 0.86 respectively in Table 9. Theory[37, 39] predicts that for 6-arm stars should have g' of approximately 0.70, but experimental values for 6-arm polystyrene[39] and polyisoprene[40] stars were approximately 0.57 and for an 8-arm polyisoprene star were 0.43. Asymmetric stars S60 and S80 (f=6.6) have g'-values in between this reported data, but agree with them to the extent that they are both less than Zimm and Kilb[39] and pre-averaged Kirkwood-Riseman theory.[37] No dependence on asymmetric arm length could be seen for these two stars. The longest asymmetric arm star polymer S300 with a functionality similar to S60 and S80, had the highest g'-ratio of 0.86, that was greater than the values obtained for 6-arm stars by the theoretical models.[37,29] S300 had branching ratio of g'that approached a value determined for a linear polymer (g'= 1.0).

Table 9: Branching ratios g, h and g'for miktoarm star polybutadienes.

Star	g	h	g'
S30	0.38	0.93	0.44
S60	0.46	1.00	0.56
S80	0.67	0.97	0.49
S300	1.27	-	0.86

3.4.2 Dilute solutions in 1,4-Dioxane

3.4.2.1 Linear Polybutadienes

Static and dynamic light scattering and viscometry experiments were performed on dilute solutions of linear polybutadienes in a θ-solvent. The θ-solvent used was 1,4-dioxane and measurements were obtained over the temperature range of 298 K to 323 K. Table 10, Table 11 and Table 12 are the static and dynamic light scattering results for linear polybutadienes LH50, LH100 and LH300 respectively. The weight-average molecular weights obtained were constant over the temperature range of measurement. The $\bar{M}_W$ of LH50 in dioxane was approximately 5.0×10^4 g mol^{-1} over the temperature range, which was comparable to a $\bar{M}_W$ of 5.8×10^4 g mol^{-1} obtained in cyclohexane. The same comparison was found for LH100, where the $\bar{M}_W$ in dioxane was approximately 9.9×10^4 g mol^{-1} and in cyclohexane was 1.2×10^5 g mol^{-1}. A larger discrepancy can be seen between $\bar{M}_W$ obtained for LH300 in dioxane and in cyclohexane, where the $\bar{M}_W$ determined in the θ-solvent was approximately 2.25×10^5 g mol^{-1} and in the good solvent was 3.69×10^5 g mol^{-1}.

Table 10: Light scattering studies on LH50 in 1,4-dioxane over the temperature range of 299.5 K to 323 K.

Temperature (K)	$\bar{M}_W/10^4$ (g mol^{-1})	R_G (nm)	$A_2/10^{-4}$ (mol ml g^{-2})
299.5	5.03 ± 0.01	9.6 ± 0.8	-1.12 ± 0.26
303.0	5.13 ± 0.12	13.9 ± 1.0	0.09 ± 0.41
308.0	4.96 ± 0.09	11.0 ± 1.4	0.90 ± 0.33
313.0	5.00 ± 0.12	9.3 ± 1.6	2.16 ± 0.41
323.0	5.21 ± 0.13	12.2 ± 1.1	4.53 ± 0.44

Table 11: Light scattering studies on LH100 in 1,4-dioxane over the temperature range of 299.5 K to 323 K.

Temperature (K)	$\bar{M}_W/10^4$ (g mol^{-1})	R_G (nm)	$A_2/10^{-4}$ (mol ml g^{-2})	$D_0/10^{-7}$ (cm^2 s^{-1})	k_D
299.5	9.78 ± 0.15	12.4 ± 1.0	-0.60 ± 0.28	2.16 ± 0.02	-46.6 ± 3.3
303.0	9.90 ± 0.17	14.8 ± 1.2	0.32 ± 0.31	2.31 ± 0.06	-41.4 ± 7.1
308.0	-	-	-	2.33 ± 0.04	-13.4 ± 4.1
313.0	9.72 ± 0.18	12.8 ± 0.2	2.00 ± 0.34	2.51 ± 0.05	-10.7 ± 6.0
323.0	10.08 ± 0.21	17.3 ± 0.9	4.02 ± 0.37	-	-

Table 12: Light scattering studies on LH300 in 1,4-dioxane over the temperature range of 299.5 K to 323 K.

Temperature (K)	$\bar{M}_W/10^5$ (g mol^{-1})	R_G (nm)	$A_2/10^{-4}$ (mol ml g^{-2})	$D_0/10^{-7}$ (cm^2 s^{-1})	k_D
299.5	2.25 ± 0.13	19.8 ± 0.7	-0.85 ± 0.47	1.24 ± 0.11	-64.8 ± 25.7
303.0	2.29 ± 0.07	19.7 ± 0.6	0.67 ± 0.24	1.37 ± 0.09	-50.9 ± 21.1
313.0	2.19 ± 0.41	19.3 ± 0.6	1.21 ± 0.41	1.72 ± 0.08	-36.9 ± 13.5
323.0	2.27 ± 0.02	22.3 ± 0.7	2.83 ± 0.50	-	-

The θ-temperature of the polymer-solvent system is defined as the temperature at which the second virial coefficient (A_2) for an infinite molecular weight polymer equals zero. For high molecular weight polymers, this limit is reached.[28] The θ-temperatures were obtained from plots of A_2 versus temperature in Figure 25. A non-linear dependency can be seen for A_2 with temperature. The temperature at which A_2 equalled zero for linear polybutadienes LH50, LH100 and LH300 were 305 K, 302 K and 298 K respectively. A decrease in θ-temperature with increasing molecular weight can be seen for these linear polybutadienes. A θ-temperatures of 299.5 K has been determined for linear polybutadienes in 1,4-dioxane with a microstructure of 93% of 1,4- and 7 % of 1,2-content by Hadjichristidis *et al.*[41] A similar microstructure of approximately 90% of 1,4- and 10% of 1,2-content (as determined

in section 2.3.3) was obtained for LH30, LH100 and LH300. As the microstructures were similar for both sets of samples, and the linear polybutadiene LH300 with the highest molecular weight has a θ-temperature in close agreement with the value obtained by Hadjichristidis[42], then this literature value of 299.5 K can be taken as the θ-temperature.

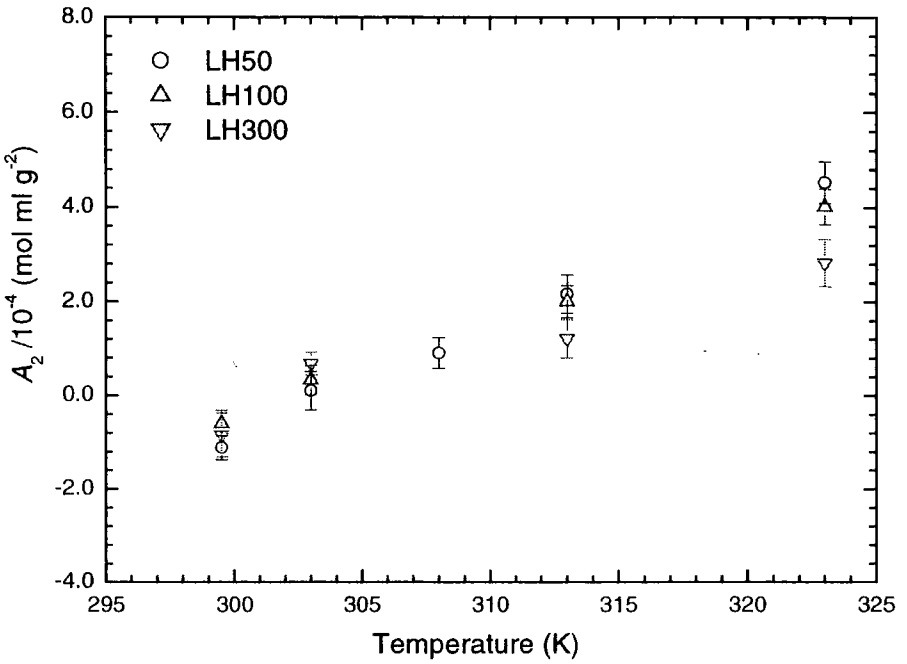

Figure 25: The temperature dependence for A_2 for linear polybutadienes LH50, LH100 and LH300 in dioxane.

The radii of gyration for the linear polybutadienes measured over the same temperature range are given in Table 10, Table 11 and Table 12 for LH50, LH100 and LH300 respectively. An overall increase in R_G with higher temperatures can be seen, demonstrating the increase in global dimensions as the solution became thermodynamically more favourable. The R_G for the linear polymers in dioxane were also lower than those obtained under good solvent conditions, demonstrating the collapse of the polymer dimensions in a poorer solvent. An increase in R_G with increasing molecular weight was noticed for the linear polybutadienes, as reported by Roovers.[16] Figure 26 is a log-log plot of R_G versus $\bar{M}_W$ for the linear polymers in dioxane at the θ-temperature of 299.5 K, with a molecular weight dependence of:

$$R_G = 4.84\times10^{-2}\,\bar{M}_W^{0.49} \qquad (117)$$

The exponent in equation 117 is in close agreement to the characteristic exponent of 0.50 for unperturbed polymers in θ-solvents.[26] This value is also lower than the exponent of 0.54 obtained in good solvent conditions. The translational diffusion coefficient at infinite dilution (D_0) and the concentration dependence for the translational diffusion coefficient (k_D) for the linear polybutadienes LH100 and LH300 are listed in Table 11 and Table 12 respectively. An decrease in D_0 with increasing molecular weight between LH100 and LH300 was found, as reported by Roovers.[16] A decrease in D_0 with temperature can be seen for each polymer as the solvent became thermodynamically poorer. At the θ-temperature of 299.5 K, D_0 values were lower than those obtained in cyclohexane. The k_D was negative for these polymers in dioxane and decreased with temperature and molecular weight, as seen by Roovers.[16] The decrease in k_D with temperature also is a measure of the reduction of the thermodynamic quality of the solution. The intrinsic viscosity ($[\eta]$) and the Huggins constant (k_H) for each linear polymer measured at the θ-temperature of 299.5 K are reported in Table 13. An increase in $[\eta]$ with molecular weight can be seen, that was also noticed by Roovers[16] for the same polymer-solvent system. The values were also lower than those characterised under good solvent conditions. A log-log plot of $[\eta]$ versus $\overline{M}_W$ for the linear polybutadienes in dioxane at a temperature of 299.5 K is shown in Figure 27 and a linear fit to this graph yields:

$$[\eta] = 8.43 \times 10^{-2} \overline{M}_W^{0.57} \qquad (118)$$

The Mark-Houwink-Sakaruda (MHS) exponent in equation 118 was 0.57, higher than the value of 0.50 obtained for linear polybutadienes under θ-solvent conditions by Roovers[16] but is lower than 0.69 obtained under good solvent conditions. The MHS parameter K_θ of 8.43×10^{-2} ml g^{-1} was higher than the value obtained in good solvent conditions of 3.67×10^{-2} ml g^{-1}, but not as high as a values of 1.99×10^{-1} ml g^{-1} and 1.98×10^{-1} ml g^{-1} determined by experimental and theoretical methods respectively for linear polybutadienes in dioxane at 299.5 K by Ioan *et al.*[16] The Huggins constants (k_H) for LH50, LH100 and LH300 were 0.65, 1.10 and 1.40 respectively and are higher than 0.5 to 0.6 that are usually determined for k_H under θ-conditions.[11] Values of k_H tend only to become molecular weight dependent in aggregated systems.[12] An increase in k_H with molecular weight can be seen for the linear polymers in Table 13, which suggests aggregation in this θ-solvent, but was not seen in the molecular weight data.

Table 13: Viscometry data for the linear polybutadienes LH50, LH100 and LH300 in dioxane at a temperature of 299.5 K.

Sample	$[\eta]$ (ml g^{-1})	k_H
LH50	41.4 ± 0.5	0.65 ± 0.06
LH100	56.1 ± 0.1	1.10 ± 0.01
LH300	96.7 ± 1.0	1.40 ± 0.09

The hydrodynamic (R_H) and viscometric (R_V) radii were calculated for these polymers from equations 36 and 42 in chapter 1. Table 14 lists R_H and R_V for LH50, LH100 and LH300 in dioxane over the temperature range of 299.5 K to 313 K. No hydrodynamic radii data was obtained for LH50. The equivalent sphere radii both increased with molecular weight for the linear polybutadienes. R_H and R_V are practically identical for the linear polymers at the θ-temperature. At 299.5 K, R_H and R_V for these polymers were less than those ascertained under good solvent conditions (see Table 6). A small decrease with temperature can be seen for R_H for LH100 as the solution becomes thermodynamically poorer. The R_H remained practically constant for LH300 over the temperature range, but the errors in R_H increased with decreasing temperature.

Table 14: The hydrodynamic and viscometric radii for linear polybutadienes in dioxane over the temperature range of 299.5 K to 313 K.

Temp (K)	LH50		LH100		LH300	
	R_H (nm)	R_V (nm)	R_H (nm)	R_V (nm)	R_H (nm)	R_V (nm)
299.5	-	6.9 ± 0.1	8.6 ± 0.1	9.5 ± 0.1	15.0 ± 1.3	15.1 ± 0.3
303.0	-	-	8.7 ± 0.2	-	14.7 ± 1.0	-
308.0	-	-	9.7 ± 0.2	-	-	-
313.0	-	-	10.0 ± 0.2	-	14.6 ± 0.7	-

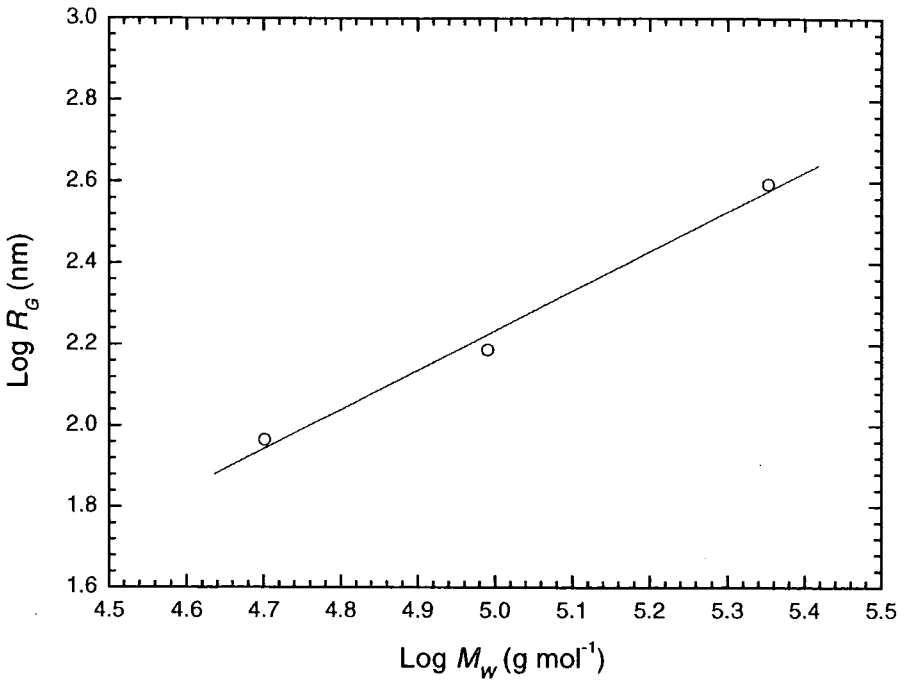

Figure 26: A log-log plot of R_G versus $\bar{M}_W$ for linear polybutadienes in 1,4- dioxane at a temperature of 299.5 K.

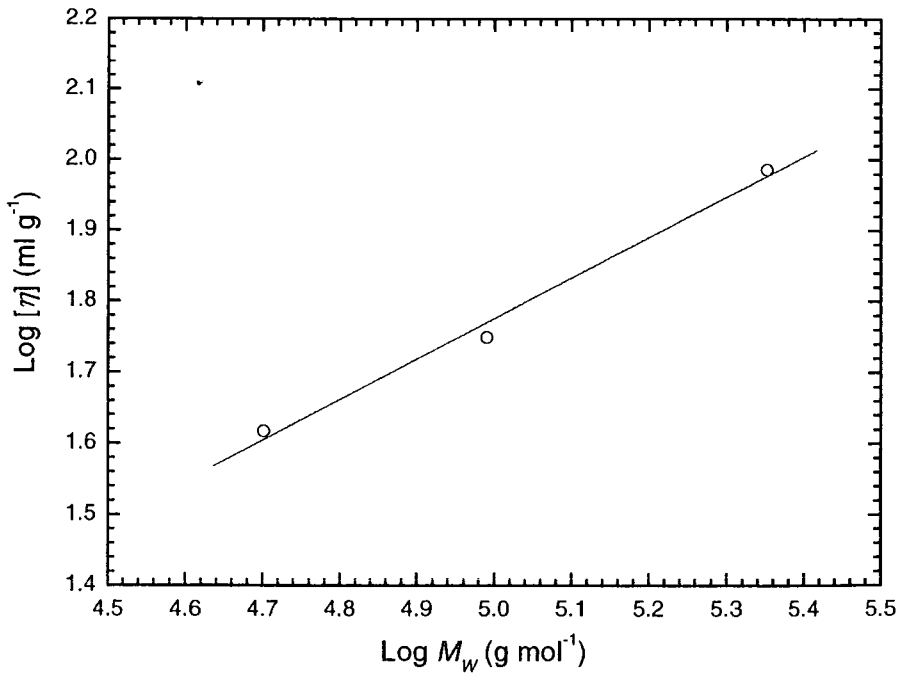

Figure 27: A log-log plot of [η] versus $\bar{M}_W$ for linear polybutadienes in 1,4- dioxane at a temperature of 299.5 K.

The size ratios R_H/R_G and R_V/R_G compare the equivalent sphere radii to the directly measurable radius of gyration. R_H/R_G ratios for LH100 and LH300, and R_V/R_G ratios for LH50, LH100 and LH300 in dioxane at the θ-temperature are reported in Table 15. In dioxane, R_H/R_G ratios were 0.69 and 0.75 for LH100 and LH300 respectively. R_H/R_G ratios of 0.52 and 0.59 were obtained for LH100 and LH300 in cyclohexane (see Table 7), that were lower than determined in dioxane. Roovers[18] obtained similar R_H/R_G ratios of 0.72 and 0.74 in good and θ-solvent conditions respectively. R_H/R_G ratios for the linear polybutadienes in Table 15 are similar to the values obtained by Roovers for θ-conditions, but are lower than the data obtained in cyclohexane. This behaviour is contrary to that observed by Roovers.

In Table 15, the R_V/R_G ratios are 0.72, 0.77 and 0.76 for LH50, LH100 and LH300 in dioxane, and appear to be independent of molecular weight. These values are similar to those determined in cyclohexane of 0.72, 0.75 and 0.75 for LH50, LH100 and LH300 respectively. Roovers[18] obtained an of R_V/R_G of 0.84 for both solvent conditions. The linear polybutadienes LH50, LH100 and LH300 have identical R_V/R_G ratios in good and in θ-solvents in agreement to the data of Roovers, but are both lower than the ratios calculated by Roovers[18] for each solvent condition. The friction constants were calculated from k_D and for LH100 and LH300 were 2.06 and 0.69 respectively (see Table 11). The linear polymer LH100 had k_0 in good approximation to that obtained by Roovers of 2.5 and the Pyun and Fixman[8] value of 2.20. A lower value of 0.69 was obtained for LH300, which reflects the sensitivity in the calculation of k_0 in equation 39, chapter 1, to the molecular weight and hydrodynamic radius determined.

Table 15: Size ratios of R_H/R_G and R_V/R_G and the friction constant for the linear polybutadienes LH50, LH100 and LH300 in dioxane at a temperature of 299.5 K.

Sample	R_H/R_G	R_V/R_G	k_0
LH50	-	0.72 ± 0.07	-
LH100	0.69 ± 0.06	0.77 ± 0.07	2.06 ± 1.24
LH300	0.75 ± 0.09	0.76 ± 0.04	0.69 ± 0.89

3.4.2.2 Miktoarm Star Polybutadienes

Static and dynamic light scattering experiments were performed on miktoarm star polymers in 1,4-dioxane over a temperature range of 298 K to 323 K. The values of $\bar{M}_W$, R_G, A_2, D_0 and k_D obtained from these experiments for the stars S30, S60, S80 and S300 are reported in Table 16, Table 17, Table 18 and Table 19 respectively. The weight-average molecular weights for these stars tended to increase with decreasing temperature (see Figure 28), where for the linear polymers they remained constant. In dioxane at a temperature of 299.5 K, the star polymers S300, S80 and S60 had $\bar{M}_W$ of 7.51×10^5 g mol^{-1}, 4.96×10^5 g mol^{-1} and 3.26×10^5 g mol^{-1} respectively. In cyclohexane, lower $\bar{M}_W$ of 5.81×10^5 g mol^{-1}, 3.58×10^5 g mol^{-1} and 2.39×10^5 g mol^{-1} were measured respectively (see Table 4). The $\bar{M}_W$ data in cyclohexane was comparable to values obtained for the stars by SEC in THF (see Table 4, section 2.3.5). At higher temperatures in dioxane, these stars approached $\bar{M}_W$ values comparable to those obtained under good solvent conditions. Light scattering values could not be obtained for the 8-arm regular star S30 in dioxane at a temperature less than 308 K, because the polymer precipitated out of solution. For S30, a $\bar{M}_W$ of 5.79×10^5 g mol^{-1} was measured at 308 K, greater than that obtained in cyclohexane ($\bar{M}_W$ of 3.75×10^5 g mol^{-1} in Table 4). The $\bar{M}_W$ for 4- and 6-arm polystyrene stars in a θ-solvent were found to be constant over the temperature range of measurement.[42, 43]

Table 16: Light scattering studies on star S30 in 1,4-dioxane over the temperature range of 308 K to 323 K.

Temperature (K)	$\bar{M}_W/10^5$ (g mol^{-1})	R_G (nm)	$A_2/10^{-4}$ (mol ml g^{-2})	$D_0/10^{-7}$ (cm^2 s^{-1})	k_D (cm^3 g^{-1})
308.0	5.79 ± 0.08	23.0 ± 0.8	0.09 ± 0.18	1.52 ± 0.14	-34.3 ± 30.8
313.0	5.35 ± 0.05	22.6 ± 1.0	0.22 ± 0.09	1.41 ± 0.07	-19.8 ± 15.1
323 .0	4.79 ± 0.14	24.3 ± 0.6	1.24 ± 0.48	1.31 ± 0.06	26.0 ± 18.8

Table 17: Light scattering studies on star S60 in 1,4-dioxane over the temperature range of 298 K to 323 K.

Temperature (K)	$\bar{M}_W/10^5$ (g mol^{-1})	R_G (nm)	$A_2/10^{-4}$ (mol ml g^{-2})	$D_0/10^{-7}$ (cm^2 s^{-1})	k_D (cm^3 g^{-1})
298.0	-	-	-	1.50 ± 0.01	-32.7 ± 1.5
299.5	3.26 ± 0.11	12.5 ± 1.1	-0.02 ± 0.19	1.56 ± 0.04	-34.5 ± 7.2
303.0	2.99 ± 0.07	13.1 ± 1.0	0.33 ± 0.14	1.64 ± 0.03	-22.6 ± 4.7
308.0	2.76 ± 0.10	14.3 ± 0.8	0.92 ± 0.22	1.80 ± 0.06	-20.5 ± 9.0
313.0	2.61 ± 0.09	15.8 ± 0.8	1.54 ± 0.25	1.88 ± 0.03	-3.7 ± 3.2
323.0	2.25 ± 0.08	16.2 ± 1.2	2.70 ± 0.30	2.24 ± 0.14	-3.6 ± 13.6

Table 18: Light scattering studies on star S80 in 1,4-dioxane over the temperature range of 298 K to 323 K.

Temperature (K)	$\bar{M}_W/10^5$ (g mol^{-1})	R_G (nm)	$A_2/10^{-4}$ (mol ml g^{-2})	$D_0/10^{-7}$ (cm^2 s^{-1})	k_D (cm^3 g^{-1})
298.0	5.08 ± 0.07	19.4 ± 0.8	-0.02 ± 0.18	-	-
299.5	4.96 ± 0.08	19.3 ± 0.8	-0.08 ± 0.21	1.78 ± 0.43	-49.4 ± 46.8
303.0	4.74 ± 0.09	19.2 ± 0.6	0.17 ± 0.27	1.51 ± 0.19	-15.9 ± 27.9
308.0	4.03 ± 0.10	20.0 ± 0.6	0.36 ± 0.40	1.63 ± 0.14	-19.7 ± 16.5
313.0	3.70 ± 0.12	20.2 ± 0.8	0.52 ± 0.58	1.50 ± 0.07	5.3 ± 9.6
323.0	-	-	-	1.69 ± 0.01	14.2 ± 0.6

The radius of gyration for the stars (see Table 16-Table 19) tended to increase with temperature (see Figure 29), as dioxane became a more thermodynamically favourable solvent at higher temperatures. This behaviour was also noticed for 4- and 6-arm polystyrene stars in the θ-solvent of cyclohexane.[43, 44] The R_G of the miktoarm stars S300, S80 and S60 in dioxane over the temperature range were lower than in cyclohexane (Table 4), demonstrating the perturbed dimensions gained within a good solvent. The opposite behaviour was noticed for the star S30, where an R_G of 18 nm and 23 nm were measured in

cyclohexane at 298 K and in dioxane at 308 K respectively. This increase in R_G for S30 within a thermodynamically poorer solvent could be due to aggregation of the stars into larger species in this solution. If the star polymers were aggregating, then a range of species would exist in solution, defined by the number of stars per aggregate and the functionality of the star. The average arm-functionality for the star S30 of 8 suggested full coupling, then aggregation for this star would just become dependent on the number of stars per aggregate.

Table 19: Light scattering studies on S300 in 1,4-dioxane over the temperature range of 298 K to 323 K.

Temperature (K)	$\bar{M}_W/10^5$ (g mol^{-1})	R_G (nm)	$A_2/10^{-4}$ (mol ml g^{-2})	$D_0/10^{-7}$ (cm^2 s^{-1})	k_D (cm^3 g^{-1})
298.0	7.87 ± 0.20	29.1 ± 1.0	0.34 ± 0.21	0.84 ± 0.05	-51.1 ± 16.2
299.5	7.51 ± 0.15	29.1 ± 0.6	0.46 ± 0.18	0.86 ± 0.04	-45.2 ± 15.2
303.0	7.10 ± 0.17	29.4 ± 1.3	0.82 ± 0.23	0.89 ± 0.05	-26.9 ± 7.5
308.0	6.52 ± 0.12	31.7 ± 0.7	1.44 ± 0.19	0.99 ± 0.02	-14.2 ± 4.3
313.0	6.09 ± 0.16	31.4 ± 0.9	1.89 ± 0.29	1.08 ± 0.01	-3.7 ± 1.9
323.0	5.59 ± 0.05	34.7 ± 0.6	2.79 ± 0.11	1.33 ± 0.01	5.2 ± 0.8

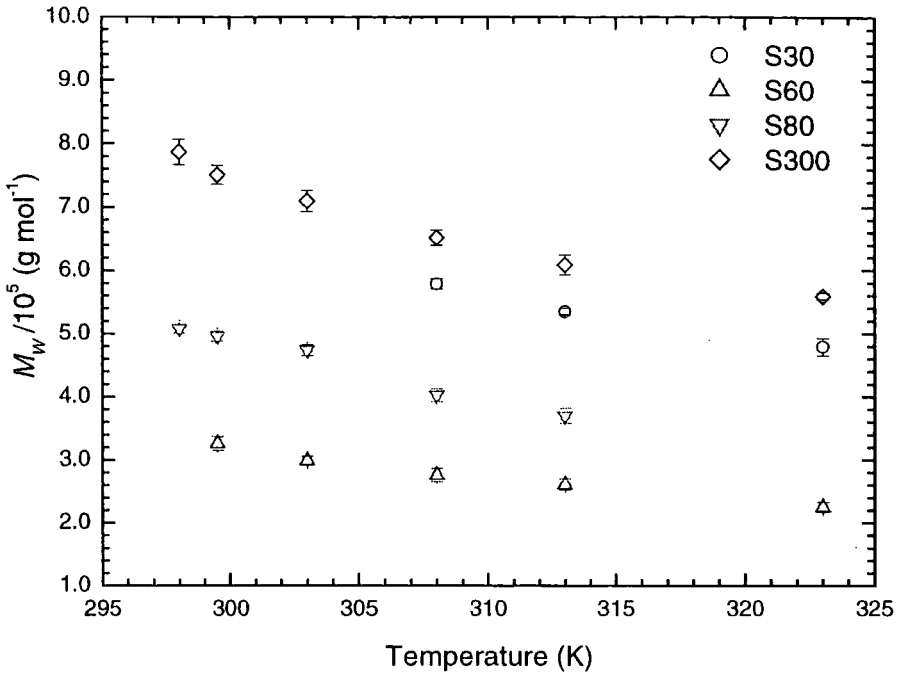

Figure 28:The temperature dependence of the $\overline{M}_W$ of the miktoarm star polymers in dioxane.

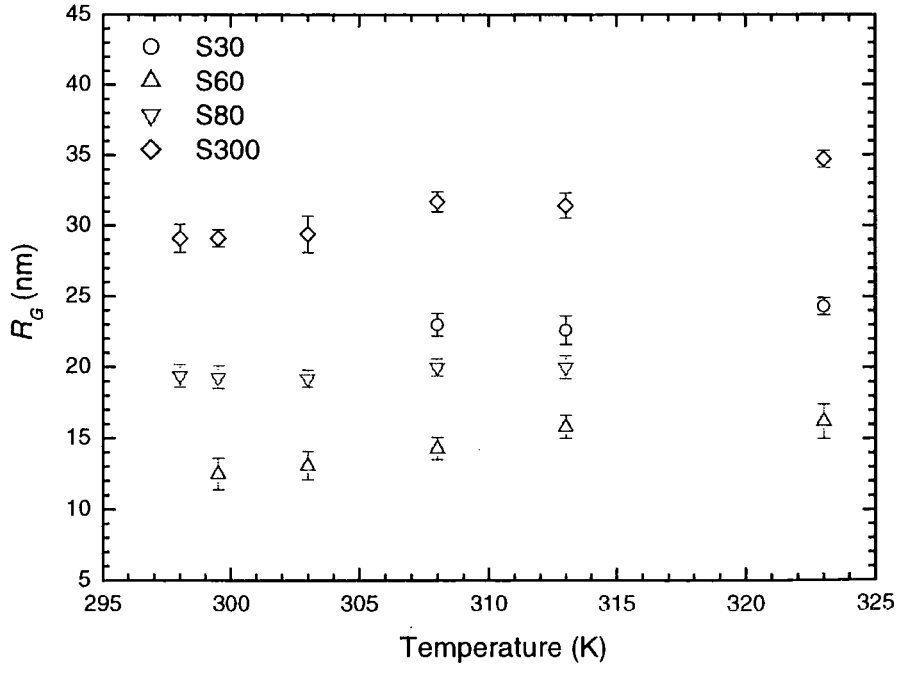

Figure 29:The temperature dependence of the R_G of the miktoarm star polymers in dioxane.

An increase in the second virial coefficients with temperature (see Figure 30) can be seen in Table 16 to Table 19 for the miktoarm star polymers. The θ-temperature point is determined as the temperature at which A_2 equals zero and were ascertained for the stars by from non-linear plots of A_2 versus temperature in Figure 30. Non-linear dependencies of A_2 with temperature was also noticed for 4- and 6-arm polystyrene stars within a θ-solvent.[43, 44] The θ-temperatures for miktoarm star polymers S30, S60, S80 and S300 were determined to be 308.4 K, 300.0 K, 299.5 K and 294.4 K respectively. A decreasing "θ-temperature" with increasing length of the asymmetric arm was noted. Theoretical and experimental work performed on star polymers in solution reported a θ-temperature depression when compared to linear polymers of the same molecular weight.[44-49] Bauer *et al*[45] reported a θ-temperature depression for low molecular weight 8- and 12-arm polyisoprene stars in dioxane. An increase in the molecular weight of the star arms increased the θ-temperature to a value similar to those of a linear polyisoprene of the same molecular weight. The θ-temperature depression was also reported for low molecular weight 8-arm polystyrenes in cyclohexane.[46]

Ganazzoli and Allegra[47] used a model to describe the θ-temperature lowering of star polymers by a theoretical free energy contribution approach. A equivalent bead-and-spring model was considered comprising of N atoms with N/f atoms per arm. The θ-temperature was determined analytically as the temperature at which a balance was reached between the repulsive 3-body interactions and attractive 2-body interactions, where the latter increased with decreasing temperature and the former remained constant. Their model predicted that for a branched star ($f > 4$) with short arms, the segment density at the core will be high and a large number of ternary contacts will exist. Lowering of the θ-temperature for this star will occur so that the 3-body interactions can be compensated by a larger number of 2-body interactions. For a star polymer with long arms, the fraction of segments near the star core diminishes and the number of 3-body interactions became negligible and therefore the same θ-temperature will be obtained for any architecture. Okumoto *et al*[43, 44] noticed that the binary cluster integral breaks down for ternary interactions near the θ-temperature, where it holds for the case of linear chains. Monte-Carlo lattice models have also found a depression in θ-temperature for model 4-, 5- and 6-arm regular stars.[48]

Dondos *et al*[49] applied the blob theory to obtain the θ-temperature of star polymers. The polymer chains were divided into a series of blobs where inside each blob the polymer had single chain behaviour. If the molecular mass of a star blob and hence size was less than for a linear blob, then the θ-temperature of the star was calculated to be lower than the corresponding linear. If the molecular mass of the star blob was greater than for the linear blob, then the θ-temperature was deemed to be higher for a star. This model was applied to lightly branched stars (up to 6-arms) and the θ-temperature was calculated to be less than a linear counterpart, up to a molecular weight limit. For a highly branched star with a short arms, the θ-temperature was less than the linear counter part, but increased above the linear θ-value with increasing arm length. The authors used the Daoud and Cotton model[50] to explain the θ-temperature depression for short arm stars as the model predicted that the blob size decreased as the branched point was approached. The Boothroyd and Ball model[51] was used to explain the increase in θ-temperature for highly branched stars compared to the linear counter parts, as this model described the interior of a highly branched star to be a impenetrable sphere that can be considered to be one large blob.

Striolo *et al*[50] measured an increase in A_2 with temperature for a 7-arm poly(ethylene oxide) stars in the polar solvent of water. The θ-temperature was found to be near 328 K to 333 K for the star, where a lower θ-temperature of 323 K was reported for a linear analogue. This increase in θ-temperature with branching was suggested to occur because of the repulsion generated by the high segment density around the centre of mass of the star, that causes an increase in solubility in hydrogen-bond forming solvents.

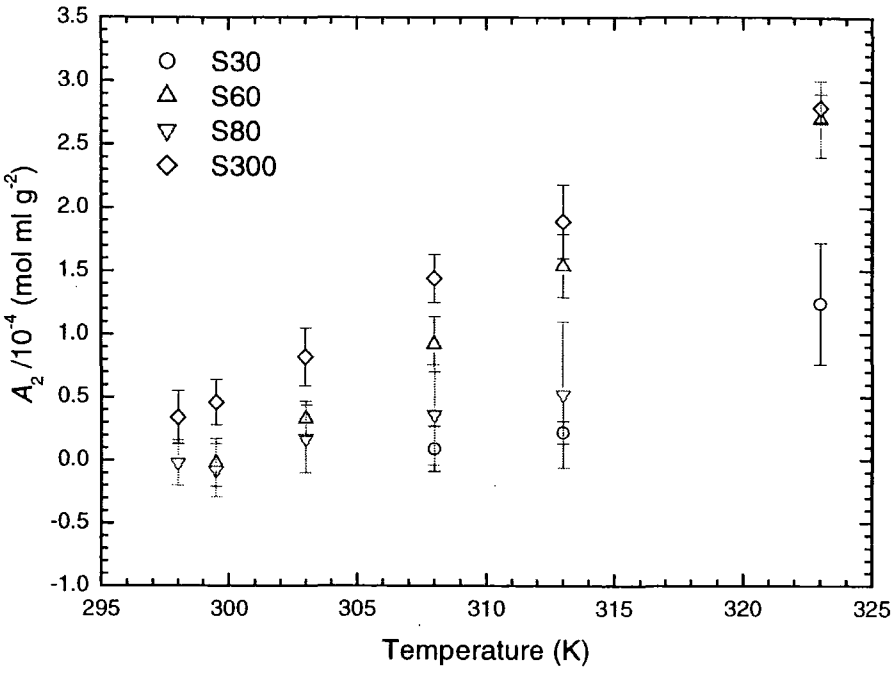

Figure 30: The temperature dependence of the A_2 of the miktoarm star polymers in dioxane.

The 8-arm regular star polymer S30 was found to have a θ-temperature of 308.4 K that was higher than the value predicted for a linear polybutadiene of 299.5 K. This regular star has a high segment density near the core. Over the temperature range of measurement, this star had $\bar{M}_W$ and R_G data that were greater than obtained in cyclohexane solutions and suggested aggregation within this solvent. Aggregation of this star in dioxane, would allow the star cores to approach each other and allow plenty of contacts for the arms to entangle or a physical cross-links to be formed. Regular star polymers would have a more spherical shape than linear polymers in solution and would find it easier to compact together. The entanglement or cross-linking of the arms within the formed aggregates would yield a high segment density and therefore yield an impenetrable core. The application of the blob model of Dondos *et al*[49] treats this impenetrable core as an overall large blob, as predicted by the model of Boothroyd and Ball[52], and a higher θ-temperature would be expected over its linear counterpart as observed.

The miktoarm star polymer S300, with the longest asymmetric arm length was found to have a θ-temperature of 294.4 K, lower than obtained for linear polybutadienes. The $\bar{M}_W$ of

this star in dioxane at 299.5 K was greater than measured in cyclohexane, suggesting the formation of higher molecular weight species at this temperature. The R_G of the star was less than the value ascertained in cyclohexane, as would be expected in this thermodynamically poorer solvent. The asymmetric star S300 will have a lower segment density near the core when compared to the regular star S30. The θ-temperature lowering for this star would be due to the compensation of 3-body interactions at the branch point by an increased number of two-body interactions, according to the model of Ganazzoli and Allegra.[34] If the model of Daoud and Cotton[37] is applied to this star, then the size of the blobs along the arms become smaller as the core is approached and the Dondos model[36] predicts a lower θ-temperature. Asymmetric star S300 would have a more aspherical shape in solution when compared to regular star S30 and star cores would find it more difficult to aggregate. This means that a lower extent of aggregation might occur for S300, when compared to the regular star S30.

The miktoarm stars S60 and S80 have asymmetric arm lengths that were in between those obtained for S30 and S300. The θ-temperatures determined for S60 and S80 were 300 K and 299.5 K respectively, which are in close agreement to the value of 299.5 K predicted for linear polybutadienes. The weight-average molecular weights for these stars in dioxane solutions near the θ-temperature were higher and R_G values lower than obtained in cyclohexane. The presence of the shorter asymmetric arms will produce more-spherical shapes than for the star S300. This would allow the cores of the star polymers to approach each other easier and allow the formation of compact aggregates. Aggregation would occur to a lesser extent when compared to the more-spherical regular star S30. This lower extent of aggregation would not cause the formation of an interpenetratable core and no θ-temperature increase would be observed. The effect of aggregation appears to have no effect at all on the θ-temperature of these two star polymers.

Translational diffusion coefficients at infinite dilution (D_0) and concentration dependence coefficient (k_D) for the star polymers in dioxane over a range of temperatures, can be seen in Table 16 to Table 19. Star polymers have higher translational diffusion coefficients than for linear polymers of equivalent molecular weight, in both solvent conditions. Insufficient data for the linear polymers and the aggregating nature of the stars cause these predictions to be unreliable. Regular polybutadiene stars have been found to have a lower D_0 in θ-solvents,

than in good solvents, but became higher as the molecular weight of the arms increased.[15-17] The translational diffusion coefficients at infinite dilution obtained in cyclohexane for S30, S60 and S80 were 1.29×10^{-7} cm^2 s^{-1}, 1.58×10^{-7} cm^2 s^{-1} and 1.27×10^{-7} cm^2 s^{-1} respectively (see Table 4). No data are available for S300 in cyclohexane.

Only the star polymer S60 had D_0 lower at the θ-condition than in the good solvent. The molecular weights of all the stars increased with decreasing temperature in dioxane. A decrease in D_0 with temperature was noticed for stars S60 and S300, where the opposite occurred for stars S30 and S80. The higher values for S30 and S80 could be due to the extent of aggregation of these stars in solution. The stars S60 and S300 had a decrease in D_0 as the decrease in the temperature caused slower translational motion of the stars in a the cooler thermodynamically poorer solvent. The differences experienced for D_0 demonstrate the complex nature of the aggregating solutions. The concentration dependence coefficient (k_D) is a measure of the thermodynamic ability of the solvent as well (see equation 39, chapter 1). All the stars had k_D values that decreased with temperature, showing that dioxane was becoming a thermodynamically poorer solvent. Roovers noticed a decrease in k_D with increasing molecular weight for these 18-arm polybutadiene stars.[15] Near the θ-temperature for these miktoarm stars, a decrease in k_D with increasing molecular weight between each star was observed.

Viscometry data for the miktoarm star polymers S60 and S300 in dioxane are reported in Table 20. Values for the intrinsic viscosity ($[\eta]$) and Huggins constant (k_H) for these two stars were measured over a temperature range of 298 K to 323 K. Figure 31 is the plot of the temperature dependence of $[\eta]$ for the stars, and an increase in $[\eta]$ with temperature can be seen. The intrinsic viscosity for the stars reduces as the temperature decreases as the stars adopt smaller dimensions in a thermodynamically poorer solution. An increase in the intrinsic viscosity with temperature has been measured for 4-arm and 6-arm polystyrene stars near the θ-temperature.[43, 44] Model polybutadiene stars[15-19], polyisoprene stars[20-22] and polystyrene stars[23-25] had lower intrinsic viscosities in θ-solvents, than under good solvent conditions. The intrinsic viscosities for S60 and S300 were smaller than obtained in cyclohexane (see Table 5). Star polymers S60 and S300 had intrinsic viscosities of 105.8 ml g^{-1} and 299.6 ml g^{-1} in cyclohexane. This demonstrates the reduction in size of the star polymers in a thermodynamically poorer solvent.

The Huggins constants (k_H) for these stars are plotted against temperature in Figure 32. An increase in k_H can be seen with decreasing temperature for both S60 and S300. Star polymer S60 has greater values of k_H than for S300 over this temperature range. The Huggins constants measured in dioxane were greater than the values obtained in cyclohexane of 0.54 and 0.36 for S60 and S300 respectively. Bauer *et al*[21] noticed for regular polyisoprene stars in θ-solvents, k_H increased with star functionality and arm molecular weight. Star S300 has approximately the same functionality as S60, but a larger difference in k_H can be seen at lower temperature, whereas at higher temperatures similar values were obtained. An increase in the Huggins constants as the θ-temperature was approached was due to the poorer thermodynamic quality of this solvent (more polymer-polymer contacts). As S60 was found to have an higher θ-temperature than S300, the solvent becomes thermodynamically poorer at higher temperatures for S60 than for S300. This means that S60 was more likely to aggregate at lower temperatures and have an increase in k_H. The miktoarm star S60 has a shorter asymmetric arm than S300 and hence more spherical shape. A higher extent of aggregation can be expected for S60 when compared to S300 at lower temperatures, due to its poorer polymer-solvent interactions and greater ease for the star cores to approach each other.

Table 20: Viscometry data for miktoarm star polymers over the temperature range of 299.5 K to 323 K.

Temp. (K)	S60		S300	
	$[\eta]$ (ml g^{-1})	k_H	$[\eta]$ (ml g^{-1})	k_H
299.5	52.0 ± 0.2	0.97 ± 0.03	117.6 ± 0.7	0.74 ± 0.04
303.0	55.1 ± 0.1	0.79 ± 0.02	126.6 ± 1.2	0.67 ± 0.06
308.0	-	-	133.7 ± 0.4	0.72 ± 0.02
313.0	60.7 ± 0.1	0.70 ± 0.01	146.1 ± 1.0	0.58 ± 0.03
323.0	64.9 ± 0.1	0.69 ± 0.01	158.0 ± 0.5	0.66 ± 0.01

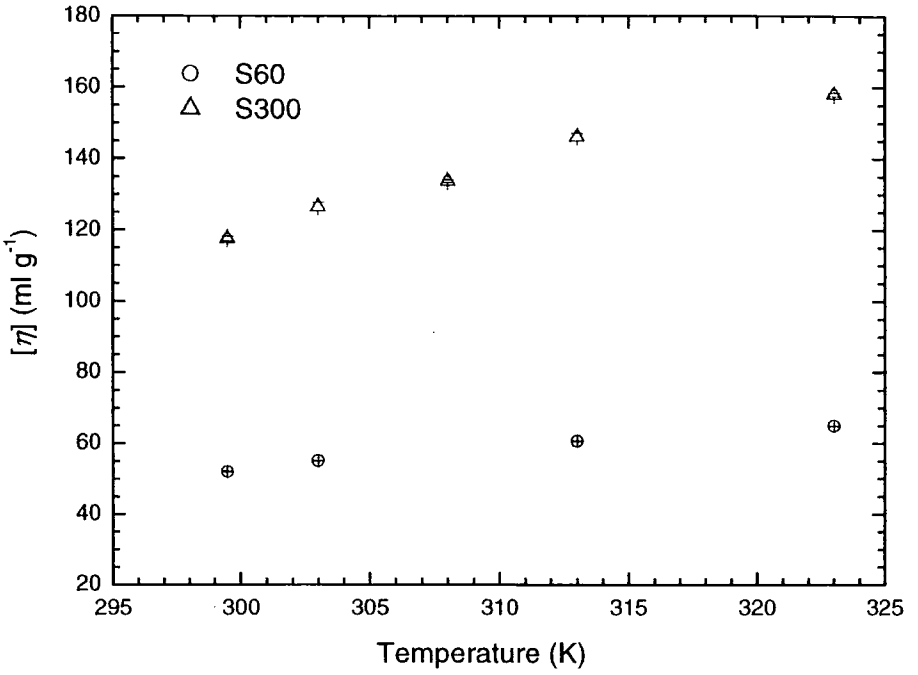

Figure 31: Temperature dependence on the [η] for miktoarm star polymers S60 and S300.

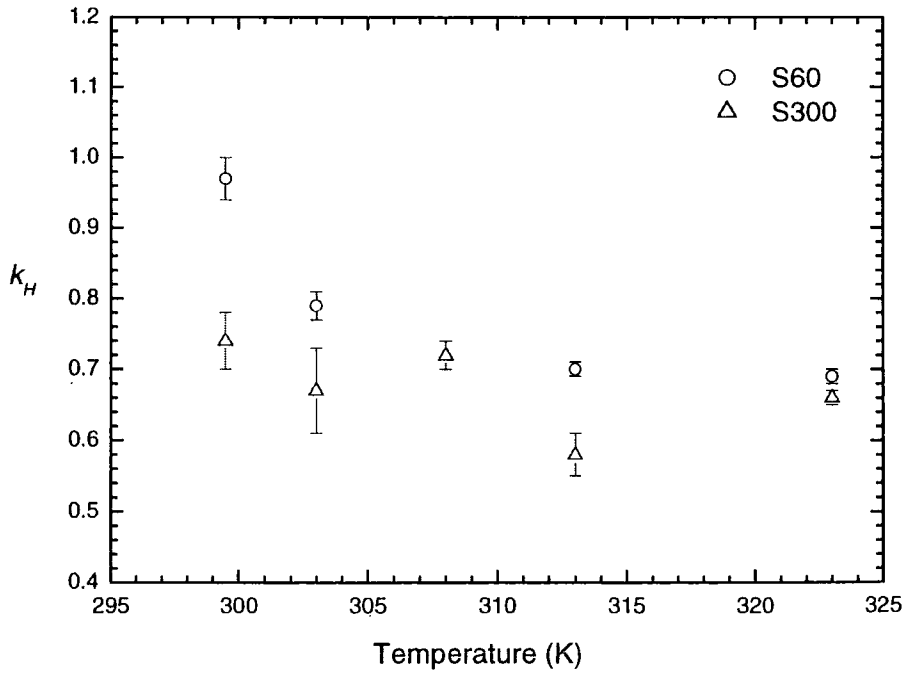

Figure 32: Temperature dependence on k_H for miktoarm star polymers S60 and S300.

The hydrodynamic radii (R_H) were calculated for the miktoarm star polymers from D_0, using the Stokes-Einstein equation (equation 36, chapter 1) and are shown in Table 21. A decrease in R_H towards lower temperature was evident. The rate of decrease of R_H with temperature was higher for stars S30 and S80 than for stars S60 and S300. This reflects the sensitivity of the calculated hydrodynamic radii from the Stokes-Einstein equation to the measured diffusion coefficients. In cyclohexane, the R_H for star polymers S30, S60 and S80 were 18.8 nm, 15.4 nm and 19.1 nm respectively. The hydrodynamic radii for the miktoarm star polymers S30, S60 and S80, were lower than those ascertained under good solvent conditions, apart from the higher temperature values for aggregating regular star S30. For 64- and 128-arm polybutadiene stars a smaller R_H in dioxane than in cyclohexane was noted.[18] This reflects the reduction of the star dimensions in a thermodynamically poorer solvent and hence lower R_H.

Table 21: Hydrodynamic radii (R_H) for miktoarm stars S30, S60, S80 and S80 in dioxane over the temperature range 298 K to 323 K.

Temperature (K)	S30 R_H (nm)	S60 R_H (nm)	S80 R_H (nm)	S300 R_H (nm)
298.0	-	12.0 ± 0.1	-	21.4 ± 1.3
299.5	-	11.9 ± 0.3	10.5 ± 2.5	21.7 ± 1.0
303.0	-	12.3 ± 0.2	13.4 ± 1.7	22.7 ± 1.3
308.0	14.8 ± 1.4	12.5 ± 0.4	13.8 ± 1.2	22.8 ± 0.5
313.0	17.8 ± 0.9	13.4 ± 0.2	16.7 ± 0.8	23.3 ± 0.2
323.0	23.5 ± 1.1	13.7 ± 0.9	18.2 ± 0.1	23.1 ± 0.2

The viscometric radii (R_V) calculated for star polymers S60 and S300 in dioxane are listed in Table 22. These values are lower than the radii determined under good solvent conditions of 15.4 nm and 30.2 nm for S60 and S300 respectively. Regular star polymers have been found to have smaller R_V in thermodynamically poorer solvent conditions.[18, 21] This also demonstrates the reduction of the intrinsic viscosity in a θ-solvent, due to the decrease in star dimensions. For S60, there is an increase in R_V with decreasing temperature, whereas R_V for S300 remained practically constant. An increase in R_V with decreasing temperature for S60 suggests the formation of a larger species due to aggregation, as the θ-temperature was approached.

Table 22: Viscometric radii (R_V) for miktoarm stars S30, S60, S80 and S80 in dioxane over the temperature range of 299.5 K to 323 K.

Temperature (K)	S60 R_V (nm)	S300 R_V (nm)
299.5	13.9 ± 0.2	24.1 ± 0.2
303.0	13.8 ± 0.1	24.2 ± 0.2
308.0	-	24.0 ± 0.2
313.0	13.6 ± 0.2	24.2 ± 0.3
323.0	13.2 ± 0.2	24.1 ± 0.3

The R_H/R_G ratios for each star have been calculated and are reported in Table 23. These values were smaller than for the hard sphere limit of 1.29, as the stars were able to interpenetrate each other. For regular star polymers, R_H/R_G has been found to increase with star functionality, to values higher than the hard sphere limit.[16] The size ratios R_H/R_G for both S30 and S80 decreased with temperature, but R_H/R_G increased slightly with decreasing temperature for S60 and essentially remained constant for S300. This variation for these size ratios are related to the extent of aggregation experienced. An increase of this size ratio with decreasing temperature suggest a higher segment density at the core, as the hydrodynamic radius equals the radius of gyration. Experimental work performed on linear polybutadienes, 4-arm regular polystyrene stars and 18-arm regular polybutadiene stars under θ-conditions have yielded R_H/R_G values of 0.74, 0.94 and 1.18 respectively.[16] The

linear polybutadienes LH100 and LH300 obtained R_H/R_G of 0.69 and 0.75 respectively in dioxane at 299.5 K. At lower temperatures, the star polymers S60 and S300 have R_H/R_G similar to lower functional stars (f<4) and linear polymers respectively. The values obtained from the linear polybutadienes LH100 and LH300 are similar to those calculated for S300.

The star S300 has a longer asymmetric arm length than S60 and hence a lower segment density near the star core and R_H/R_G. The increase for S60 and independence of S300 for this size ratio with decreasing temperature (see Figure 33) could be due to the higher θ-temperature of S60. If the solvent is becoming thermodynamically poorer faster for S60, than for S300, then aggregation could be occurring at a greater rate for S60. The decrease in R_H/R_G with temperature for stars S30 and S80 suggests a decrease in segment density near the core. As these stars have been suggested to be forming higher molecular weight aggregates as the θ-temperature was approached, then an increase in R_H/R_G would be expected. The values of R_H/R_G obtained for these stars must be sensitive to the R_H obtained from the Stokes-Einstein equation, due to the measurement of D_0 from a diverse solution containing a range of functional star aggregates.

Table 23: The ratio of R_H/R_G for the miktoarm stars in dioxane over the temperature range of 298 K to 323 K.

Temperature (K)	S30	S60	S80	S300
	R_H/R_G	R_H/R_G	R_H/R_G	R_H/R_G
298.0	-	-	-	0.74 ± 0.07
299.5	-	0.95 ± 0.11	0.54 ± 0.15	0.75 ± 0.05
303.0	-	0.94 ± 0.09	0.70 ± 0.11	0.77 ± 0.08
308.0	0.64 ± 0.08	0.87 ± 0.08	0.81 ± 0.08	0.72 ± 0.03
313.0	0.79 ± 0.07	0.85 ± 0.06	0.83 ± 0.07	0.74 ± 0.03
323.0	0.97 ± 0.07	0.85 ± 0.12	-	0.67 ± 0.01

The size ratios of the viscometric radius to the radius of gyration (R_V/R_G) for the star polymers S60 and S300 in dioxane can be seen in Table 24. An increase in R_V/R_G with reduction in temperature for both S60 and S300 can be observed in Figure 34. For S60 and S300, R_V/R_G ranged from 0.81 to 1.11, and 0.69 to 0.83 respectively with decreasing temperature. Literature values have reported an increase in R_V/R_G with arm functionality up to a hard sphere limit of 1.29.[19] For linear, 4-, 6- and 8-arm regular polyisoprene stars under θ-conditions, R_V/R_G was 0.83, 0.95, 1.04 and 1.03 respectively.[21] R_V/R_G obtained for linear polybutadienes LH50, LH100 and LH300 in dioxane at 299.5 K were 0.72, 0.77 and 0.76 respectively. The star S300 has a longer asymmetric arm length than S60 and therefore has a lower segment density near the core. The R_V/R_G values for S300 over the range of temperatures are similar to a linear polymer and suggests lower segment density. The star S60 with the shorter asymmetric arm length has a R_V/R_G similar to a higher functional star at lower temperatures. The high values experienced for S60 near its θ-temperature, could be due to increased segment densities formed from a greater extent of aggregation.

Table 24: The ratio of R_V/R_G for the miktoarm stars S60 and S300 in dioxane over the temperature range of 299.5 K to 323 K.

Temperature (K)	S60 R_V/R_G	S300 R_V/R_G
299.5	1.11 ± 0.11	0.83 ± 0.02
303.0	1.05 ± 0.09	0.82 ± 0.04
308.0	-	0.76 ± 0.02
313.0	0.86 ± 0.06	0.77 ± 0.03
323.0	0.81 ± 0.07	0.69 ± 0.02

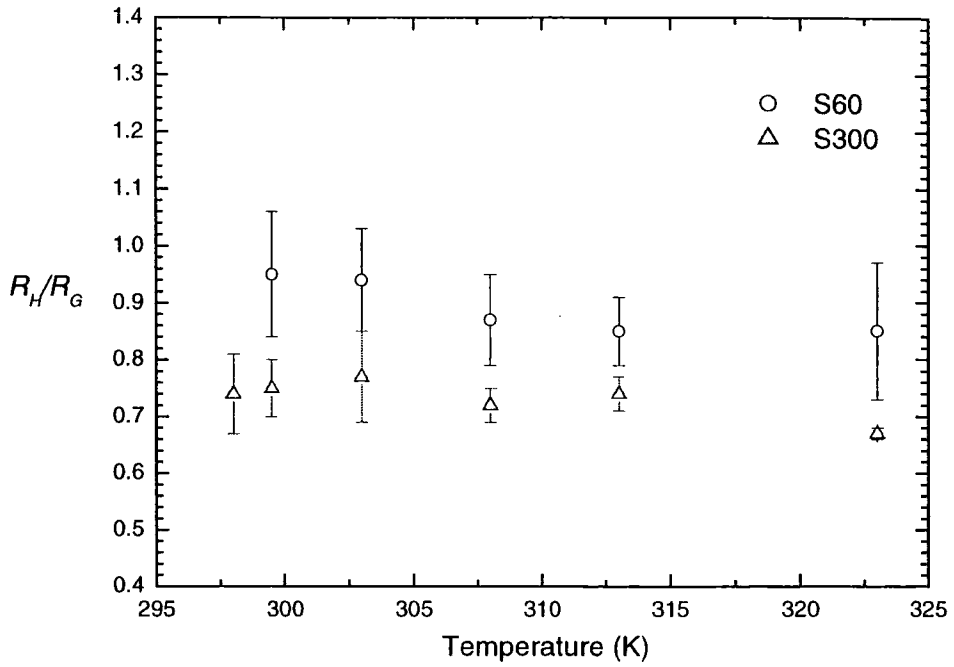

Figure 33: A plot of R_H/R_G versus temperature for miktoarm stars S60 and S300 in dioxane.

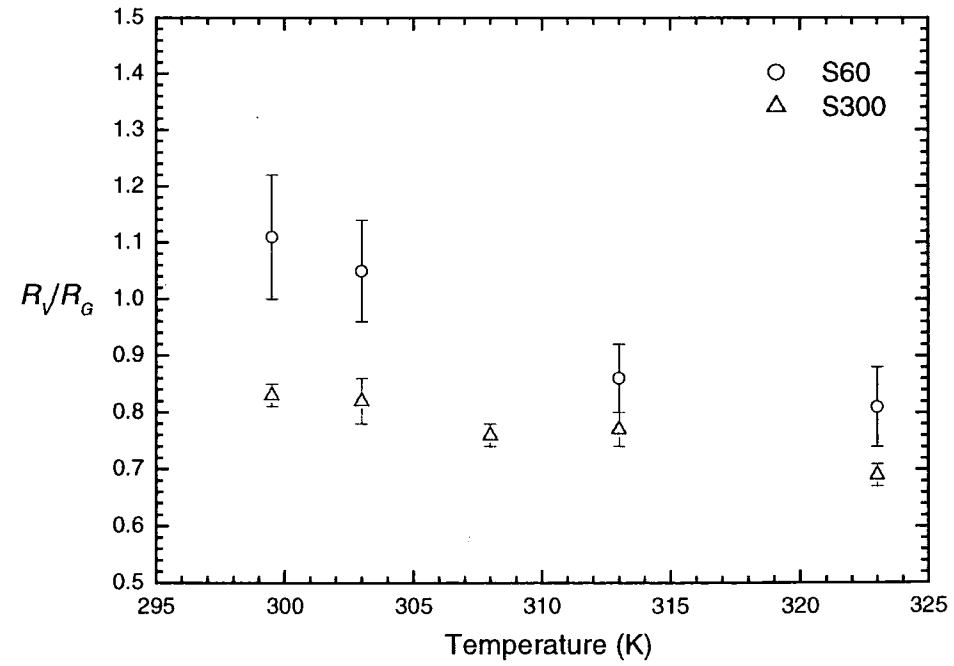

Figure 34: A plot of R_V/R_G versus temperature for miktoarm stars S60 and S300 in dioxane.

The friction constants (k_0) were calculated from equation 39, chapter 1, and are reported in Table 25. The friction constants for all the star polymers were lower than the values obtained in cyclohexane. The miktoarm star polymers S30, S60 and S80 in cyclohexane had k_0 as 3.64, 6.82 and 7.73 respectively. All the star polymers in Table 4 have friction constants below the hard sphere limit of 7.16. Roovers *et al*[14] found for 18-arm polybutadiene stars in dioxane under θ-conditions that k_0 were below values obtained for linear polybutadienes and for star polybutadienes under good solvent conditions. The friction constants for linear polybutadiene LH100 and LH300 in dioxane at 299.5 K were 2.06 and 0.69 respectively. For star S60, the friction constants obtained in dioxane are less than the values determined under good solvent conditions and decrease with temperature to a value similar to that of a linear polymer. The star polymer S300 also has k_0 decreasing with temperature towards a value obtained for a linear polymer. The friction constants increase with decreasing temperature for stars S30 and S80. The friction constants calculated for the stars depends on the sensitivity of equation 39, chapter 1, to the measured global properties.

Table 25: Friction constants (k_0) for the miktoarm star polymers over the temperature range of 298 K to 323 K.

Temperature (K)	S30	S60	S80	S300
	k_0	k_0	k_0	k_0
298.0	-	-	-	3.30 ± 3.85
299.5	-	2.46 ± 24.24	6.86 ± 17.44	3.30 ± 2.99
303.0	-	2.63 ± 1.91	2.41 ± 6.85	3.42 ± 2.66
308.0	3.09 ± 4.37	3.93 ± 3.32	2.89 ± 9.34	4.38 ± 2.35
313.0	1.59 ± 2.13	3.57 ± 4.07	1.01 ± 1.38	4.44 ± 3.31
323.0	1.34 ± 1.75	4.30 ± 17.10	-	5.49 ± 1.30

The cross linking of the miktoarm star polymers in dioxane can be seen by the size exclusion chromatograms in Figure 35 and Figure 36. The light scattering detector was used and hence the higher molecular weight material can be seen more clearly. Figure 35 is the SEC for the 8-arm regular star polymer before exposure to 1,4-dioxane and a monodisperse peak can be seen at 19.5 ml, with molecular weights corresponding to those ascertained by light scattering in cyclohexane. Figure 36 is the chromatogram for the star polymer after dissolution in 1,4-dioxane for 7 days and an overlapping second peak can be seen. In this chromatogram a peak can be seen at a retention volume of 19.5 ml for the original star polymer and a second peak can be seen at a retention volume of 17.8 ml for the crosslinked stars. This broad peak suggests that the solution was polydisperse and contains a range of aggregates that consisted of two or more stars and single star species as well. The sample prepared for SEC was precipitated from the dioxane solution and re-dissolved in THF (the solvent used for SEC analysis producing the results in Figure 36). This suggests the formation of permanent physical cross-links.

Cross-linking of the star arms could be due to peroxide linkages formed whilst dissolved in dioxane. The solvent dioxane is a cyclic ether which is susceptible to the formation of peroxides. The polybutadiene arms contain unsaturated double bonds that can undergo attack from the free radicals of the peroxides, subsequently forming chemical bonds with other polybutadiene arms on the same or neighbouring stars. Cross-linking with peroxides is achieved by free radical attack at the methylene group alpha to the double bond (the allylic position) and abstraction of a hydrogen.[52] The free radical formed adds to the double bond of another polymer chain and addition reactions continue until the radical undergoes termination. Only one cross-link needs to be formed between two arms of differing stars to generate a coupled species, and therefore the presence of very trace amount of peroxide can still lead to coupled stars. Heating the star polymer solutions to a temperature of 323 K could facilitate chain degradation and cross-linking as well. The use of θ-solvents yield polymer-polymer contacts that are thermodynamically more favourable than polymer-solvent contacts, which allow the easier overlapping of the arms and greater chance of cross-linking.

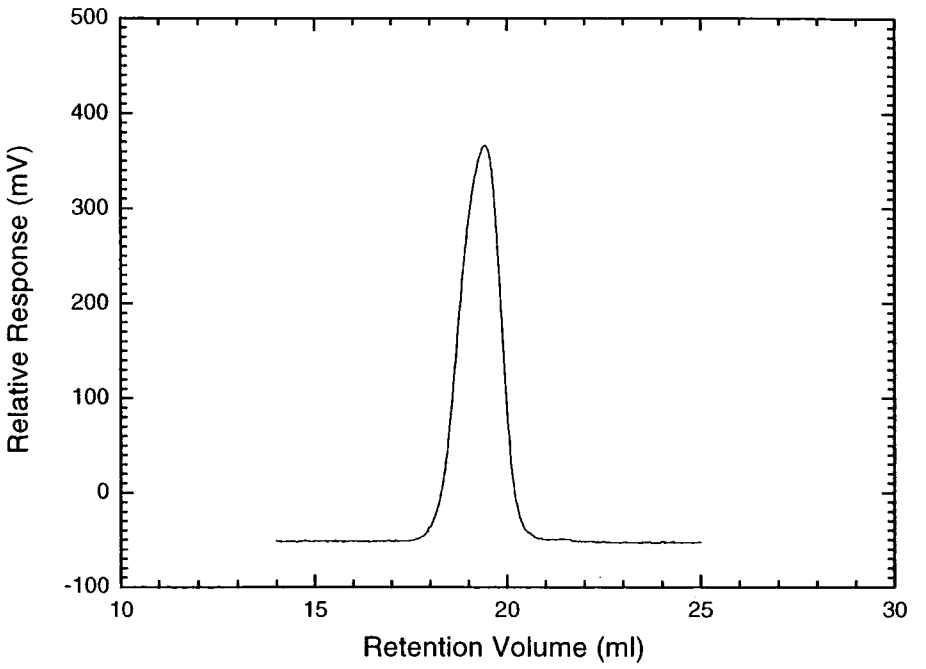

Figure 35: Size exclusion chromatogram for star polymer S30 before exposure to dioxane.

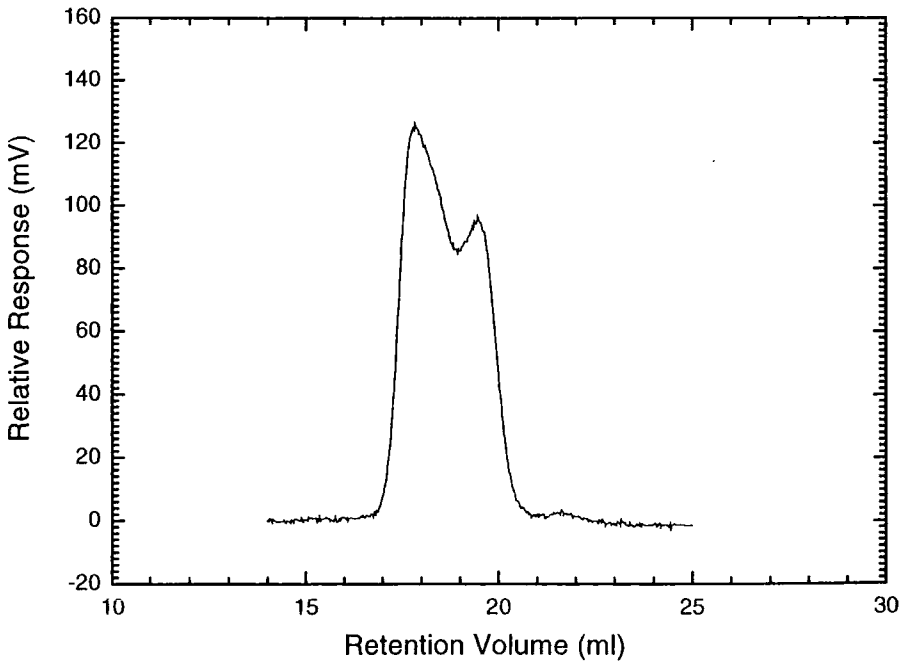

Figure 36: Size exclusion chromatogram for star polymer S30 after exposure to dioxane.

3.4.3 Summary of Results

A series of linear and star polybutadienes have been characterised in dilute solution by static and dynamic light scattering and viscometry techniques. Cyclohexane and dioxane were used as good and θ-solvents respectively. The cyclohexane solutions were analysed at a temperature of 298 K and the dioxane solutions were characterised over a temperature range of 298 K to 323 K. The weight-average molecular weights ($\bar{M}_W$) for the linear and star polybutadienes in cyclohexane solutions were in close agreement to those obtained by size exclusion chromatography (SEC) in THF. In dioxane, the $\bar{M}_W$ for the linear polybutadienes were approximately constant over the temperature range of measurement and equal to those measured in cyclohexane and by SEC (apart from the highest molecular weight polybutadiene, LH300). The star polymers were found to have increasing $\bar{M}_W$ with decreasing temperature, which was due to an aggregation process. At higher temperatures, the $\bar{M}_W$ for stars S60, S80 and S300 were similar to those obtained in cyclohexane and by SEC. At higher temperatures, the regular star polymer S30 had a $\bar{M}_W$ greater than that determined in cyclohexane and SEC, suggesting a greater extent of aggregation.

The second virial coefficients (A_2) for the linear polybutadienes in cyclohexane were found to decrease with increasing molecular weight with a scaling exponent of –0.20, that was similar to the exponent of –0.21 obtained by Roovers[16] for the same polymer-solvent system. In cyclohexane, the miktoarm star polymers had lower A_2 than for linear polymers of the same molecular weight, reflecting the presence of the branch point on segment density. Star polymer S300 with the longest asymmetric arm length had A_2 approaching those of a linear polymer of comparable molecular weight. The double logarithmic plot of A_2 versus normalised molecular weight ($\bar{M}_W/f$) yielded a positive scaling exponent of 0.21, that was partly due to the presence of the higher functional star S30. If the datum point for this star was ignored then a slight positive dependence on A_2 with asymmetric arm molecular weight can still be seen, suggesting the second virial coefficients were increasing to have values similar to those of a linear polymer of equal molecular weight. In dioxane, the θ-temperatures were determined for the linear and star polybutadienes from curved plots of A_2 versus temperature. The θ-temperature for the linear polymers were found to decrease with molecular weight to a value similar to those determined by Roovers[16] of 299.5 K and

this was subsequently taken as the θ-temperature for these linear species. For the star-branched polymers, the θ-temperature was found to decrease with increasing asymmetric arm length. The θ-temperatures for S30, S60, S80 and S300 were 308.4 K, 300 K, 299.5 K and 294.4 K respectively.

The radius of gyration (R_G) for the linear polybutadienes were found to increase with molecular weight in both good and θ-solvents. The values of R_G in cyclohexane were larger than those obtained in the dioxane, reflecting the perturbed dimensions obtained in the thermodynamically more favourable solvent. A double logarithmic plot of R_G versus molecular weight yielded the scaling exponent of 0.54 in cyclohexane, higher than the characteristic exponent of 0.49 for dioxane at 299.5 K for the θ-state, but less than the predicted value of 3/5 for good solvent systems.[26] In cyclohexane, a double logarithmic plot of R_G versus normalised molecular weight for the miktoarm star polymers yielded the scaling exponent of 1.09, that suggested an increase in R_G with asymmetric arm length to values similar to linear polymers of equal molecular weight. This also could be seen by the calculation of the branching ratio g, where an increase in asymmetric arm length yielded a value of g greater than that of a linear polymer. In dioxane, an overall increase in R_G with increasing temperature was seen for the stars, reflecting larger dimensions in a thermodynamically more favourable solution. Over the temperature range used, stars S60, S80 and S300 had R_G lower than those obtained under good solvent conditions. The R_G for the regular star S30 over the temperature range of measurement were found to be larger in dioxane than in cyclohexane, suggesting the formation of a higher molecular weight species. The interpenetration functions calculated for the linear polybutadienes in cyclohexane were in close agreement to theoretical and experimental predictions.[29-31] A decrease in Ψ^* with asymmetric arm length was seen for the stars towards values obtained for linear polymers.

The variation of the θ-temperatures for the star polymers were analysed by the theories proposed by Ganazzoli and Allegra[47] and Dondos *et al.*[49] The θ-temperature increase for regular star S30 when compared to a linear polymer of equal molecular weight was due to the formation of a aggregated species, as seen by the increased $\bar{M}_W$ and R_G greater than good solvent values. The more spherical nature of the regular stars allows for more compact

aggregates to be formed, that yielded increased segment densities near the star core. The theory of Boothroyd and Ball[52] allowed the high segment density to be treated as an impenetrable core that can be treated as an overall large blob, and the θ-temperature increase was predicted according to the theory of Dondos *et al.*[49] The star S300 with the longest asymmetric arm length had a θ-temperature depressed from that determined for a linear polymer. The $\bar{M}_W$ were still larger at lower temperatures than obtained under good solvent conditions, but the R_G value was still smaller than measured under good solvent conditions, which suggested a lower extent of aggregation. The star S300 has a more aspherical shape than S30, making it more difficult to form compact aggregates, and therefore more likely to exist as single species in solution as well. According to the blob model of Daoud and Cotton[51], the size of blobs decreased in size towards the core, due to the higher segment density. This in turn will lead to a calculation of θ-temperature depression by models of Ganazzoli and Allegra[47] and Dondos *et al.*[49] The stars S60 and S80 had a θ-temperature equal to those ascertained for linear polymers. These stars still had an increase in $\bar{M}_W$ at lower temperatures, but R_G were still lower than those obtained under good solvent conditions. The stars have a more spherical shape than S300, but do not aggregate to the same degree as the regular star S30.

The translational diffusion coefficients (D_0) at infinite dilution for the linear polybutadienes were found to decrease with increasing molecular weight in both cyclohexane and in dioxane. The values in cyclohexane were higher than those obtained in dioxane, which was also noticed by Roovers.[15] The double logarithmic plot of D_0 versus $\bar{M}_W$ for these polymers in good solvent conditions found a scaling exponent of –0.59, that was in good agreement of the values of –0.57 obtained by Roovers for the same polymer-solvent system. In cyclohexane, the star polymers (no data available for S300) had D_0 approximately identical to linear polymers of comparable molecular weight, contrary to what was observed by Roovers.[16] A double logarithmic plot of D_0 versus normalised molecular weight for these stars in this solvent, led to the scaling exponent of –0.57. This showed that D_0 decreased with molecular weight, but no dependence on asymmetric arm length could be seen. In dioxane, D_0 was found to decrease with temperature for the linear polymers, as the solution became thermodynamically poorer. This same temperature decrease was only found for stars S60 and S300, and only star S60 had D_0 lower than values determined under good solvent conditions, suggesting a variation of D_0 with extent of star aggregation.

The concentration dependence coefficients (k_D) for the star polymers in cyclohexane were lower than those of linear polymers with comparable molecular weight and this was also observed for 18-arm polybutadienes in cyclohexane.[15] Lower concentration dependence coefficients for the star polymers reflects the smaller A_2 obtained. An overall increase in k_D with molecular weight was observed in cyclohexane for the linear polymers, but not for the miktoarm stars. The k_D were negative for the linear polybutadienes in dioxane, and decreased with temperature and molecular weight in the same fashion as A_2. The star polymers also had negative k_D in dioxane, which decreased with temperature, but no decrease in molecular weight was observed. The star polymers had higher k_D than for linear polymers with comparable molecular weights in the θ-solvent, and this was also observed by Roovers for 18-arm polybutadienes stars.[16] The friction constants (k_0) calculated were found to be highly sensitive to the global properties measured. An increase in k_0 with star asymmetric arm length was noticed in cyclohexane. No molecular weight dependence was seen for the stars in dioxane, due to the range of aggregation, but a decrease in k_0 with temperature from good solvent to linear polymers values were observed. In dioxane, linear polybutadiene LH100 had k_0 similar to the data of Roovers[16] and the Pyun and Fixman[9] calculated value of 2.23.

A decrease in the intrinsic viscosity ($[\eta]$) with molecular weight was observed for the linear polybutadienes in both good and θ-solvents. Double logarithmic plots yielded a molecular weight scaling exponent of 0.69 in a good solvent, that was similar to value of 0.70 by Roovers[16] and higher than 0.57 obtained under θ-conditions. In cyclohexane, the star polymers were noticed to have lower $[\eta]$ than for linear polymers of comparable molecular weight. The double logarithmic plot of $[\eta]$ versus normalised molecular weight yielded a scaling exponent of 1.18, that suggested an increase in $[\eta]$ with asymmetric arm length to values similar to linear polymers of equal molecular weight. This was also seen by the calculation of the branching ratio g', where an increase in asymmetric arm length yielded g' in close agreement with a linear polymer. Lower intrinsic viscosities were obtained for both linear and star polymers in dioxane than in cyclohexane, demonstrating the reduction in global dimensions in a thermodynamically poorer solvent. Star polymer S60 and S300 had an increase in $[\eta]$ with increasing temperature in dioxane, as the solution became a thermodynamically more favourable.

The Huggins constants (k_H) of approximately 0.4 determined for the linear polybutadienes in cyclohexane, were in close agreement with data for good solvent conditions. Branched polymers are expected to have higher values of k_H due to higher segment densities near the branch point and this was seen for regular star S30 with a k_H of 0.63. A decrease in k_H with asymmetric arm length was noticed in cyclohexane, where star S300 had a k_H similar to that of a linear polymer. Values of k_H greater than 0.5 were found for the linear polybutadienes in dioxane, that increased with molecular weight and suggested the formation of a aggregated species. Aggregation could be the cause of increasing k_H with decreasing temperature for star polymers S60 and S300. A greater increase in k_H towards lower temperatures was observed for S60, when compared to S300, which could be due to a greater extent of aggregation for this star in the θ-solvent.

For the linear polybutadienes in cyclohexane, the equivalent sphere radii of R_T and R_V were calculated to be identical over the molecular weight range, where R_H were slightly lower. The radii of gyration were constantly greater than the equivalent sphere radii for the linear polymers over this molecular weight range, demonstrating no change in segment density for these linear species The equivalent sphere radii were identical for each respective star in cyclohexane. The R_G for the regular star polymer S30 was similar to the equivalent sphere radii, reflecting the high segment density near the core. A steady increase in the difference between R_G and equivalent sphere radii with asymmetric arm length could be seen, describing the reduction of segment density near the core and this was seen more clearly by calculating size ratios. The size ratios R_T/R_G and R_V/R_G for the linear polybutadienes were similar to the values reported by Roovers, where the size ratio R_H/R_G were slightly lower than the Roovers data.[16] Star S30 had a size ratio in close agreement to data calculated for an 8-arm regular star.[23] The size ratios decreased from this regular star value with increasing asymmetric arm length, where star S300 had similar size ratios to that of linear polymer. An increase in the branching ratio h in cyclohexane could be seen from regular star S30 to asymmetric stars S60 and S80, with a decrease in average star functionality, but with no dependence on asymmetric arm length.

The R_H and R_V for the linear polybutadienes in dioxane were smaller than those obtained under good solvent conditions, where they increased with molecular weight and were identical for each linear. A decrease in R_H with temperature was noticed, describing the

reduction in hydrodynamic volume in a thermodynamically poorer solution. In dioxane, higher size ratios of R_H/R_G were obtained than in cyclohexane, that was contrary to the data of Roovers.[16] The R_V/R_G ratio was identical in both solvent conditions, which obeys the data of Roovers.[16] A decrease in R_H was also noticed for the star polymers in a θ-solvent, but the rate of decrease for stars S30 and S80 was higher than for S60 and S300, reflecting the sensitivity of the Stokes-Einstein equation to the measured D_0. The hydrodynamic radii for the stars were lower than those obtained under good solvent conditions, apart from the regular star S30, at higher temperatures. The viscometric radii for the stars S60 and S300 were lower than those obtained under good solvent conditions. R_V for star S60 increased with decreasing temperature, where for S300 remained essentially constant. An increase in R_V with decreasing temperature suggests aggregation of S60 as the θ-temperature was approached.

In dioxane, the size ratio R_H/R_G increased with decreasing temperature for S60 and remained constant for S300. An increase in R_H/R_G can be described by greater segment density near the core, as the equivalent sphere radius equals the radius of gyration. This means that star S60 might be aggregating to a greater extent than S300. Decreases in R_H/R_G with temperature were found for stars S30 and S60, that suggested the formation of smaller species, which was contrary to the molecular weight data and demonstrates the sensitivity of these values to the obtained global properties and the aggregation process. The size ratios R_V/R_G also increased with decreasing temperature, which describes the formation of a higher molecular weight species. At lower temperatures, the stars S60 and S300 had R_V/R_G resembling highly functional stars and linear polymers respectively, when compared to the polyisoprene star data of Bauer *et al.*[21] This can also be linked to a higher aggregation of the more spherical star S60, when compared to S300 at lower temperatures.

Overall an increase in the asymmetric arm length of the miktoarm star polymers yielded global properties similar to those of linear polymers of equal molecular weight. This was seen for R_G, $[\eta]$, k_H, Ψ^*, R_T/R_G, R_V/R_G, g and g' for the star polymers with increasing asymmetric arm molecular weight. Aggregation of the star polymers was noticed in dioxane as the molecular weights increased with decreasing temperature, where for linear polymers it remained constant over the temperature range. The variation of the θ-temperatures for the stars were observed, that were explained by the differing extents of aggregation between

regular and asymmetric stars. It was postulated that the regular stars find it easier to form compact aggregates than for the asymmetric stars, and the extent of aggregation could be linked to the length of the asymmetric arm. The different extents of aggregation were seen by the regular star having R_G greater than those obtained in good solvent conditions and the variation of k_H, R_H/R_G and R_V/R_G between stars S60 and S300 with decreasing measurement temperature.

3.5 References

[1] Katime, I. A.; Quintana, J. R. *Comprehensive Polymer Science*; Ed. Allen, G.; Bevington, J. C.; Pergamon Press: Oxford, 1989, vol.1, p103.

[2] Kratchovil, P, *Polymer Science Library 5: Classical Light Scattering from Polymer Solutions*; Ed. Jenkins, A. D.; Elsevier: Amsterdam,1987.

[3] Benoit, H. *J. Polym. Sci.* **1953**, 11, 507.

[4] Phillies, G. D. J. *J. App. Polym. Sci.: App. Polym. Symp.* **1989**, 43, 275.

[5] Ford, N. C. *Dynamic Light Scattering: Applications of Photon Correlation Spectroscopy*; Ed. Pecora, R.; Plenum Press: New York, 1985, p 7.

[6] Berne, B. J.; Pecora, R. *Dynamic Light Scattering*; Wiley –Interscience: New York, 1976.

[7] King, T. A. Comprehensive Polymer Science, Ed. Allen, G.; Bevington, J. C.; 1989, Pergamon Press, vol.1, p 911.

[8] Koppel, D. E. *J. Chem. Phys.* **1972**, 57, 4814.

[9] Lovell, P. *Comprehensive Polymer Science*; Ed. Allen, G.; Bevington, J. C.; Pergamon Press: Oxford, 1989, vol.1, p 173.

[10] Mays, J.W.; Hadjichristidis, N. *Modern Methods of Polymer Characterisation*; Ed. Barth, H.G.; Mays, J. W. John Wiley & Sons: New York, 1991, 227.

[11] Bohdanecky, M.; Kovar, J. *Polymer Science Library 2: Viscosity of polymer Solutions*, Ed. Jenkins, A. D.: Elsevier, Amsterdam, 1982.

[12] Bandrup, J.; Immergut, E. H.; Grulke, E. A. *Polymer Handbook*; 4th ed.;Wiley-Interscience: New York, 1999.

[13] Burchard, W *Adv. Polym. Sci.* **1999**, 143, 113.

[14] Toporowski, P. M.; Roovers J. *J. Polym. Sci.: Part A* **1986**, 24, 3009.

[15] Martin, J.E.; Roovers, J. *J. Polym. Sci: Part B* **1989**, 27, 2513.

[16] Zhou, L. L.; Hadjichristidis, N.; Toporowski, P. M.; Roovers, J. *Rubber Chem. Technol.* **1992**, 65, 303.

[17] Roovers, J; Zhou, L. L.; Toporowski, P. M.; van der Zwan, M.; Iatrou, H.; Hadjichristidis, N. *Macromolecules* **1993**, 26, 4324.

[18] Roovers, J.; Toporowski, P. M.; Martin, J. *Macromolecules* **1989**, 22, 1897.

[19] Hajichristidis, N.; Roovers, J. *J. Polym. Sci., Poly. Phys. Ed.* **1974**, 12, 2521.

[20] Bauer, B. J.; Fetters, L. J.; Graessley, W. W.; Hadjichristidis, N.; Quack, G. *Macromolecules* **1989**, 22, 2337.

[21] Adam, M.; Fetters, L. J.; Graessley, W. W.; Witten, T. A. *Macromolecules* **1991**, 24, 2434.

[22] Berry, G. C. *J. Polym. Sci.: Part A-2* **1971**, 9, 687.

[23] Roovers, J; Hadjichristidis, N.; Fetters, L. J. *Macromolecules* **1983**, 16, 214.

[24] Okumoto, M.; Nakamura, Y.; Norisuye, T.; Teramoto, A. *Macromolecules* **1998**, 31, 1615.

[25] Freire, J. J. *Adv. Polym. Sci.* **1999**, 143, 34.

[26] Ioan, C.; Ioan, S.; Simionescu, B. C. *Macromol. Symp.* **1999**, 138, 191.

[27] Yamakawa, H. *Modern theory of Polymer Solutions*; Harper and Row: New York, 1971.

[28] Grest, G. S.; Fetters, L. J.; Huang, J. S. *Adv. Chem. Phys.* **1996**, Volume XCIV, 67.

[29] Douglas, J. F.; Roovers, J.; Freed, K. F. *Macromolecules* **1990**, 23, 4168.

[30] Douglas, J. F.; Freed, K. L.; *Macromolecules* **1984**, 17, 2344.

[31] Rubio, A. M.; Freire, J. J.; *Macromolecules* **1996**, 29, 6946.

[32] Roovers, J; Zhou, L. L.; Toporowski, P. M.; van der Zwan, M.; Iatrou, H.; Hadjichristidis, N. *Macromolecules* **1993**, 26, 4324.

[33] Zimm, B. H.; Stockmayer, W. H. *J. Chem Phys* **1949**, 17, 1301.

[34] Barrett, A. J.; Tremain, D. L. *Macromolecules* **1987**, 20, 1687.

[35] Stockmayer, W.; Fixman, M. *Ann. N.Y. Acad. Sci.* **1953**, 57, 334.

[36] Prats, R.; Pla, J.; Freire, J. J. *Macromolecules* **1983**, 16, 1701.

[37] Roovers, J.; Toporowski, P. M. *J. Polym. Sci: Polym. Phys. Ed* **1980**, 18, 1907.

[38] Zimm, B. H.; Kilb, R. W. *J. Polym Sci.* **1959**, 37, 19.

[39] Roovers, J.; Bywater, S. *Macromolecules* **1974**, 7, 443.

[40] Hajichristidis, N.; Roovers, J. *J. Polym. Sci., Poly. Phys. Ed.* **1974**, 12, 2521.

[41] Hajichristidis, N.; Zhoungde, X.; Fetters, L. J.; *J. Polym. Sci., Poly. Phys. Ed.* **1982**, 20, 743.

[42] Okumoto, M.; Terao, K.; Nakamura, Y.; Norisuye, T.; Teramoto, A. *Macromolecules* **1997**, 30, 7493.

[43] Okumoto, M.; Tasaka, Y.; Nakamura, Y.; Norisuye, T.; *Macromolecules* **1999**, 32, 7430.

[44] Bauer, B. J.; Hajichristidis, N.; Fetters, L. J.; Roovers, J. E. L. *J. Am. Chem. Soc* **1980**, 102, 2410.

[45] Striolo, A.; Prausnitz, J. M.; Bertucco, A. *Macromolecules* **2000**, 33, 9583.

[46] Ganazzoli, F.; Allegra, G. *Macromolecules* **1990**, 23, 262.

[47] Bruns, W.; Carl, W. *Macromolecules* **1991**, 24, 209.

[48] Dondos, A.; Papanagopoulos, D. *Polymer* **1997**, 38, 6255.

[49] Striolo, A.; Prausnitz, J. M. *Polymer Communication* **2001**, 42, 4773.

[50] Daoud, M.; Cotton, P. *J. Physique* **1982**, 43, 531.

[51] Boothroyd, A. T.; Ball, R. C. *Macromolecules* **1990**, 23, 1729.

[52] Bikales, N. M.; Kroschwitz, J. I.; Mark, H. F.; Menges, G.; Overberger, C. G. *Encyclopaedia of Polymer Science and Engineering*; 2nd ed.; John Wiley & Sons: New York, 1988, vol. 4, p380.

Chapter 4

Characterisation of Miktoarm Star-Branched Polymers by Small Angle Neutron Scattering

4.1 Introduction

This chapter outlines the characterisation of the miktoarm star-branched polymers in the melt and solution state by the technique of small-angle neutron scattering (SANS). The polybutadiene star polymers had a single deuterated arm that was a different chain length to the other hydrogenous arms. Previous work has been performed on single-labelled star polymers in solution and in the melt state, but not on stars with varying chain length. The scattering cross sections obtained were fitted by a scattering law derived from the random phase approximation. Section 4.2 describes the characteristics of this technique and the scattering law used for these partially labelled stars. The experimental section 4.3 discusses the instrumental set up, the experiments performed, the data reduction procedures and the fitting of the scattering law to obtain the parameters of interest. The results of the small angle neutron scattering of asymmetric star polymers S60 and S80 are presented in section 4.4, where S80 has a longer asymmetric arm than S60. The radius of gyration of the asymmetric deuterated arms and the thermodynamic interaction parameters were determined from fits of the scattering law to the obtained cross sections. A summary of results is presented at the end of this section.

4.2 Small Angle Neutron Scattering

4.2.1 Introduction

Small-angle neutron scattering is a simple diffraction technique that provides information on the size and shape of polymers and assemblies.[1, 2] SANS is particularly useful for the investigation of hydrocarbon systems, as the exploitation of the differing neutron-nucleus interactions of hydrogen and deuterium enables the investigation of deuterium labelled model materials. The SANS technique exploits the wave-particle duality of the neutron, that was first formulated by Louis de Broglie in 1924. The wavelength (λ) of the neutron is related to a particle of mass, m, with a velocity of v, by the Plank constant, h:

$$\lambda = \frac{h}{mv} \tag{1}$$

The principles involved in small angle neutron scattering are analogous to light scattering, but SANS has a greater scope as an investigative tool, due to the shorter wavelength of radiation used. The main advantage of using short wavelengths is that smaller length scales can be probed, a wider range of the particle scattering law becomes accessible and global dimensions of smaller particles can be determined. The wave-particle duality of the neutron yields radiation of a wavelength of between 0.15 to 2.5 nm, where a light scattering laser source has wavelengths from 400 to 700 nm. When a sample is exposed to a beam of neutrons, the neutrons are scattered isotropically, as the wavelength of the incident neutron is orders of magnitude larger than the size of the scattering nucleus, which can be considered as a point scatterer. This is contrary to light scattering, where the wavelength is comparable to the size of the scatterer. SANS experiments are only possible at few sites, due to the availability of suitable neutron sources, where light scattering experiments are cheaper and widely available. All neutron sources are less intense than lasers and the spectrometer design is always a compromise between resolution and signal to noise ratio.

4.2.2 Scattering Vector Q

The independent variable in a SANS experiment is the scattering vector Q, which is sometimes called the wavevector transfer or momentum transfer as well. The scattering vector is the magnitude of the difference between the incident (k_i) and scattered (k_s) wavevectors (see Figure 1). Each wavevector has a magnitude of $2\pi/\lambda$ and points in the direction of travel of the neutrons. If the neutron does not lose any energy (elastic scattering), then Q is only dependent on scattering direction and its vectorial change is represented as:

$$Q = |\boldsymbol{Q}| = |\boldsymbol{k}_s - \boldsymbol{k}_i| = \frac{4\pi n}{\lambda}\sin\left(\frac{\theta}{2}\right) \tag{2}$$

The neutron refractive index of n is taken as unity and Q has dimensions of (length)$^{-1}$. The importance of Q is that its modulus $|Q|$ quantifies length scales in reciprocal space and is the independent variable in SANS. The insertion of the Bragg diffraction equation into equation 2 yields:

$$d = \frac{2\pi}{Q} \tag{3}$$

Equation 3 relates the molecular length scale to the Q-range accessible. Large scale structures can be investigated with small values of Q and conversely small distance scales are observed with large values of Q.

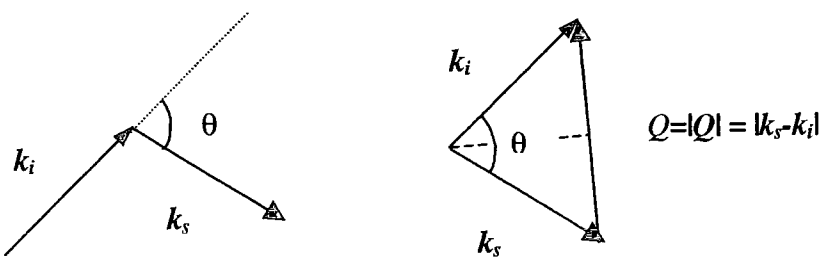

Figure 1: Vector diagram for Q.

4.2.3 Scattering Lengths and Cross Sections

Every nucleus within the sample can be considered as a source for a scattered wave. The location of this scattered neutron in space is related to the square of the amplitude of the scattered wave. The amplitude of the scattered wave is determined by the scattering length b of the nucleus, which is the ratio of the amplitude of the scattered wave to the amplitude of the incident wave. Scattering lengths vary throughout the periodic table and are listed for common nuclei in Table 1. The difference in scattering lengths for deuterium and hydrogen can be seen, and its importance in deuterium labelling of model polymers. The negative scattering length obtained for hydrogen signifies a half wavelength phase shift on scattering that leads to destructive interference. The square of the scattering length is the probability of finding a neutron from the incident beam within the scattered beam, and can also be described as the probability of scattering per nucleus, per neutron, per solid angle, where the angle is expressed in steradians (4π steradians within a scattering sphere). Thus the total probability of scattering is $4\pi b^2$, which is given the name of cross section (σ). Negative scattering lengths for a sample thus yield a positive cross sections.

All the scattering nuclei within a sample are in a spatial arrangement of some form. The probability of a beam of neutrons being scattered from the sample will be governed by the sum of the amplitudes of the scattered neutrons by each individual nuclei. The net signal is the sum of all the scattered wave amplitudes, and scattering lengths for all the nuclei need to be averaged, before squaring them to obtain the net probability of scattering. Deuterium labelling specific polymer chains in a sample results in spatial correlations to exist between nuclei that have the same scattering length. This leads to characteristic information about their shape, obtained from nuclei scattering coherently. If there are no spatial correlations between the nuclei of the same scattering length (as in naturally occurring isotopes), then there will be a random or incoherent part of the scattering probability, that yields isotope incoherent scattering. The isotope incoherent scattering is not the only source of destructive interference. The scattering nuclei have different spin states that are generally uncorrelated within a sample and can lead to another source of incoherent scattering.

Table 1: The Scattering Lengths for Common Nuclei.

Nucleus	Scattering Length b /10^{-5} (Å)
^{1}H	-3.742
^{2}D	6.674
C	6.648
O	5.805

4.2.4 The SANS Apparatus

Neutron scattering experiments are extremely expensive and are usually performed at special sites, with international co-ownership. They are usually large scale instruments buried beneath massive biological shielding, which serves to protect the user and decrease background noise to the detectors. Neutrons can be produced from two different types of sources. The first source of neutrons is from continuous nuclear fission in a nuclear reactor, where the emitted neutrons have thermal energies. The highest-intensity reactor source in the world is the 58 MW high-flux reactor at the Institute Laue-Langevin (ILL) in Grenoble, France. Another type of neutron source is spallation from a metal target, that has been bombarded by protons with velocities near the speed of light. The neutrons from this type of source are produced as pulses and the highest intensity spallation source in the world is at the ISIS facility, near Oxford, UK.

Neutrons from whatever source generally need to be moderated. i.e. have their wavelength distribution altered. Moderation of emitted neutrons to longer wavelengths is usually achieved by dense hydrogenous materials, such as water, liquid methane and liquid hydrogen. The neutrons are scattered many times within the moderator and lose energy until they reach the appropriate thermal equilibrium. The moderated neutrons can be used by two different methods. The first method is to use a band pass filter to select a very narrow range of incident wavelengths and the second method is to use a broad range of wavelengths and time of flight techniques. The former method results in fixed wavelength instruments, where the latter results in fixed geometry instruments.

The SANS experiments performed at ILL use a fixed-wavelength instrument (see Figure 2), the reactor is a hot source that allows a shift of the distribution of neutron wavelengths to higher wavelengths. The apparatus size is large scale with distances from neutron source to sample to detector being up to 180 m. The wavelength of the moderated neutrons were selected by a band pass filter, which consists of a mechanical chopper, the speed of rotation determining the wavelength. The neutrons must be collimated before they reach the sample, as they cannot be focussed onto the sample. Collimators of up to 40 m in length, shape the neutron beam to a size of a few millimetres, with the use of apertures made from neutron absorbing material. A low-efficiency detector positioned before the sample was used as a beam monitor to determine the count rate of the incident beam, and the count rate is integrated to put the scattering data on a per neutron basis.

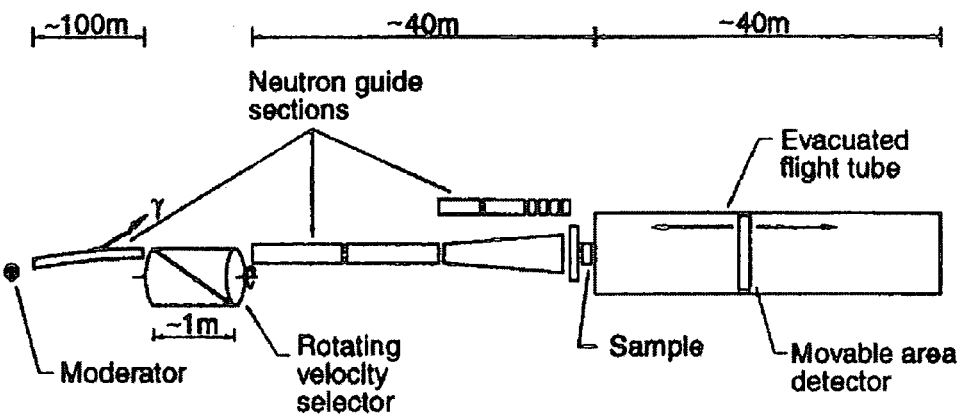

Figure 2: A fixed-wavelength SANS instrument.

The scattered neutron intensity is recorded by 2-dimensional detectors positioned behind the sample. Detectors being up to 1.5 m in diameter allow for large solid angle coverage, because of the low neutron flux by present-day neutron sources. The 2-dimensional detectors consist of an array of smaller gas detectors of the Geiger-Muller type that contain either ^3He or BF_3 detection medium. An array of 64 × 64 or 128 × 128 of gas detectors per 2-dimensional detector are used at ILL. The transmitted beam is prevented from reaching the detector by the use of a beam stop. The beam stop may be removed after appropriate attenuation of the incident beam in order to measure the neutron transmission of the sample. The detectors can be moved between 0.5 m to 40 m away from the sample and air

scattering is prevented by housing the detector in a evacuated chamber. In a fixed-wavelength SANS apparatus (Figure 3), the Q-range is dependent on the sample-detector distance (L_{sd}) and the radial detector distance (R_{det}):

$$Q = \frac{4\pi}{\lambda}\frac{R_{\text{det}}}{L_{sd}} \tag{4}$$

The neutrons arriving at the centre of the detector have small Q-values and *vice-versa*. The minimum and maximum values of radial detector distances are fixed and causes the Q-range to be limited. The Q-range can be expanded by changing the sample detector distance. If the sample detector distances are increased, then this causes the range of Q-values to be smaller and *vice-versa*. Use of more than one sample to detector distances provides overlapping Q-ranges increasing the range of length scales that can be investigated.

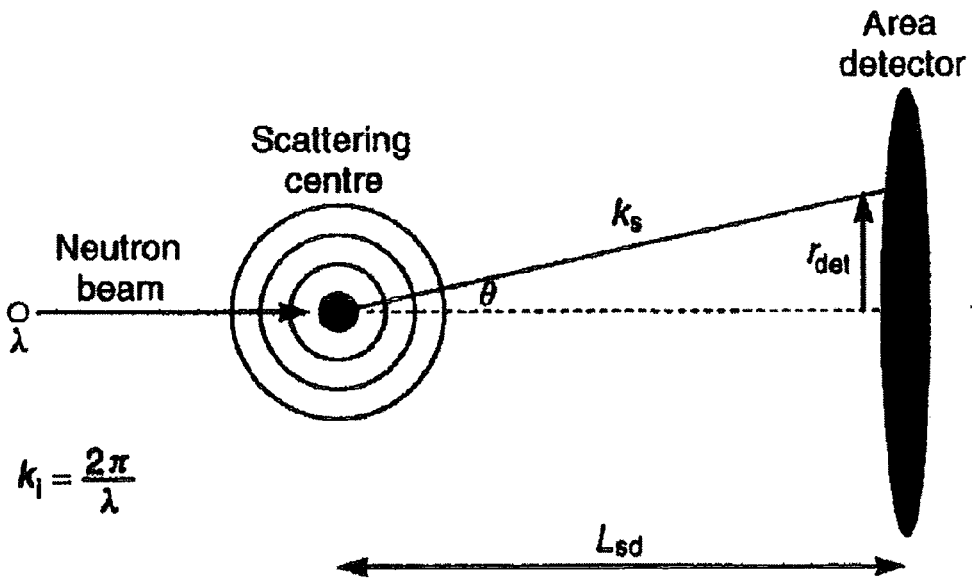

Figure 3: *The geometry of a SANS experiment.*

4.2.5 Differential Scattering Cross Section

The differential scattering scattering cross section ($d\Sigma/d\Omega(Q)$) is the dependent variable determined by SANS and is the fraction of neutrons scattered in a defined solid angle element. The coherent differential scattering cross section contains all the information on the size, shape and interactions between the scattering nuclei in the sample. The differential scattering cross section has units of $(\text{length})^{-1}$ and can be related to the microscopic differential cross section ($d\sigma/d\Omega(Q)$) of each nucleus, by multiplying this cross section with by the number concentration of scattering nuclei. Neutron detectors do not measure the intensity of scattered radiation, but measure the number of neutrons of a given wavelength, scattered through a particular angle that arrive on a small area of the detector in a unit time (i.e. a flux). The flux of neutrons may be expressed as:

$$I(Q) = I_0(\lambda)\Delta\Omega\eta(\lambda)T(\lambda)V_S\frac{d\Sigma}{d\Omega}(Q) \tag{5}$$

I_0 is the incident flux, $\Delta\Omega$ is the solid angle element defined by the size of the detector pixel, η is the detector efficiency, T is the neutron transmission and V_S is the sample volume illuminated by the beam. The first 3 terms in equation 5 are instrument specific, whereas the last three terms are sample dependent. The differential scattering cross section is related to the parameters that describe structural and morphological factors by the relation:

$$\frac{d\Sigma}{d\Omega}(Q) = NV^2(\Delta\rho)^2 P(Q)S(Q) + B \tag{6}$$

N is the number concentration of scattering centres, V is the volume of one scattering centre, $(\Delta\rho)^2$ is the contrast factor and B is the background signal. $S(Q)$ and $P(Q)$ are the structure and form factors respectively. The scattering length density (ρ) is the sum of the scattering lengths for all the nuclei within the sample and can be calculated from the following simple expression:

$$\rho = N\sum_i b_i = \frac{\delta N_A}{M}\sum_i b_i \tag{7}$$

The bulk density of the molecule is δ, M is the molecular weight of the scattering species and b_i is the coherent scattering length for nucleus i. The scattering lengths and densities for common polymers and solvents are listed in Table 2. The contrast factor ($(\Delta\rho)^2$) is the square of the difference between the scattering length densities between solute (ρ) and surrounding medium or matrix (ρ_m):

$$(\Delta\rho)^2 = (\rho - \rho_m)^2 \tag{8}$$

Equation 8 shows that if the scattering length density is negative, the contrast factor and hence ($d\Sigma/d\Omega(Q)$) are always positive or zero. When $(\Delta\rho)^2$ is zero, the scattering centres are said to be in contrast match. The usefulness of contrast matching in SANS is that it provides a means of dramatically simplifying scattering patterns by having identical scattering length densities for specific parts of the sample under investigation.

Table 2: Scattering lengths (b) and densities (ρ) for common polymers and solvents.

Polymer/Solvent	b /Å	ρ /Å^{-2}
Polydeuterobutadiene	6.664×10^{-4}	5.952×10^{-6}
Polybutadiene	4.140×10^{-5}	4.109×10^{-7}
Cyclohexane	-5.016×10^{-6}	-2.795×10^{-8}
Cyclohexane-d_{12}	1.200×10^{-3}	6.274×10^{-6}
1,4-Dioxane	8.266×10^{-5}	5.840×10^{-7}

4.2.6 Structure Factor S(Q)

The term $S(Q)$ in equation 6 is the structure factor of the sample. It is a dimensionless function which describes how $d\Sigma/d\Omega(Q)$ is modulated by interference effects between neutrons scattered by different scattering centres within the sample. The structure factor is dependent on the local degree of order in the sample (the spatial distribution of nuclei) and the interaction potential between scattering centres. The structure factor is a damped oscillatory function whose maxima correspond to a distance of r, of each nearest-neighbour coordination shell. The differential scattering cross section is independent of the structure factor for polymer samples containing identical species as no intermolecular interferences exist. This is also the case in dilute systems and the scattering is dependent upon the form factor alone.

4.2.7 Form Factor P(Q)

The term $P(Q)$ in equation 6 is the form factor or shape factor. It is a dimensionless function which describes how $d\Sigma/d\Omega(Q)$ is modulated by interference effects between neutrons scattered by different parts of the same scattering centre. The form factors are therefore dependent on the size and shape of the scattering centre. Functions of $P(Q)$ versus $Q^2R_G^2$ lead to functions for scattering centres of various shapes and sizes. The Debye equation for the form factor of a Gaussian polymer chain is:

$$P(Q)=\frac{2\left(\exp\left(-Q^2R_G^2\right)+Q^2R_G^2-1\right)}{\left(Q^2R_G^2\right)^2} \tag{9}$$

The form factor for a regular Gaussian star polymer with f arms was derived by Benoit:[3]

$$P(Q)=\frac{2}{y^2}\left[\frac{y}{f}-\frac{1}{f}\left(1-e^{-y}\right)+\frac{(f-1)}{2f}\left(1-e^{-y}\right)^2\right] \tag{10}$$

Where:

$$y=\frac{f}{3f-2}Q^2\left\langle R_G^2\right\rangle \tag{11}$$

The form factor for a regular star polymer with excluded volume was calculated by renormalization group techniques by Alessandrini and Carignano.[4] The scattering form factor was devised for scattering from either star polymers or from a single arm. Increasing deviations from the Gaussian predictions were found with stars with higher arm functionalities.

4.2.8 Random Phase Approximation

A more specific application of the Debye scattering form factor is in the description of the scattering from polymer blends. In this system the scattering arises out of composition fluctuations and is therefore directly proportional to the density correlation function for the system, a quantity that can be expressed using a generalisation of random phase approximation (RPA).[5] The resulting scattering function for a two component system is:

$$\frac{(\Delta\rho)^2}{\frac{\partial\Sigma}{\partial\Omega}(Q)} = \frac{1}{n_1 v_1 \phi_1 P(Q, R_{G,1})_{Debye}} + \frac{1}{n_2 v_2 \phi_2 P(Q, R_{G,2})_{Debye}} - \frac{2\chi}{(v_1 v_2)^{1/2}} \qquad (12)$$

The number of polymer segments of type i is n_i with volume v_i. $P(Q, R_G)_{Debye}$ is the form factor for a polymer chain with a Gaussian distribution, as in equation 9, and χ is the Flory-Huggins interaction parameter between the two polymers.

4.2.9 The SANS Experiment and Data Reduction

To obtain the differential scattering cross section ($d\Sigma/d\Omega(Q)$) of the sample, the scattering of a sample is not the only measurement required. For every sample analysed a transmission needs to be recorded, to place $d\Sigma/d\Omega(Q)$ on an absolute scale. The absolute scale is calibrated from the neutron scattering and transmission of a standard, and this also divides out the $\Delta\Omega\eta(\lambda)$ term in equation 5. The transmission of a sample of species i can be defined as:

$$T_i = \frac{\frac{I(r_{\det} \approx 0)_i}{Mon_i}}{\frac{I(r_{\det} \approx 0)_{mt}}{Mon_{mt}}} \tag{13}$$

$I(r_{det} \approx 0)_i$ is the intensity of the neutron beam at approximately zero angle, Mon is the integrated monitor counts recorded and the subscript mt is for empty sample position. The scattering of an empty sample holder is subtracted from the sample data. The electronic and cosmic radiation background noise of the detector can be determined by inserting a cadmium (Cd) stop into the beam, which is a neutron absorber. The calibration standards used in SANS experiments are known as flat scatterers, as the standard has predominantly incoherent scattering and therefore Q-independent (or flat) over the Q-range of interest. The primary standard is a homogeneous single crystal of unstressed, hydrogen free, vanadium. The disadvantage of vanadium is that its $d\Sigma/d\Omega(Q)$ is very small and long measurement times are required. The 1 mm path length of water is sometimes used instead, but the scattering of water is wavelength and temperature dependent and hence correction formulae are used to relate the data to the vanadium cross section. Good sample and transmission counting statistics are required to reduce the size of the error bars in the $d\Sigma/d\Omega(Q)$ data.

The process of data reduction recovers the differential scattering cross section from what has been recorded by the detector. The scattered neutrons arrive at the detector and generate a series of diffraction rings, as the detector intercepts a conic section of the sphere of scattering. Analysis of the scattering rings is complicated as the detector is a square array of pixels. To overcome this problem, the detector is divided up into a series of imaginary concentric rings, where the width of each ring is of order of a pixel. Then a radial

integration is performed within each ring, over the same range of solid angles. The radially integrated data are then normalised (i.e. placed on a per neutron basis) using the transmission and the integrated counts recorded by the monitor detector. The processed background is removed ring by ring and the data is then divided by the calibrant scattering also by a ring by ring basis to remove the area efficiency term. Finally the position of each ring is converted to Q by the small angle approximation in equation 4 to yield the fully reduced dataset. The equation to determine $d\Sigma/d\Omega(Q)$ for a sample of thickness of t for a fixed wavelength instrument is:

$$\frac{d\Sigma}{d\Omega}(Q)_{sa} = \frac{\left[\left(\frac{I(Q)_{sa}}{Mon_{sa}} - \frac{I(Q)_{cd}}{Mon_{cd}}\right) - \frac{T_{sa}}{T_{sc}} \times \left(\frac{I(Q)_{sc}}{Mon_{sc}} - \frac{I(Q)_{cd}}{Mon_{cd}}\right)\right]}{\left[\left(\frac{I(Q)_{no}}{Mon_{no}} - \frac{I(Q)_{cd}}{Mon_{cd}}\right) - \frac{T_{no}}{T_{nc}} \times \left(\frac{I(Q)_{nc}}{Mon_{nc}} - \frac{I(Q)_{cd}}{Mon_{cd}}\right)\right]} \times \frac{t_{no}}{t_{sa}} \frac{T_{no}}{T_{nc}} \frac{d\Sigma}{d\Omega}(Q)_{no} \quad (14)$$

The subscripts in equation 14 of *sa*, *sc*, *cd*, *no* and *nc* are sample, sample container, cadmium, standard and standard container respectively.

4.2.10 The Theoretical Scattering Law for a Miktoarm Star Polymer

A miktoarm star polymer was considered with f equal arms. The star has a single deuterated D-arm and the rest are hydrogenous H-arms. The form factor associated with this star, assuming incompressibility and no interactions between H- and D-arms, is:[6]

$$S_{inc}(Q) = \frac{S_0^{HH} S_0^{DD} - \left(S^{HD}\right)^2}{S_0^{HH} + S_0^{DD} + 2S^{HD}} \quad (15)$$

S_0^{HH} and S_0^{DD} are the Q-dependent partial form factors for the H- and D-arms respectively, and S^{HD} was the Q-dependent cross-partial form factor. The partial form factors determines the self-correlation of the local order of the respective polymer species in Fourier space. The cross-partial form factor describes the correlation between the order parameter of two species. As the stars have an average star functionality, a diverse mixture of polymer species might exist in a sample and therefore a form factor was required for each species. A

method of determining the form factors for copolymers of arbitrary architecture was proposed by Read.[6] The partial form factors can be considered by self-, co- and propagator terms, and the method was applicable to polymers with a Gaussian distribution of segments. The self-terms describe the correlations within a molecular species and the Q-variation of the Gaussian distribution of species in space is related to the Debye equation scaled by the square of the degree of polymerisation. The co-terms were used for the correlations between like-chains and the propagator-term only applies if a different species intervenes between the two like species and connects them in some way. For a star polymer with f arms, there is one self-term for the single deuterated arm, and $(f\text{-}1)$ self-terms for the hydrogenous arms.[7] Each H-arm is correlated to $(f\text{-}2)$ other H-arms, but as they are all connected at a common junction point, there are no propagator terms. The form factor in equation 15 assumes no interaction between the polymer species. The application of random phase approximation introduces the interaction parameter (χ) between two polymer species and the differential scattering cross section can be expressed as:

$$\frac{d\Sigma(Q)}{d\Omega} \propto \left(\frac{1}{S_{inc}(Q)} - 2\chi \right)^{-1} \tag{16}$$

The constant of proportionality in equation 16 is the contrast factor between the H- and D-arms. The differential cross section for partially labelled stars predicted by the model as shown in Figure 4. The typical RPA or correlation hole maximum is seen at a constant value of Q, defined by the radius of gyration of the arm ($Q_{max} \sim R_G^{-1}$). The maximum of the peak increases with increasing χ and a decrease in star functionality, due to a higher deuterium content within the star. If the star polymer is mixed with a third component, then all thermodynamic interactions with this third component must be considered as well. Balsara *et al*[8] devised a series of interaction parameters χ_{DM}, χ_{HM} and χ_{HD} for a copolymer dispersed in the 3rd component matrix (M). This leads to the final expression for the cross section accounting for all the contrast factors in the system:

$$\frac{d\Sigma(Q)}{d\Omega} = K^T S(Q) K \tag{17}$$

For a m-component mixture, K is an (m-1) column vector of contrast factors between the selected H- and D-arms, and the matrix:

$$K = \frac{b_i}{v_i} - \frac{b_M}{v_M} \tag{18}$$

K^T is the transpose of the column vector, b_i and v_i were the scattering length and volume occupied by the monomer unit of species i of the H- or D-arm, and b_M and v_M were the corresponding values for the matrix. $S(Q)$ in equation 17 represents the full scattering law and is equal to the right hand side of equation 16. The full scattering law for a 3-component system can be seen in Appendix A. If the sample is a polymer melt, the matrix component will be the other star polymers and only two interaction parameters need to be considered. The interaction parameter χ_{HD}, that was associated with the intramolecular interactions of the star and the second, χ_{DM}, was the interaction of the deuterium arm with the surrounding star matrix. This scattering law has been applied to miktoarm star polymer solutions, where the solvent was now considered to be the matrix. Interaction parameters of χ_{HS}, χ_{DS} and χ_{HD} now result between the hydrogenous (H) and deuterated (D) star arms and the solvent (S). The influence of the excluded volume effect was incorporated within the interaction parameters. The polymer-solvent interactions for the hydrogenous and deuterated arms were the same and therefore the scattering law obtained is insensitive to the absolute values of χ_{HS} and χ_{DS}.

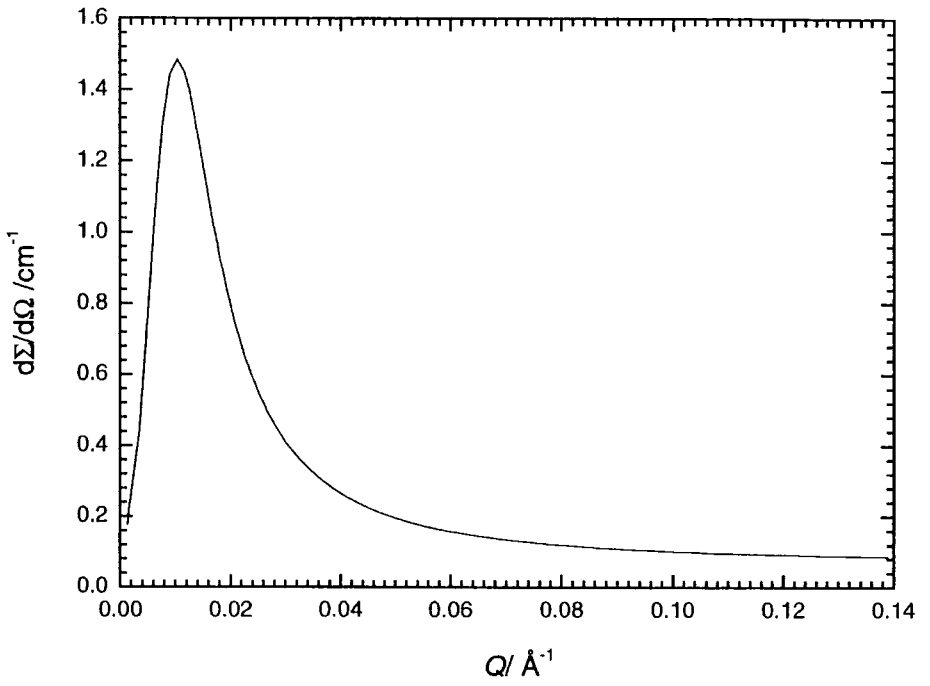

Figure 4: The scattering cross section from RPA expressions for a single-labelled-arm polybutadiene star with 8-arms .

4.3 Experimental

4.3.1 Polybutadiene Star Polymers in the Melt State

4.3.1.1 Sample Preparation

Polymer samples to be analysed by SANS in the pure melt state were stars S60 and S80 (see tables 2, 3 and 4 in chapter 2 for molecular weights), and linear hydrogenous LH100 and linear deuterated LD100 polybutadienes (see table 1 in chapter 2 for molecular weights). Both stars had an average arm functionality of 6.6. The sample were prepared by placing pure polymer between circular quartz windows (diameter of 20 mm) using a 1 mm PTFE spacer, the path length of the sample. The quartz plates were slotted into a brass/stainless steel sample holder and were held in place with a screw top. The sample holders were held in position in the beam by a rack. The temperature of the rack was maintained by a heating element, which was controlled and powered by a Eurotherm model 2132 PID controller and by a ceramic temperature sensor inserted into the top of the rack. A water standard sample was also prepared, by filling a Hellma Quartz cell (path length of 1 mm) with distilled water.

4.3.1.2 SANS Experiment

The small angle neutron scattering experiments were performed on the D11 diffractometer at ILL, Grenoble, France. Two sample to detector distances of 1.6 m and 5.0 m were used, the high and low Q-range values respectively (see equation 4). The wavelength of the incident neutron beam used was 10 Å, with a wavelength distribution ($\Delta\lambda/\lambda$) of 9 %. The scattering detector was slightly off axis and the overall Q-range obtained $3 \times 10^{-3} \leq Q/\text{Å}^{-1} \leq 1.4 \times 10^{-1}$. Transmission runs were measured at a sample to detector distance of 5.5 m, with the beam stop removed and an attenuator placed within the beam. The beam collimation for high Q-range, low Q-range and transmission runs were 4.0 m, 5.5 m and 4.0 m respectively. A series of sample, background and water standard runs were performed at these sample to detector distances. The electronic background noise of the detector was determined by inserting a cadmium beam stop into the path of the neutrons. The scattering and

transmission runs of the water standard, standard container, polymer samples and empty polymer cell were all measured at room temperature (298 K). The scattering and transmission runs of the polymer samples were also determined at temperatures of 318 K, 328 K, 338 K, 348 K, 358 K, 368 K, 378 K and 388 K.

4.3.1.3 Data Reduction

The scattering cross sections, $d\Sigma/d\Omega(Q)$, were obtained from the raw data by using the data reduction programs provided by ILL.[9] Transmissions of the samples were obtained by using WINDET. This program asked for the transmission runs of sample and sample container in a defined data window of detector pixels. To transfer the data from a 2-dimensional format to a radially re-grouped format, the program of RNILS was applied to the scattering data for each Q-range. Sample parameters such as neutron wavelength, sample to detector distance, beam stop position and collimation were applied for each respective Q-range. Unwanted data points and beam stop position were removed by formulating a mask over the 2-dimensioanl detector, by using the program RMASK and then input in to the RNILS program. Data normalisation and background subtraction was performed by SPOLLY for both range of Q. The program asked for the RNILS scattering data for the electronic background noise, water sample, empty water container, sample run and empty sample cell. The transmissions for the water and sample runs were also entered, and the macroscopic cross section of water at a neutron wavelengths of 10 Å of 0.969 cm^{-1} was used to provide absolute scattering values. The cross sections for the two Q-ranges were scaled by multiplying by a scaling factor. The incoherent scattering was removed by subtracting the cross section flat baselines of LH100 and LD100 from the star sample data at the correct volume fractions.

4.3.1.4 Data Fitting

The cross sections obtained by the reduction procedures had data points with large errors removed that were especially found near the beam stop at low-Q, so that the fitting procedures could be applied. The cross sections were fitted by the scattering law for a single labelled arm star polymer using a Fortran program. The Fortran program modelled the scattering law and asked for a number of fixed variables that included the number of

hydrogenous arms, the star volume fraction, the number average degree of polymerisation (X_n) of the hydrogenous and deuterated arms, and the background. The floating variables to be determined were the radius of gyration of the deuterated arm, and the interaction parameters χ_{HD} and χ_{DM}. The fixed variables for star polymers S60 and S80 are listed in Table 3.

Table 3: The fixed variables of stars S60 and S80 for the Fortran fitting program.

Fixed Variable	S60	S80
Number of H-arms	6.0	6.0
Star volume fraction	1.0	1.0
X_n of D-arm	973	1318
X_n of H-arm	561	643
Background	0.2-0.3	0.2-0.3

4.3.2 Polybutadiene Star Polymers in the Solution State

4.3.2.1 Sample Preparation

Stock solutions of the star polymers S60 and S80 in 1,4-dioxane and in cyclohexane were prepared. The solvents used were 1,4-dioxane (supplied from Aldrich), 99.6 % atom cyclohexane-d_{12} (Aldrich) and 99.5 % AR cyclohexane (Aldrich). The cyclohexane was contrast matched to the hydrogenous content of the stars by a using a mixture of cyclohexane and cyclohexane-d_{12}. The stock solutions were diluted to obtain a series of volume fractions (ϕ_{Star}) of stars in solution. The volume fractions of S60 in cyclohexane were 0.12, 0.09, 0.07, 0.05 and 0.02, and in dioxane were 0.12, 0.09 and 0.07. The volume fractions of S80 in cyclohexane were 0.12, 0.10, 0.05 and 0.02, and in dioxane were 0.13, 0.10, 0.07 and 0.04. These solutions were transferred by pipette into Hellma quartz cells of a path length of 1 mm. A water standard sample was also prepared as in section 4.3.1.1.

4.3.2.2 SANS Experiment

Small angle neutron scattering experiments on the polymer solutions were performed on the D22 apparatus at ILL, Grenoble, France. The neutron wavelength of the incident beam was 8 Å, with a wavelength distribution ($\Delta\lambda/\lambda$) of 10 %. The sample to detector distances used for the scattering experiments were 3.6 m and 18 m for the high and low Q-ranges respectively. These sample to detector distances yielded an overall Q-range of $3 \times 10^{-3} \leq Q/\text{Å}^{-1} \leq 1.4 \times 10^{-1}$. The transmission runs were measured at a sample to detector distance of 5.0 m, but with the beam stop removed and the attenuator placed within the beam. The collimations used for the high Q-range, low Q-range and transmission runs were 4.0 m, 17.6 m and 5.6 m respectively. The electronic background noise of the detector was measured by the same procedure as in section 4.3.1.2. The scattering and transmission runs were recorded for the polymer solutions, water standard, empty cell, and pure cyclohexane mix and dioxane solvents. The temperature of the sample rack was maintained at 298 K.

4.3.2.3 Data Reduction

The scattering cross sections, $d\Sigma/d\Omega(Q)$, were obtained from the raw data by using the data reduction programs provided by ILL, mentioned in section 4.3.1.3. In the data normalisation and background subtraction program of SPOLLY, the pure solvents were used for the respective backgrounds of the samples. The macroscopic cross section of water used for a neutron wavelength of 8 Å was 0.916 cm^{-1}. The two Q-ranges were scaled together by multiplying the cross sections by a scaling factor.

4.3.2.4 Data Fitting

The cross sections obtained by the reduction procedures had erroneous data points removed so that the fitting procedures could be applied. The cross sections were fitted by the use of the scattering law by using an Excel spreadsheet and the solver utility in Excel. The data was fitted using fixed and floating variables were used to fit the data by utilising the linear least-squares procedure. The fixed variables for the star polymers included the number of H- and D-arms, the number average degrees of polymerisation of both arms, the volumes of the monomer units, the scattering lengths of the monomer units, the Kuhn segment lengths

of each unit, the R_G of the hydrogenous arm, the volume fraction of star in solution and the background. The fixed variables for the solvent of the volume of solvent molecule, the degree of polymerisation of solvent molecule and R_G of solvent molecule were all set at unity. The Kuhn length of the solvent molecule equalled that of the monomer units. The fitting variables for the stars were the R_G of the deuterated arm and the interaction parameters χ_{DM} and χ_{HD}. Table 4 lists the fixed variables used for star polymers S60 and S80.

Table 4:The fixed variables for the miktoarm star polymers S60 and S80 in cyclohexane and dioxane.

Fixed Fitting Variable	S60 in Cyclohexane	S60 in Dioxane	S80 in Cyclohexane	S80 in Dioxane
Number of *H*-arms	6.0	6.0	6.0	6.0
Number of *D*-arms	1	1	1	1
Volume of *H*-monomer ($Å^{-3}$)	107	107	107	107
Volume of *D*-monomer ($Å^{-3}$)	101	101	101	101
X_n of *H*-arm	561	561	643	643
X_n of *D*-arm	973	973	1318	1318
Scattering length of *H*-arm (Å)	4.14×10^{-5}	4.14×10^{-5}	4.14×10^{-5}	4.14×10^{-5}
Scattering length of *D*-arm (Å)	6.66×10^{-4}	6.66×10^{-4}	6.66×10^{-4}	6.66×10^{-4}
Scattering length of solvent (Å)	4.14×10^{-5}	8.27×10^{-5}	4.14×10^{-5}	8.27×10^{-5}
Kuhn length of *H*-arm (Å)	8.19	8.19	8.19	8.19
Kuhn length of *D*-arm (Å)	8.19	8.19	8.19	8.19
R_G of *H*-arm (Å)	85	60	92	65
Background (cm^{-1})	0.01 - 0.06	0.02	0.01 - 0.07	0.01 - 0.07

4.4 SANS Results of Star Polymers

4.4.1 The Melt State

The scattering cross sections for the star polymers S60 and S80 can be seen in Figure 5 and Figure 6 respectively. The Q-range for the scattering cross section begins at 7.0×10^{-2} Å^{-1}, as the beam stop yielded data points with a high degree of error at lower wavevector. The scattering for the star polymers were dominated by a peak located at a scattering vector determined by the radius of gyration of the deuterated asymmetric arms. Hutchings *et al*[7] analysed partially labelled regular star polybutadienes with 3-, 4-, 8- and 12-arms by SANS and scattering peaks were also noticed for the deuterated arms on the $d\Sigma/d\Omega(Q)$. For these stars the scattering peaks shifted to lower-Q with increasing arm functionality, as the higher segment density at the core caused stretching of the labelled arm and an increase in the R_G. A shift in the scattering peak to lower Q can be observed between asymmetric star S60 and S80, where S80 has a larger asymmetric arm. The peaks of $d\Sigma/d\Omega(Q)$ for S60 (*Figure 5*) occurs at a wavevector of approximately 1.13×10^{-2} Å^{-1}, where a peak can just be observed for the cross sections of S80 at lower Q (Figure 6). This shift to lower Q also follows the increase in the radius of gyration of the labelled arm. Higher scattering cross sections can be seen for S80 than for S60, reflecting the greater quantity of deuterium in this sample and hence more coherent scattering.

A slight decrease in the scattering maximum with increasing temperature can be seen for both stars at fixed wavevector. This temperature dependence can be seen more clearly in Figure 7 and Figure 8, which are the scattering cross sections at low Q for S60 and S80 respectively. A decrease in the scattering cross section at fixed wavevector with increasing temperature has also been observed for deuterated linear and hydrogenous linear polybutadiene blends and for polydiene star diblock copolymers by SANS.[10, 11] The linear polybutadiene blends were found to have upper critical solution temperature (UCST) and became more miscible with increasing temperature.[10] This suggests the star polymer samples were becoming more miscible at higher temperatures.

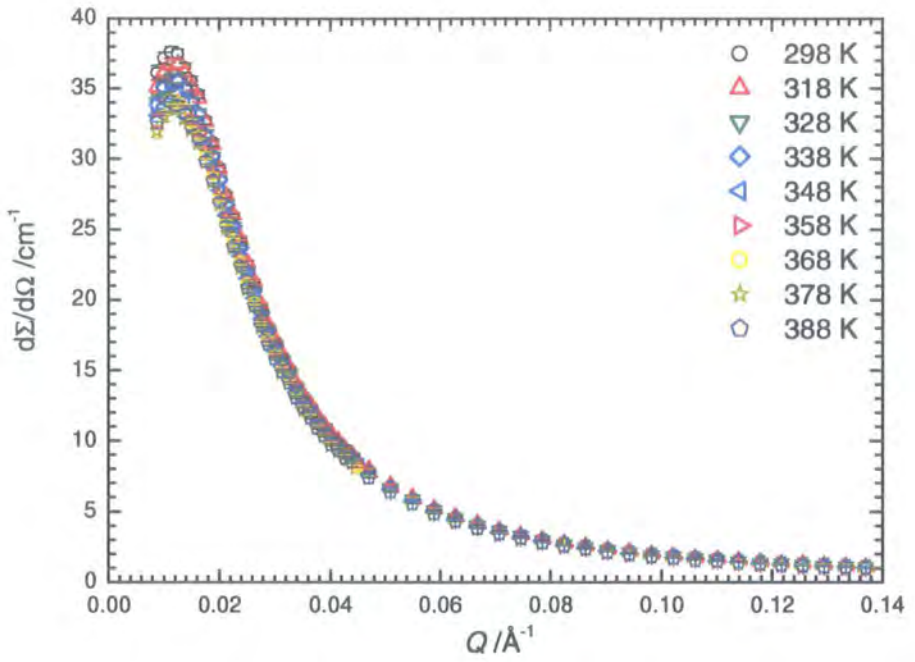

Figure 5: The scattering cross sections for star S60 in the melt at temperatures between 298 K to 388 K.

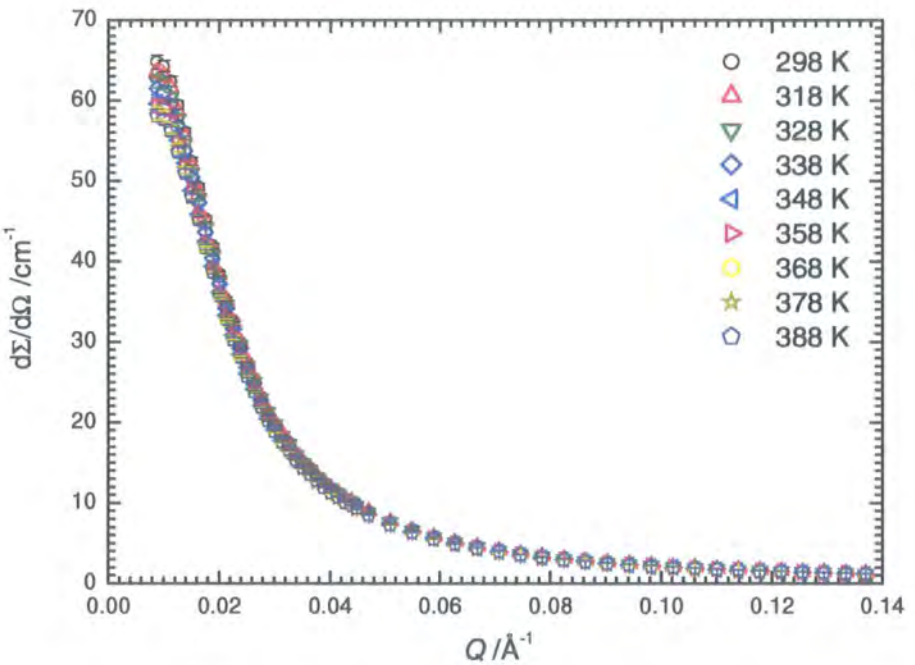

Figure 6: The scattering cross sections for star S80 in the melt at temperatures between 298 K to 388 K.

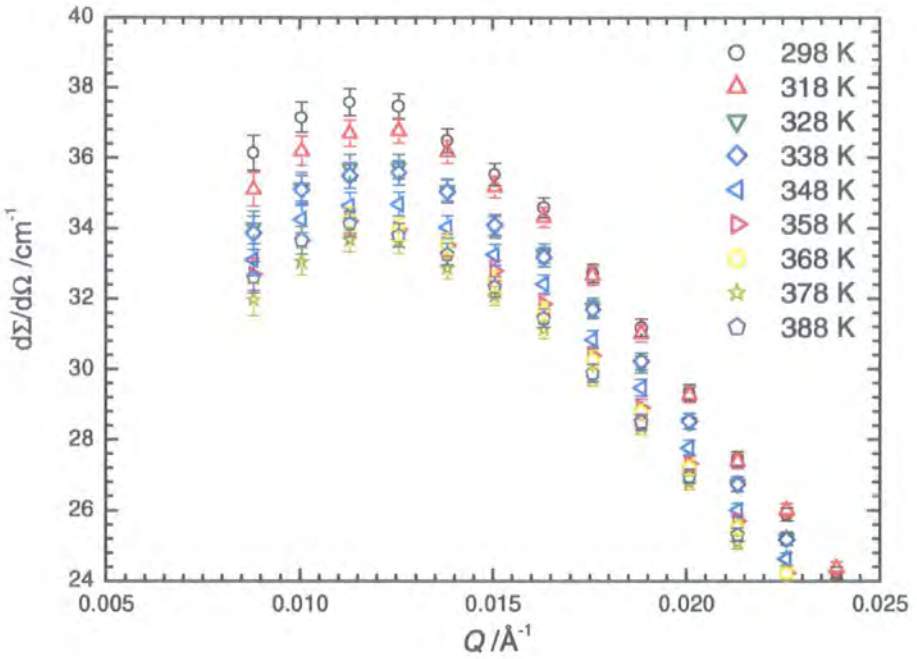

Figure 7: The scattering cross sections for star S60 in the melt at low-Q in the temperature range of 298 K to 388 K .

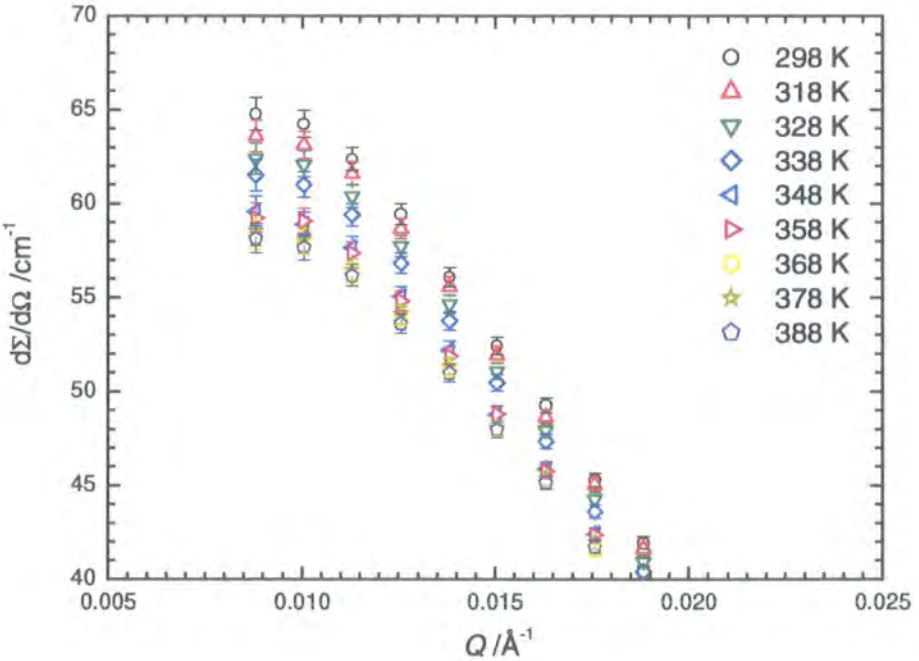

Figure 8: The scattering cross sections for star S80 in the melt at low-Q in the temperature range of 298 K to 388 K.

The scattering cross sections were fitted using the random phase approximation expression for the scattering law and are shown in Appendix B for both stars at all temperature measurements. The radius of gyration for the deuterated arms (*D*-arm) obtained from these fits are listed in Table 5 and have an error of 5 %. A small increase in the R_G of these arms with temperature was observed for both stars and this can be seen in Figure 9. The linear fit to the data in Figure 9 yields approximately identical gradients of 0.23 Å K^{-1} and 0.24 Å K^{-1} for S60 and S80 respectively, as would be expected the arms of the similar chemical composition. The calculation of the R_G for unperturbed linear polybutadiene ($\langle R^2\rangle_\theta^{1/2}/M^{1/2}$ = 0.082 nm) of equivalent molecular weight to the star arms yielded values of 82 Å and 95 Å, for S60 and S80 respectively.[12] The values of R_G for the asymmetric arms of the star polymers were slightly higher than the values determined for an unperturbed polymer of equivalent molecular weight, and demonstrates the effect of the branch point has on global dimensions. This was also observed by SANS for polyethylene stars in the molten state with 3-, 4-, 12- and 18-arms.[13] These stars were found to be swollen with respect to unperturbed dimensions.

The scattering data at a temperature of 298 K for the single deuterated arm as Kratky plot of $Q^2 d\Sigma/d\Omega$ versus Q are shown in Figure 10. The characteristic peak obtained for star polymers at low wavevector is not observed in these plots, which exhibit single arm scattering only.[14] The Kratky plots for the asymmetric stars are also different to those obtained for a linear polymer, where a plateau is obtained at high wavevector. Alessandrini and Carignano[4] calculated Kratky plots for one arm scattering and found an increase away from the plateau values of linear polymers with increasing star functionality. This increase was proposed to be due to greater star dimensions being obtained by arm stretching, to relieve the segment overcrowding at the core for stars with higher arm functionalities. In Figure 10, an upwards increase in the Kratky plots for S60 and S80 can be observed at higher-Q, demonstrating that the stars had increased dimensions in the melt state, when compared to linear polymer of the same molecular weight. The Katky plots are also sensitive to the incoherent scattering subtracted form the cross sections, and this also needs to be taken into account.

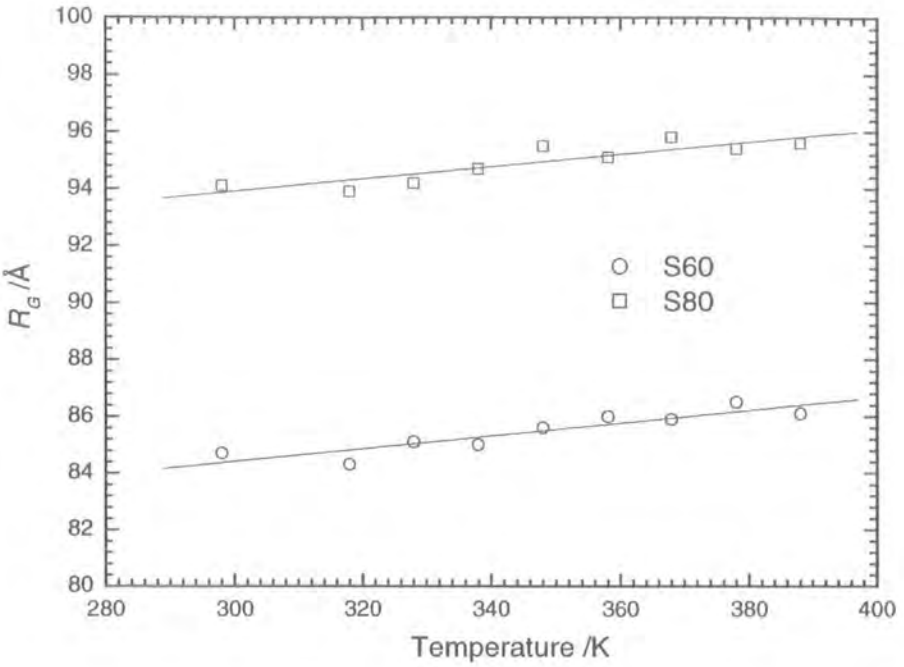

Figure 9: The temperature dependence of the R_G for the asymmetric arms of star polymers S60 and S80.

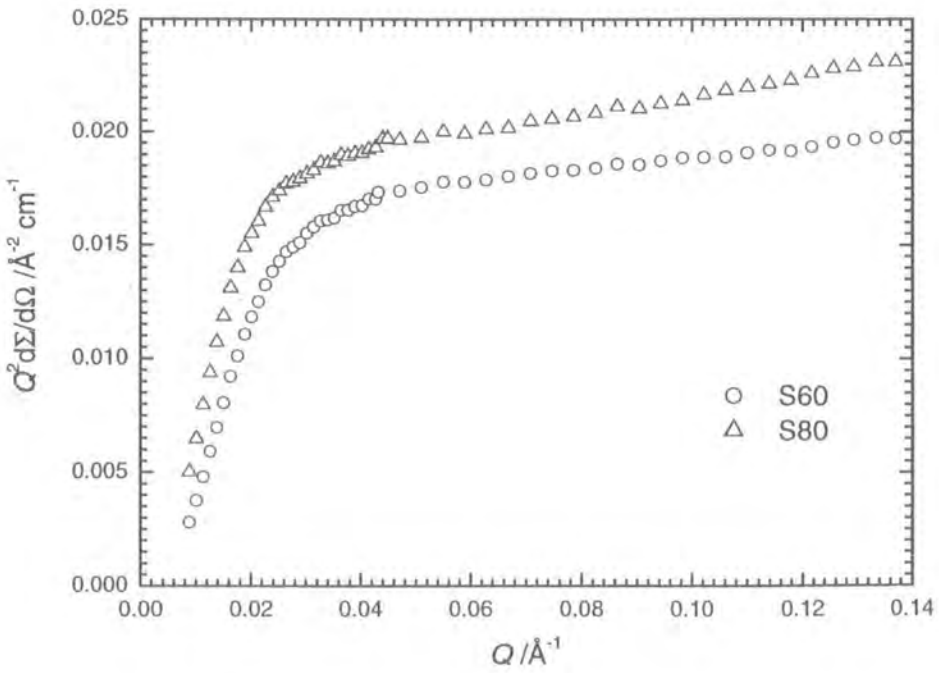

Figure 10: The Kratky plots for S60 and S80 in the melt at a temperature of 298 K.

Table 5: The R_G for the deuterated (D-arm) arm of the star polymers S60 and S80.

Temperature (K)	S60	S80
	R_G of *D*-arm (Å)	R_G of *D*-arm (Å)
298	85	94
318	84	94
328	85	94
338	85	95
348	86	96
358	86	95
368	86	96
378	87	95
388	86	97

The interaction parameters obtained for the stars are listed in Table 6 (errors are within 5 %). The temperature dependence of the interaction parameters of χ_{HD} and χ_{DM} are plotted in Figure 11 and Figure 12 for S60 and S80 respectively. The parameters of χ_{HD} and χ_{DM} represent the intramolecular and intermolecular interactions of the deuterated arm. The intramolecular interactions were between the deuterated arm and the hydrogenous arms of the same star, where the intermolecular interactions were between the deuterated arm and the arms of other stars. These parameters were found to be higher for star S80 than for star S60, due to the higher quantity of deuterium within the star. Negative interaction parameter favours miscibility of the polymer blend, where a positive value favours immiscibility. A decrease of χ_{DM} with increasing temperature suggests that the intermolecular interactions were becoming more thermodynamically favourable, where an increase in χ_{HD} suggests that the intramolecular interactions were becoming less thermodynamically favourable. This can be envisaged as greater mixing of the star polymers with each other at higher temperatures

The interaction parameters of the star polymers can be investigated further by plotting reciprocal temperature dependencies (T^{-1}) and this can be seen in Figure 13. Linear fits allows the reciprocal temperature parameters *A* and *B* (as seen in equation 30, section 1.24, chapter 1) to be determined and are listed in Table *7* for the intra- and intermolecular interaction parameters for both stars. The linear increase in the reciprocal temperature dependence suggests that the stars have a upper critical solution temperature (UCST), and the polymer becomes more miscible with increasing temperature. If a linear decrease in the reciprocal temperature dependence demonstrates a lower critical solution temperature (LCST), and the polymer becomes immiscible with increasing temperature. The linear increase for χ_{DM} and decrease for χ_{HD} show that inter-star arm mixing was becoming more favourable than intra-star arm mixing. The parameter *B* for χ_{HD} and χ_{DM} were identical and of opposite sign, showing the simultaneously mixing and de-mixing of inter- and intra-star arms. The parameter *B* has been determined for blends of linear deuterated and hydrogenous polybutadienes with UCST behaviour to be between 0.15 K^{-1} to 0.35 K^{-1}.[15-17] The parameter B for UCST behaviour for star polymer S80 has a value of 0.406 K^{-1}, which is lower than the value of 0.675 K^{-1} obtained for S60 and suggested a decrease in parameter *B* with increasing asymmetric arm length. The higher value of parameter *B* for the S60 would be due to greater mixing of the star arms in the more spherical shaped star polymer.

Table 6: Interaction parameters χ_{HD} and χ_{DM} for the star polymers S60 and S80.

Temperature (K)	Star S60		Star S80	
	$\chi_{HD}/10^{-4}$	$\chi_{DM}/10^{-4}$	$\chi_{HD}/10^{-4}$	$\chi_{DM}/10^{-4}$
298	-10.1	6.0	-8.9	7.1
318	-10.4	5.9	-8.6	6.8
328	-9.2	4.7	-8.0	6.2
338	-9.3	4.8	-7.8	5.9
348	-8.2	3.6	-7.2	5.2
358	-7.5	2.9	-6.5	4.7
368	-6.8	2.3	-6.4	4.5
378	-6.2	1.6	-6.5	4.5
388	-5.8	1.5	-6.4	4.4

Table 7: The reciprocal temperature dependence parameters A and B for the interaction parameters χ_{HD} and χ_{DM}.

Star	χ_{HD}		χ_{DM}	
	A	B /K^{-1}	A	B /K^{-1}
S60	1.03×10^{-3}	-0.635	-1.60×10^{-3}	0.675
S80	3.55×10^{-4}	-0.375	-6.30×10^{-4}	0.406

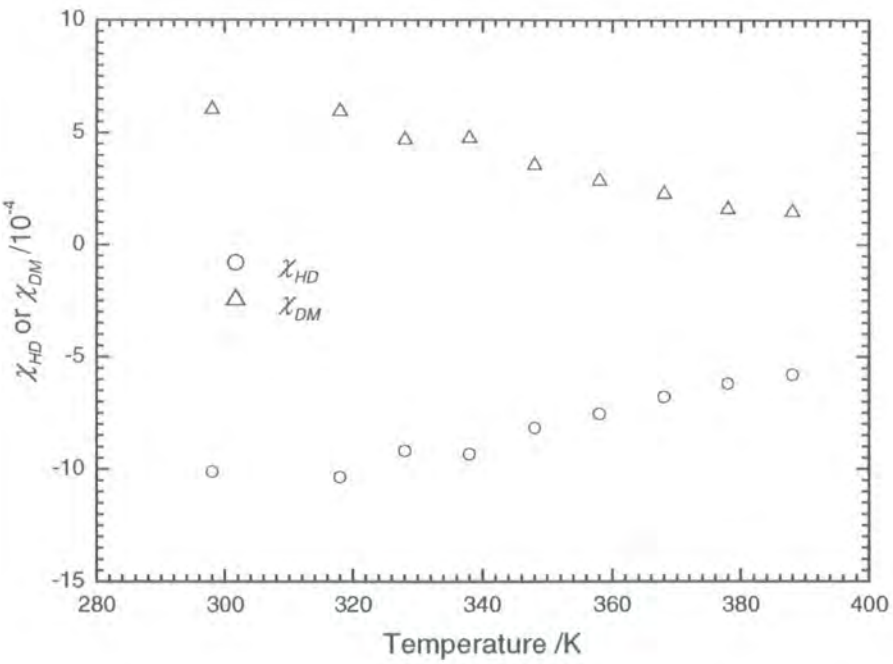

Figure 11: Temperature dependence of the interaction parameters of χ_{HD} and χ_{DM} for the star polymer S60 in the melt state.

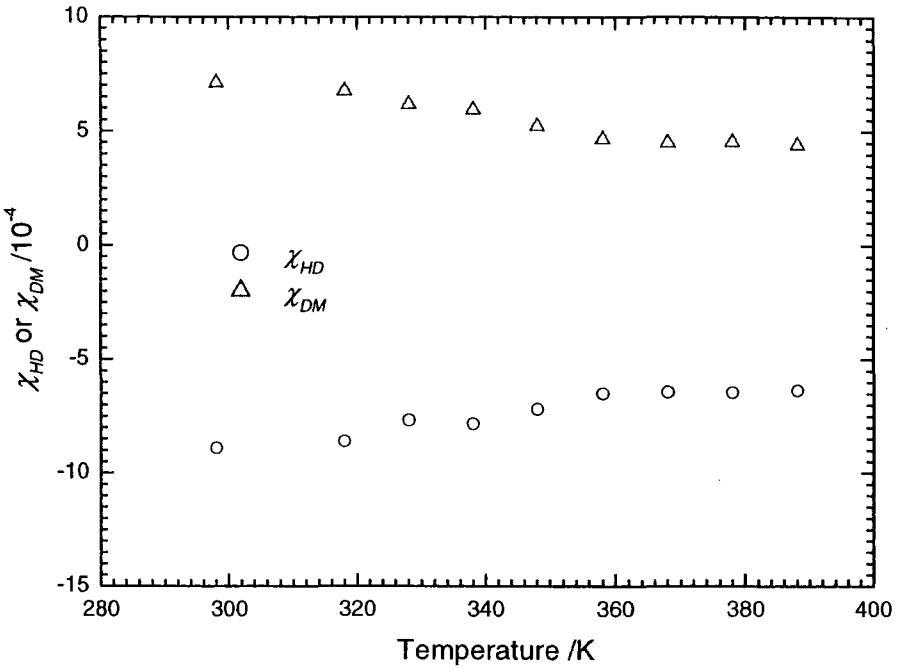

Figure 12: Temperature dependence of the interaction parameters of χ_{HD} and χ_{DM} for the star polymer S80 in the melt state.

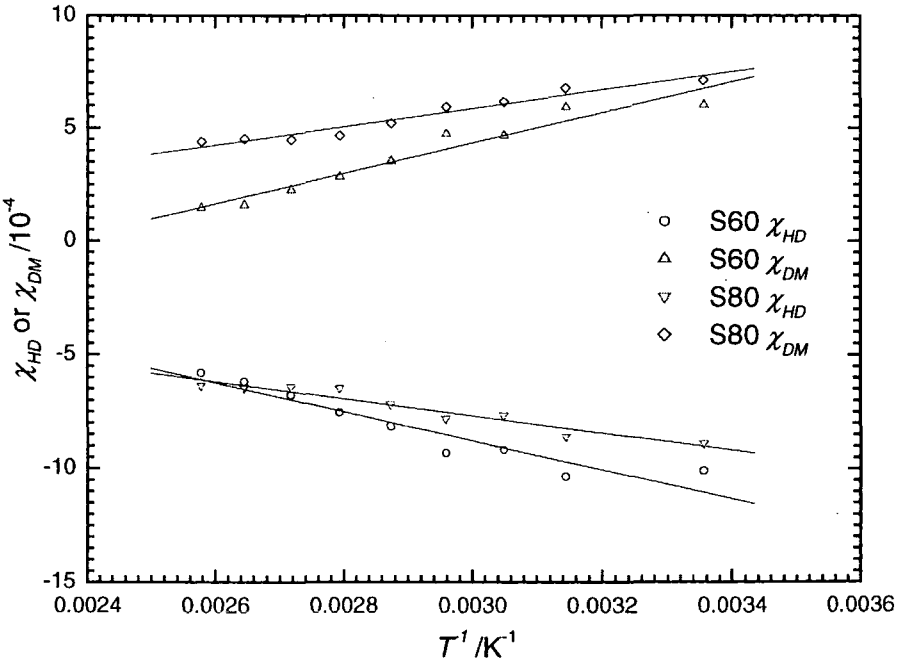

Figure 13: The reciprocal temperature dependence for the interaction parameters χ_{HD} and χ_{DM} of the star polymers S60 and S80 in the melt state.

4.4.2 The Solution State

SANS experiments were performed on the asymmetric star polymers S60 and S80 in solutions of contrast matched cyclohexane-d_{12}/cyclohexane and in 1,4-dioxane. Cyclohexane and 1,4-dioxane are a good and θ-solvent for polybutadiene respectively. The experiments were performed at a temperature of 298 K, that was close to the θ-temperature of linear polybutadiene in 1,4-dioxane of 299.5 K. The scattering cross sections obtained for S80 and S60 in cyclohexane over a range of volume fractions of star polymer (ϕ_{Star}) are shown in Figure 14 and Figure 15 respectively. The characteristic scattering peak associated with the radius of gyration of the asymmetric arm can be seen a low-Q. For both star polymers the positions of these peaks for all volume fractions are at a fixed value of Q. For the star polymers S60 and S80, the scattering peaks are located at wavevectors of approximately of 1.0×10^{-2} Å^{-1} and 7.0×10^{-3} Å^{-1} respectively. This shift of the scattering peak to lower Q for S80, is due to the presence of the longer asymmetric arm. This is also reflected in the higher $d\Sigma/d\Omega(Q)$ obtained for S80 than for S60, due to the greater quantity of deuterium within the star.

The scattering cross sections obtained for S60 and S80 in 1,4-dioxane are shown in Figure 16 and Figure 17 respectively. As this solvent was thermodynamically poorer than the good solvent of cyclohexane, a reduction in the radius of gyration of the labelled arm was expected, with a shift of the scattering peak to higher wavevector. The opposite has occurred here as the shift in the maximum was towards lower Q, and this suggested an increase in the R_G of the arm or the formation of a higher molecular weight species by star aggregation. At similar volume fractions, the $d\Sigma/d\Omega(Q)$ for the star polymers were higher in dioxane than in cyclohexane. This is another indication of the formation of higher molecular weight species in dioxane solution. Star aggregation has also been observed for 3-, 4-, 8- and 12-arm regular polybutadiene stars in dioxane by Hutchings *et al.*[18] The increase in the scattering cross sections seem to be more prevalent for S60 than for S80 with the longer asymmetric arm, suggesting a greater degree of aggregation for this star.

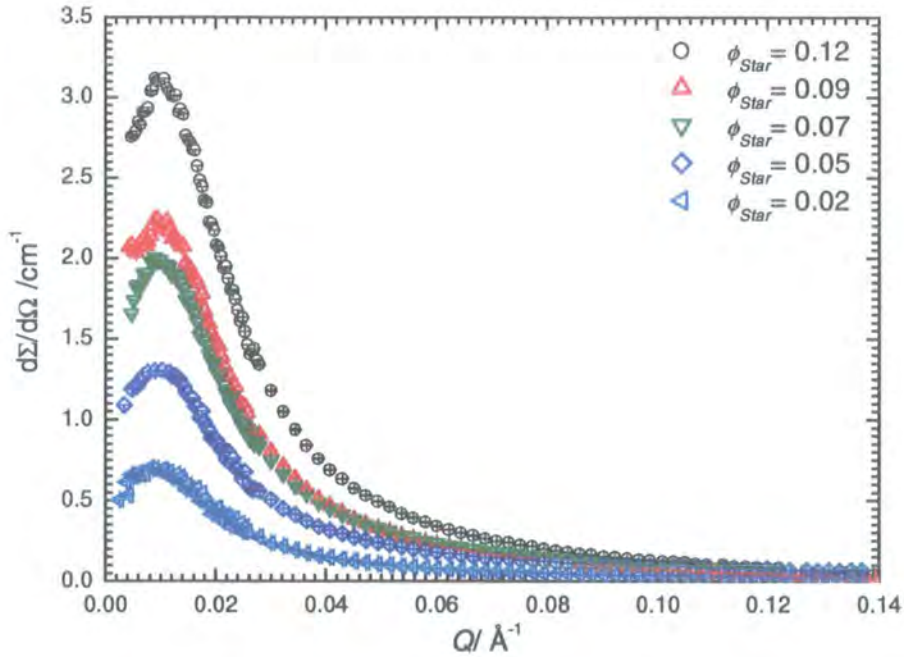

Figure 14: Scattering cross sections for star polymer S60 in contrasted matched cyclohexane-d_{12}/cyclohexane at a series of star volume fractions.

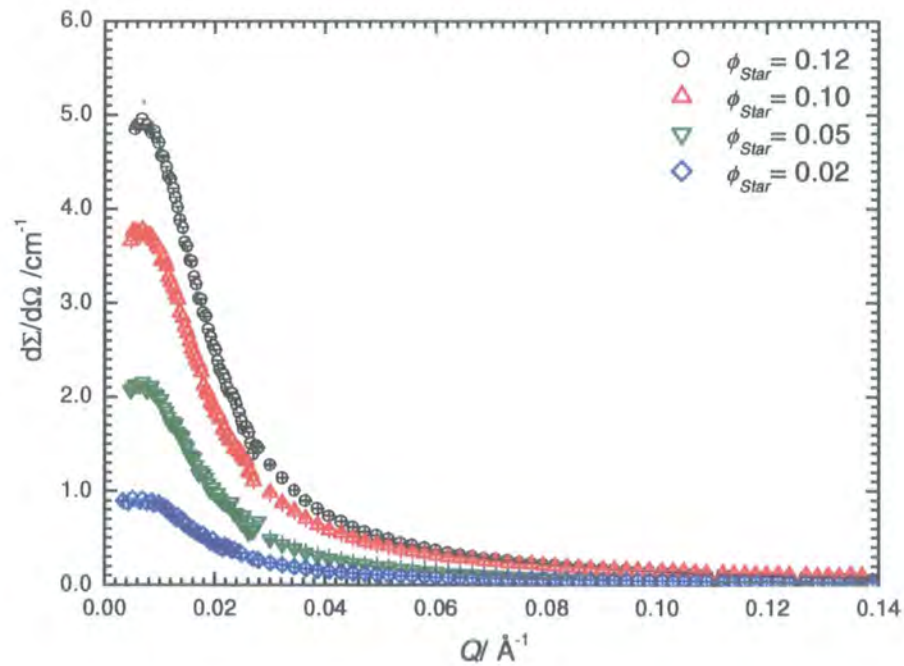

Figure 15: Scattering cross sections for star polymer S80 in contrast matched cyclohexane-d_{12}/cyclohexane at a series of star volume fractions.

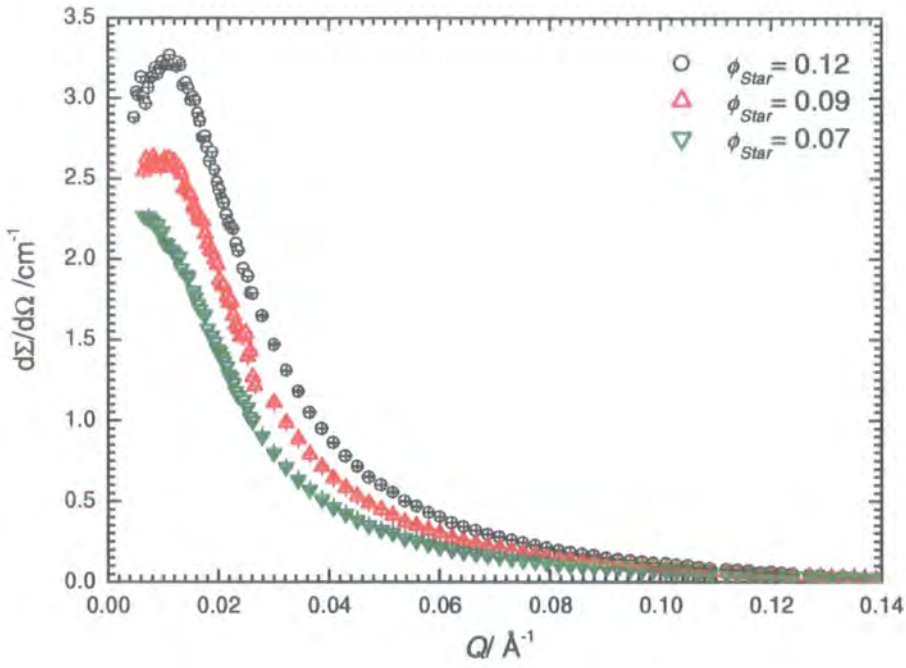

Figure 16: Scattering cross sections for star polymer S60 in 1,4-dioxane at a series of star volume fractions.

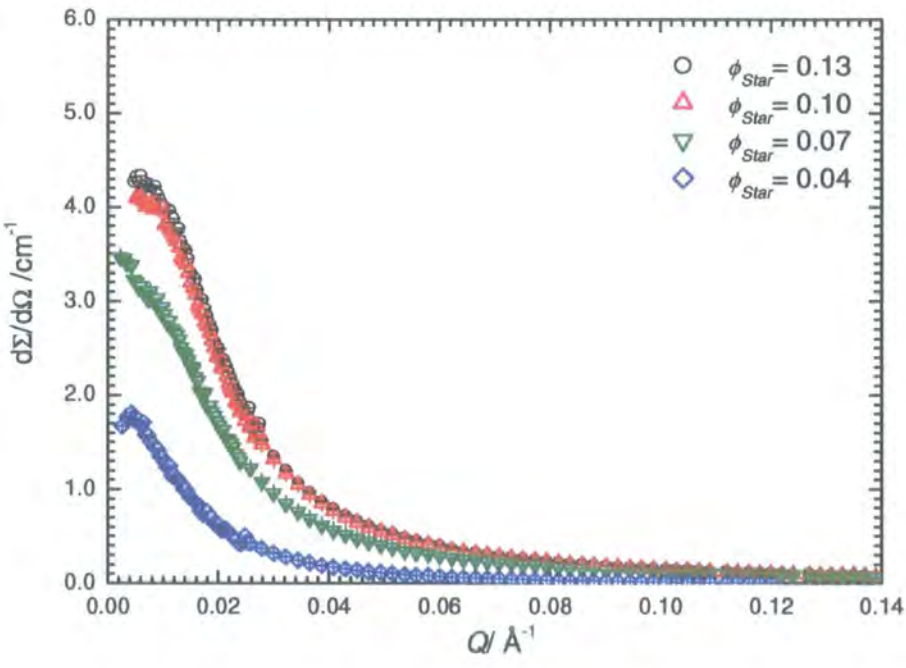

Figure 17: Scattering cross sections for star polymer S80 in 1,4-dioxane at a series of star volume fractions.

The Q-dependence of the scattering cross sections for the star polymers was determined by double logarithmic plots for cyclohexane solutions in Figure 18 and Figure 19, and for dioxane solutions in Figure 20 and Figure 21 for S60 and S80 respectively, over a range of star volume fractions. The characteristic peak observed for the deuterated arm at the low-range of Q ($Q < 0.01$ Å^{-1}) is no longer observed, whereas this peak was still evident for regular 8-arm polybutadiene star under the same solvent conditions.[18] This loss of the characteristic peak is due to the shift of the scattering maximum towards lower-Q, as observed in the linear cross sections due to the presence of the longer asymmetric arms. In the mid-range of Q $0.02 \leq Q/$ Å$^{-1} \leq 0.07$, the length scales probed correspond to the correlation lengths of the outermost blobs of the star arm, assuming the Daoud and Cotton model star. The Q-dependence of the scattering cross section in this range is related to the excluded volume effect experienced by these blobs. Cross section scaling dependencies of $Q^{-5/3}$ ($Q^{-1.67}$) and Q^{-2} are obtained if the polymer chain within the blobs has perturbed and unperturbed dimensions respectively. The scaling exponents obtained for the S60 and S80 over this mid-range of Q are shown in Table 8 for each star volume fraction and solvent condition.

The scaling exponents found for theses stars over the mid-range of Q seemed to be independent of ϕ_{Star}. In cyclohexane, the scaling exponents for S60 in cyclohexane in this mid-range of Q were higher than the perturbed dimensions prediction of $Q^{-5/3}$, but lower than the unperturbed prediction of Q^{-2}. This can be interpreted as the asymmetric star arm having perturbed dimensions in the good solvent. Higher scaling predictions were found in dioxane for this star, but were still lower than the unperturbed prediction of Q^{-2}, and therefore the arm still had stretched dimensions in this θ-solvent. The star polymer S80 had higher scaling exponents in cyclohexane than for S60, over the range of measured star volume fraction and suggested that S80 still had unperturbed dimensions. Star S80 has a longer asymmetric arm and therefore a lower proportion of this arm will be within the star core. The increase in the scaling exponent demonstrates the decrease in the influence of the high segment density at the core had on the dimensions of this longer arm. The mid–range of Q scaling dependencies for S80 in dioxane were similar to those obtained in cyclohexane. The results were still lower then the unperturbed prediction of Q^{-2}, and therefore the arms were still experiencing excluded volume effects in this solvent. At the lower star volume fraction of 0.04, a scaling exponent of 2 was obtained that correspond to

unperturbed dimensions for the arm. The scaling exponents for S80 in dioxane were slightly higher than those obtained for S60 in the same solvent, demonstrating a reduction of the influence of high segment density at the core had on the longer asymmetric arm.

Table 8: The scattering cross section scaling dependence exponent for the stars S60 and S80 over the mid-range of Q of $0.02 \leq Q/\text{Å}^{-1} \leq 0.07$.

Star Polymer S60				Star Polymer S80			
Cyclohexane mix		1,4-Dioxane		Cyclohexane mix		1,4-Dioxane	
Volume Fraction (ϕ_{Star})	*Scaling exponent*	Volume Fraction (ϕ_{Star})	*Scaling exponent*	Volume Fraction (ϕ_{Star})	*Scaling exponent*	Volume Fraction (ϕ_{Star})	*Scaling exponent*
0.12	1.83	0.12	1.76	0.12	1.80	0.13	1.89
0.09	1.79	0.09	1.80	0.10	1.83	0.10	1.88
0.07	1.79	0.07	1.84	0.05	1.89	0.07	1.87
0.05	1.76	-	-	0.02	1.84	0.04	2.02
0.02	1.74	-	-	-	-	-	-

Kratky plots of $Q^{5/3}d\Sigma/d\Omega$ versus Q for S60 and S80 in cyclohexane are shown in Figure 22 and Figure 23 respectively, over the range of volume fractions. The Kratky plots were for the stars experiencing excluded volume. The characteristic peak for star polymers, where the scattering is from all arms was not observed for these single-labelled arm stars.[19] A decrease can be seen for these plots at high-range Q, which was contrary to the increase that was modelled for single arm scattering by Alessandrini and Carignano.[4] A decrease in the Kratky plot suggests a reduction of the stretching of the labelled arm, but is more likely due to the sensitivity of these plots to the value of incoherent background. The Kratky plots are dependent on the value of incoherent scattering subtracted from the cross sections and this can be seen in the Kratky plots for S60 and S80 in Figure 24 and Figure 25 respectively, at the highest star volume fraction of 0.12. If the incoherent scattering is decreased by a half, a upwards shift in the Kratky plot at high Q is observed. The value of incoherent scattering removed is small, and therefore a slight variation in these values demonstrates the sensitivity of these plots at high Q.

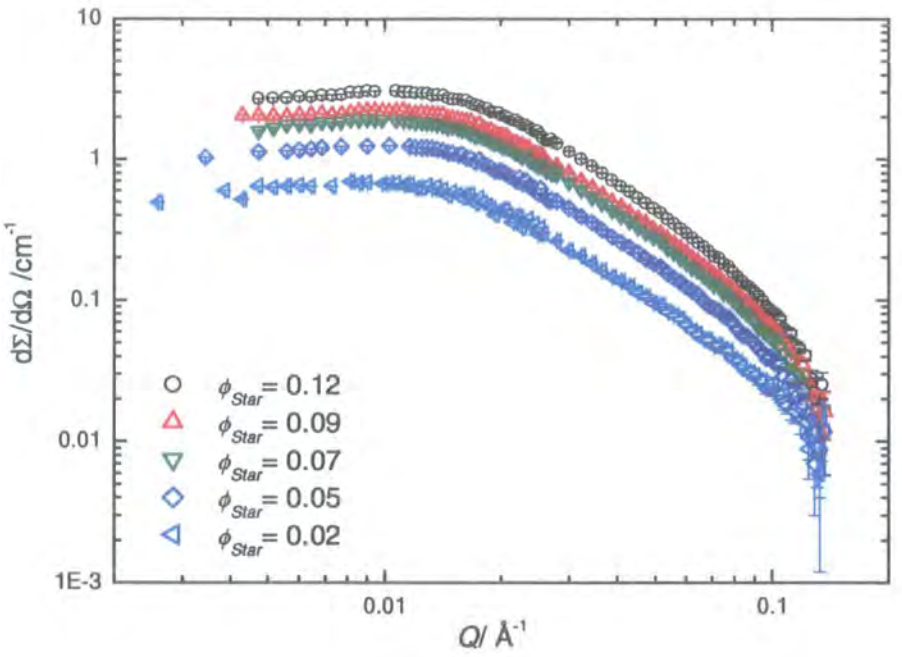

Figure 18: *Double logarithmic plot of scattering cross section versus wavevector for star S60 in cyclohexane over a range of star volume fractions.*

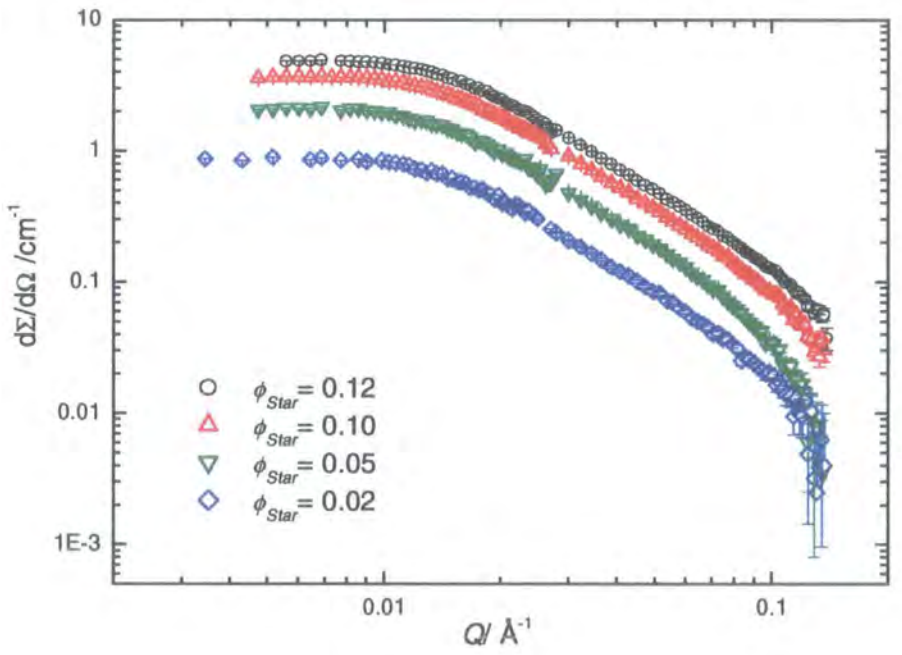

Figure 19: *Double logarithmic plot of scattering cross section versus wavevector for star S80 in cyclohexane over a range of star volume fractions.*

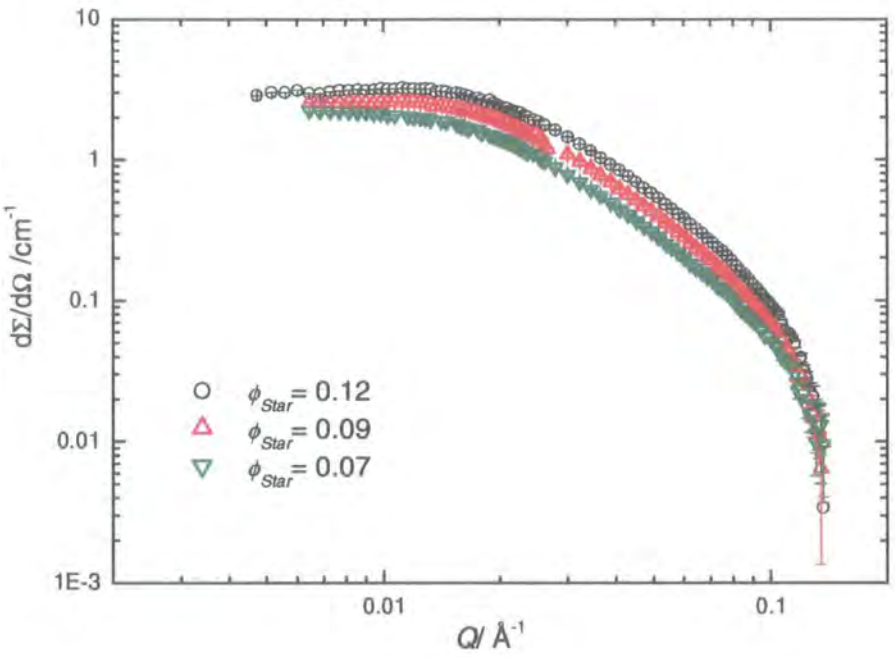

Figure 20: Double logarithmic plot of scattering cross section versus wavevector for star S60 in 1,4-dioxane over a range of star volume fractions.

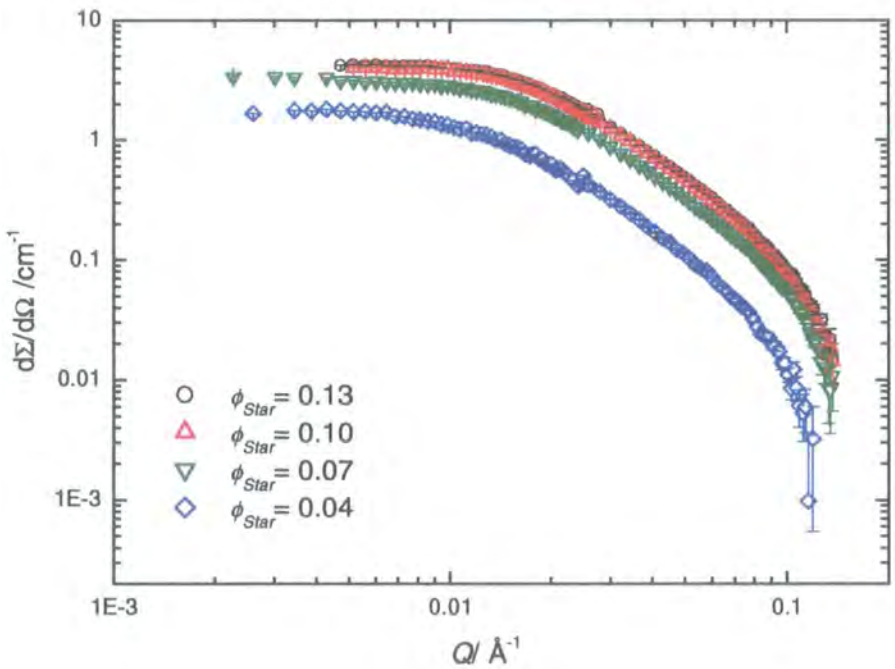

Figure 21: Double logarithmic plot of scattering cross section versus wavevector for star S80 in 1,4-dioxane over a range of star volume fractions.

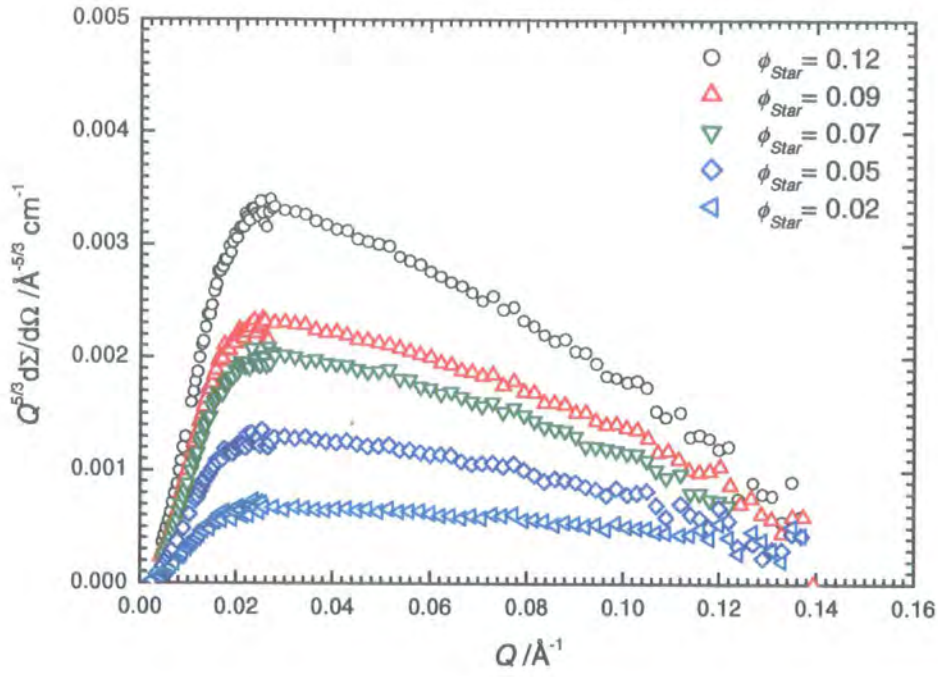

Figure 22: The Kratky plots for star polymer S60 in cyclohexane over the range of star volume fractions .

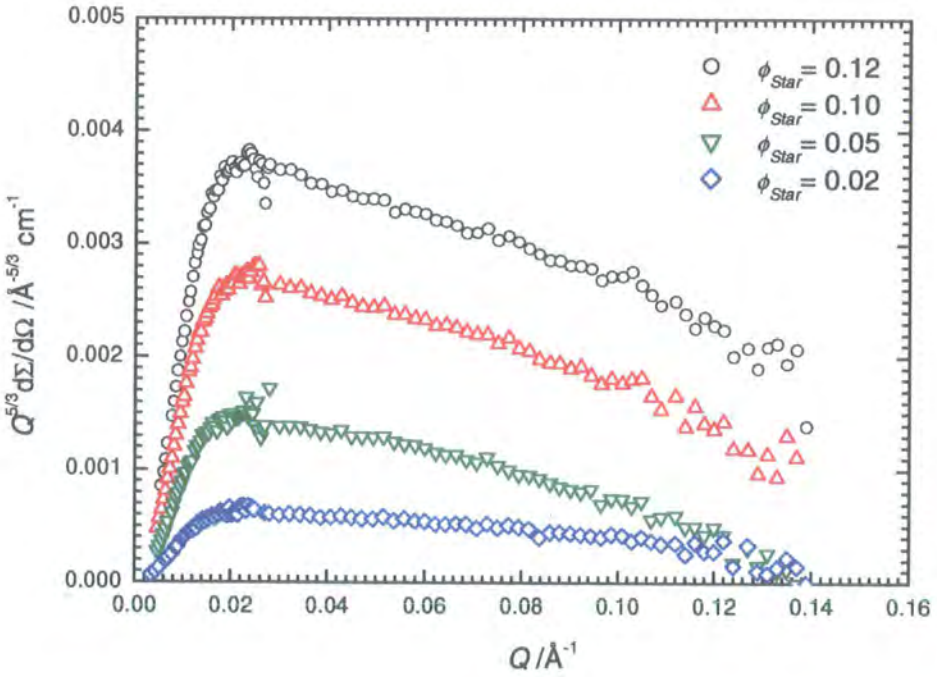

Figure 23: The Kratky plots for star polymer S80 in cyclohexane over the range of star volume fractions.

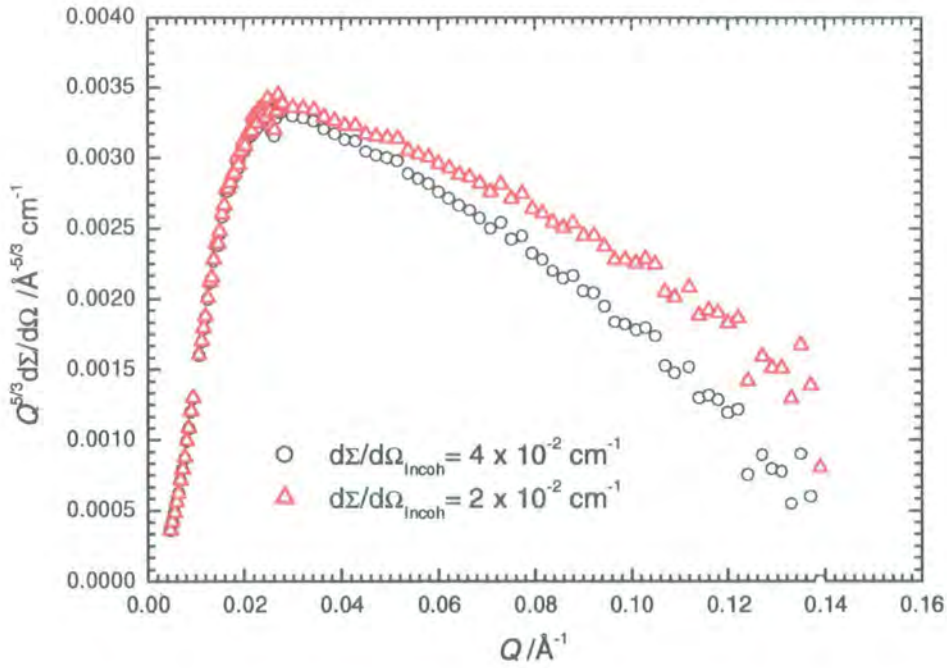

Figure 24: The variation Kratky plot with the value of incoherent scattering subtracted for the star S60 in cyclohexane at a ϕ_{Star} of 0.12.

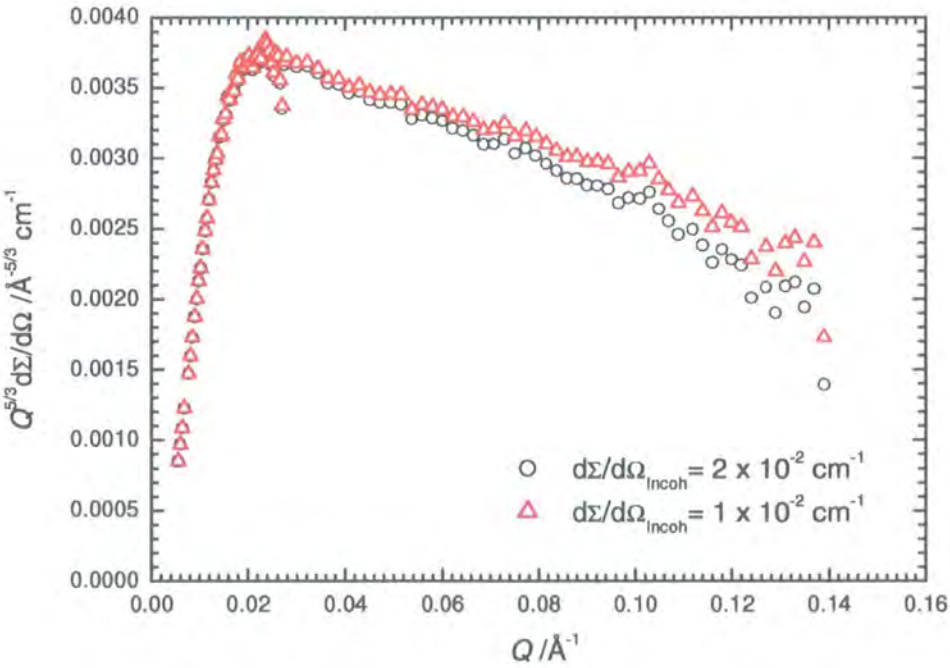

Figure 25: The variation Kratky plot with the value of incoherent scattering subtracted for the star S80 in cyclohexane at a ϕ_{Star} of 0.12.

The scattering cross sections were fitted using the random phase approximation expression for the scattering law using the parameters in Table 4 and are shown for each star volume fraction (ϕ_{Star}) in Appendix C. The fits obtained for the RPA expression for the scattering law were worse than those obtained for the stars in the melt state (as shown in Appendix B) due to the excluded volume effects experienced by the labelled arm. The scattering law was only devised for unperturbed dimensions with the Debye form factor. The radius of gyration obtained for the asymmetric deuterated arms from the data fits for each star are shown in Table 9. The R_G values had an error of 10 %.

In the good solvent of cyclohexane, the R_G remained practically constant over the each star volume fraction range, and were approximately 142 Å and 169 Å for S60 and S80 respectively. These average values were greater than 82 Å and 95 Å for unperturbed linear polymer at equivalent molecular weight, and 85 Å and 94 Å measured in the melt state at a temperature of 298 K for S60 and S80 respectively. The higher values of R_G obtained in cyclohexane demonstrates the stretching of the star arm dimensions away from unperturbed configurations, due to the excluded volume effect under good solvent conditions. Expansion factors for the asymmetric arms can be calculated by dividing the R_G obtained under good solvent conditions by the R_G of an unperturbed linear polymer ($R_{G,0}$) of equivalent molecular weight, and are listed in Table 10 for S60 and S80. The expansion factors (α_S^2) for the star S80 seemed to be greater than those for S60 over the star volume fraction of interest. Alessandrini and Carignano[4] have calculated an analytical expression for the expansion factor for a labelled arm in a f-functional star:

$$\alpha_S^2 = \frac{R_G^2}{R_{G,0}^2} = 1 + (f-1)\left[\frac{35}{64} - \frac{3}{4}\ln 2\right] \qquad (21)$$

The expansion factors calculated for a 6- and 7-arm regular star by equation 21 were 1.14 and 1.16 respectively, and are clearly much lower than those obtained for S60 and S80 over the volume fraction range. An expansion factor of approximately 2.36 was determined for an 8-arm regular polybutadiene star in cyclohexane by SANS, and allowing for the difference in star functionality, which was much lower than those obtained for asymmetric stars S60 and S80.[18] The increase in the expansion factor with asymmetric arm length suggested increased dimensions in this thermodynamically more favourable solvent due to

the excluded volume effect. As the a greater proportion of the star arm is not within the star, the arm is more influenced by the solvent, than the segment overcrowding at the core.

In the thermodynamically poorer solvent of 1,4-dioxane, Table 9 shows that higher R_G values were obtained for both stars than under good solvent conditions. Larger R_G values in this solvent could be due to aggregation or cross-linking of the stars to form higher molecular weight species. Aggregation of the stars was seen by the results of light scattering, viscometry and size exclusion chromatography experiments, as reported in section 3.4.2.2 in chapter 3. Aggregation of the stars in this θ-solvent would also reduce the accuracy of the fits of the scattering law to the cross sections, as the scattering law only assumes single star species and no excluded volume effects.

Interaction parameters were obtained from the random phase approximation data fits to the $d\Sigma/d\Omega(Q)$ (see Appendix C) for the star polymers and are shown in Table 11. The intramolecular interaction parameter of χ_{HD} are listed for S60 and S80 over a range of volume fractions in both good and θ-solvent conditions (errors are within 10 %). The interaction parameters of χ_{HD} were positive in a good solvent, due to the polymer-solvent contacts between the deuterated arms and the solvent being thermodynamically more favourable than polymer-polymer contacts between the hydrogenous and deuterated arms. An increase in χ_{HD} with decreasing volume fraction was observed for both stars, that suggested that when the stars became more isolated in solution, the effect of the polymer solvent contacts were becoming more dominant. The values of χ_{HD} were higher for S60 than for S80 over the star volume fraction range, as a greater proportion of the asymmetric arm was within the star and hence a greater likelihood of more repulsive polymer-polymer contacts.

In the θ-solvent of 1,4-dioxane, the χ_{HD} were overall lower than obtained under good solvent conditions, as the intramolecular polymer-polymer contacts between the deuterated and hydrogenous arms become more favourable. The extent of aggregation of the stars and the diversity of species produced in solution would have an pronounced effect on χ_{HD}. The star S60 at smaller star volume fractions had negative values of χ_{HD} that were lower than obtained for S80, suggesting a larger number of favourable polymer-polymer contacts.

More polymer-polymer contacts would be obtained for star S60, due to a greater proportion of the asymmetric arm being within the star.

Table 9: The R_G of the deuterated asymmetric arms (D-arm) of stars S60 and S80 in cyclohexane-d_6/cyclohexane mix and 1,4-dioxane over a range of star volume fractions.

Star Polymer S60				Star Polymer S80			
Cyclohexane mix		1,4-Dioxane		Cyclohexane mix		1,4-Dioxane	
Volume Fraction (ϕ_{Star})	R_G (Å) of *D*-arm	Volume Fraction (ϕ_{Star})	R_G (Å) of *D*-arm	Volume Fraction (ϕ_{Star})	R_G (Å) of *D*-arm	Volume Fraction (ϕ_{Star})	R_G (Å) of *D*-arm
0.12	138	0.12	131	0.12	161	0.13	165
0.09	145	0.09	259	0.10	172	0.10	153
0.07	139	0.07	279	0.05	174	0.07	179
0.05	142	-	-	0.02	170	0.04	236
0.02	146	-	-	-	-	-	-

Table 10: Expansion factors for the labelled arms for star polymers S60 and S80 over the range of star volume fractions.

Volume Fraction (ϕ_{Star})	Star (S60) α_S^2	Volume Fraction (ϕ_{Star})	Star S80 α_S^2
0.12	2.83	0.12	2.87
0.09	3.13	0.10	3.27
0.07	2.87	0.05	3.35
0.05	3.00	0.02	3.20
0.02	3.17	-	-

Table 11: The interaction parameters χ_{HD} for stars S60 and S80 in cyclohexane-d_6/cyclohexane mix and 1,4-dioxane over the range of star volume fractions.

Star Polymer S60				Star Polymer S80			
Cyclohexane mix		1,4-Dioxane		Cyclohexane mix		1,4-Dioxane	
Volume Fraction (ϕ_{Star})	$\chi_{HD}/10^{-2}$	Volume Fraction (ϕ_{Star})	$\chi_{HD}/10^{-2}$	Volume Fraction (ϕ_{Star})	$\chi_{HD}/10^{-2}$	Volume Fraction (ϕ_{Star})	$\chi_{HD}/10^{-2}$
0.12	1.5	0.12	2.9	0.12	1.1	0.13	0.2
0.09	1.3	0.09	-7.7	0.10	1.2	0.10	1.9
0.07	3.1	0.07	-8.9	0.05	3.7	0.07	5.0
0.05	6.0	-	-	0.02	13.3	0.04	3.0
0.02	18.7	-	-	-	-	-	-

4.4.3 Summary of Results

Star polymers S60 and S80 have been characterised in the melt and in dilute solutions by SANS. In the melt state, the scattering cross sections were obtained over the temperature range of 288 K to 388 K. In the solution state, the scattering cross sections were determined in the good solvent of cyclohexane and in the θ-solvent of 1,4-dioxane, over a range of star volume fractions. The hydrogenous content of the polymer was contrast matched to the a mixture of cyclohexane-d_{12} and cyclohexane. In both melt and solution states, a maximum in the $d\Sigma/d\Omega(Q)$ was observed due to the radius of gyration of the deuterated asymmetric arms and its wavevector position was determined by its value. The peaks of scattering cross sections of the both stars in the melt state were at fixed wavevector over the temperature range of measurement and decreased with increasing temperature. In the cyclohexane solution, the $d\Sigma/d\Omega(Q)$ peaks were also at fixed wavevector for both stars and increased with star volume fraction. A shift to lower Q was observed for star S80 with the longer asymmetric arm, in both melt and cyclohexane solution states. The proposed shift to higher-Q for the stars in dioxane solutions did not occur, and the shift of lower wavevector was interpreted as aggregation of the stars in this solution. Aggregation of the stars was seen by the results of light scattering, viscometry and size exclusion chromatography experiments, as reported in section 3.4.2.2 in chapter 3.

The Kratky plots of the scattering data in the melt suggested an increase in star dimensions from linear polymers due to the presence of the single branch point. In cyclohexane solutions, a decrease in the Kratky plot (plotted for excluded volume) at high wavevector was due to the sensitivity of these plots to value of incoherent scattering subtracted. The scaling exponents of the scattering cross sections in the solution states were also determined by the double logarithmic plots. Over the mid range of the scattering cross section, the scaling exponents for the Q-dependence suggested that the labelled arms were experiencing excluded volume effects in both solvent conditions. The exponents increased with arm length under both solvents as a greater proportion of the arm was not within the star region, demonstrating a lower influence the high segment density at the core had on arm stretching.

The radii of gyration of the deuterated arms were found by fitting the scattering law with the random phase approximation expression to the cross section data. The R_G determined

for the star arms in the melt state were found to increase slightly with temperature and were higher than calculated for a linear unperturbed polymer of equivalent molecular weight. In cyclohexane solutions, the R_G were found to be constant over the range of star volume fraction of interest, and were greater than determined in the melt state and for unperturbed linear polymer, demonstrating the excluded volume effect. Larger R_G values were found in dioxane solutions when compared to cyclohexane data, suggesting aggregation within this solvent. The expansion factors were calculated for the asymmetric arms of the stars and showed that stretching of the asymmetric arm became greater with chain length.

The interaction parameters of χ_{HD} and χ_{DM} were determined from the RPA fits to the scattering cross sections for the deuterated arms of S60 and S80 in the melt state. The intrastar interaction parameters χ_{HD}, were found to be negative, and increased with increasing temperature suggesting greater immiscibility, whereas the interstar interaction parameters χ_{DM}, were positive and decreased with increasing temperature due to greater miscibility of the deuterated arms. Increasing temperature was found to promote greater interstar mixing of the deuterated arms and this was found to be more prevalent for S60, with the more spherical star shape.

In cyclohexane and dioxane solutions, the interaction parameters χ_{HD}, were obtained from fits to the scattering cross sections. The χ_{HD} values were positive in cyclohexane, due to the repulsive nature of the polymer and polymer contacts between the deuterated and hydrogenous arms in a good solvent, and increased with decreasing star volume fraction. This increase was proposed to be due to the star becoming more isolated in solution and the attractive polymer-solvent contacts became more dominant. The χ_{HD} values were found to be greater for S60 than for S80, as a greater proportion of the deuterated asymmetric arm was within the star. The interaction parameters were overall lower in dioxane solutions, as the polymer-polymer contacts became more thermodynamically favourable. The interaction parameters would be effected by the extent of aggregation of the stars in the dioxane solutions.

4.5 References

[1] King, S. M. *Modern Techniques for Polymer Characterisation*, Ed. Pethrick, R. A.; Dawkins, J. V.; John Wiley and Sons: Chichester, 1999.

[2] Higgins, J. S.; Benoit, H. C.; *Polymers and Neutron Scattering*, Clarendon Press: Oxford, 1994.

[3] Benoit, H. *J. Polym. Sci.* **1953**, 11, 507.

[4] Alessandrini, J. L.; Carignano, M. A. *Macromolecules* **1992**, 25, 1157.

[5] De Gennes, P. G. *Scaling Concepts in Polymer Physics*, Cornell University Press; Ithaca, 1979.

[6] Read, D. J. *Macromolecules* **1998**, 31, 399.

[7] Hutchings, L.R.; Richards, R.W.; *Macromolecules* **1999**, 32, 880.

[8] Balsara, N. P.; Jonnalagadda, S. V.; Lin, C. C.; Han, C. C.; Krishnamoorti, R. *J. Chem. Phys.* **1993**, 99, 10011.

[9] Engelhaaf, S. U.; Ghosh, R. E.; Rennie, A. R. *A Computing Guide for Small-Angle Scattering Experiments*; Institut Max von Laue-Paul Langevin.

[10] Sakurai, S.; Hasegawa, H.; Hashimoto, T.; Hargis, I. G.; Aggarwal, S. L. Han, C. C. *Macromolecules* **1990**, 23, 451.

[11] Brunacci, A. S.; Kiff, F. T.; Richards, R. W.; Thompson, R. L.; King, S. M. *Polymer* **2000**, 41, 2557.

[12]Bandrup, J.; Immergut, E. H.; Grulke, E. A. *Polymer Handbook*; 4th ed.;Wiley-Interscience: New York, 1999.

[13] Horton, J. C.; Squires, G. L.; Boothroyd, A. T., Fetters, L. J.; Rennie, A. R.; Glinka, C, J.; Robinson, R. A. *Macromolecules* **1989**, 22, 681.

[14] Freire, J. J. *Adv. Polym. Sci.* **1999**, 143, 34.

[15] Bates, F. S.; Dierker, S. B.; Wignall, G. D. *Macromolecules* **1986**, 19, 1938.

[16] Bates, F. S.; Wignall, G. D. *Phys. Rev. Lett.* **1986**, 57, 1429.

[17] Bates, F. S.; Fetters, L. J.; Wignall, G. D. *Macromolecules* **1988**, 21, 1086.

[18] Hutchings, L. R.; Richards, R. W.; Reynolds, S. W.; Thompson, R. L. unpublished.

[19] Willner, L,; Jucknischke, O.; Richter, D.; Roovers, J.; Zhou, L.-L.; Toporowski, P. M.; Fetters, L. J.; Huang, J. S.; Lin, M. Y.; Hajichristidis, N. *Macromolecules* **1994**, 27, 3821.

Chapter 5

Conclusions and Future Work

A series of asymmetric star-branched polybutadienes were synthesised with a single deuterium labelled arm of varying molecular weight. Living anionic polymerisation methods were used to control the molecular weight of the arms, and to produce narrow molecular weight distributions. Chlorosilanes were found to be effective coupling agents to link the arms of the star and especially more so for regular stars. Difficulties arose in the preparation of the longer asymmetric arm stars and this could be due to steric hindrance of the coupling centre by these arms to the approaching uncoupled living hydrogenous arms. Increasing the reaction times to facilitate greater linking also has the detrimental effect of further termination of the living uncoupled hydrogenous arms. Four star polymers were synthesised with increasing the asymmetric arm length.

Investigation of the these star polymers was achieved in dilute solutions by static and dynamic light scattering and viscometry techniques. Increasing the length of the asymmetric arm yielded global properties in good solvent conditions similar to those ascertained for linear polymers of equivalent molecular weight. This was seen more clearly by calculating branching and size ratios for the stars. Aggregation was observed for the stars in θ-solvents conditions with a increase molecular weight with decreasing temperature. The molecular weights ascertained at higher temperatures were similar to those characterised under good solvent conditions, apart from the regular star S30. Aggregation could be seen by the formation of a higher molecular weight peak by size exclusion chromatography and occurred by cross-linking of the arms between stars. Global properties obtained in the θ-

solvent suggested that the extent of aggregation was linked to the length of the asymmetric arm, and this was observed between the stars S60 and S300 by the calculated size ratios and Huggins constants. The θ-temperatures ascertained for the star polymers were dependent on the asymmetric arm length. Star S300 with the longest asymmetric arm only experienced a θ-depression from the value obtained for linear polymer of equivalent molecular weight, where the regular star was found to have an increase in θ-temperature over linear values. The stars with intervening asymmetric arm lengths had a θ-temperature similar to the value ascertained for linear polymers. The variation of the θ-temperatures was suggested to be due to the increase of aggregation of the more spherical star, compared to the other stars.

Small angle neutron scattering studies were performed on the stars in good and θ-solvents, and in the melt state. A random phase approximation expression for the scattering law was used to determine R_G and the interaction parameters, and poorer fits were obtained in solution due to excluded volume effects. In good solvents, the R_G ascertained for the labelled asymmetric arms were found to be constant over the volume fraction range of interest, and greater than those obtained in the melt state, demonstrating the excluded volume effect. Under θ-conditions, the R_G of the labelled arms were found to be higher than those determined under good solvent conditions, due to the aggregation of the stars to higher molecular weight species in this solvent. The scaling dependencies of the scattering cross-sections over the mid-range of Q, suggested the asymmetric arms were being influenced by excluded volume effects in both good and θ-solvents. This influence was reduced in the thermodynamically poorer solvent and with the increase in the asymmetric arm length, due to a reduction of the influence of the high segment density at the star core had on R_G.

Intra- and inter-star interaction parameters of the deuterated asymmetric arm were determined for the stars in the melt state by neutron scattering. Inter-star mixing was found to increase with increasing temperature, and this was found to be more prevalent for more spherical shaped stars. In cyclohexane solutions, positive intra-star interaction parameters were obtained demonstrating that polymer-solvent contacts became more thermodynamically favourable than the polymer-polymer contacts between the asymmetric deuterated and hydrogenous arms. As the length of the asymmetric arm increased, the intra-

star interaction parameter decreased as a smaller proportion of this arm was now within the star core. In dioxane solutions, the intra-star interaction parameter was lower than obtained under good solvent conditions, as the polymer-polymer contacts became thermodynamically more favourable. The interpretation of the interaction parameters in this solvent were dependent on the diversity of the star aggregation.

The global properties of these miktoarm star polymers can be investigated further by synthesising more stars with a range of molecular weights for the asymmetric arm, especially in the mid to higher molecular weight range of between 1×10^5 g mol^{-1} to 3×10^5 g mol^{-1}. The global properties obtained from the characterisation of these stars in dilute solutions of good and θ-solvents, can be used to calculate branching and size ratios to obtain a better understanding of the cross-over from star to linear polymer behaviour. Investigation of the stars in dilute solutions of various θ-solvents can be performed to see if aggregation is still occurring, as it does in 1,4-dioxane. θ-solvents of n-propyl acetate, 2-pentanone and propylene oxide can be used with θ-temperatures ascertained for linear polybutadienes of 308.5 K, 332.7 K and 308 K respectively.

Neutron scattering studies on the miktoarm star polymers in the melt and solution state can be performed to obtain radii of gyration and interaction parameters for the asymmetric arms. The values of R_G obtained in the melt state and under good and θ-solvent conditions can be compared to see the increase of these arms with excluded volume. Expansion factors can be calculated for these stars to see whether the relative increase in star dimensions follows the increase in arm length. The inter- and intra-star interaction parameters can be obtained in the melt state to see if increasing asymmetric arm length causes the inter-star mixing of this arm to approach behaviour of that of a linear polymer. The intra-star interaction parameters can be ascertained in good and θ-solvents respectively. The increase of the interaction parameter with increasing asymmetric arm length can be investigated further, and whether lower values are obtained under θ-solvent conditions.

Appendix A

The general from of the scattering cross section for a three component system is given by:

$$\frac{d\Sigma(Q)}{d\Omega} = K_{HM} S_{AA}(Q) + 2K_{DM} K_{HM} S_{AB}(Q) + K_{DM} S_{BB}(Q)$$

$$S_{AA}(Q) = \frac{S1_{BB}(Q)}{S1_{AA}(Q) S1_{BB}(Q) - S1_{AB}{}^2(Q)}$$

$$S1_{BB}(Q) = SO1_{BB}(Q) + V_{BB}(Q)$$

$$SO1_{BB}(Q) = \frac{SO_{AA}(Q)}{SO_{AA}(Q) SO_{BB}(Q) - SO_{BB}{}^2(Q)}$$

$$SO_{AA}(Q) = n_H D_H \phi_H v_H \left(g_{dH} + (n-1)\left[\left(\frac{1}{u_H}\right)(1-\exp(u_H))\right]^2 \right)$$

$$SO_{BB}(Q) = n_D D_D \phi_D v_D \left(g_{dD} + (n-1)\left[\left(\frac{1}{u_D}\right)(1-\exp(u_D))\right]^2 \right)$$

$$SO_{AB}(Q) = \sqrt{n_H n_D D_H D_D v_H v_D \phi_H \phi_D} \times \left[\left(\frac{1}{u_H}\right)(1-\exp(u_H))\right]\left[\left(\frac{1}{u_D}\right)(1-\exp(u_D))\right]$$

$$V_{BB}(Q) = \frac{1}{D_M \phi_M v_M g_{dM}} - \frac{2\chi_{DM}}{v_{norm}}$$

The term $S_{BB}(Q)$ is constructed in a similar manner as that above for $S_{AA}(Q)$. The cross term $S_{AB}(Q)$ is given by:

$$S_{AB}(Q) = \frac{-S1_{AB}(Q)}{S1_{AA}(Q) S1_{BB}(Q) - S1_{AB}{}^2(Q)}$$

$$S1_{AB}(Q) = SO1_{AB}(Q) + V_{AB}(Q)$$

$$SO1_{AB}(Q) = \frac{-SO_{AB}(Q)}{SO_{AA}(Q) SO_{BB}(Q) - SO_{AB}{}^2(Q)}$$

$$V_{AB}(Q) = \frac{1}{D_M \phi_M v_M g_{dM}} - \frac{\chi_{HM} + \chi_{DM} + \chi_{HD}}{v_{norm}}$$

K_{IJ} is the contrast factor between species I and J, and D, H, and M refer to deuterated, hydrogenous and matrix species respectively. n, D, ϕ and υ are the number of arms, degrees of polymerisation, volume fraction, and monomer unit volume, respectively, of the species specified by the subscript. υ_{norm} is the reference volume calculated as the appropriate root of the product of the individual monomer unit volumes (square root for $V_{II}(Q)$ terms and cube root for $V_{IJ}(Q)$ terms). The Debye function for the scattering of a Gaussian coil is represented by g_{dI} for species I.

Appendix B

RPA fits to star polymers S60 in the melt state.

B1: RPA fit to $d\Sigma/d\Omega(Q)$ for S60 in the melt state at a temperature of 298 K.

B2: RPA fit to $d\Sigma/d\Omega(Q)$ for S60 in the melt state at a temperature of 318 K.

B3: RPA fit to $d\Sigma/d\Omega(Q)$ for S60 in the melt state at a temperature of 328 K.

B4: RPA fit to $d\Sigma/d\Omega(Q)$ for S60 in the melt state at a temperature of 338 K.

B5: RPA fit to $d\Sigma/d\Omega(Q)$ for S60 in the melt state at a temperature of 348 K.

B6: RPA fit to $d\Sigma/d\Omega(Q)$ for S60 in the melt state at a temperature of 358 K.

B7: RPA fit to $d\Sigma/d\Omega(Q)$ for S60 in the melt state at a temperature of 368 K.

B8: RPA fit to $d\Sigma/d\Omega(Q)$ for S60 in the melt state at a temperature of 378 K.

B9: RPA fit to $d\Sigma/d\Omega(Q)$ for S60 in the melt state at a temperature of 388 K.

RPA fits to star polymers S80 in the melt state.

B10: RPA fit to $d\Sigma/d\Omega(Q)$ for S80 in the melt state at a temperature of 298 K.

B11: RPA fit to $d\Sigma/d\Omega(Q)$ for S80 in the melt state at a temperature of 318 K.

B12: RPA fit to $d\Sigma/d\Omega(Q)$ for S80 in the melt state at a temperature of 328 K.

B13: RPA fit to $d\Sigma/d\Omega(Q)$ for S80 in the melt state at a temperature of 338 K.

B14: RPA fit to $d\Sigma/d\Omega(Q)$ for S80 in the melt state at a temperature of 348 K.

B15: RPA fit to $d\Sigma/d\Omega(Q)$ for S80 in the melt state at a temperature of 358 K.

B16: RPA fit to $d\Sigma/d\Omega(Q)$ for S80 in the melt state at a temperature of 368 K.

B17: RPA fit to $d\Sigma/d\Omega(Q)$ for S80 in the melt state at a temperature of 378 K.

B18: RPA fit to $d\Sigma/d\Omega(Q)$ for S80 in the melt state at a temperature of 388 K.

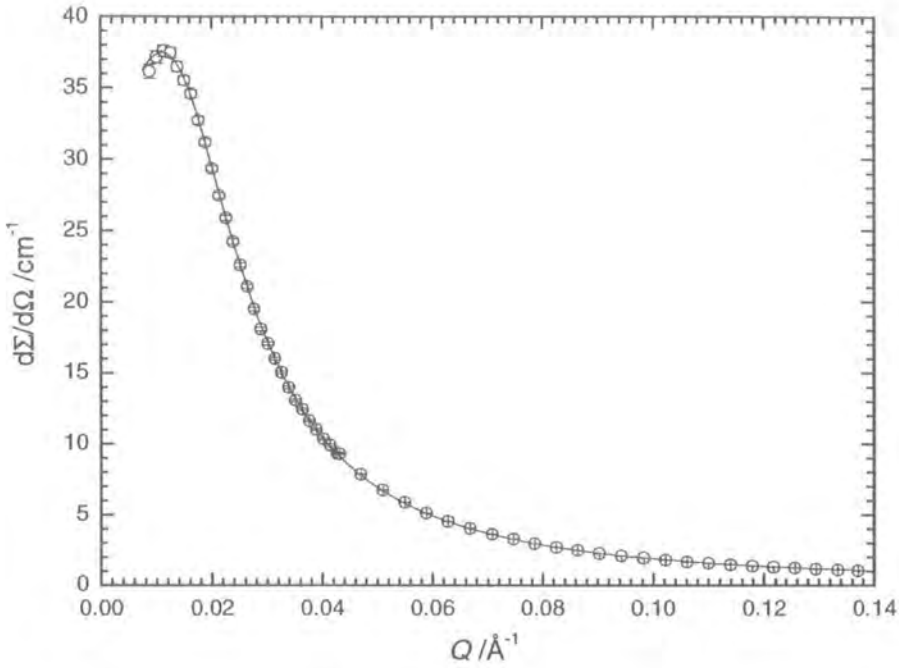

B1: RPA fit to dΣ/dΩ(Q) for S60 in the melt state at a temperature of 298 K.

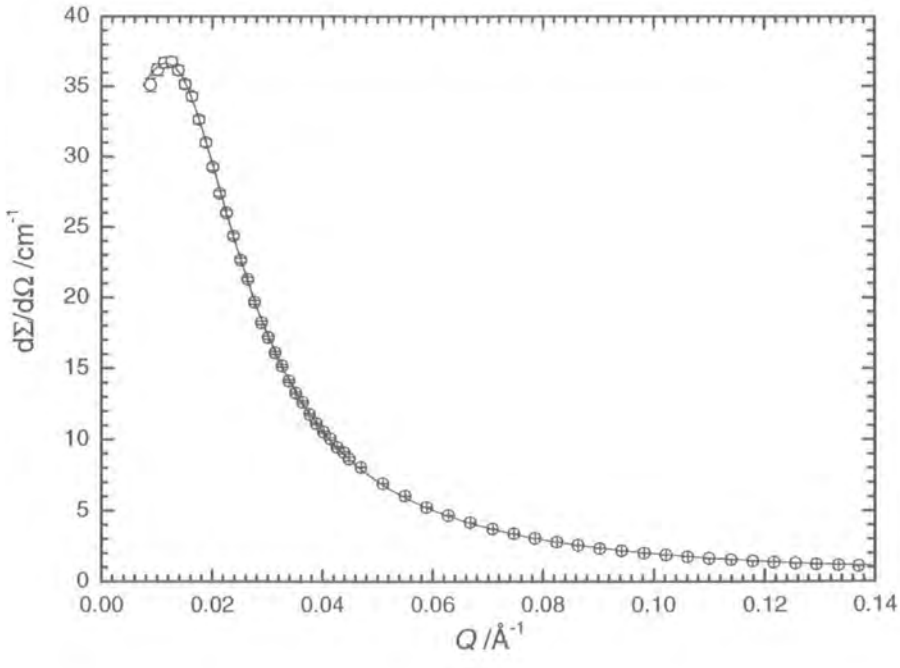

B2: RPA fit to dΣ/dΩ(Q) for S60 in the melt state at a temperature of 318 K.

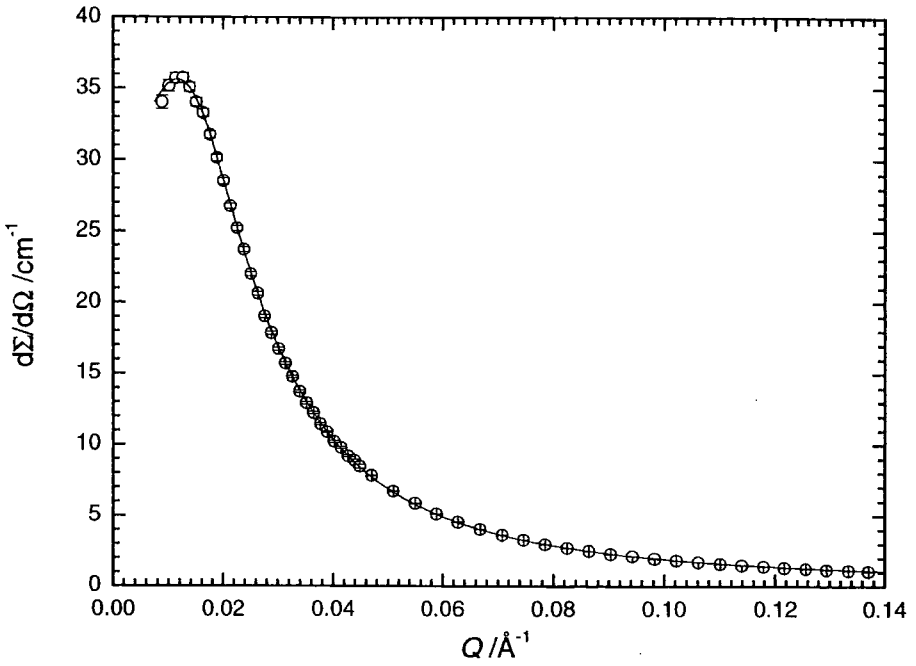

B3: RPA fit to dΣ/dΩ(Q) for S60 in the melt state at a temperature of 328 K.

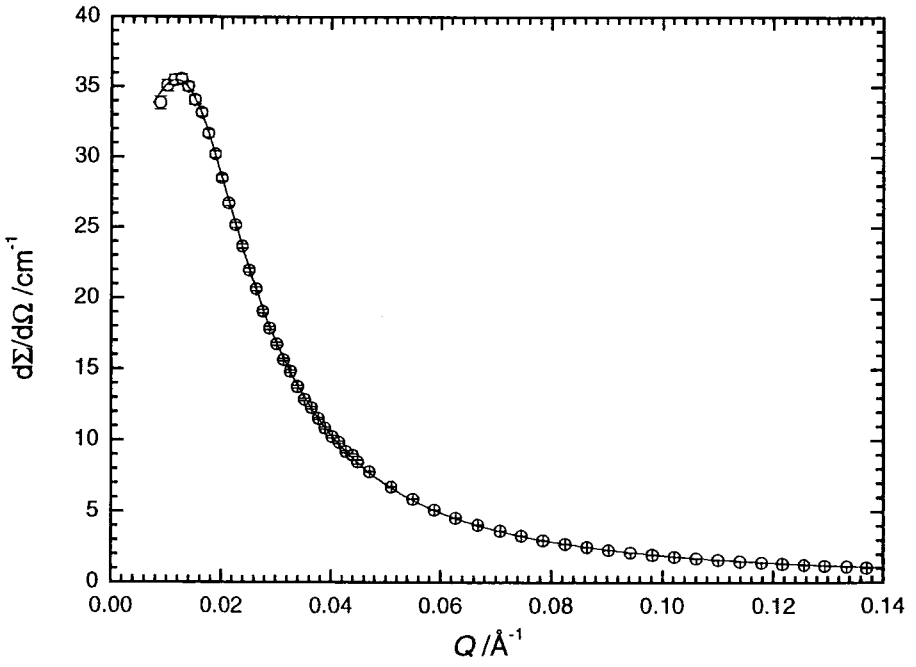

B4: RPA fit to dΣ/dΩ(Q) for S60 in the melt state at a temperature of 338 K.

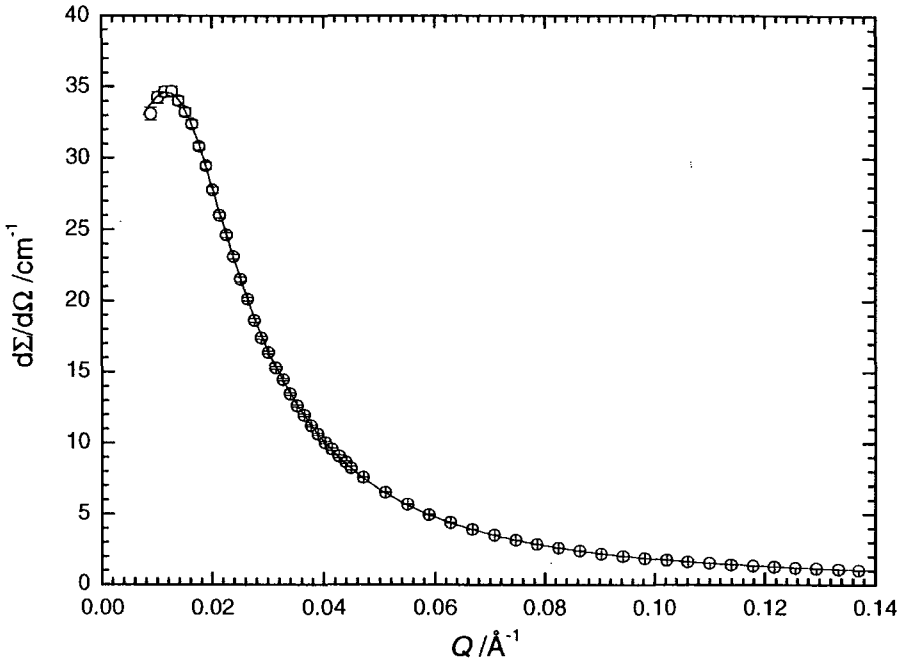

B5: RPA fit to dΣ/dΩ(Q) for S60 in the melt state at a temperature of 348 K.

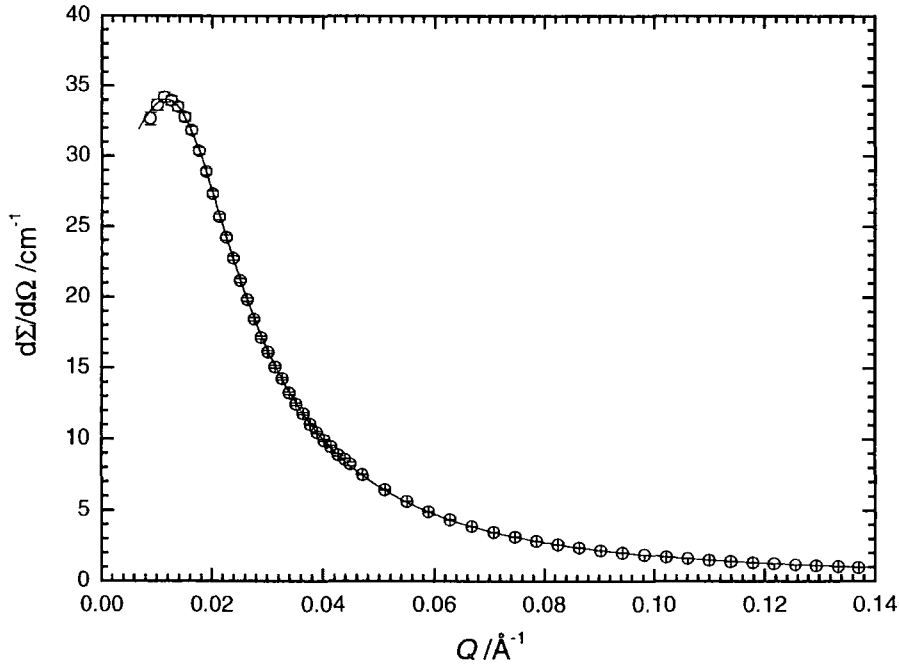

B6: RPA fit to dΣ/dΩ(Q) for S60 in the melt state at a temperature of 358 K.

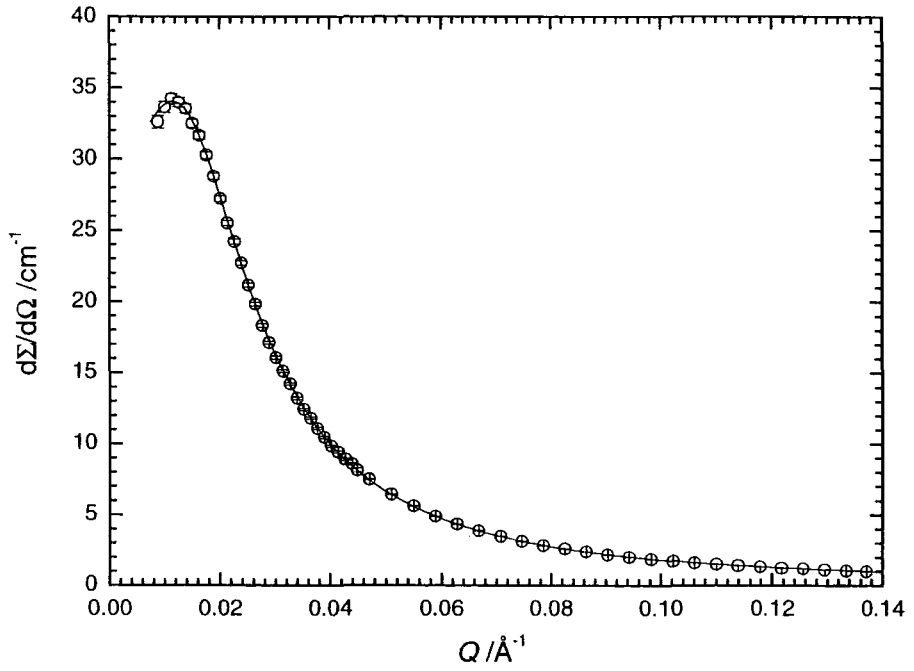

B7: RPA fit to dΣ/dΩ(Q) for S60 in the melt state at a temperature of 368 K.

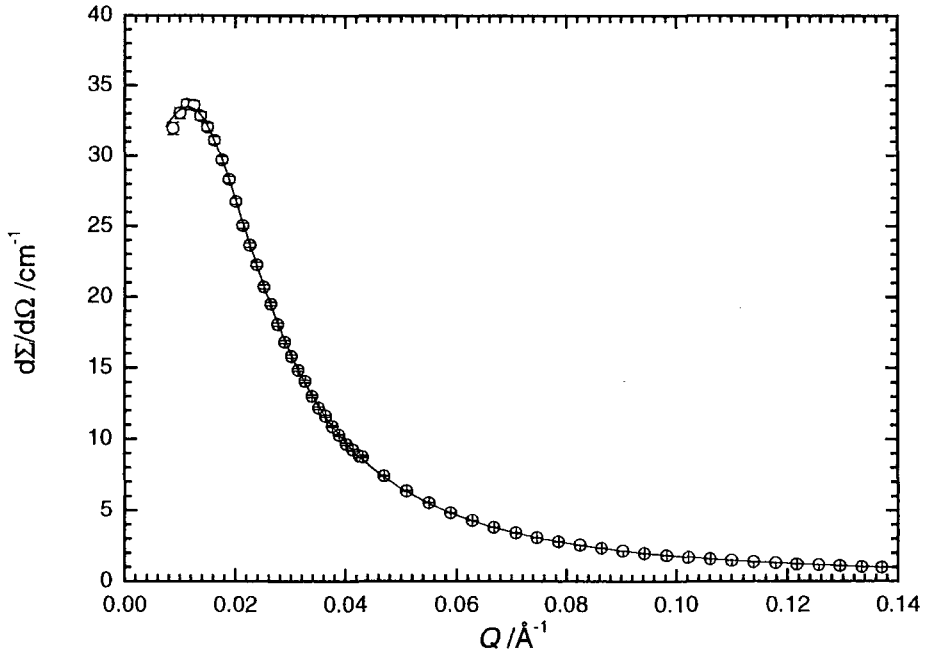

B8: RPA fit to dΣ/dΩ(Q) for S60 in the melt state at a temperature of 378 K.

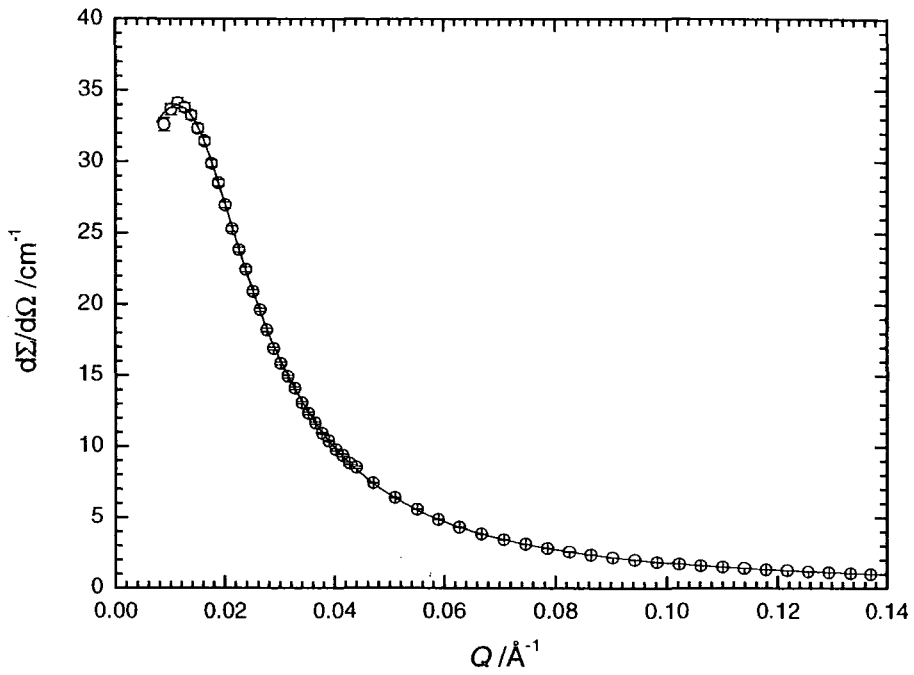

B9: RPA fit to dΣ/dΩ(Q) for S60 in the melt state at a temperature of 388 K.

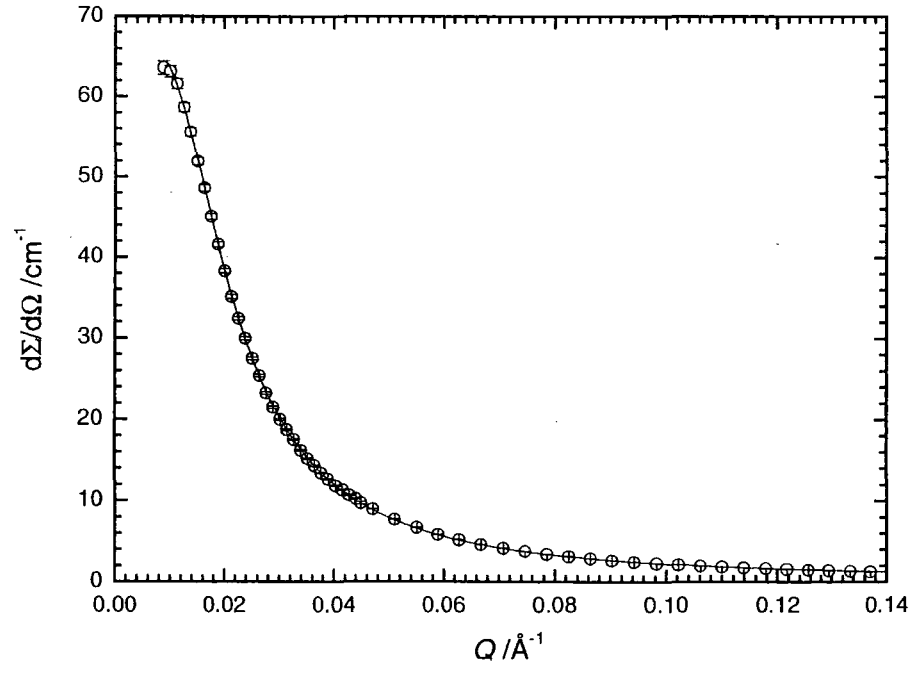

B10: RPA fit to dΣ/dΩ(Q) for S80 in the melt state at a temperature of 298 K.

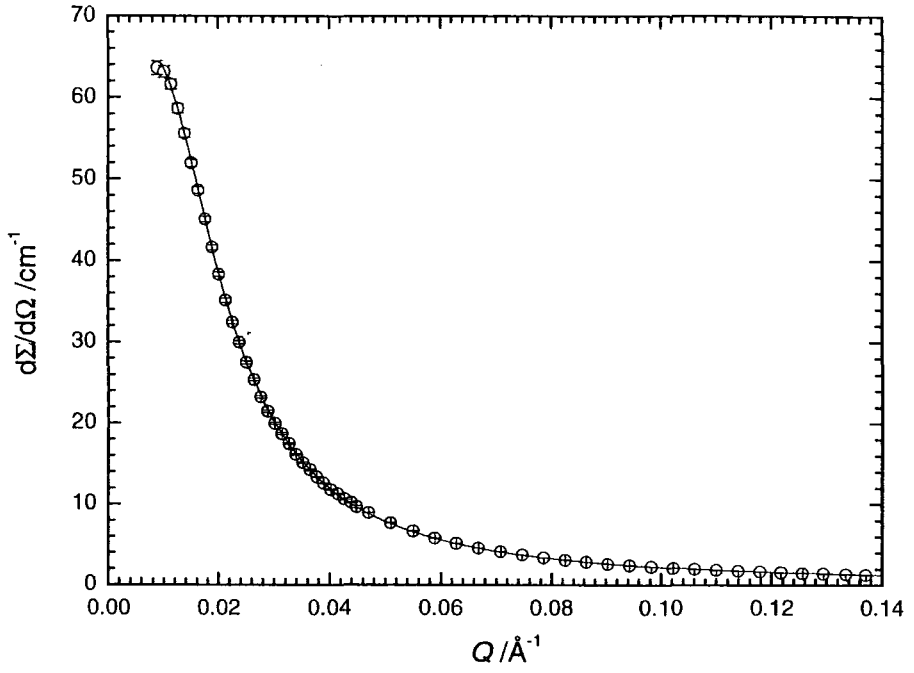

B11: RPA fit to dΣ/dΩ(Q) for S80 in the melt state at a temperature of 318 K.

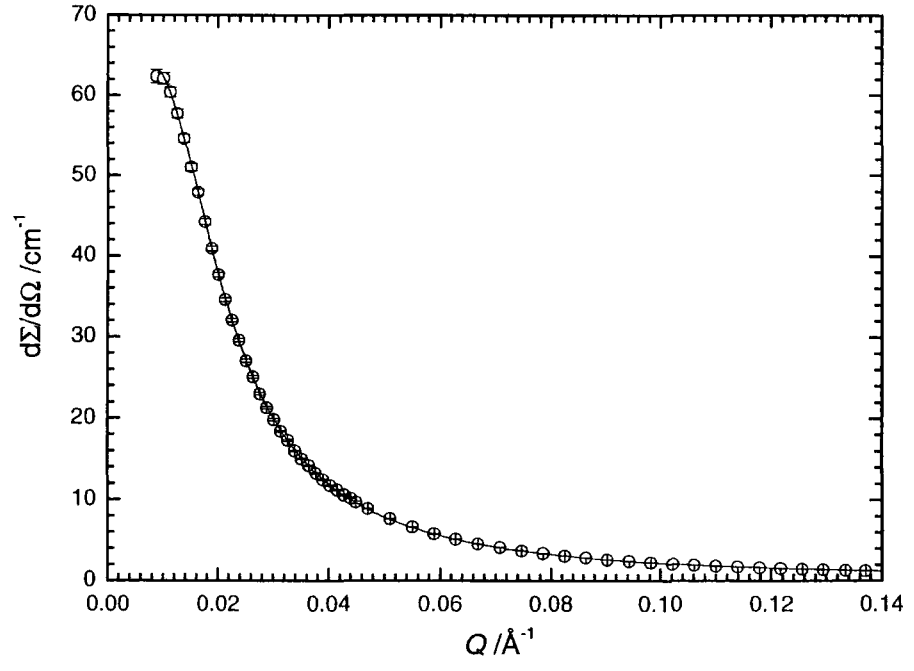

B12: RPA fit to dΣ/dΩ(Q) for S80 in the melt state at a temperature of 328 K.

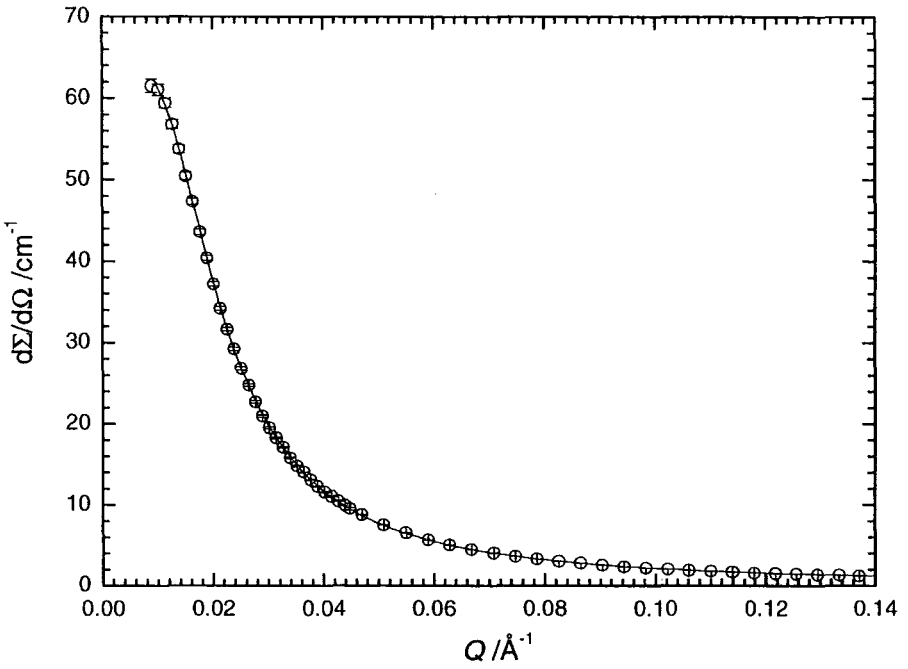

B13: RPA fit to dΣ/dΩ(Q) for S80 in the melt state at a temperature of 338 K.

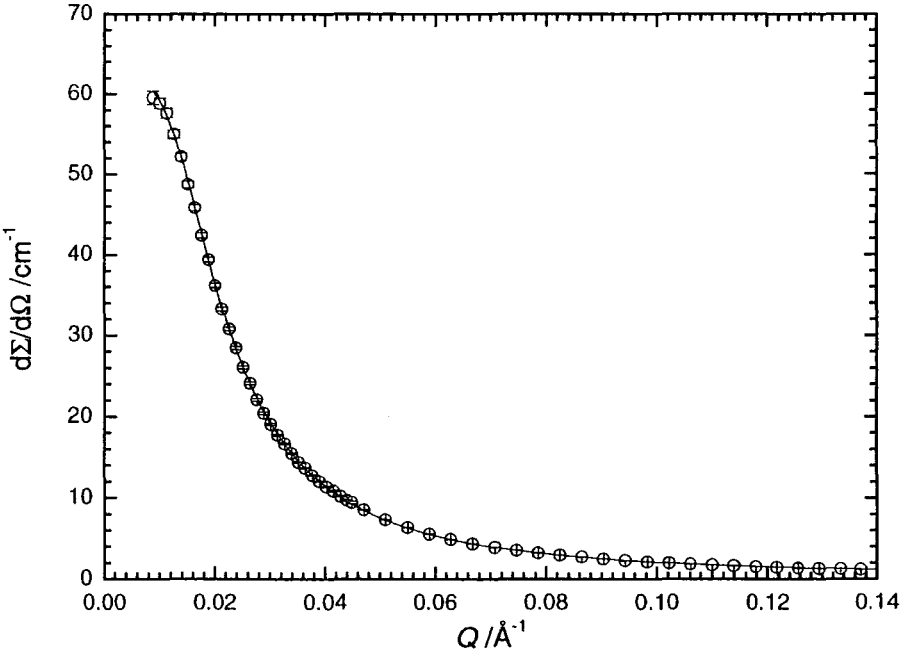

B14: RPA fit to dΣ/dΩ(Q) for S80 in the melt state at a temperature of 348 K.

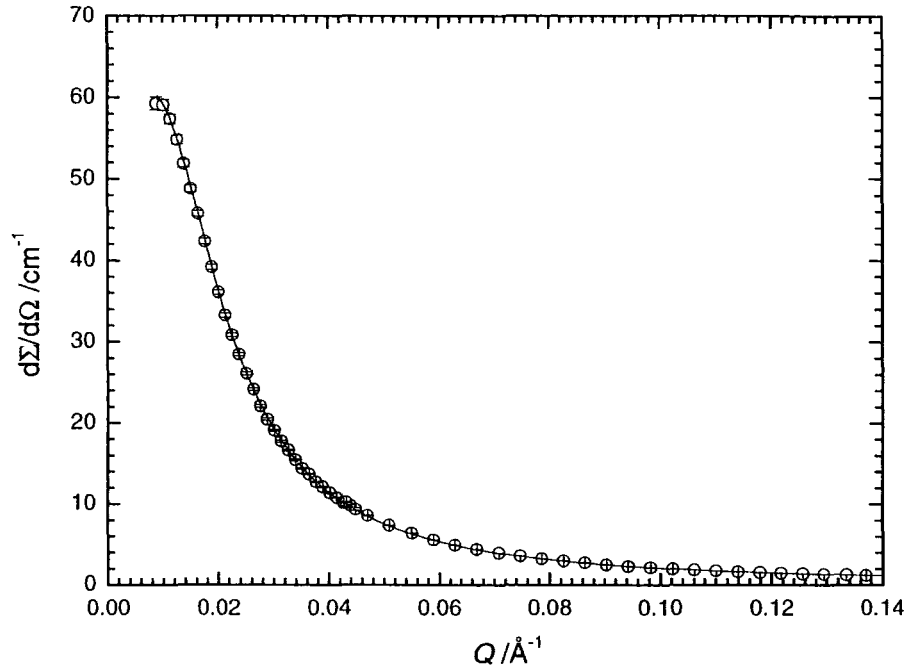

B15: RPA fit to dΣ/dΩ(Q) for S80 in the melt state at a temperature of 358 K.

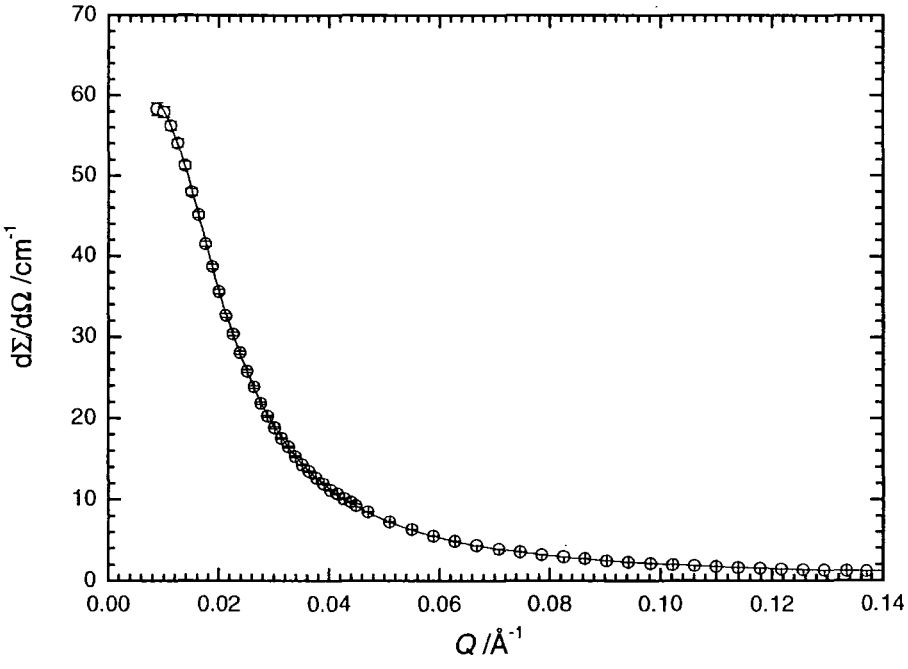

B16: RPA fit to dΣ/dΩ(Q) for S80 in the melt state at a temperature of 368 K.

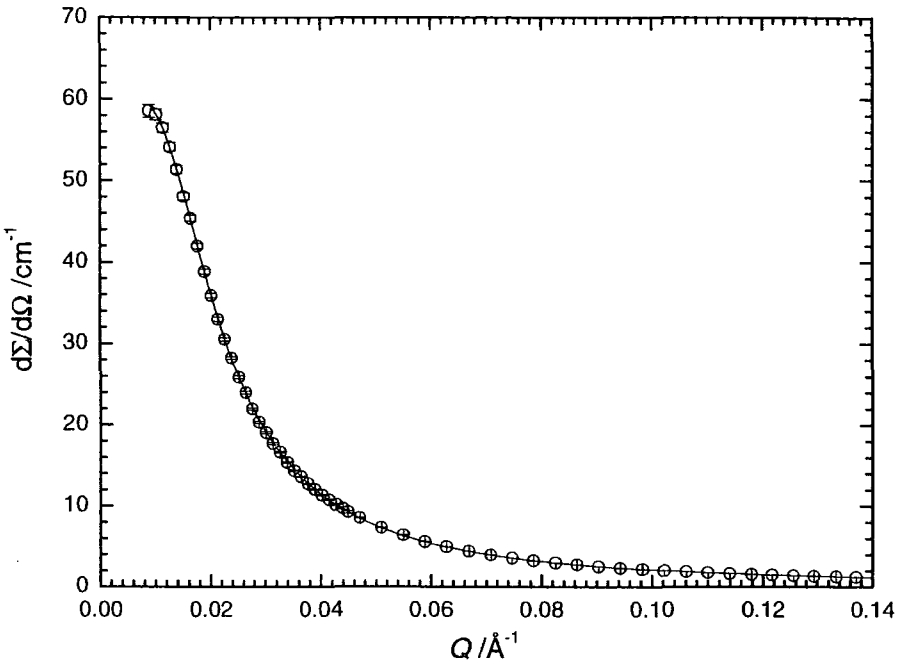

B17: RPA fit to dΣ/dΩ(Q) for S80 in the melt state at a temperature of 378 K.

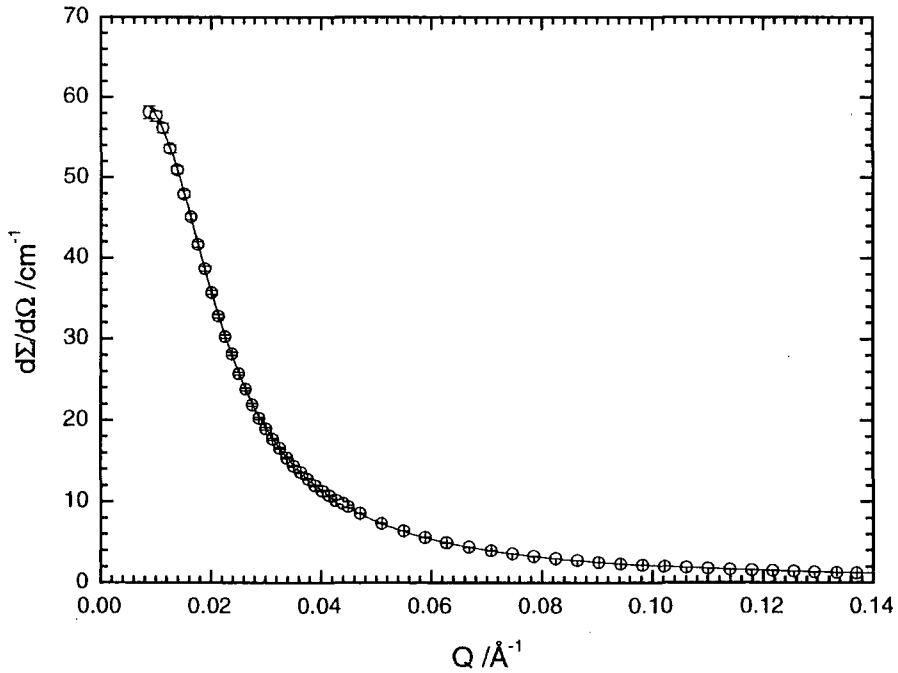

B18: RPA fit to dΣ/dΩ(Q) for S80 in the melt state at a temperature of 388 K.

Appendix C

RPA fits to S60 and S80 in contrast matched cyclohexane/cyclohexane-d_{12} at range of star volume fractions (ϕ_{Star}).

C1: RPA fit to S60 in contrast matched cyclohexane/cyclohexane-d_{12} at a ϕ_{Star} of 0.12.

C2: RPA fit to S60 in contrast matched cyclohexane/cyclohexane-d_{12} at a ϕ_{Star} of 0.09.

C3: RPA fit to S60 in contrast matched cyclohexane/cyclohexane-d_{12} at a ϕ_{Star} of 0.07.

C4: RPA fit to S60 in contrast matched cyclohexane/cyclohexane-d_{12} at a ϕ_{Star} of 0.05.

C5: RPA fit to S60 in contrast matched cyclohexane/cyclohexane-d_{12} at a ϕ_{Star} of 0.02.

C6: RPA fit to S80 in contrast matched cyclohexane/cyclohexane-d_{12} at a ϕ_{Star} of 0.12.

C7: RPA fit to S80 in contrast matched cyclohexane/cyclohexane-d_{12} at a ϕ_{Star} of 0.10.

C8: RPA fit to S80 in contrast matched cyclohexane/cyclohexane-d_{12} at a ϕ_{Star} of 0.05.

C9: RPA fit to S80 in contrast matched cyclohexane/cyclohexane-d_{12} at a ϕ_{Star} of 0.02.

RPA fits to S60 and S80 in 1,4-dioxane at range of star volume fractions (ϕ_{Star}).

C10: RPA fit to S60 in 1,4-dioxane at a ϕ_{Star} of 0.12.

C11: RPA fit to S60 in 1,4-dioxane at a ϕ_{Star} of 0.09.

C12: RPA fit to S60 in 1,4-dioxane at a ϕ_{Star} of 0.07.

C13: RPA fit to S80 in 1,4-dioxane at a ϕ_{Star} of 0.13.

C14: RPA fit to S80 in 1,4-dioxane at a ϕ_{Star} of 0.10.

C15: RPA fit to S80 in 1,4-dioxane at a ϕ_{Star} of 0.07.

C16: RPA fit to S80 in 1,4-dioxane at a ϕ_{Star} of 0.04.

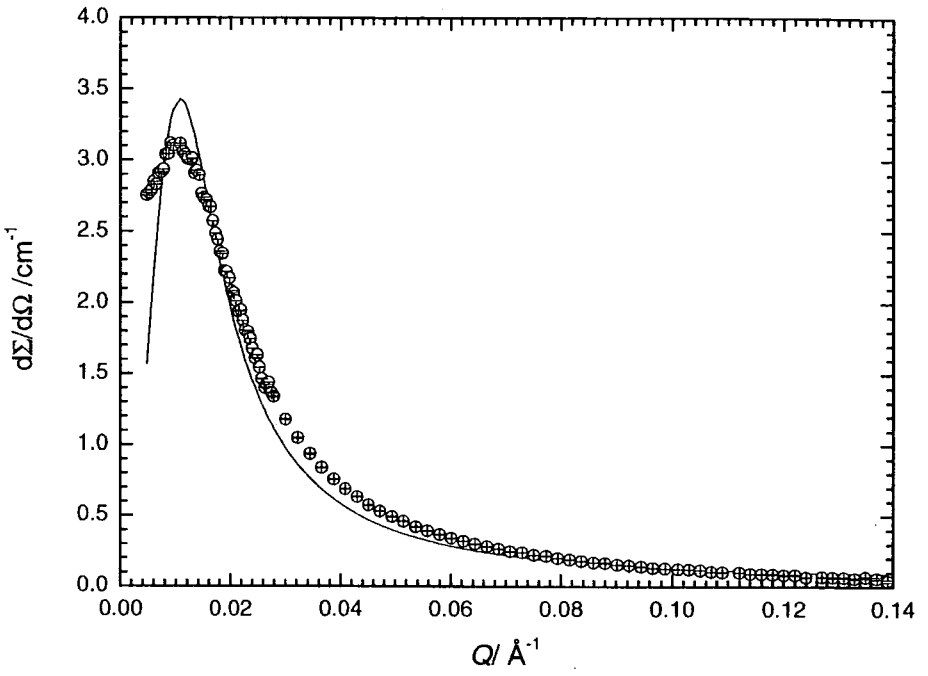

C1: RPA fit to S60 in contrast matched cyclohexane/cyclohexane-d_{12} at a ϕ_{Star} of 0.12.

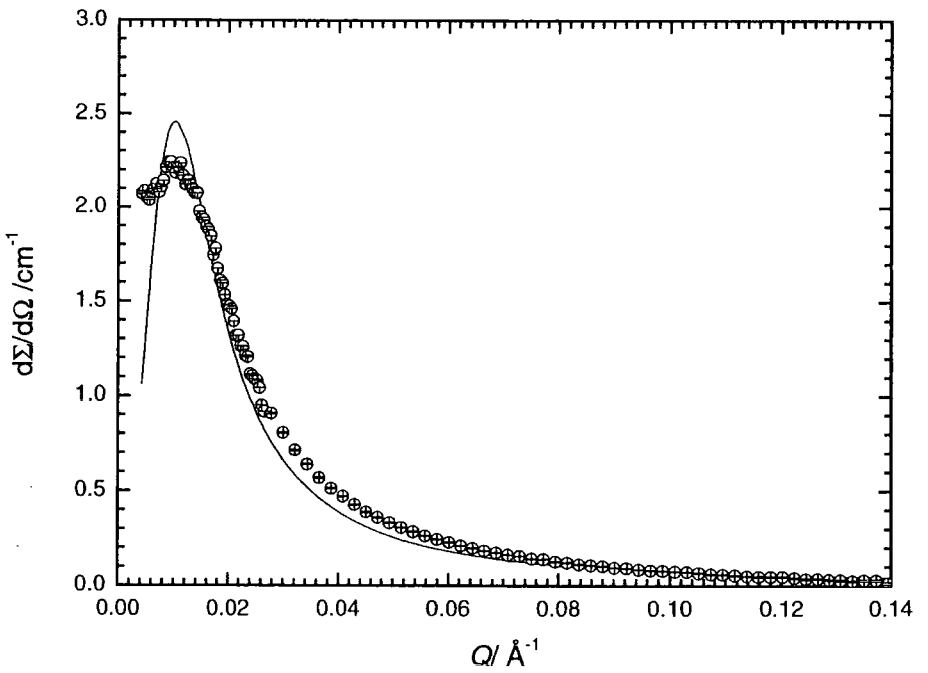

C2: RPA fit to S60 in contrast matched cyclohexane/cyclohexane-d_{12} at a ϕ_{Star} of 0.09.

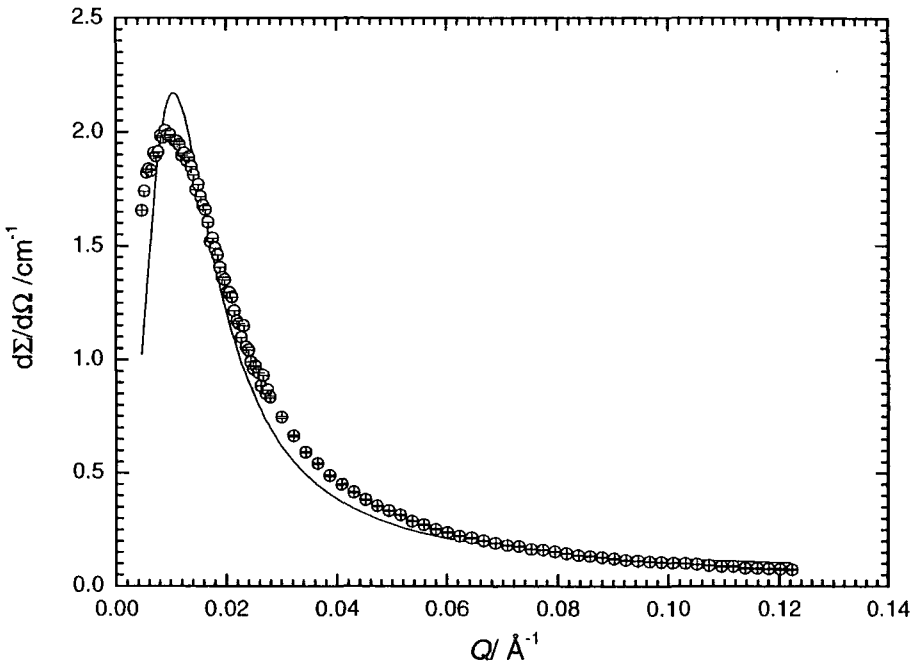

C3: RPA fit to S60 in contrast matched cyclohexane/cyclohexane-d_{12} at a ϕ_{Star} of 0.07.

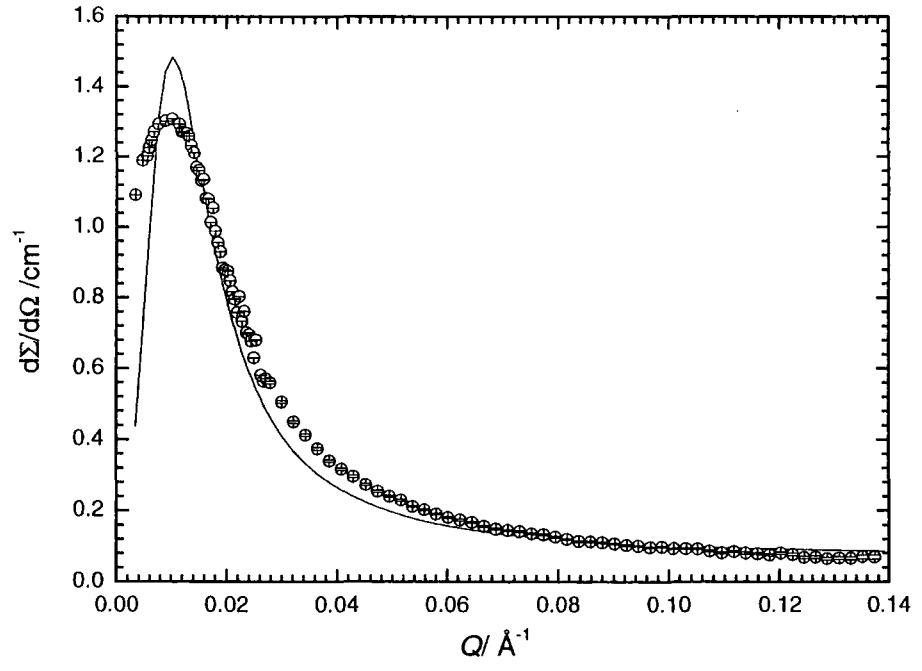

C4: RPA fit to S60 in contrast matched cyclohexane/cyclohexane-d_{12} at a ϕ_{Star} of 0.05.

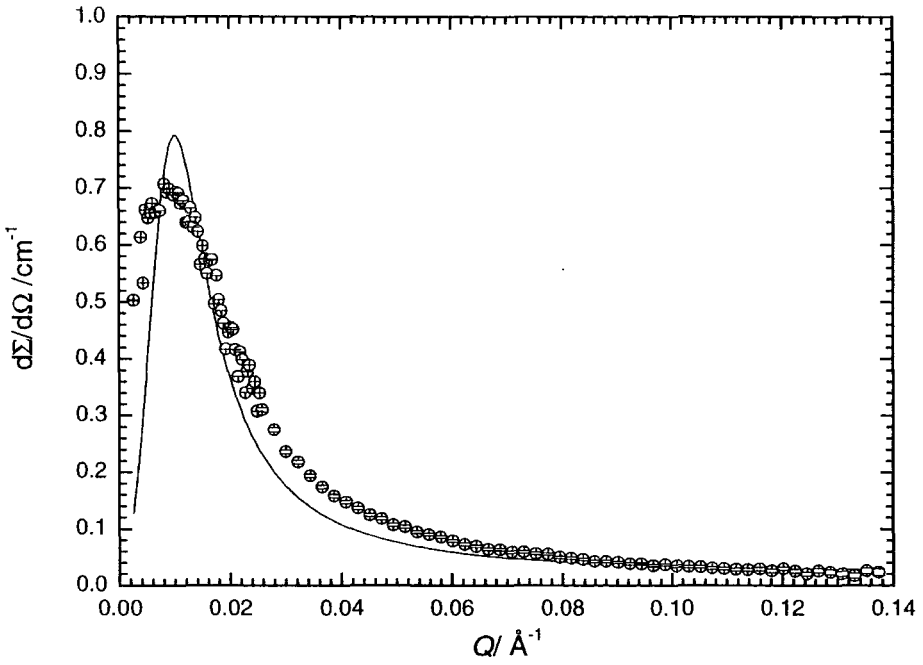

C5: RPA fit to S60 in contrast matched cyclohexane/cyclohexane-d_{12} at a ϕ_{Star} of 0.02.

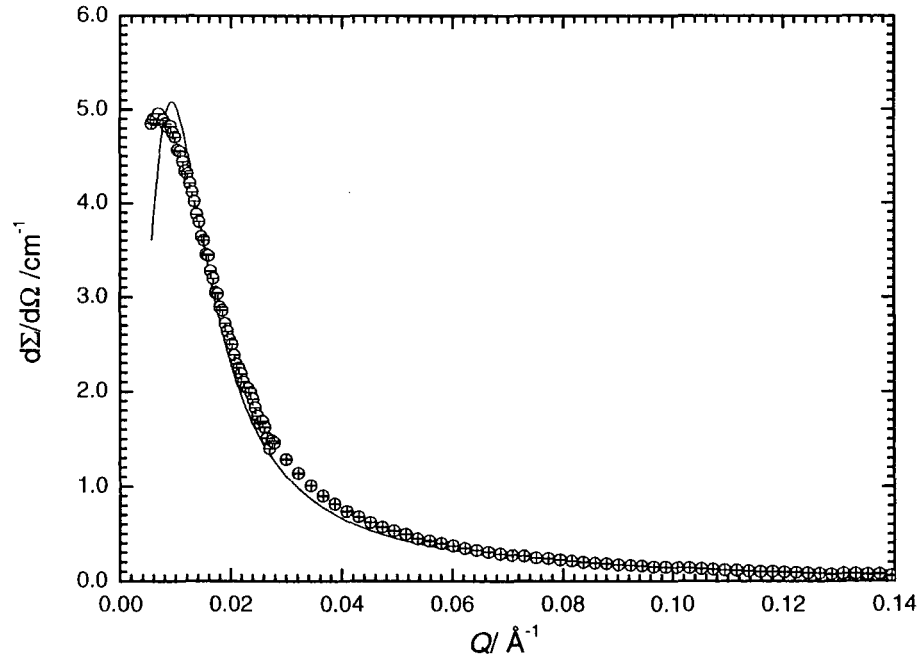

C6: RPA fit to S80 in contrast matched cyclohexane/cyclohexane-d_{12} at a ϕ_{Star} of 0.12.

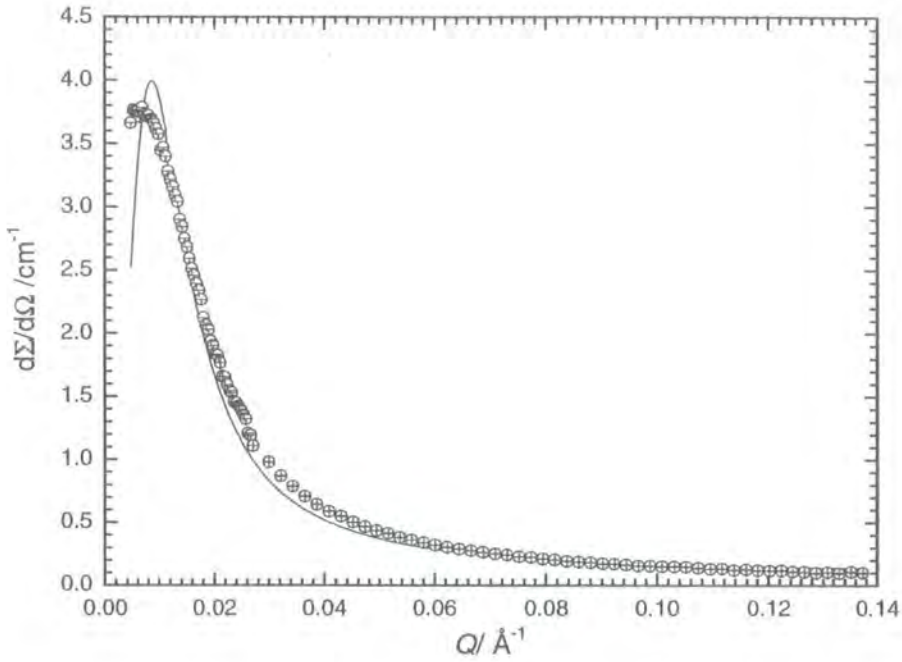

C7: RPA fit to S80 in contrast matched cyclohexane/cyclohexane-d_{12} at a ϕ_{Star} of 0.10.

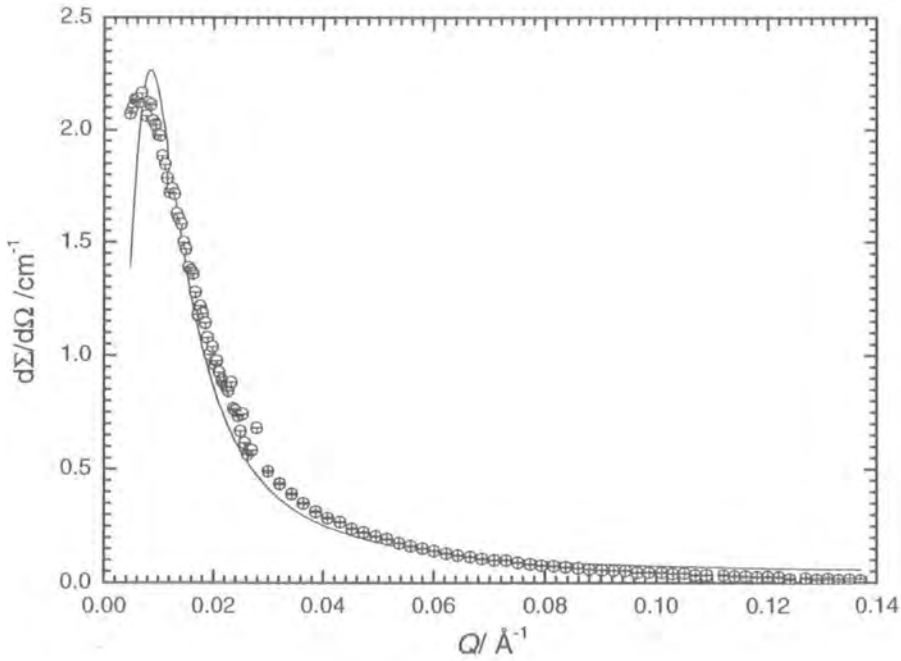

C8: RPA fit to S80 in contrast matched cyclohexane/cyclohexane-d_{12} at a ϕ_{Star} of 0.05.

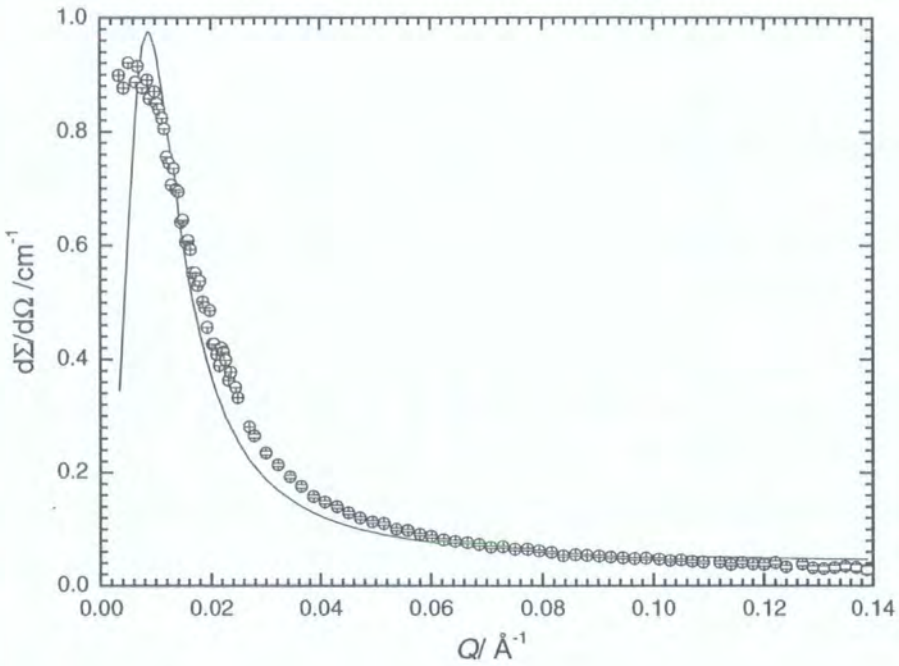

C9: RPA fit to S80 in contrast matched cyclohexane/cyclohexane-d_{12} at a ϕ_{Star} of 0.02.

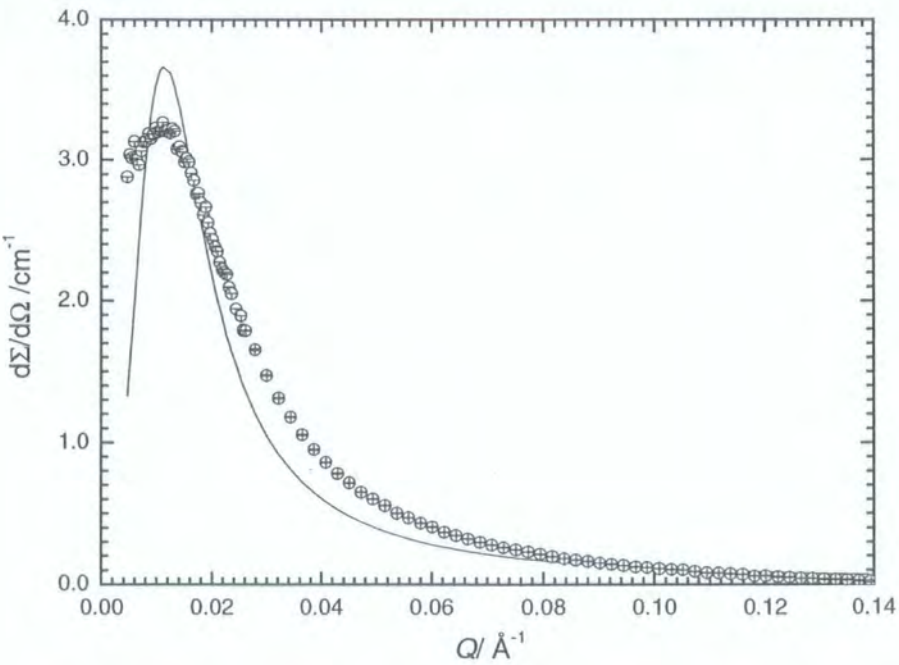

C10: RPA fit to S60 in 1,4-dioxane-d_8 at a ϕ_{Star} of 0.12.

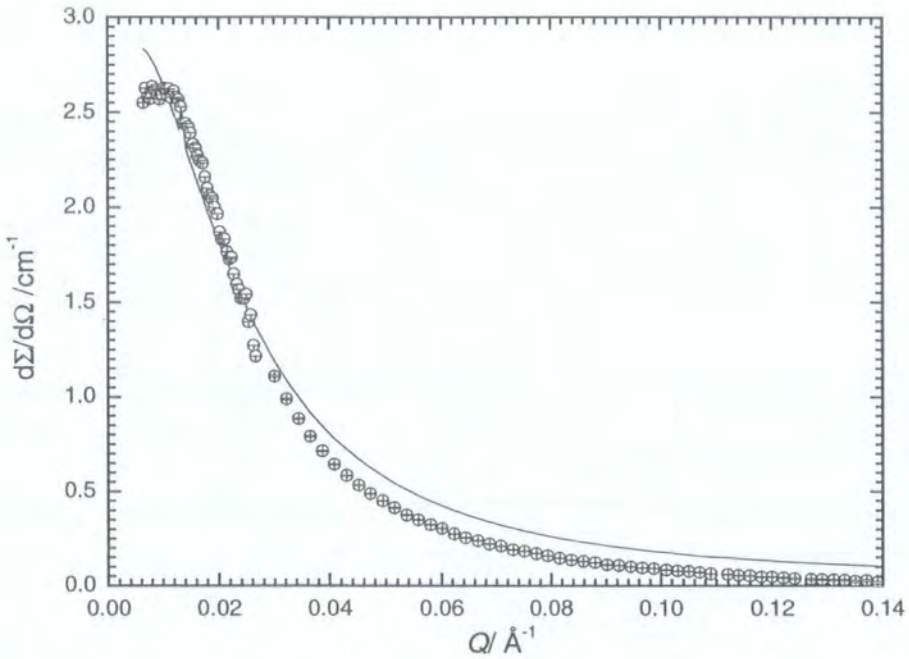

C11: RPA fit to S60 in 1,4-dioxane-d_8 at a ϕ_{Star} of 0.09.

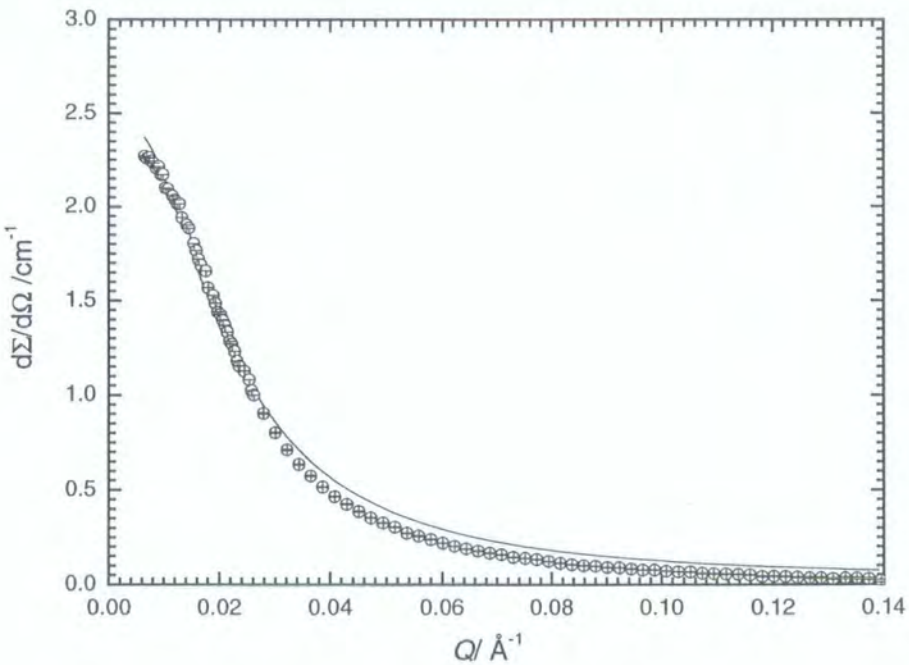

C12: RPA fit to S60 in 1,4-dioxane-d_8 at a ϕ_{Star} of 0.07.

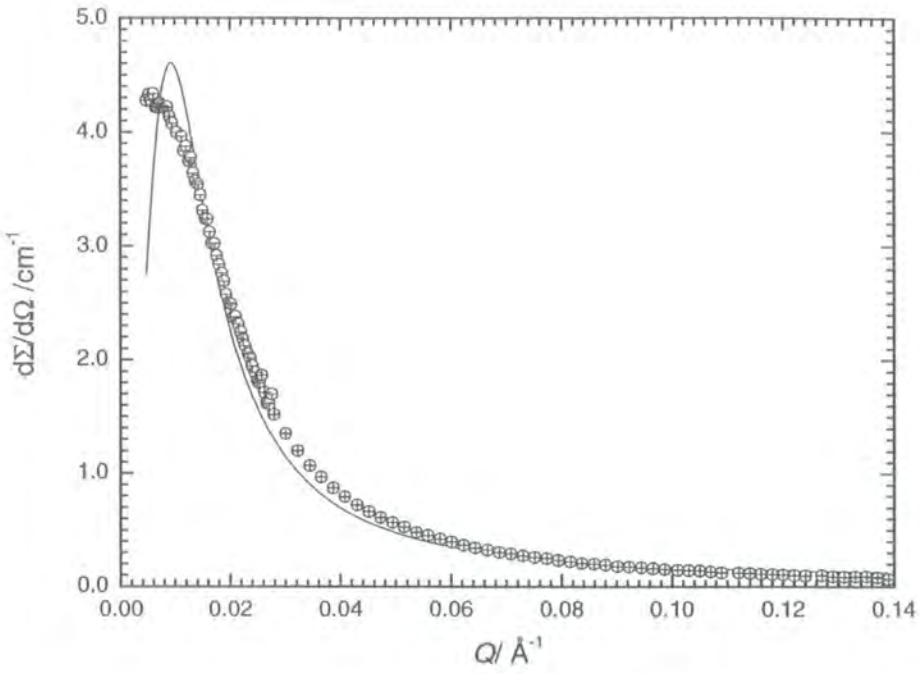

C13: RPA fit to S80 in 1,4-dioxane-d_8 at a ϕ_{Star} of 0.13.

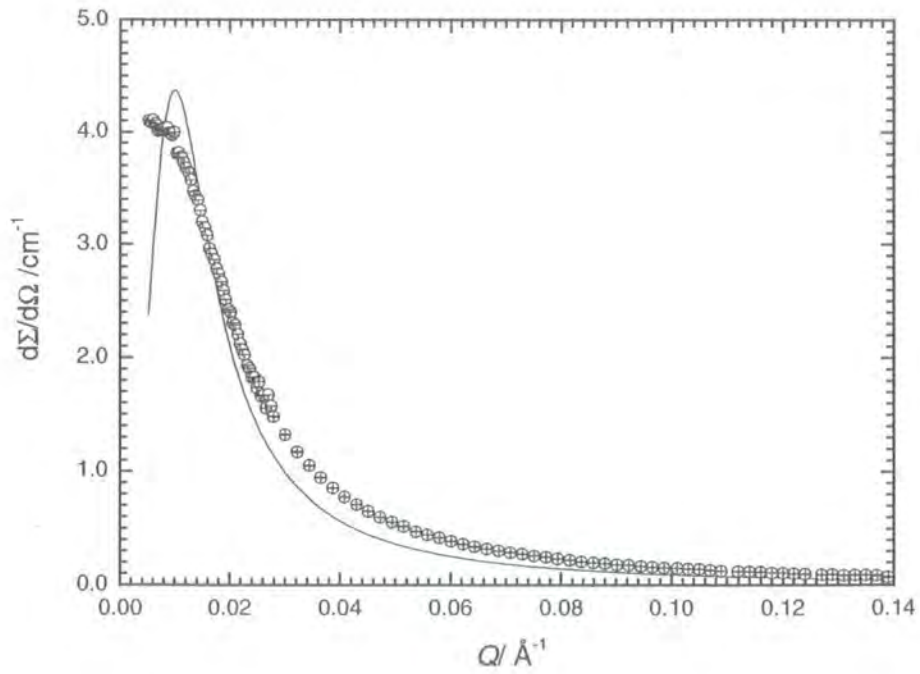

C14: RPA fit to S80 in 1,4-dioxane-d_8 at a ϕ_{Star} of 0.10.

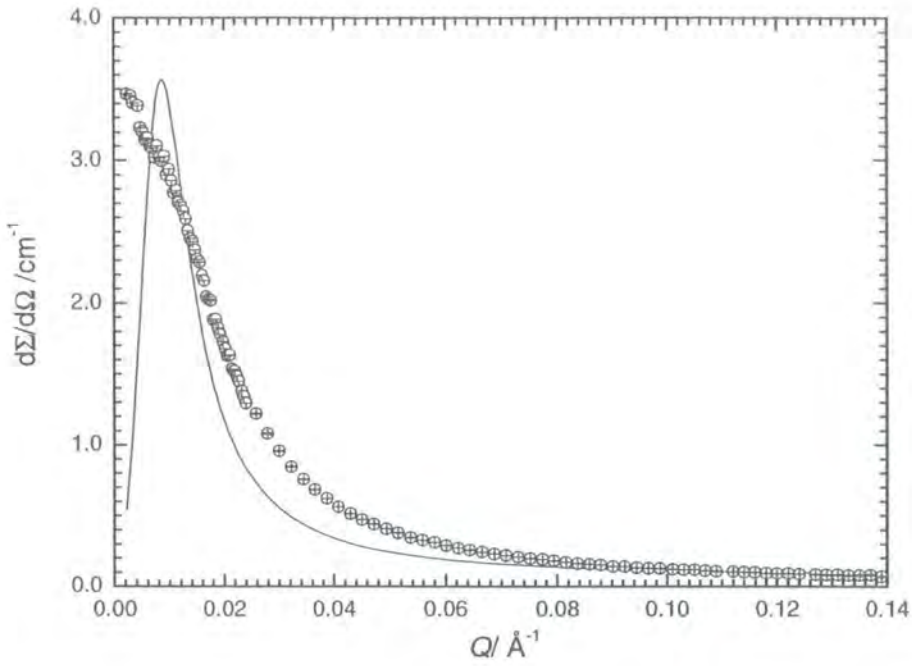

C15: RPA fit to S80 in 1,4-dioxane-d_8 at a ϕ_{Star} of 0.07.

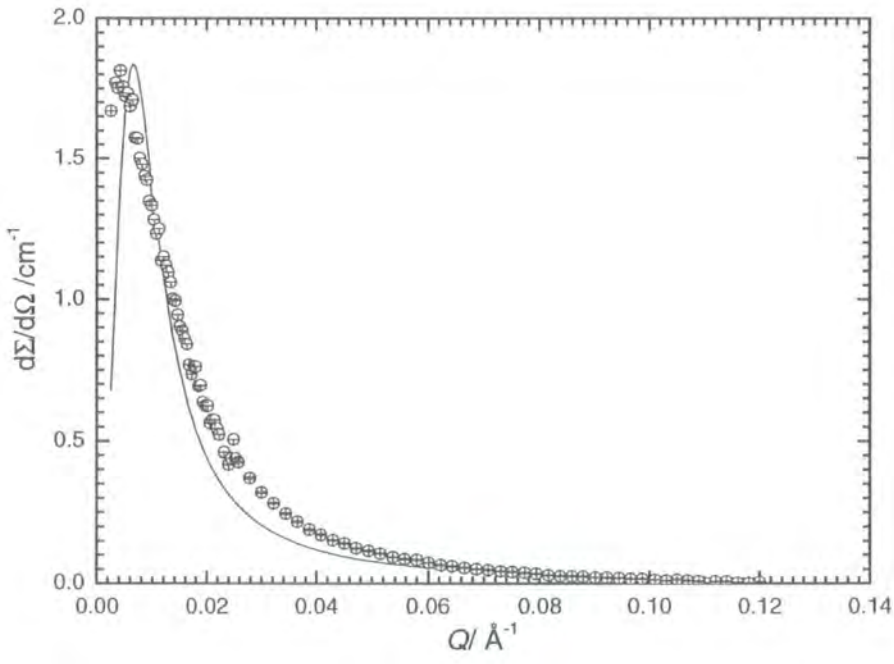

C16: RPA fit to S80 in 1,4-dioxane-d_8 at a ϕ_{Star} of 0.04.